

University of Bath



**PHD**

**Transient optimisation of a diesel engine**

Wijetunge, Roshan

*Award date:*  
2001

*Awarding institution:*  
University of Bath

[Link to publication](#)

**General rights**

Copyright and moral rights for the publications made accessible in the public portal are retained by the authors and/or other copyright owners and it is a condition of accessing publications that users recognise and abide by the legal requirements associated with these rights.

- Users may download and print one copy of any publication from the public portal for the purpose of private study or research.
- You may not further distribute the material or use it for any profit-making activity or commercial gain
- You may freely distribute the URL identifying the publication in the public portal ?

**Take down policy**

If you believe that this document breaches copyright please contact us providing details, and we will remove access to the work immediately and investigate your claim.

Download date: 13. May. 2019

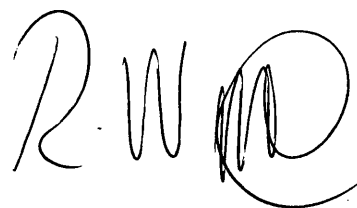
# **TRANSIENT OPTIMISATION OF A DIESEL ENGINE**

submitted by Roshan Wijetunge  
for the degree of PhD  
of the University of Bath  
2001

## **COPYRIGHT**

Attention is drawn to the fact that copyright of this thesis rests with its author.  
This copy of the thesis has been supplied on condition that anyone who consults  
it is understood to recognise that its copyright rests with its author and that no quotation from the thesis  
and no information derived from it may be published  
without the prior written consent of the author.

This thesis may be made available for consultation within  
the University Library and may be photocopied or lent to other libraries  
for the purposes of consultation.

A handwritten signature in black ink, consisting of the letters 'R', 'W', and 'J' in a stylized, cursive script.

UMI Number: U135980

All rights reserved

INFORMATION TO ALL USERS

The quality of this reproduction is dependent upon the quality of the copy submitted.

In the unlikely event that the author did not send a complete manuscript and there are missing pages, these will be noted. Also, if material had to be removed, a note will indicate the deletion.



UMI U135980

Published by ProQuest LLC 2013. Copyright in the Dissertation held by the Author.  
Microform Edition © ProQuest LLC.

All rights reserved. This work is protected against  
unauthorized copying under Title 17, United States Code.



ProQuest LLC  
789 East Eisenhower Parkway  
P.O. Box 1346  
Ann Arbor, MI 48106-1346

UNIVERSITY OF BATH	
6	24 JUL 2001
Ph.D.	

# **TRANSIENT OPTIMISATION OF A DIESEL ENGINE**

**PHD THESIS**

**ROSHAN WIJETUNGE**

**UNIVERSITY OF BATH**

**Supervised by N.D.Vaughan & J.G.Hawley**

## **SYNOPSIS**

The drive to reduce emissions and fuel consumption whilst simultaneously meeting vehicle performance targets has led to many advances in Diesel engine technology in recent years. In particular, exhaust gas recirculation (EGR) and variable geometry turbocharging (VGT) have played a key role in achieving these aims by permitting flexible control of the engine inlet gas charge. However, the added flexibility comes at the cost of increased control system complexity, and as a result, increased calibration effort. The full potential of these devices are difficult to achieve due to limitations in the control methods employed, the actuation hardware used, as well as the additional production and cost constraints. This thesis aims to devise simple strategies that provide improved control and exploit more fully the potential of the EGR VGT system during transient operation, a regime widely accepted as offering much room for improvement in terms of exhaust emissions and fuel consumption.

An extensive study of engine behaviour utilising a fully transient engine test bed is described and a dynamic engine model is introduced and validated. Control strategies are developed in simulation and on the test bed engine using rapid prototyping hardware. A new control scheme for improved VGT performance during large load transients based on exhaust manifold pressure feedback is developed and evaluated. Two methods of achieving coordinated control of the EGR and VGT systems for a more rapid transient airflow response are demonstrated. An investigation into Exhaust Gas Oxygen concentration feedback for EGR-VGT control is also performed and a feedforward with feedback control scheme proposed.

The new control schemes have been evaluated using constant speed fuel transients and full legislative drive cycles. Comparisons with the existing control strategy are made for cumulative emissions and fuel consumption.

It is concluded that the new control schemes offer scope for improved engine performance but careful consideration of control strategy setpoint values is required to achieve good drive cycle emissions and fuel consumption. Throughout the strategy development process the calibration ease and strategy complexity are considered, the final control schemes are simple extensions to the existing strategy and offer improved control system performance with little increase in calibration requirements or transparency of the control strategy.

# ACKNOWLEDGEMENTS

I would like to express my gratitude to the following people:

My supervisors, Dr. Nick Vaughan and Dr. Gary Hawley for their support and guidance. Dr. Chris Brace for his expertise and enthusiasm. Professor Frank Wallace for advice on all things turbocharged. Dr. Torquil Ross-Martin for setting me off in the right direction. Terry Wilson, Jeff Brewster, Alan Brewer and all the technical staff past and present involved in running and maintaining the transient test facility. Roger Tilley for his software expertise. Matt Cole, Paul Geurrier and Professor Kevin Edge for their advice on control systems. My colleagues Allan Cox, Chris Mobley, Sam Akehurst, Robin Maugham, Volker Wicke, Jon Hall and Adrian Cooper for their input, coffee breaks, frisbee tournaments and general good-humour. Hugh Burnham-Slipper for keeping me sane through the most difficult periods and for his invaluable advice and support.

The staff at the collaborative organisations who have advised or assisted this research: From the Ford Motor Company, Gordon Bird, Roy Horrocks, Brian Cummings, Paul Moraal, Ilya Kolmanovsky, Micheal Van Nieuwstadt, Urs Christiansen, Jim Bromham, Mike Watts and Trevor Taylor. Kleinknecht, Lance Keene. NTK Insulators, Dan Boon. Honeywell Turbocharging Systems, Phil Halsall. Cambridge Control, Steve Pole.

Finally I would like to thank my family and Caroline for all their support, encouragement and understanding.

Roshan Wijetunge

May 2001

# Table of Contents

ABBREVIATIONS & NOMENCLATURE.....	11
CHAPTER 1 INTRODUCTION .....	14
1.1 BACKGROUND.....	14
1.2 OBJECTIVES .....	15
1.3 RESEARCH METHODOLOGY AND THESIS OUTLINE.....	15
CHAPTER 2 BACKGROUND AND LITERATURE REVIEW .....	17
2.1 BACKGROUND.....	17
2.1.1 DIESEL ENGINE.....	17
2.1.2 DIESEL COMBUSTION.....	17
2.1.3 DIESEL ENGINE EXHAUST EMISSIONS .....	18
2.2 EXHAUST GAS RECIRCULATION .....	19
2.3 VARIABLE GEOMETRY TURBOCHARGER.....	20
2.4 ELECTRONIC ENGINE CONTROL .....	20
2.4.1 EGR AND VGT CONTROL.....	21
2.5 ALTERNATIVE EGR CONTROL STRATEGIES .....	22
2.6 ALTERNATIVE VGT CONTROL STRATEGIES .....	23
2.7 COORDINATED EGR AND VGT CONTROL STRATEGIES .....	25
2.8 ALTERNATIVE CONTROL TECHNIQUES .....	28
2.8.1 SLIDING MODE CONTROL.....	28
2.8.2 MINIMAL CONTROLLER SYNTHESIS.....	29
2.8.3 OPTIMISATION-BASED CONTROL.....	29
2.8.4 INTELLIGENT CONTROL .....	30
2.8.5 NEURAL NETWORKS.....	30
2.8.6 FUZZY LOGIC .....	31
2.9 CONSIDERATIONS FOR EGR-VGT CONTROLLER DESIGN .....	31
2.9.1 MINIMUM BSFC .....	31
2.9.2 BEST TIP-IN RESPONSE .....	32
2.9.3 MINIMUM NO <sub>x</sub> .....	32
2.9.4 TRANSIENT SMOKE .....	33
2.9.5 DRIVEABILITY .....	33
2.10 GENERAL REMARKS.....	33
CHAPTER 3 EXPERIMENTAL CHARACTERISATION OF THE ENGINE.....	44
3.1 INTRODUCTION.....	44
3.2 TRANSIENT TEST CELL .....	44
3.2.1 ENGINE .....	44
3.2.2 TRANSMISSION.....	45
3.2.3 DYNAMOMETER.....	45
3.2.4 TEST CELL CONTROL.....	45
3.2.5 ENGINE CONTROL AND CALIBRATION.....	46
3.2.6 RAPID PROTOTYPING EQUIPMENT.....	46
3.2.7 EMISSIONS MEASUREMENT.....	46
3.2.8 FUEL FLOW .....	47
3.2.9 IN-CYLINDER PRESSURE.....	47
3.2.10 DATA ACQUISITION.....	47
3.3 ENGINE TESTING.....	47
3.4 STEADY STATE ENGINE TESTING .....	48
3.4.1 MODAL TESTS.....	48
3.4.2 LIMITING TORQUE CURVE .....	50
3.4.3 EGR AND VGT SWEEPS .....	51
3.5 DYNAMIC TESTING .....	52

3.5.1	CONSTANT SPEED FUEL STEP TESTING .....	52
3.5.2	COMPARISON OF FUEL STEP RESPONSE WITH AND WITHOUT EGR	56
3.5.3	DRIVE CYCLE TESTING .....	56
3.6	SUMMARY OF RESULTS.....	58
CHAPTER 4 DYNAMIC ENGINE SIMULATION.....		76
4.1	INTRODUCTION .....	76
4.2	MODELLING FOR CONTROL.....	76
4.3	FORD PUMA 2.0 LITRE VGT DIESEL ENGINE MODEL .....	77
4.3.1	INLET, COMPRESSOR, INTERCOOLER AND EGR .....	78
4.3.2	CYLINDERS.....	79
4.3.3	EXHAUST MANIFOLD AND TURBINE.....	80
4.3.4	TURBOCHARGER SHAFT .....	81
4.4	ADDITIONAL SUB-MODELS.....	82
4.4.1	VGT ACTUATOR AND VANE MODEL .....	82
4.4.2	EGR VALVE.....	83
4.4.3	DRIVER MODEL .....	84
4.4.4	STANDARD CONTROLLER .....	84
4.4.5	DYNAMOMETER MODEL.....	84
4.5	MODEL VALIDATION.....	85
4.5.1	VGT VANE MECHANISM MODEL VALIDATION.....	85
4.5.2	FUEL STEP TRANSIENTS.....	85
4.5.3	DRIVE CYCLE VALIDATION .....	89
4.6	SUMMARY OF RESULTS.....	90
CHAPTER 5 EXHAUST PRESSURE CONTROLLER.....		103
5.1	INTRODUCTION .....	103
5.2	TRANSIENT TURBINE BEHAVIOUR .....	103
5.3	EXHAUST PRESSURE MEASUREMENT .....	105
5.4	TRANSIENT DETECTION .....	106
5.5	PROPOSED CONTROL SCHEME .....	107
5.6	SIMULINK IMPLEMENTATION .....	107
5.7	COMPARISON IN SIMULATION OF CONTROLLERS .....	109
5.7.1	INLET MANIFOLD PRESSURE .....	109
5.7.2	VGT VANE POSITION.....	110
5.7.3	EXHAUST MANIFOLD PRESSURE.....	110
5.7.4	FUELLING.....	110
5.8	EXHAUST PRESSURE CONTROLLER EXPERIMENTAL EVALUATION ON TEST BED	111
5.8.1	Implementation on test bed using dSpace.....	111
5.8.2	Comparison of controllers over 2500 rev/min tip-in response .....	111
5.8.3	Summary of performance at different engine speeds .....	114
5.9	SUMMARY OF RESULTS.....	115
CHAPTER 6 COORDINATED EGR VGT CONTROL 1 .....		130
6.1	INTRODUCTION .....	130
6.2	MOTIVATION FOR COORDINATED EGR AND VGT CONTROL.....	130
6.2.1	EGR FLOW BEHAVIOUR.....	131
6.2.2	EGR BEHAVIOUR UNDER THE STANDARD CONTROL SCHEME.....	131
6.2.3	OPERATING REGION DEPENDENCY .....	132
6.3	COORDINATED EGR AND VGT CONTROL .....	133
6.4	FUZZY LOGIC FOR COORDINATED CONTROL .....	133
6.4.1	FUZZY LOGIC .....	134
6.5	FUZZY CONTROLLER DESIGN.....	134
6.6	PROPOSED CONTROLLER.....	135
6.6.1	OVERVIEW .....	135
6.6.2	CONTROLLER DESIGN .....	135



6.6.3	CONTROLLER INPUT AND OUTPUT CLASSIFICATION.....	136
6.6.4	CONTROLLER RULE BASE .....	137
6.6.5	EXAMPLE INFERENCE OPERATION .....	139
6.7	COORDINATED CONTROLLER PERFORMANCE TESTING .....	141
6.7.1	1500 REV/MIN FUELLING PROFILE WITH ACTIVE OPEN-LOOP.....	142
6.7.2	SUMMARY 1500 REV/MIN FUELLING PROFILE WITH FIXED OPEN- LOOP .....	143
6.8	EXPERIMENTAL RESULTS DISCUSSION .....	143
6.8.1	GENERAL PERFORMANCE .....	143
6.8.2	PROPORTIONAL TERMS.....	143
6.8.3	FUZZY INFERENCE .....	144
6.9	REVISED CONTROL SCHEME.....	144
6.9.1	REVISED FUZZY CONTROLLER SIMULATED PERFORMANCE EVALUATION .....	145
6.10	REVISED CONTROLLER DISCUSSION .....	146
6.10.1	GENERAL PERFORMANCE.....	146
6.10.2	STABILITY .....	146
6.11	SUMMARY OF RESULTS.....	147
<b>CHAPTER 7 COORDINATED CONTROL USING CROSS-COUPLED INDEPENDENT CONTROLLERS .....</b>		<b>156</b>
7.1	INTRODUCTION .....	156
7.2	COORDINATED CONTROL REVISITED .....	156
7.3	CROSS-COUPLED APPROACH .....	156
7.4	PROPOSED CONTROL SCHEME .....	157
7.4.1	OVERVIEW .....	157
7.4.2	SWITCHING MECHANISM.....	157
7.5	FUZZY OPERATING POINT IDENTIFICATION.....	159
7.5.1	EXAMPLE INFERENCE.....	159
7.6	SIMULINK IMPLEMENTATION .....	160
7.7	SIMULATED PERFORMANCE .....	160
7.7.1	1500 rev/min FUELLING PROFILE FIXED OPEN-LOOP TERM .....	160
7.7.2	1500 rev/min FUELLING PROFILE ACTIVE OPEN-LOOP TERM .....	161
7.8	ENGINE-BASED CONTROLLER EVALUATION .....	161
7.8.1	ENGINE IMPLEMENTATION.....	161
7.8.2	TEST PROCEDURE.....	161
7.8.3	TEST RESULTS .....	162
7.9	SUMMARY OF RESULTS.....	167
<b>CHAPTER 8 EXHAUST OXYGEN FEEDBACK CONTROL .....</b>		<b>181</b>
8.1	INTRODUCTION .....	181
8.2	MOTIVATION FOR FEEDBACK EGR CONTROL .....	182
8.3	OXYGEN SENSORS FOR AUTOMOTIVE DIESEL APPLICATION .....	182
8.3.1	Operating Principle.....	182
8.3.2	Requirements for Application to Diesel Engines .....	183
8.3.3	Sensor .....	183
8.4	POSSIBLE SENSOR INSTALLATION CONFIGURATIONS.....	183
8.4.1	INLET MANIFOLD INSTALLATION.....	183
8.4.2	EXHAUST MANIFOLD INSTALLATION.....	185
8.4.3	EXHAUST MANIFOLD MOUNTING DETAILS .....	185
8.5	INITIAL INVESTIGATION .....	186
8.6	UEGO APPLICATIONS FOR CONTROL.....	187
8.6.1	RECONSTRUCTING INLET MANIFOLD BURNT GAS FRACTION .....	187
8.6.2	MODELLING INLET BURNT GAS FRACTION.....	189
8.6.3	CONTROL TO AN EXHAUST GAS OXYGEN CONCENTRATION .....	189
8.7	FEEDBACK CONTROLLER DEVELOPMENT 1.....	190

8.7.1	TEST RESULTS FOR FEEDBACK CONTROLLER 1 .....	190
8.8	FEEDBACK CONTROLLER DEVELOPMENT 2.....	190
8.8.1	TEST RESULTS FOR FEEDBACK CONTROLLER 2 .....	191
8.9	FEEDFORWARD CONTROLLER DEVELOPMENT.....	192
8.9.1	FEEDFORWARD COMPENSATION OF FUELLING DISTURBANCE....	193
8.9.2	OXYGEN DISTURBANCE MODEL .....	193
8.9.3	MODEL IDENTIFICATION .....	193
8.10	SIMULATED CONTROL SYSTEM PERFORMANCE.....	195
8.10.1	FUEL STEP PERFORMANCE.....	195
8.10.2	FUEL RAMP PERFORMANCE .....	195
8.11	OVERVIEW OF RESULTS AND DISCUSSION.....	196
CHAPTER 9 CONTROLLER EVALUATION OVER DRIVE CYCLE.....		213
9.1	INTRODUCTION .....	213
9.2	TEST PROCEDURE .....	214
9.3	STABILITY .....	214
9.4	LIMITATIONS .....	215
9.5	CUMULATIVE RESULTS .....	216
9.5.1	URBAN SECTION OF CYCLE .....	216
9.5.2	EXTRA-URBAN SECTION OF THE CYCLE.....	218
9.6	TIME-RESOLVED DATA .....	220
9.6.1	Urban Section of Cycle.....	220
9.6.2	Extra Urban Section of Cycle .....	221
9.7	SUMMARY OF RESULTS & DISCUSSION .....	223
CHAPTER 10 CONCLUSIONS & FURTHER WORK .....		239
10.1	CONCLUSIONS.....	239
10.2	FURTHER WORK .....	241

## Table of Figures

FIGURE 2.1 SCHEMATIC OF A TURBOCHARGED HSDI DIESEL ENGINE WITH EGR	35
FIGURE 2.2 HSDI DIESEL ENGINE COMBUSTION PROCESS ON CYLINDER PRESSURE VERSUS CRANK ANGLE DIAGRAM	36
FIGURE 2.3 DIFFERENT VARIABLE GEOMETRY TURBOCHARGER TURBINE ARRANGEMENTS	37
FIGURE 2.4 EGR AND VGT STANDARD CONTROL STRATEGY SCHEMATIC	38
FIGURE 2.5 NO <sub>x</sub> REDUCTION AND AIR FUEL RATIO TRACKING DUE TO OXYGEN SENSOR FEEDBACK EGR CONTROL ( <i>AMSTUTZ ET AL [4]</i> )	39
FIGURE 2.6 ACTUATION FORCE VS. VANE ANGLE FOR VGT VANE MECHANISM ( <i>WALKER [7]</i> )	39
FIGURE 2.7 COMPARISON OF AIRFLOW (MAF) AND BOOST TRACKING(MAP) FOR COORDINATED AND INDEPENDENT CONTROL OF EGR AND VGT ( <i>VAN NIEUWSTADT ET AL [16]</i> )	40
FIGURE 2.8 NO <sub>x</sub> / PM TRADE-OFF RESULTS FOR COMPARISON BETWEEN DIFFERENT EGR VGT CONTROL SCHEMES ( <i>VAN NIEUWSTADT ET AL [17]</i> )	41
FIGURE 2.9 SIMPLE SLIDING MODE SCHEME	41
FIGURE 2.10 BLOCK DIAGRAM FOR NON-LINEAR CYLINDER PRESSURE OBSERVER ( <i>KAO AND MOSKWA [28]</i> )	42
FIGURE 2.11 SIMULINK IMPLEMENTATION OF AN MCS CONTROLLER	42
FIGURE 2.12 NEURAL NETWORK EXAMPLE FOR AUTOMOTIVE APPLICATION (EMISSIONS MAPPING TO ENGINE PARAMETERS)	43
FIGURE 3.1 SCHEMATIC REPRESENTATION OF DYNAMIC ENGINE TEST FACILITY	59
FIGURE 3.2 MODAL TEST RESULTS: BOOST, AIRFLOW, TURBOCHARGER SPEED AND EXHAUST PRESSURE	60
FIGURE 3.3 MODAL TEST RESULTS: EGR RATE, BSFC, SMOKE, MASS NO <sub>x</sub>	61
FIGURE 3.4 LIMITING TORQUE CURVE RESULTS: TORQUE, POWER, FUELLING, SMOKE, BSFC	62
FIGURE 3.5 LIMITING TORQUE CURVE RESULTS: AIR FUEL RATIO, CYLINDER PRESSURE, EXHAUST PRESSURE, TURBOCHARGER SPEED	63
FIGURE 3.6 VGT SWEEP WITH EGR VALVE CLOSED: BOOST, EXHAUST PRESSURE AND TORQUE	64
FIGURE 3.7 BRAKE SPECIFIC FUEL CONSUMPTION VARIATION WITH EGR AND VGT SETTING ( <i>PEASE ET AL [76]</i> )	65
FIGURE 3.8 SPECIFIC NO <sub>x</sub> EMISSIONS VARIATION WITH EGR AND VGT SETTING ( <i>PEASE ET AL [76]</i> )	65
FIGURE 3.9 1500 REV/MIN FUEL STEP TRANSIENT – ENGINE PERFORMANCE PARAMETERS	66
FIGURE 3.10 1500 REV/MIN FUEL STEP TRANSIENT - TURBOCHARGER PHYSICAL PARAMETERS	66
FIGURE 3.11 1500 REV/MIN FUEL STEP TRANSIENT - ENGINE CONTROL PARAMETERS	67
FIGURE 3.12 2500 REV/MIN FUEL STEP TRANSIENT – ENGINE PERFORMANCE PARAMETERS	67
FIGURE 3.13 2500 REV/MIN FUEL STEP TRANSIENT - TURBOCHARGER PHYSICAL PARAMETERS	68
FIGURE 3.14 2500 REV/MIN FUEL STEP TRANSIENT - ENGINE CONTROL PARAMETERS	68
FIGURE 3.15 3500 REV/MIN FUEL STEP TRANSIENT – ENGINE PERFORMANCE PARAMETERS	69

FIGURE 3.16 3500 REV/MIN FUEL STEP TRANSIENT - TURBOCHARGER PHYSICAL PARAMETERS .....	69
FIGURE 3.17 3500 REV/MIN FUEL STEP TRANSIENT - ENGINE CONTROL PARAMETERS .....	70
FIGURE 3.18 COMPARISON OF FUEL STEP TRANSIENT RESPONSE AT 2500 REV/MIN FOR VGT TURBOCHARGER WITH AND WITHOUT THE EGR SYSTEM ACTIVE.....	71
FIGURE 3.19 EXHAUST GAS ANALYSER SIGNAL RECONSTRUCTION .....	72
FIGURE 3.20 DRIVE CYCLE PERFORMANCE (URBAN SECTION OF ECE15 CYCLE) .....	72
FIGURE 3.21 DRIVE CYCLE PERFORMANCE (URBAN SECTION OF ECE15 CYCLE) .....	73
FIGURE 3.22 DRIVE CYCLE PERFORMANCE (EXTRA-URBAN SECTION OF ECE15 CYCLE).....	74
FIGURE 3.23 DRIVE CYCLE PERFORMANCE (EXTRA-URBAN SECTION OF ECE15 CYCLE).....	75
FIGURE 4.1 TOP LAYER OF SIMULINK ENGINE MODEL .....	92
FIGURE 4.2 SCHEMATIC OF VGT VANE AND ACTUATOR MECHANISM.....	92
FIGURE 4.3 SIMULINK IMPLEMENTATION OF VGT ACTUATOR AND VANE MODEL .....	93
FIGURE 4.4 DRIVE CYCLE CONTROLLER NON-LINEAR INTEGRAL PEDAL MAP	93
FIGURE 4.5 DETAIL OF SIMULINK DRIVER MODEL.....	94
FIGURE 4.6 STANDARD CONTROLLER SIMULINK IMPLEMENTATION .....	94
FIGURE 4.7 COMPLETE ENGINE AND SUBSYSTEM MODELS .....	95
FIGURE 4.8 VGT VANE RESPONSE, SIMULATED AND EXPERIMENTAL .....	95
FIGURE 4.9 COMPARISON OF SIMULATED AND EXPERIMENTAL ENGINE BEHAVIOUR FOR A LARGE FUEL STEP AT 1500 REV/MIN.....	96
FIGURE 4.10 COMPARISON OF SIMULATED AND EXPERIMENTAL ENGINE BEHAVIOUR FOR A LARGE FUEL STEP AT 2500 REV/MIN.....	97
FIGURE 4.11 COMPARISON OF SIMULATED AND EXPERIMENTAL ENGINE BEHAVIOUR FOR A LARGE FUEL STEP AT 3500 REV/MIN.....	98
FIGURE 4.12 SIMULATION VALIDATION OVER URBAN SECTION OF ECE DRIVE CYCLE, GENERAL PERFORMANCE COMPARISON .....	99
FIGURE 4.13 SIMULATION VALIDATION OVER URBAN SECTION OF ECE DRIVE CYCLE, EGR AND VGT SYSTEM BEHAVIOUR COMPARISON .....	100
FIGURE 4.14 SIMULATION VALIDATION OVER EXTRA-URBAN SECTION OF ECE DRIVE CYCLE, GENERAL PERFORMANCE COMPARISON .....	101
FIGURE 4.15 SIMULATION VALIDATION OVER EXTRA-URBAN SECTION OF ECE DRIVE CYCLE, EGR AND VGT SYSTEM BEHAVIOUR COMPARISON.....	102
FIGURE 5.1 2500 REV/MIN TIP-IN TRANSIENT .....	116
FIGURE 5.2 3500 REV/MIN TIP-IN TRANSIENT .....	117
FIGURE 5.3 VGT BOOST CONTROL LOOP SYSTEM DELAYS.....	118
FIGURE 5.4 TURBINE CHARACTERISTIC INDICATING CHOKING REGION .....	118
FIGURE 5.5 TURBINE CHARACTERISTIC WITH ACTUAL AND IDEAL TRANSIENT TRAJECTORIES.....	119
FIGURE 5.6 SCHEMATIC REPRESENTATION OF CONTROL STRATEGY .....	119
FIGURE 5.7 SIMULINK IMPLEMENTATION OF EXHAUST PRESSURE CONTROLLER.....	120
FIGURE 5.8 TRANSIENT DETECTION ROUTINE.....	120
FIGURE 5.9 SIMULATION OF THE EXHAUST PRESSURE CONTROLLER COMPARED WITH STANDARD CONTROLLER.....	121
FIGURE 5.10 ENGINE OPERATING CONDITIONS COVERED BY THE EXHAUST PRESSURE CONTROLLER .....	122
FIGURE 5.11 EXPERIMENTAL COMPARISON OF CONTROLLERS: ENGINE PERFORMANCE.....	122

FIGURE 5.12 EXPERIMENTAL COMPARISON OF CONTROLLERS: TURBOCHARGER AND ENGINE PRESSURE BEHAVIOUR .....	123
FIGURE 5.13 EXPERIMENTAL COMPARISON OF CONTROLLERS: VGT VANE POSITION AND CONTROLLER TERMS.....	123
FIGURE 5.14 TURBINE FLOW VERSUS PRESSURE RATIO .....	124
FIGURE 5.15 COMPARISON OF CONTROLLER PERFORMANCE AT DIFFERENT ENGINE SPEEDS: EXHAUST MANIFOLD PRESSURE.....	125
FIGURE 5.16 COMPARISON OF CONTROLLER PERFORMANCE AT DIFFERENT ENGINE SPEEDS: TURBOCHARGER SPEED .....	126
FIGURE 5.17 COMPARISON OF CONTROLLER PERFORMANCE AT DIFFERENT ENGINE SPEEDS: INLET MANIFOLD PRESSURE.....	127
FIGURE 5.18 COMPARISON OF CONTROLLER PERFORMANCE AT DIFFERENT ENGINE SPEEDS: VGT VANE POSITION.....	128
FIGURE 5.19 TURBINE PRESSURE RATIO VS. EXHAUST MANIFOLD PRESSURE	129
FIGURE 6.1 TYPICAL ARRANGEMENT OF A FUZZY FEEDBACK CONTROL SCHEME.....	148
FIGURE 6.2 SCHEMATIC REPRESENTATION OF CONTROLLER .....	148
FIGURE 6.3 MEMBERSHIP FUNCTIONS FOR FUZZY CONTROLLER INPUTS AND OUTPUTS .....	149
FIGURE 6.4 EXAMPLE OF FUZZY INFERENCE ENGINE .....	149
FIGURE 6.5 SIMULINK IMPLEMENTATION OF FUZZY CONTROLLER .....	150
FIGURE 6.6 EXPERIMENTAL EVALUATION OF FUZZY CONTROLLER.....	151
FIGURE 6.7 EXPERIMENTAL EVALUATION OF FUZZY CONTROLLER (FIXED 50 % OPEN-LOOP TERM).....	152
FIGURE 6.8 SCHEMATIC OF REVISED FUZZY CONTROLLER .....	153
FIGURE 6.9 SIMULINK IMPLEMENTATION OF REVISED FUZZY CONTROLLER	153
FIGURE 6.10 SIMULATED COMPARISON OF REVISED FUZZY CONTROLLER WITH STANDARD CONTROLLER OVER 1500 REV/MIN FUELLING PROFILE.....	154
FIGURE 6.11 DETAIL OF SIMULATED PERFORMANCE OF REVISED FUZZY CONTROLLER OVER 1500 REV/MIN FUEL PROFILE .....	155
FIGURE 7.1 COUPLING OF THE INDEPENDENT CONTROL LOOP OUTPUTS TO ACHIEVE COORDINATED CONTROL ACTION .....	168
FIGURE 7.2 COUPLING OF THE INDEPENDENT CONTROL LOOP INPUTS TO ACHIEVE COORDINATED CONTROL ACTION .....	168
FIGURE 7.3 INPUT MEMBERSHIP FUNCTIONS (ENGINE SPEED AND FUELLING DEMAND) .....	169
FIGURE 7.4 OUTPUT MEMBERSHIP FUNCTIONS (AIRFLOW ERROR TO VGT LOOP INPUT GAIN) .....	169
FIGURE 7.5 EXAMPLE OF FUZZY INFERENCE IN OPERATION IN THE LOW SPEED AND LOW LOAD ENGINE OPERATING RANGE .....	169
FIGURE 7.6 EXAMPLE OF FUZZY INFERENCE IN OPERATION IN THE TRANSITION REGION FROM LOW SPEED AND LOAD TO HIGH SPEED AND LOAD .....	170
FIGURE 7.7 SIMULINK IMPLEMENTATION OF CROSS-COUPLED CONTROLLER (ADDITIONAL ELEMENTS SHOWN IN RED) .....	170
FIGURE 7.8 SIMULATED FUEL STEP RESPONSE AT 1500REV/MIN (CUSTOM SETPOINTS AND FIXED OPEN-LOOP) .....	171
FIGURE 7.9 SIMULATED FUEL STEP RESPONSE AT 1500 REV/MIN (CUSTOM SETPOINTS AND ACTIVE OPEN-LOOP).....	172
FIGURE 7.10 TIP-IN 1 AIRFLOW AND BOOST TRACKING DETAILS .....	173
FIGURE 7.11 TIP-IN 1 PERFORMANCE DETAILS .....	173
FIGURE 7.12 TIP-IN 1 CONTROL DETAIL.....	174
FIGURE 7.13 TIP-IN 2 AIRFLOW AND BOOST PRESSURE TRACKING .....	174
FIGURE 7.14 TIP-IN 2 PERFORMANCE DETAIL .....	175
FIGURE 7.15 TIP-IN 2 CONTROL DETAIL.....	175

FIGURE 7.16 TIP-IN 3 AIRFLOW AND BOOST PRESSURE TRACKING .....	176
FIGURE 7.17 TIP-IN 3 PERFORMANCE DETAIL .....	176
FIGURE 7.18 TIP-IN 3 CONTROL DETAIL .....	177
FIGURE 7.19 TIP-OUT 1 AIRFLOW AND BOOST PRESSURE TRACKING .....	177
FIGURE 7.20 TIP-OUT 1 PERFORMANCE DETAIL .....	178
FIGURE 7.21 TIP-OUT 1 CONTROL DETAIL .....	178
FIGURE 7.22 TIP-OUT 2 AIRFLOW AND BOOST PRESSURE TRACKING .....	179
FIGURE 7.23 TIP-OUT 2 PERFORMANCE DETAIL .....	179
FIGURE 7.24 TIP-OUT 2 CONTROL DETAIL .....	180
FIGURE 8.1 RELATIONSHIP BETWEEN OXYGEN CONCENTRATION AND AIR FUEL RATIO (NO EGR PRESENT) .....	197
FIGURE 8.2 UEGO SENSOR OUTPUT CURVE .....	197
FIGURE 8.3 RELATIONSHIP BETWEEN AIR FUEL RATIO, EXHAUST OXYGEN CONCENTRATION AND EGR RATE .....	198
FIGURE 8.4 INSTALLATION DETAILS FOR UEGO SENSOR (EXHAUST SIDE ON VIEW OF ENGINE) .....	198
FIGURE 8.5 NOISE REDUCTION ON SENSOR OUTPUT .....	199
FIGURE 8.6 FREQUENCY CONTENT OF UEGO SENSOR SIGNAL FOR TRANSIENTS AT VARIOUS ENGINE SPEEDS .....	200
FIGURE 8.7 EXHAUST OXYGEN SENSOR RESPONSE TO A FUEL STEPS AT VARIOUS ENGINE SPEEDS .....	201
FIGURE 8.8 CONTOURS OF EXHAUST GAS OXYGEN CONCENTRATION [%] COMPARED TO FUELLING AND EGR RATE FOR FIXED TOTAL ENGINE GAS FLOW CONDITIONS .....	201
FIGURE 8.9 CONSTANT SPEED FUEL PROFILE PERFORMANCE FOR DIRECT REPLACEMENT OF MAF SENSOR WITH UEGO SENSOR .....	202
FIGURE 8.10 SIMULATED OXYGEN CONCENTRATION RESPONSE TO EGR, VGT AND FUEL CHANGES .....	203
FIGURE 8.11 FUELLING PROFILE RESPONSE FOR COORDINATED OXYGEN CONCENTRATION CONTROLLER .....	204
FIGURE 8.12 FORMULATION FOR A PREDICTIVE, OPTIMISATION-BASED APPROACH TO THE EXHAUST OXYGEN CONCENTRATION CONTROL PROBLEM .....	205
FIGURE 8.13 SCHEMATIC OF FEEDFORWARD AND FEEDBACK CONTROL SCHEME .....	205
FIGURE 8.14 FREQUENCY RESPONSE FOR FUEL TO OXYGEN CONCENTRATION MODELS AT VARIOUS NOMINAL FUEL LEVELS IN THE RANGE 5-20 MG/SHOT .....	206
FIGURE 8.15 STEP RESPONSES FOR FUEL TO OXYGEN CONCENTRATION MODELS AT VARIOUS NOMINAL FUEL LEVELS IN THE RANGE 5-20 MG/SHOT .....	206
FIGURE 8.16 SIMULINK IMPLEMENTATION OF OXYGEN CONCENTRATION DISTURBANCE PREDICTOR .....	207
FIGURE 8.17 DETAIL OF SIMULINK IMPLEMENTATION OF RECURSIVE ALGORITHM .....	207
FIGURE 8.18 PREDICTION PERFORMANCE OF FUEL TO OXYGEN CONCENTRATION MODEL FOR VARIOUS FUEL STEP CHANGES .....	208
FIGURE 8.19 COMPARISON OF OXYGEN CONCENTRATION TRACKING OVER FUEL STEP PROFILE FOR UEGO FEEDBACK CONTROL WITH MODEL-BASED FEEDFORWARD AGAINST FIXED FEEDFORWARD TERMS .....	209
FIGURE 8.20 COMPARISON OF OXYGEN CONCENTRATION TRACKING OVER FUEL STEP PROFILE FOR UEGO FEEDBACK CONTROL WITH MODEL-BASED FEEDFORWARD AGAINST FIXED FEEDFORWARD TERMS - DETAIL .....	210

FIGURE 8.21 COMPARISON OF OXYGEN CONCENTRATION TRACKING OVER FUEL RAMP PROFILE FOR UEGO FEEDBACK CONTROL WITH MODEL-BASED FEEDFORWARD AGAINST FIXED FEEDFORWARD TERMS .....	211
FIGURE 8.22 COMPARISON OF OXYGEN CONCENTRATION TRACKING OVER FUEL RAMP PROFILE FOR UEGO FEEDBACK CONTROL WITH MODEL-BASED FEEDFORWARD AGAINST FIXED FEEDFORWARD TERMS – DETAIL .....	212
FIGURE 9.1 NO <sub>x</sub> / SMOKE TRADE-OFF OVER URBAN (FIRST 200 SECONDS) SECTION OF DRIVE CYCLE .....	226
FIGURE 9.2 FUEL CONSUMPTION / NO <sub>x</sub> TRADE-OFF OVER URBAN SECTION OF CYCLE .....	226
FIGURE 9.3 EGR AND VGT POSITIONS OVER URBAN SECTION OF CYCLE FOR STANDARD CONTROLLER WITH NEW SETPOINTS .....	227
FIGURE 9.4 EGR AND VGT POSITIONS OVER URBAN SECTION OF CYCLE FOR COORDINATED CONTROLLER WITH NEW SETPOINTS.....	227
FIGURE 9.5 OPERATING ENVELOPE FOR COORDINATED CONTROLLER OVER URBAN SECTION OF CYCLE .....	228
FIGURE 9.6 AIRFLOW VS BOOST TRACKING ERROR COMPARISON FOR STANDARD AND COORDINATED CONTROLLERS OVER URBAN SECTION OF CYCLE .....	228
FIGURE 9.7 ENGINE COOLANT TEMPERATURE OVER EXTRA-URBAN SECTION OF CYCLE, ILLUSTRATING THE 2 INSTANCES WHERE COOLANT TEMPERATURE DROPPED DURING THE TEST .....	229
FIGURE 9.8 NO <sub>x</sub> / SMOKE TRADE-OFF OVER EUDC SECTION OF DRIVE CYCLE	229
FIGURE 9.9 NO <sub>x</sub> / FUEL CONSUMPTION TRADE-OFF OVER EUDC SECTION OF CYCLE .....	230
FIGURE 9.10 EGR AND VGT POSITIONS OVER EXTRA-URBAN SECTION FOR THE DIFFERENT CONTROLLERS .....	230
FIGURE 9.11 USE OF COORDINATED ACTION FOR COORDINATED CONTROLLER OVER EXTRA-URBAN SECTION OF CYCLE.....	231
FIGURE 9.12 AIRFLOW VS. BOOST TRACKING ERROR COMPARISON FOR STANDARD AND COORDINATED CONTROLLER OVER EUDC SECTION OF CYCLE .....	231
FIGURE 9.13 TRANSIENT EVENTS AND COORDINATED ACTION OVER URBAN SECTION OF CYCLE .....	232
FIGURE 9.14 AIRFLOW TRACKING AND EGR VGT POSITION DETAIL FOR COORDINATED CONTROLLER OVER URBAN SECTION OF CYCLE .....	232
FIGURE 9.15 AIRFLOW TRACKING AND EGR VGT POSITION DETAIL FOR STANDARD CONTROLLER OVER URBAN SECTION OF CYCLE .....	233
FIGURE 9.16 AIRFLOW TRACKING AND EGR VGT POSITION DETAIL FOR COORDINATED CONTROLLER WITH FIXED 50% OPEN-LOOP TERM OVER URBAN SECTION OF CYCLE .....	233
FIGURE 9.17 EMISSIONS COMPARISON OF STANDARD AND COORDINATED CONTROLLERS OVER URBAN SECTION OF CYCLE .....	234
FIGURE 9.18 TRANSIENT EVENTS AND COORDINATED ACTION OVER EXTRA-URBAN SECTION OF CYCLE .....	234
FIGURE 9.19 AIRFLOW TRACKING AND EGR VGT POSITION DETAIL FOR COORDINATED CONTROLLER OVER EXTRA-URBAN SECTION OF CYCLE	235
FIGURE 9.20 AIRFLOW TRACKING AND EGR VGT POSITION DETAIL FOR STANDARD CONTROLLER OVER EXTRA-URBAN SECTION OF CYCLE.....	235
FIGURE 9.21 AIRFLOW TRACKING AND EGR VGT POSITION DETAIL FOR COORDINATED CONTROLLER WITH FIXED 50% OPEN-LOOP TERM OVER EXTRA-URBAN SECTION OF CYCLE.....	236
FIGURE 9.22 EMISSIONS COMPARISON OF STANDARD AND COORDINATED CONTROLLERS OVER EXTRA-URBAN SECTION OF CYCLE .....	236

FIGURE 9.23 EMISSIONS COMPARISON OF COORDINATED CONTROLLER WITH  
FIXED AND ACTIVE OPEN-LOOP TERM OVER EXTRA-URBAN SECTION OF  
CYCLE ..... 237

FIGURE 9.24 EXHAUST OXYGEN TRACKING AND EGR VGT POSITION DETAIL  
FOR UEGO CONTROLLER OVER EXTRA-URBAN SECTION OF CYCLE..... 237

FIGURE 9.25 EMISSIONS COMPARISON OF UEGO CONTROLLER OVER EXTRA-  
URBAN SECTION OF CYCLE ..... 238



## Abbreviations & Nomenclature

AFR	- Air to Fuel Ratio
BMEP	- Brake Mean Effective Pressure
BSFC	- Brake Specific Fuel Consumption
CAN	- Control Area Network
CCP	- CAN Calibration Protocol
CO	- Carbon Monoxide
CO <sub>2</sub>	- Carbon Dioxide
CVT	- Continuously Variable Transmission
DC	- Direct Current
DSP	- Digital Signal Processor
ECU	- Engine Control Unit
EEPROM	- Electronically Erasable Programmable Read Only Memory
EGO	- Exhaust Gas Oxygen (sensor)
EGR	- Exhaust Gas Recirculation
EUDC	- Extra Urban Drive Cycle
EVR	- Electronic Vacuum Regulator
FGT	- Fixed Geometry Turbocharger
FID	- Flame Ionisation Detector
GPC	- General Predictive Control
HC	- Hydrocarbons
HSDI	- High Speed Direct Injection (Diesel Engine)
I/O	- Input / Output
LTC	- Limiting Torque Curve
MAF	- Mass Air Flow
MAP	- Manifold Absolute Pressure
MIMO	- Multiple Input Multiple Output
NO <sub>x</sub>	- Oxides of Nitrogen
NVH	- Noise, Vibration and Harshness
OBD	- On Board Diagnostics
PC	- Personal Computer
PD	- Proportional Derivative
PI	- Proportional Integral
PID	- Proportional Integral Derivative
PM	- Particulate Matter

PWM	- Pulse Width Modulation
SISO	- Single Input Single Output
TDC	- Top Dead Centre
UEGO	- Universal Exhaust Gas Oxygen (sensor)
VGT	- Variable Geometry Turbocharger

**For all equations presented in this work:**

$A$	- Area
$c_p$	- Specific Heat Capacity (Constant pressure)
$D$	- Distance
$F$	- Fraction
$J$	- Rotational Inertia
$k$	- Coefficient
$m$	- Mass
$N$	- Rotational Speed
$n$	- Number of
$p$	- Pressure
$Q$	- Heat energy
$R$	- Universal Gas Constant
$t$	- Time
$T$	- Temperature
$Tq$	- Torque
$V$	- Volume
$W$	- Mass Flow
$x$	- Position
$X$	- Concentration
$z$	- Delay operator
$\eta$	- Efficiency
$\rho$	- Density

**Subscripts:**

$a$	- Air
$act$	- Actuator
$aero$	- Aerodynamic
$amb$	- Ambient Conditions
$b$	- Burnt Gas
$c$	- Compressor
$e$	- Engine Cylinders
$eff$	- Effective
$EGR$	- EGR valve
$eng$	- Engine
$f$	- Fuel
$i$	- Inlet Manifold
$mech$	- Mechanical
$O_2$	- Oxygen
$stoich$	- Stoichiometric
$t$	- Turbine
$vac$	- Vacuum
$vol$	- Volumetric

$x$  - Exhaust Manifold

All other subscripts used are self-explanatory.

Where several subscripts appear together, this represents a transition from the condition described by the first subscript to that defined by the second. Where subscripts are used to indicate transitions for variables where a subscript is already employed (e.g. to denote a property) then an underscore is used to separate the subscripts.

For example:

$W_{a\_ie}$  describes the mass flow ( $W$ ) of air ( $a$ ) from inlet manifold ( $i$ ) to the Cylinders ( $e$ )

# Chapter 1 INTRODUCTION

## 1.1 BACKGROUND

In recent years the Diesel engine has become considerably more common as the choice of powerplant in passenger vehicles, to the extent that now even luxury automobile manufacturers offer Diesel engines across their vehicle range. Increasing environmental awareness on the part of society through concerns about pollution, climate change and depletion of natural resources has led to pressure to develop more and more efficient solutions to our transportation needs.

The compression ignition Diesel engine has adapted well to this new environment; compared with the spark ignition gasoline engine, its inherently higher efficiency and the accompanying fuel economy advantages give it a better starting position. Advances in automotive technology such as the widespread adoption of electronic control and new emissions and performance enhancing devices have allowed Diesel engines to evolve into powerful, flexible, efficient and clean automotive prime movers. This trend looks set to continue. With realistic zero emissions vehicles still several years from mass production, the Diesel market share will continue to grow and new applications such as hybrid powertrains will ensure continued interest in engine development.

Against this optimistic background for Diesel engine development, ever stricter emissions regulations pose considerable challenges for Diesel engineers. The real challenge is to develop systems that meet these stringent regulations whilst being cost-effective enough for mass-production. No single innovation will solve these development issues, rather a combination of improvements to engine, powertrain and vehicle design, combustion control, exhaust aftertreatment and powertrain control will be required.

Key engine technologies that have led to significant emissions and performance improvements are electronically controlled Exhaust Gas Recirculation and turbocharging. However, the extra degrees of freedom introduced by these systems have increased the complexity and hence cost of engine electronic controls. Due to the expensive nature of transient testing and advanced control system development, these new systems have been applied to the engine using a combination of well-established classical control techniques and steady state mapping programs, which although time consuming are less complex when considered against the development of full transient control.

The steady state engine behaviour is now well optimised to the extent that very little performance improvement can be extracted from further steady state optimisation. The

development emphasis is therefore on how the system behaves as it moves between these steady states.

Very little real life driving is steady state; even the seemingly constant motorway cruising conditions are permeated with small variations in speed, load and temperature for example. Transient emissions form a significant contribution to the totals in the legislative emissions tests [1] and the deviation of transient emissions from steady state values is also considerable [2].

## **1.2 OBJECTIVES**

The research presented in this thesis aims to address the issue of transient optimisation of Diesel engine turbocharging and exhaust gas recirculation through the conception of new control strategies for these systems. Improvements to emissions, fuel consumption and control system performance are sought that remain feasible within the framework of the mass produced vehicle market and the limitations to control system complexity and calibration effort that this imposes.

## **1.3 RESEARCH METHODOLOGY AND THESIS OUTLINE**

The arrangement of this thesis documents the procedure used to arrive at a set of solutions to the engine control problem that has been outlined. An extensive literature survey is given in Chapter 2 which presents the necessary background on Diesel engine combustion, emissions and performance. The concept of electronic control is introduced and a detailed review of the published work on the control of Exhaust Gas Recirculation and turbocharging is given. A variety of control techniques that may be applicable in the course of this research are also introduced. The important factors that must be considered when designing an Exhaust Gas Recirculation / turbocharging controller are also discussed.

An important aspect in the design of control strategies is a thorough understanding of the nature and behaviour of the plant to be controlled. Chapter 3 presents and discusses the results of the engine test program undertaken using the transient engine dynamometer facility. The engine is characterised in steady state and transiently, and key interactions and control issues are identified.

Computer power has increased greatly in recent years, as has the availability of flexible, easy to use simulation and analysis packages for dynamic systems. Therefore, computer modelling is now used extensively as a tool for control system design, allowing rapid development and testing of new systems in a safe environment, as well as the exploration of many areas that may not be feasible by empirical research. A dynamic engine model was provided for this

study, Chapter 4 describes the model and describes additional elements that have been generated to improve the accuracy and utility of the basic model. A validation is performed and the suitability of the model for control system design is discussed.

The first new control scheme to be developed is described in Chapter 5, it is designed to address certain generic deficiencies in the transient control of VGT systems. The presented control scheme shows performance improvements in simulation that are then confirmed through experimental application of the strategy to the test bed engine.

In Chapter 6 the concept of co-ordinated control of the EGR and VGT systems is developed and a fuzzy logic control scheme proposed. Initial test bed experiments highlight difficulties involved in the use of such a method, but further iterations in simulation show improvements in transient airflow behaviour.

The control scheme devised in Chapter 6 incurs large computational penalties due to the use of a fuzzy inference system to generate the control law. In Chapter 7 an alternative method of obtaining co-ordinated control is demonstrated, making use of the existing engine feedback control schemes and a very simple fuzzy logic system to co-ordinate the action of the independent EGR and VGT control loops. The new system is demonstrated in simulation then implemented on the test bed engine, improvements to transient airflow are shown.

An investigation into the use of oxygen feedback as a parameter to allow better, more accurate control of the EGR-VGT system is given in Chapter 8. Sensor installation and information processing are discussed and simple feedback controllers are implemented using similar techniques to those developed in previous chapters. Experimental results show the inherent difficulty in using feedback compensation schemes for such a system, and a model-based feedforward strategy is developed in simulation and shown to improve the oxygen sensor-based system performance.

All the control schemes shown here have been developed using test schedules that apply fuelling transients at constant engine speed, this is because fuelling is the fastest external disturbance to which the EGR-VGT systems must respond to. In Chapter 10, the co-ordinated and oxygen feedback control schemes are evaluated using the legislative drive cycle on the transient test bed, the performance of the new systems is contrasted against that of the existing control strategy for emissions and fuel consumption.

The final chapter outlines what has been achieved by this work and discusses to what extent the objectives have been met. The thesis is concluded by a brief description of further work that could be performed in the wake of this research.

## **Chapter 2 BACKGROUND AND LITERATURE REVIEW**

This chapter provides an introduction to important aspects of Diesel engine combustion, emissions and performance. Electronic engine control is introduced and discussed further under the context of Exhaust Gas Recirculation and Variable Geometry Turbocharging control. An extensive literature review of relevant research into this control problem is given followed by a discussion of the performance requirements of an EGR-VGT control system .

### **2.1 BACKGROUND**

#### **2.1.1 DIESEL ENGINE**

A schematic representation of a typical modern high speed direct injection Diesel engine is shown in **Figure 2.1**. Fresh air enters the turbocharger compressor where its density is increased. The compressed air then flows from the compressor to the inlet manifold; usually a charge air cooler (not shown here) is used to remove some of the heat added due to the non-isentropic nature of the compression process.

The air in the inlet manifold mixes with exhaust gases that arrive via the Exhaust Gas Recirculation (EGR) valve; this mixture then flows into the combustion chamber when the inlet valve opens. Fuel is added to the mixture via a high pressure injector nozzle located within the combustion chamber and the exhaust gases resulting from combustion leave the chamber through the exhaust port into the exhaust manifold.

From the exhaust manifold, a portion of the gases flows back to the inlet via the EGR valve; often a heat exchanger is used to reduce the EGR temperature and the remainder of the gases expand through the Variable Geometry Turbocharger (VGT) turbine. The turbine extracts energy from the gases and transfers this energy mechanically to the compressor via the turbocharger shaft. The compressor uses this energy to increase the incoming air density.

#### **2.1.2 DIESEL COMBUSTION**

The Diesel combustion process is illustrated on a crank angle versus cylinder pressure diagram in **Figure 2.2**. This diagram illustrates the in-cylinder pressure over the middle section of the four-stroke cycle, from just before inlet valve closure after the induction stroke to just after exhaust valve opening at the end of the expansion stroke. The piston rises and compresses the air charge in the cylinder resulting in the increase in pressure shown by the blue line. If no fuel were injected the cylinder pressure would follow the behaviour shown by this line all the way to bottom centre at the right of the figure; this is the unfired cycle

pressure trace. In the fired cycle, fuel is injected into the combustion chamber several degrees before the piston reaches top dead centre (TDC); the liquid fuel jet atomises and is entrained by the rapid movements within the air charge. The compression process heats the air charge considerably and the fuel vaporises and mixes with the air. Where the mixture reaches combustible limits for the fuel being used, *autoignition* occurs due to the air temperature and pressure. This happens within a few degrees crank angle and is known as the *premixed combustion*, the cylinder pressure rises sharply during this phase. The duration between the *start of injection* and the *autoignition* (or *start of combustion*) is known as the *delay period*. The combustion process propagates to other areas where the local air fuel mixture is within combustible limits; this is the *mixing-controlled combustion* phase. As mixing of air, fuel and burnt gases continues into the expansion stroke, so does the *mixing-controlled* combustion [3].

The Diesel combustion process is limited by oxygen availability; upper limits for fuel injection quantities will be chosen depending on the levels of smoke that are produced when in-cylinder oxygen availability is low; this limits the torque output for a given engine speed. Diesel engine speeds are also limited by the combustion process to around 5000 rev/min; this is determined by the minimum time required for complete combustion.

### 2.1.3 DIESEL ENGINE EXHAUST EMISSIONS

The principal exhaust emissions species of concern for Diesel engines are oxides of nitrogen ( $\text{NO}_x$ ), unburned hydrocarbons (uHC or HC) and particulate matter (PM) [4]. Carbon monoxide (CO) is not usually considered a problem for Diesel engines as the combustion conditions are predominantly lean. Carbon Dioxide emissions are often monitored due to concerns over the greenhouse effect; Carbon Dioxide production is directly related to fuel consumption.

$\text{NO}_x$  and HC react in the presence of sunlight in the atmosphere to form a dangerous photochemical smog that has choked many cities around the world. This is why up until recently emissions regulations have specified combined total emissions limits for  $\text{NO}_x$  and HC [5].

Particulate Matter describes a host of fine particles made up of agglomerated and soluble organic fractions, sulphur-based and carbon-based compounds. These particles are thought to carry carcinogenic material deep into the lung tissue [6] and are a particular problem for Diesel combustion.

Diesel  $\text{NO}_x$  emissions result from the oxidation of atmospheric nitrogen during combustion, a process described by the Zeldovich Mechanism [7].  $\text{NO}_x$  formation shows a strong



dependence on high temperatures, oxygen concentration and residence times; unfortunately these factors are characteristic of the Diesel combustion process.

Diesel exhaust hydrocarbon emissions generally derive from fuel that was either locally in too rich or too lean a mixture to combust and was not subsequently consumed in the slow thermal oxidation reactions that occur during the expansion [8]. Thus incomplete mixing or quenching of the oxidation process is the significant source of HC emission, this can occur from impingement of the fuel spray onto the cylinder wall as discussed in [9].

Particulates originate mainly from the incomplete combustion of Diesel fuel. Particle formation is followed by an agglomeration phase where the particle grows in size by 'soaking-up' compounds and coagulating with other particles [10]. The particles can be oxidised to form gaseous products at any point in these two phases, therefore the actual quantity of particulates in the Diesel exhaust will depend on the balance between formation and oxidation processes during the expansion [11].

## **2.2 EXHAUST GAS RECIRCULATION**

EGR is a well-established technique for reducing engine NO<sub>x</sub> emissions [12]. A fraction of the exhaust gas is fed into the inlet manifold to mix with the incoming fresh air. Anything up to 50% of the intake air can be substituted with exhaust gas, depending on the engine operating point, but EGR is applied predominantly at part-load due to oxygen availability in the exhaust. The EGR flow rate is regulated by a valve as illustrated in **Figure 2.1**. The flow is a function of the EGR valve position, the pressure difference between inlet and outlet manifolds and the upstream (exhaust) conditions.

**Ladommatos et al [13,14,15]** have shown through experimental investigation that EGR works by reducing the combustion flame temperature, heat release rate and oxygen concentration - the critical factors in NO<sub>x</sub> formation. This is achieved by reducing oxygen availability in the inlet charge (the *dilution effect*), increasing the specific heat capacity of the charge (the *thermal effect*) and through the dissociation of CO<sub>2</sub> (the *chemical effect*). The dominant effect is that of reduced oxygen availability.

The adverse effects of EGR include increases in other emissions. The reduction in oxygen availability leads to less soot oxidation in the latter part of the Diesel combustion process which will increase soot and PM [16]. CO, HC and Brake Specific Fuel Consumption (BSFC) will also increase with increasing EGR. Application of EGR can also increase engine wear and erosion, particularly in heavy-duty Diesel engines, and fouling of the EGR valve itself can create emissions and driveability problems.

## **2.3 VARIABLE GEOMETRY TURBOCHARGER**

Turbocharging provides a method of increasing the power output from a Diesel engine without increasing its size. The excess energy of the exhaust gases is harnessed via a turbine to drive a compressor that increases inlet air charge density. Increasing the charge air density means that more fuel can be combusted for a given cylinder displacement and hence more power developed from the engine [17].

The variable geometry turbocharger (VGT) has an adjustable nozzle that guides exhaust gas onto the turbine. Two different variable geometry turbines are illustrated in **Figure 2.3**, the swivelling vane and sliding sheath arrangements. The speed of the exhaust flow and the angle at which it impinges on the turbine blades determine the energy transfer from the gases to the turbine. At low exhaust flows the geometry can be adjusted to maximise energy transfer to the turbine, whilst at high flows the geometry can be set to limit energy transfer to the turbine to prevent excessive inlet and exhaust manifold pressures. The VGT supersedes the Fixed Geometry Turbocharger (FGT) which uses a turbine bypass valve (a wastegate) to limit the manifold pressures. The greatest benefit gained from a VGT is the ability to optimise the inlet manifold pressure over a wide speed range in comparison with an FGT, a detailed treatment of the VGT is given by **Hawley et al** in [18]

Very little has been published about the use of VGT as an emissions reduction device other than its effect on smoke. However, at low speed and high load the higher AFR available can reduce smoke and PM; at cold start increased backpressure can be used to reduce HC and at high speed/light load conditions the boost and temperature can be used to reduce ignition delay [19]. The strong effect of VGT vane position on exhaust manifold pressure can also be used to increase EGR flow rates.

## **2.4 ELECTRONIC ENGINE CONTROL**

The first applications of electronic engine control were for fuel injection timing in spark ignition engines. Since then, electronics have gradually taken over most of the regulating functions of both spark and compression ignition engines to the point where now the mechanical linkage from the accelerator pedal to the engine has been replaced with so-called 'drive-by-wire' systems.

The microprocessors for engine control (often referred to as ECU – Engine Control Unit) have steadily grown in performance to cope with the increase in electronic engine systems, however, many are still based on 16-bit fixed-point arithmetic which does limit the complexity of control strategy that can be used and incurs significant amounts of time and

specialist resources in programming and calibrating. Systems are now becoming available with floating-point processors that offer much more power and functionality but at increased hardware cost and power consumption.

### 2.4.1 EGR AND VGT CONTROL

Although EGR and VGT systems are coupled by virtue of the exhaust manifold, the trend for in-production control strategies is to control each device with an independent loop. A schematic representation of this is shown in **Figure 2.4**.

The EGR uses mapped steady state values of compressor mass airflow (MAF) to generate PWM duty cycle commands for the EGR valve actuator. These targets or setpoints are scheduled according to engine speed and fuel quantity: the measured mass airflow is compared with the setpoint and the resultant error passed to a Proportional plus Integral (PI) compensation scheme, which calculates a command for the EGR actuator based on this error. This output is added to a feed forward term of the nominal actuator duty cycles, again from steady state mapping data and the total output sent to the EGR valve driver. To account for the strong non-linear nature of the airflow to EGR valve position relationship with engine operating point, the controller gains are scheduled with speed and load.

This approach controls the amount of airflow entering the inlet manifold and eventually the cylinders, ideally inducing enough fresh air for good combustion quality with the remainder of the charge being made up of EGR. Increasing the EGR valve position will allow more EGR flow and hence reduce fresh airflow into the engine. Most systems will shut the EGR valve during any large changes in demanded fuelling [20], such as can occur during acceleration, gearshifts and load changes. The principal aim of the system under such manoeuvres is to reduce the amount of exhaust gas residuals in the inlet charge as quickly as possible to prevent poor combustion quality.

The VGT is controlled in a similar manner: a steady state map of inlet manifold boost pressure (MAP) against speed and fuelling is used to generate setpoints for the VGT controller. The difference between measured and target boost pressure is fed to a PI compensator to generate a PWM duty cycle demand to the VGT vane actuator. This is added to a feedforward term of the nominal actuator duty cycle, scheduled with engine speed and fuelling. As was the case for the EGR system, the controller gains are scheduled with speed and fuel to accommodate the non-linear response of inlet pressure to vane position with engine operating point. The manifold pressure sensor response time can have significant effects on the overall dynamic response of the control system [21].

This control scheme is widely adopted because PI control is well understood by engineers and is very easy to implement using basic hardware, the calibration can be easily interpreted and directly related to the physical system. Although the aforementioned control scheme is common for production EGR-VGT engine, much research into improved control strategies (in terms of performance, complexity and calibration) has been performed, these are described in the following sections.

## **2.5 Alternative EGR Control Strategies**

**Itoyama et al [22]** describe a model based EGR controller where the intake and exhaust systems are dynamically modelled in order to estimate pressures in both manifolds. With knowledge of EGR valve position, an accurate estimate of EGR flow rate can be made which in turn can be used to control the valve. They also illustrate that as the pressure difference between the inlet and exhaust manifold reduces, the sensitivity of EGR flow to this pressure difference increases, making accurate EGR control difficult.

**Amstutz et al [23]** have developed and tested a feedback controller for EGR using an exhaust gas oxygen (EGO) sensor combined with a model-based robust control system. The system controls the air fuel ratio to a fixed value, though the choice of set point has a significant influence on NO<sub>x</sub> and PM emissions. The controller design is based on linearised system models and the fuel injection is treated as a disturbance to the plant to be rejected by the EGR system. The strategy is compared to the performance of the engine with no EGR over part of transient test cycle (see **Figure 2.5**), therefore it is hard to determine if the NO<sub>x</sub> reduction is any better than an airflow- based feedback control scheme. The dynamics of the oxygen sensor are cited as being of particular importance in the performance of the control system. Transient EGR performance can be better managed using a parameter that relates directly to the combustion conditions. Additionally, oxygen sensor technology has progressed a great deal since, offering good potential for further research.

**Olbrot et al [24]** use a windowing technique to identify nine linear models of the EGR system across the engine load and speed range from on-engine perturbation experiments. The models allow the non-linear EGR valve response to be approximated as a first order lag with variable delay, gain and time constant. Robust PI controllers are designed for the nine operating points using the models and linear interpolation is used to schedule the parameters of the controllers between the operating points where the models were identified. This methodology facilitates robust controllers and rapid calibration.

## 2.6 Alternative VGT Control Strategies

The transient response of the turbocharger is critical to the vehicle feel or driveability as well as emissions and fuel consumption. As a result, much research has been performed on the dynamic control aspects of the VGT. Small changes in load can be dealt with adequately by conventional feedback controllers such as the standard strategy, but the large load transients often experienced by HSDI Diesel engines can cause control problems.

The feedback path from manifold pressure to VGT vane position includes delays and non-linearities that make control by classical linear methods (such as PID control) difficult. The response of the vanes to actuator control demands can be non-linear due to aerodynamic effects acting on the vanes themselves. **Walker [25]** quantifies this effect using strain gauge measurements of the actuation force required to move the turbocharger vane mechanism. As can be seen in **Figure 2.6** there is actually a reversal in the force acting on the vanes. The significant hysteresis levels present in the mechanism are also identified in this work.

**Moraal et al [26]** describe a more detailed study where the actuator and electronic vacuum regulator (EVR) are analysed and models are identified. The presented model has two states, both pressures, and represents the actuator behaviour well. The system displays different response times depending on which direction it is travelling. This is due to the spring return mechanism that guarantees the VGT to fail-safe (i.e. open); this is also identified in the experimental characterisation performed by **Brace et al [27]**.

**Jain [28]** identifies two transient load conditions for the Diesel engine: 'power transients' where there is a sudden increase in load such as encountering a hill or an overtaking manoeuvre and 'gearshift transients', where a rapidly increasing load is momentarily interrupted whilst the gearshift occurs. In both cases oscillatory VGT behaviour can result, to combat this an anticipation function is used to generate a feedforward demand for the VGT vanes which is added to the feedback control signal. The feedforward term is based on the rate of change of pedal position. During rapid increases the vanes are closed further than by the feedback controller alone; during gearshifts they are held in the current position for a delay period proportional to the rate of decrease in load.

**Arcoumanis et al [29]** examined various simple control strategies on an engine simulation, such as opening the vane position with increasing engine speed or fuelling demand. It was found that controllers which give a good transient response hold the turbine flow area at a minimum over the low speed/low load operating range. This does compromise the steady state part-load fuel consumption because the exhaust backpressure is higher.

**Pilley et al [30]** detail a systematic approach to transient VGT control strategy design and implementation for heavy-duty Diesel engines. System identification techniques are applied

in order to generate linear models of the engine at various operating points. Variables that normally cannot be measured on-line can be modelled and included in the control strategy providing their behaviour does not change with age. Using the techniques of General Predictive Control (GPC), dynamic models are used in a predictive manner to assess how the system will respond to changes in the control inputs. Appropriate control action is then calculated from the minimisation of a cost function (i.e. lowest fuel consumption or HC emissions). This method also supports the simultaneous control of more than one output, allowing interactive systems to be better controlled. The controller gave significant reductions in HC's, smoke and particulates over a transient cycle but with a slight fuel economy penalty. No detail is given on the complexity of implementation; optimisation routines need to be performed on-line in order to minimise the cost functions, therefore the processor requirements are likely to be significant. Additionally, the quality of the control action will depend greatly on the quality of the models used.

**Dekker et al [31]** use a simulation environment to design a simple VGT controller that discriminates between large and small changes in boost pressure demand and applies different controllers accordingly. **Buratti et al [32]** describe a boost control strategy for VGT that uses two different controllers for different operating conditions. A Proportional plus Integral (PI) controller is employed for “steady state” operation, while a Proportional plus Derivative (PD) controller is used under transient conditions, switching is governed by the rate of change of boost pressure. Transient control is performed when the rate of change of boost pressure exceeds a predefined limit. The results of using this control strategy are shown as greatly improving the response to step changes in acceleration.

In [33] **Fredriksson** develops a non-linear VGT engine model and applies a non-linear methodology to synthesise a controller. This “backstepping” method has the benefit of retaining the physical interpretation of the parameters in the model, and because of the non-linear nature of the process, a non-linear control technique should perform better. The technique is used to design an engine speed controller and an air fuel ratio controller via command of VGT and fuel injection using a much simplified version of the original model. A control function is derived but is found to be rather aggressive with respect to the VGT control, resulting in large overshoots in boost response. Although these and other issues, such as the error present in torque estimation (an observer can be used to correct the estimate) are addressed, in general the resultant controller is complex and ultimately appears to give similar responses to other, more simple control approaches. Also, this work is performed in simulation with perfect signals, access to all parameters and large computational headroom; an on-engine implementation may be difficult in practice. Again, the control performance will depend on accuracy of the model employed.

## **2.7 Coordinated EGR and VGT control strategies**

In recent years, several works have been published (predominantly from the same source) on the coordinated control of EGR and VGT systems for improved performance. Due to the fact that both the EGR and VGT systems are driven by exhaust gas, it is not surprising that a strong coupling exists between them, or that exploiting this coupling will lead to improved performance.

In [34] **Kolmanovsky et al** describe a non-linear engine model and subsequently use it to analyse the plant behaviour. It is demonstrated that in the low load and low speed operating region, co-ordination between EGR and VGT systems will yield faster fresh air flow dynamics than by modulation of the EGR valve alone. This is shown to be due to the strong coupling of EGR and VGT systems. It is also shown that as the engine operating point moves towards higher speeds and higher fuelling levels, the dominance of the coupling reduces and the devices can be controlled independently, justifying the independent loop controllers commonly applied to this system.

The work presented by **Van Nieuwstadt et al** in [35] is from the same group and continues from [34], using the model with an H-infinity control design method. This is a frequency-based design technique that effectively allows specification of the system frequency response. The tracking error and actuator effort frequency functions can be defined: for instance, tracking error can be specified as having high gain at low frequency for good tracking, and low gain at high frequency for good noise rejection. The technique is a branch of Optimal Control and requires linear plant models which are derived from the non-linear model at various operating points where local controllers are to be designed. The procedure is used to design two controllers: one a multivariable PI controller from EGR and VGT to airflow and boost, the other a twin SISO system from EGR to airflow and VGT to boost. The comparative results from simulation and test bed indicate that the coordinated controller can increase the airflow response to a tip-in at the cost of boost response for low load and speed operation (see **Figure 2.7**). The development effort and computational demands for such a controller are not discussed, however they are unlikely to be favourable.

**Van Nieuwstadt et al** continue the EGR VGT control strategy research in [36,37]. These papers describe the application and evaluation of five different EGR-VGT control strategies on a test bed engine over the EUDC section of the drive cycle. Several of the controllers make use of additional sensors or estimation schemes for control parameters. Interestingly, the choice of setpoints is cited as being more important in terms of engine performance than the feedback scheme used to attain them, as emissions, fuel consumption and driveability are directly affected by this choice.

Only two of the controllers described employ coordinated EGR VGT action. One achieves this using a single integrator design to generate position demands for the EGR and VGT actuators, necessitating inner closed-loop controllers on actuator position, which in itself is a non-trivial task. The weighted sum of airflow and boost errors is fed into a single PI controller, the output is distributed to the EGR and VGT position loops according to output weightings. Although the setpoints are designed for maximum inlet burnt gas fraction (low  $\text{NO}_x$ ) with an Air Fuel Ratio constraint, these constraints can be violated because the controller tracks a linear combination of airflow and boost, as opposed to individual tracking. This also makes dynamometer calibration more difficult. The use of only one compensator does however allow simple co-ordination of the EGR and VGT actions, depending on the choice of the weightings.

The other coordinated controller is derived from a control Lyapunov function with certain simplifications to aid stability and robustness -a more detailed treatment of the derivation of this controller is given by **Jankovic and Kolmanovsky** in [38]. Although this is a non-linear control technique, all non-linear gains are approximated with constant gains and gains on the boost pressure error have been zeroed. The resultant controller is a multivariable, linear proportional controller from airflow and exhaust manifold pressure to EGR and VGT *flow*. The output values of flow demand are converted to actuator position demands using orifice flow equations and measurements/estimations of conditions either side of the valves. These are then attained with inner position control loops. There is no integral action, and the strategy requires turbine and EGR flow models.

The drive cycle results for the different controllers tested are summarised on a  $\text{NO}_x$  / Particulates trade-off graph (see **Figure 2.8**). The results show the effect of the different controllers was to shift the emissions to a new point on the trade-off, i.e. more particulates and less  $\text{NO}_x$ , consistent with higher EGR, though this is much more to do with the choice of setpoint than control scheme.

**Walker [25]** describes another study of EGR VGT control, this time focusing on the interactive behaviour of the system. Linear analysis is performed locally on a non-linear engine model to study the relationship between EGR and VGT to airflow and boost. As in [34] the cross-coupled nature between EGR and VGT inputs to airflow and boost outputs is illustrated, the linearised models are used to design a 'diagonalising pre-compensator' allowing standard SISO frequency domain design techniques to be applied to each individual loop (EGR to airflow and VGT to boost pressure). The resultant controller compensates the VGT loop for any changes made to the EGR loop and vice versa. The scheme does not attempt to address the improvements in airflow response offered by coordinated control.



An interesting idea is proposed for switchable calibrations, addressing the fact that actual vehicles are driven in different ways by different people, and there are times when the driver will be driving economically, and times when they will be driving more aggressively. It is impossible to optimise the engine controls for all these conditions simultaneously, but it makes a great deal of sense to provide different calibrations (e.g. economy, sport, motorway cruise etc.) and some logic to decide which calibration to apply. The proposed scheme looks at pedal position history and engine speed to determine what driving style is being used and selects between sport and economy calibrations accordingly. However, the scheme is not implemented.

**Moynihan [39]** presents a comprehensive study of robust Diesel engine control in a generic framework. A non-linear engine model is again used as the basis of this work: a control scheme based on robust control design techniques is motivated using Air Fuel Ratio and inlet manifold burnt gas fraction as control parameters for the engine. These are cited as being more suitable than airflow and boost from a controllability point of view. These signals are recreated using a non-linear sliding mode observer, and H-infinity loop-shaping is used to design single point multivariable linear controllers. The proposed scheme uses additional pressure sensing (exhaust) and torque measurements, limiting the practicality of this simulation-based investigation under current industry conditions. Although the non-linearities of integrator wind-up and smoke-limited fuelling are addressed in this work, the highly non-linear behaviour of the actuation mechanism is ignored. An EGR throttle is also motivated in this control scheme to improve control over the EGR rate.

**Porter et al [40]** describe a model-based EGR-VGT control strategy that uses a transient detection based on fuelling to trigger transient EGR control using an Air Fuel Ratio estimate. Manifold dynamics and inlet CO<sub>2</sub> concentration are included in a model of the EGR circuit using volumetric efficiency, exhaust and inlet temperature estimates, and exhaust pressure measurements. The fuel limiting strategy is also model-based: comparisons between this full model-based strategy and variations on the same theme (no fuel limiting, no EGR valve closure) are presented though these schemes appear to perform worse than a well calibrated decentralised PI controller (particularly in terms of minimum air fuel ratio) so the favourable performance of the model-based controller is slightly exaggerated. Even so, the benefits of model-based control are given as being the improved calibration and generic nature of the resulting controller.

Steady state schedules of VGT vane position and EGR valve position have been investigated in several publications [41,42,43]. The results from [41] show optimum combinations of EGR and VGT settings achieved by manual sweeping at various engine operating points. The settings achieve good steady state NO<sub>x</sub> reduction and BSFC through the use of large EGR

valve settings and small turbine openings to drive the EGR. As this is a steady state study, the consequences of such high EGR levels when moving from one condition to another are not addressed. Although these are still applied via independent PID control loops, they illustrate that the control system design must be considered from a coordinated as well as a holistic point of view in order to access the full potential of emissions reduction from the engine system.

## **2.8 Alternative Control Techniques**

As more engine systems come under electronic command, the opportunities to exploit this increased flexibility have precipitated the use of a variety of “exotic” control techniques throughout the automotive field. A selection of techniques from the automotive field and beyond that could be used in this study are discussed in the following section.

### **2.8.1 SLIDING MODE CONTROL**

Sliding mode is part of a family of control systems known as variable structure systems. As the name suggests, these controllers can change their structure depending on the input. The basic principles are defined in [44,45]; the sliding mode controller in its simplest form will switch from full positive control action to full negative control action, with no in-between condition. This switching is derived from a function of the input error to the controller and the result is that the output is forced to follow a user-defined trajectory. The plant will be forced towards this trajectory as rapidly as possible due to the use of full control action. Once converged upon this trajectory, rapid switching keeps the output on the trajectory; this condition is known as sliding. One consequence of this control scheme is that the system dynamics become independent of the plant dynamics, however, the rapid switching can cause problems of chattering in certain applications and is ultimately limited by the switching frequency of the hardware. Full state feedback is also necessary for the controller implementation; a simple sliding mode scheme is illustrated in **Figure 2.9**.

**Moskwa** has published several works on automotive applications of sliding mode. In [46] he describes the design of a sliding mode throttle and spark controller to allow the following of ideal engine and torque converter speed trajectories in order to improve automatic shift quality. The work is performed in simulation, the control law derivation is non-trivial. **Kao and Moskwa** [47] describe the use of sliding mode for speed tracking of a Diesel engine, and also present the use of sliding mode observers for in-cylinder pressure and fuel mass burn rate. In this example, the crankshaft is modelled and variations in the modelled speed are compared with measured variations in speed. The difference is used to drive a cylinder pressure estimate towards the correct value to achieve the measured speed variation, as

illustrated in **Figure 2.10**. Similar sliding mode applications for fuelling and speed control of spark ignition engines are presented in [48,49,50].

### 2.8.2 MINIMAL CONTROLLER SYNTHESIS

Another interesting tracking controller scheme is the Minimal Controller Synthesis design (MCS) which is a form of model reference adaptive control. It requires neither plant model identification nor linear control design, instead the algorithm uses a model of the ideal behaviour of the system (for example a first order lag) and forces the plant output to match the model output; an example implementation is shown in **Figure 2.11**. However, the tuning of the four gain parameters has no straightforward physical interpretation and the system adaptive gains can drift significantly during steady state operation causing unexpected behaviour when the next transient occurs. An extension to this technique known as Gain Bounded MCS is described by **Stoten and Sebusang [51]**, which addresses the problem of instability due to the drifting of the adaptive gains of the controller by defining bounds within which the controller is allowed to drift.

### 2.8.3 OPTIMISATION-BASED CONTROL

When a system has to be controlled to achieve a desired performance target whilst also satisfying other defined constraints, an optimisation-based approach can be adopted. **Kolmanovsky and Stefanopoulou [52]** use constrained optimisation to determine the ideal energy addition trajectory over time for an electrically assisted turbocharger subject to constraints of zero net energy utilisation (the device can be used as a generator as well as a motor), minimum smoke and maximum vehicle acceleration. The technique is very powerful as it allows any objective function to be included in the trajectory design. However in this work it only defines the optimum trajectory for a system, it does not provide the control law to achieve this trajectory.

**Karlsson [53]** also describes such an approach, using genetic algorithms to determine the optimal torque modulation pattern required to cancel vibrations in a vehicle driveline, the aim being to then choose a control law that can actually achieve such a torque profile. These techniques are too cumbersome to apply on-line, and are more for establishing the required behaviour of the system. On-line optimal control can be achieved using the cost function based approaches such as General Predictive Control as previously discussed [30] in this chapter under VGT control. This is a form of optimal control as the control law is based on the least squares minimisation of the cost function.

## 2.8.4 INTELLIGENT CONTROL

Intelligent control has been much lauded as the future of control systems, by intelligent it is meant that the system incorporates some aspect of the way humans behave and operate though it is questionable as to whether this should always be considered intelligent. The main strands of activity in this field are Fuzzy Logic and Neural Networks and both have already found extensive application to the automotive field.

## 2.8.5 NEURAL NETWORKS

**Shoureshi [54]** gives an informative introduction to both techniques in the context of building climate control, showing how the neural network can be used for adaptive non-linear modelling and the fuzzy logic for rule-based control law application. They can be combined to provide a powerful, self-adapting and generalised controller. Neural networks can be considered as universal function approximators; they consist of interconnected activation functions (neurons) with individual weights and biases. The weights and biases are determined via the process of training; this is where an initial set of values for the weights and biases are iterated until the output of the network matches the training data for the given input. This has obvious applications for modelling, where the network can represent a linear or non-linear process without the need to actually understand the physical process. An example is shown in **Figure 2.12**: the network is used to approximate NO<sub>x</sub> and HC's from speed, fuel and timing inputs. Such modelling approaches are known as 'black-box' models as they bear no resemblance to the physical system. The models can be placed in control systems to give feedback of unmeasurable parameters. For example **Brace [1]** generates neural models of exhaust emissions and fuel consumption for use by the control system to determine optimum operating lines for a CVT and Diesel engine powertrain. An important point demonstrated here is the need to train the networks with sufficiently diverse data to ensure that they predict accurately for all possible parameter variations that could affect the result in reality. Also, extrapolative behaviour must be carefully verified.

Virtual sensing utilises neural networks to provide predicted engine performance from sensor input data. This can be used for on-board diagnostic (OBD) applications as demonstrated by **Atkinson et al [55]** where emissions can be predicted or the output of critical sensors can be verified. **Ortmann et al [56]** use neural networks for identifying spark ignition engine knock from accelerometer feedback, based on extensive training data for a knocking engine. Spark ignition fuel film compensation applications of neural networks have also been published by several authors [57,58,59]. Neural networks can be easily integrated into feedforward control schemes by training them using inverted data; the desired output is fed into the network and the required input is produced. **Moraal [60]** tackled the problem of modelling the highly non-

linear flow characteristic of a Variable Geometry Turbocharger turbine using neural networks, though the result was less effective than a physical interpretation-based approach where the parameters of a proposed equation were fitted using optimisation techniques. Neural models are generally computationally intensive, especially if an adaptive element is required.

### **2.8.6 FUZZY LOGIC**

Fuzzy Logic is a control structure which emulates the way humans arrive at decisions of what to do given a certain set of circumstances; the interested reader is referred to [61, 62, 63,64] for a more complete description of its workings. The basis of fuzzy logic is the degree to which an input to a system belongs a particular set. Once this is established, logical rules can be applied to the sets in order to map the inputs to the outputs. Fuzzy logic offers an intuitive approach to control, allowing complex control laws to be built up from simple linguistic rules; these rules can embody operator knowledge and system behaviour.

Automotive applications of fuzzy logic are varied, such as automatic gearshift control as described by **Bolander** [65], fault diagnosis for OBD applications as illustrated by **Soliman et al** [66], engine idle speed control [67] and the tracking of ideal engine and Continuously Variable Transmission operating trajectories [68]. In the last example a fuzzy logic controller is designed as a supervisory controller, the outputs of the controller are increments to the engine speed and torque demands generated from rules about pedal position, sensor feedback and operating point history.

## **2.9 CONSIDERATIONS FOR EGR-VGT CONTROLLER DESIGN**

The choice of control scheme depends very much on the nature of the plant to be controlled. The EGR VGT plant is a complex dynamic system many difficult behavioural phenomena such as non-minimum phase responses and DC gain reversal with operating point [34]. There are additional, often conflicting constraints that are applied to the system in order to satisfy the driveability, Noise Vibration and Harshness (NVH), fuel economy, aftertreatment system and engine durability requirements. The principal factors that must be considered when designing the EGR and VGT control systems are given below.

### **2.9.1 MINIMUM BSFC**

The EGR VGT system has a strong effect on fuel consumption due to the influence the system has on the exhaust manifold pressure and hence engine pumping work. To drive large

EGR flow rates a reasonable pressure difference between the manifolds must be established and this does imply a high backpressure. Achieving low engine pressure differential requires the use of wider VGT vane settings when no boost is required, or minimal boost for the given conditions.

### **2.9.2 BEST TIP-IN RESPONSE**

When a large tip-in occurs, it is assumed that the driver requires torque as soon as possible. The only way to achieve this is by ensuring that the maximum amount of air (oxygen) is available (i.e. high Air Fuel Ratio) to permit the demanded fuel quantity to be burnt. This comes into direct conflict with the use of EGR which reduces the air available in the charge for combustion. Even if the EGR valve is closed immediately upon detection of the transient, there is still a certain amount of time required for the inlet manifold to clear of residual exhaust gases: the higher the preceding EGR level and the lower the engine speed, the longer this time will be. To a certain extent this limits the improvements that can be made to tip-in response without making physical changes such as smaller EGR transport volumes or mounting the valve nearer the manifold.

If the demanded fuelling quantity requires more air than is available, fuel limiting is applied until the boost pressure responds and air density increases. This can take a significant amount of time, particularly at low engine speed conditions. A protracted period spent under limited fuelling will be interpreted as poor driveability. Transiently, the need to generate boost as quickly as possible will necessitate high backpressure in order to accelerate the turbine, conflicting with the fuel consumption requirements.

### **2.9.3 MINIMUM NO<sub>x</sub>**

The use of EGR is currently the most effective practical means of reducing Diesel NO<sub>x</sub> emissions, however, tight control over the EGR level is essential in avoiding driveability problems and increased smoke and PM. Maximising the EGR rate at any given condition will provide the best NO<sub>x</sub> performance, particularly in the higher load/speed ranges where current EGR strategies tend to be more conservative due to the potential for detrimental effects on smoke emissions.

During tip-ins from low to high fuelling, large transient NO<sub>x</sub> peaks are inevitable as EGR must be sacrificed for torque response. This can be improved to a certain extent through retarding the injection timing which will have the additional benefit of increasing the exhaust enthalpy and providing the turbine with more power to accelerate. However, torque production can suffer if this is not carefully controlled.

#### **2.9.4 TRANSIENT SMOKE**

Transient smoke is minimised by limiting the fuelling using an air density estimate, the effect of this is most noticeable during large tip-ins as explained previously.

Transient smoke can also manifest itself during gear changes, where a sudden drop in fuelling as the accelerator is released and the clutch depressed will cause the turbocharger speed to fall and hence reduce boost and airflow. When the fuelling comes back in after the gear and clutch are re-engaged, the turbo may have decelerated sufficiently for there to be inadequate boost pressure, resulting in fuel-limiting or transient smoke.

#### **2.9.5 DRIVEABILITY**

Although driveability is implicit in at least one of the aforementioned criteria (best tip-in response), there is very little in the way of objective targets that can be set to in order to achieve 'good driveability'. The inclusion of driveability is usually left to the calibration stage, where engineers will test the vehicle over a number of manoeuvres and modify strategy variables to achieve the subjective quantity of 'good driveability'.

Several people have worked on the development of metrics that can be used to relate subjective to objective data [69,70,71]. For example, identifying what features of the acceleration versus time trace for a vehicle are important to the performance feel of the vehicle. All the work in this field appears to deal exclusively with the complete powertrain as installed in the vehicle. From this point of view, the most important driveability feature of the engine is its ability to produce torque and the manner in which the transient torque evolves. Although fuelling has the dominant effect over torque, subtle modifications to the torque production are caused by factors such as engine pumping and air fuel ratio, and to this extent it is a feature of the VGT EGR control system.

For best driveability, a rapid fresh air rise in response to a tip-in, with minimal overshoot and smoke limited fuelling stages, followed by stable charge composition during high load operation are required.

### **2.10 GENERAL REMARKS**

From the review of control systems, it can be seen that there is a distinct trend of including knowledge of the system behaviour into the control strategy, be it in the form of a model or in heuristic rules that define system behaviour. Many of the more ambitious control schemes have only found application in the simulation environment, or if transferred to real engines they have been demonstrated over a very limited operating range.

The control system needs to work within realistic constraints for a system that would be mass-produced in a vehicle ECU. The primary limitations are those of computational overhead, as the EGR and VGT control features are just two (or one) of many tasks performed by the automotive control unit; the chronometric requirements of these tasks must be kept low. This does make certain types of model-based approach less attractive, though not all model-based controllers have a large computational requirement. Techniques involving neural networks, fuzzy logic or on-line optimisation can also place large demands on the processor.

Another important consideration is that of calibration: the task of calibration should ideally not require the same level of expertise as the task of controller design. The calibration needs to be intuitive and easily related to the process in order to be understandable.

From the review of EGR VGT system performance requirements, it is clear that a controller that simultaneously satisfies all constraints is unfeasible, some trade-off needs to be made as to which constraints are to be given priority, this could well be performed adaptively depending on driving conditions. Clearly, any improvements in airflow and EGR flow response will help transient performance and emissions, as will better knowledge of EGR levels present in the inlet charge.



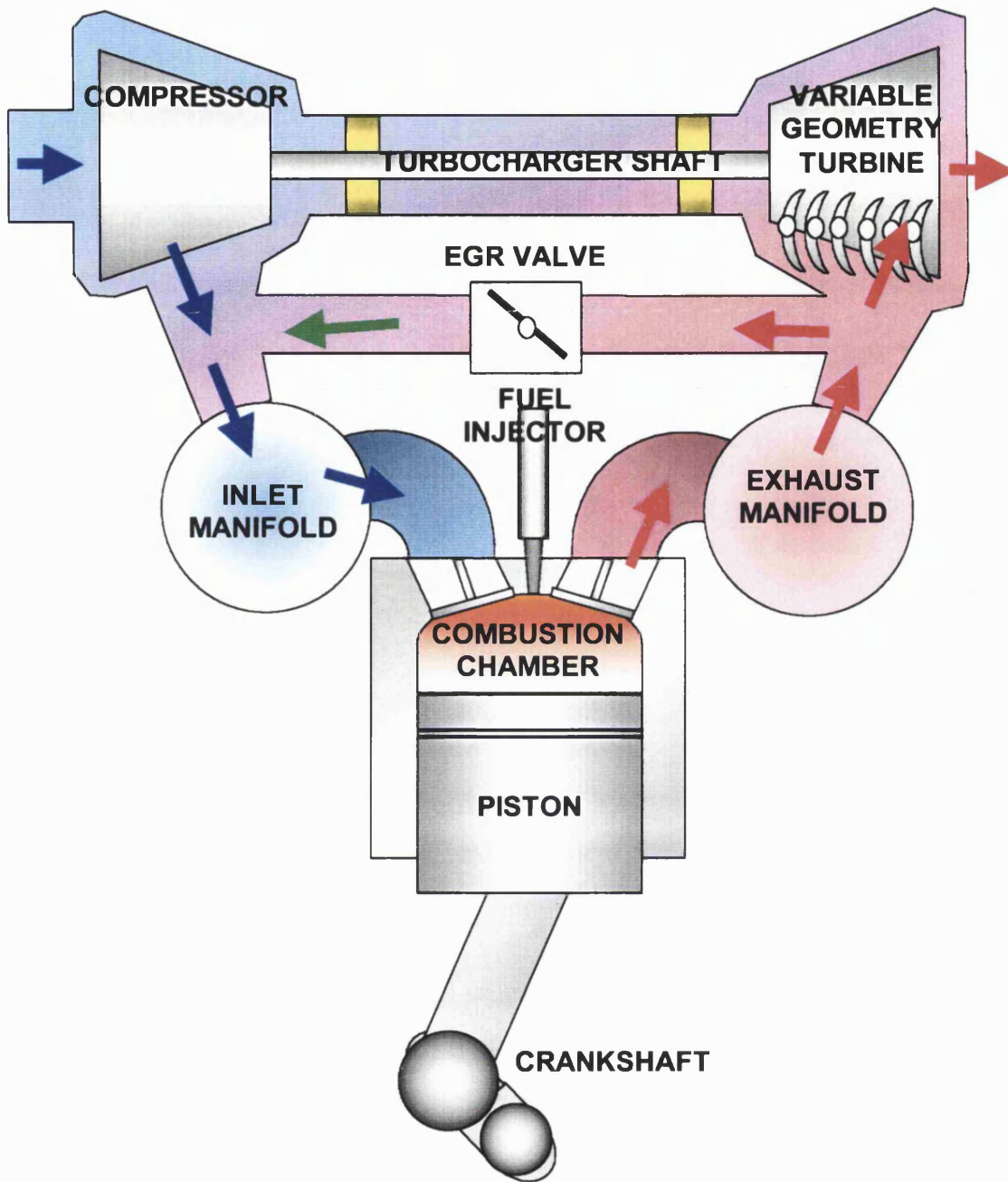
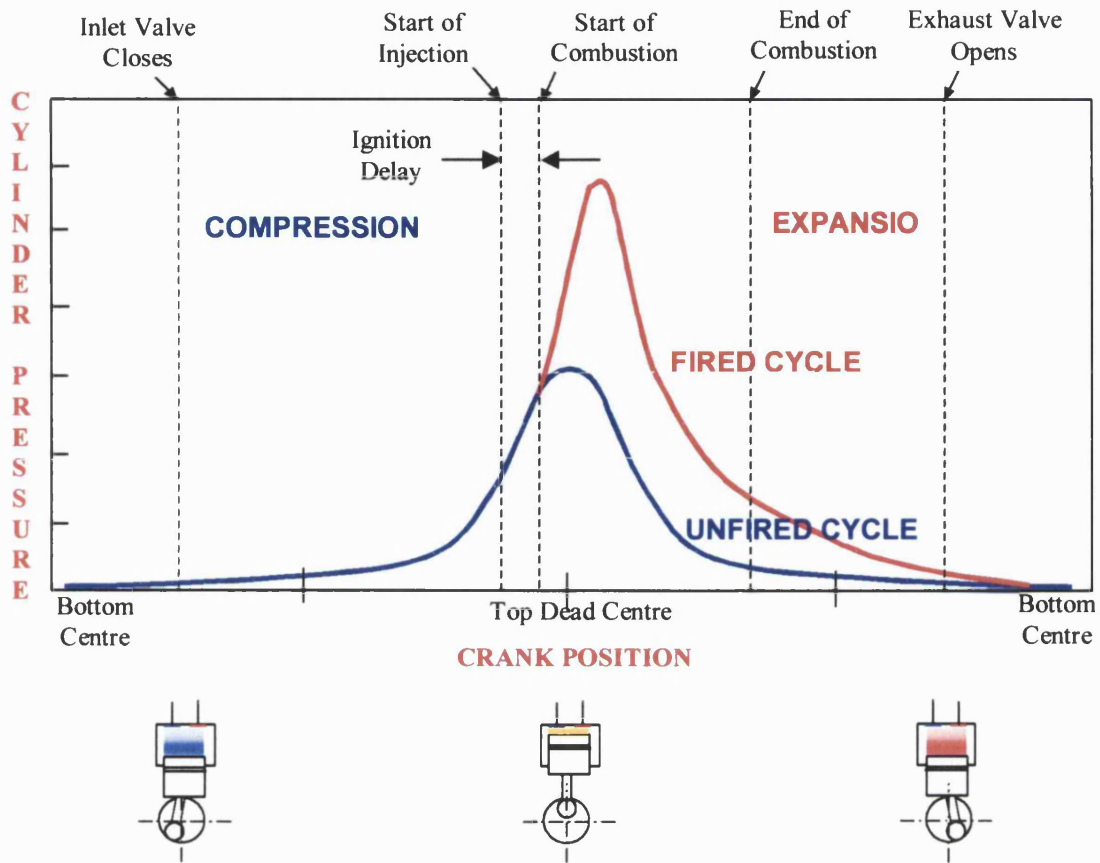
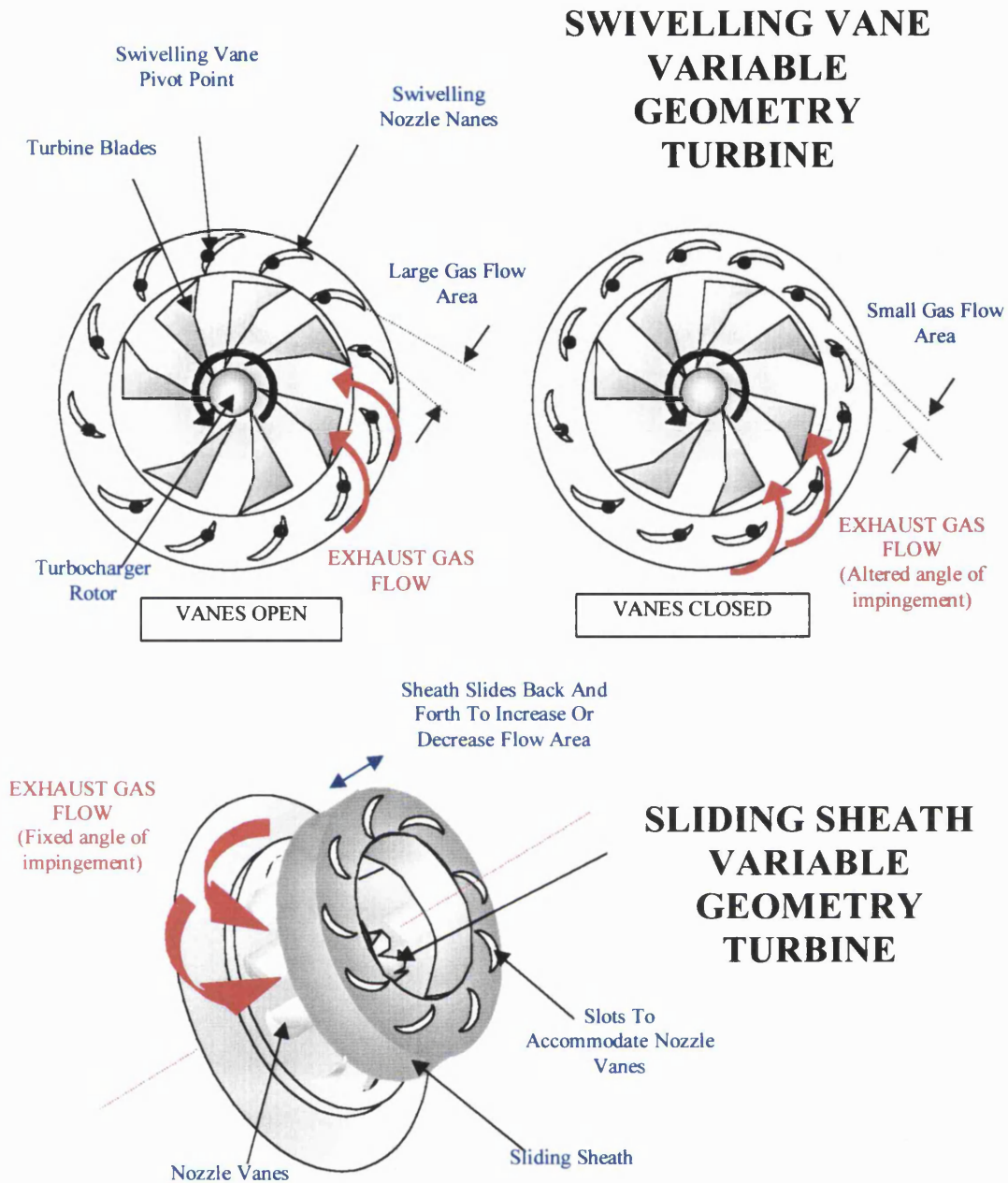


Figure 2.1 Schematic of a turbocharged HSDI Diesel engine with EGR



**Figure 2.2 HSDI Diesel engine combustion process on cylinder pressure versus crank angle diagram**



**Figure 2.3 Different Variable Geometry Turbocharger turbine arrangements**

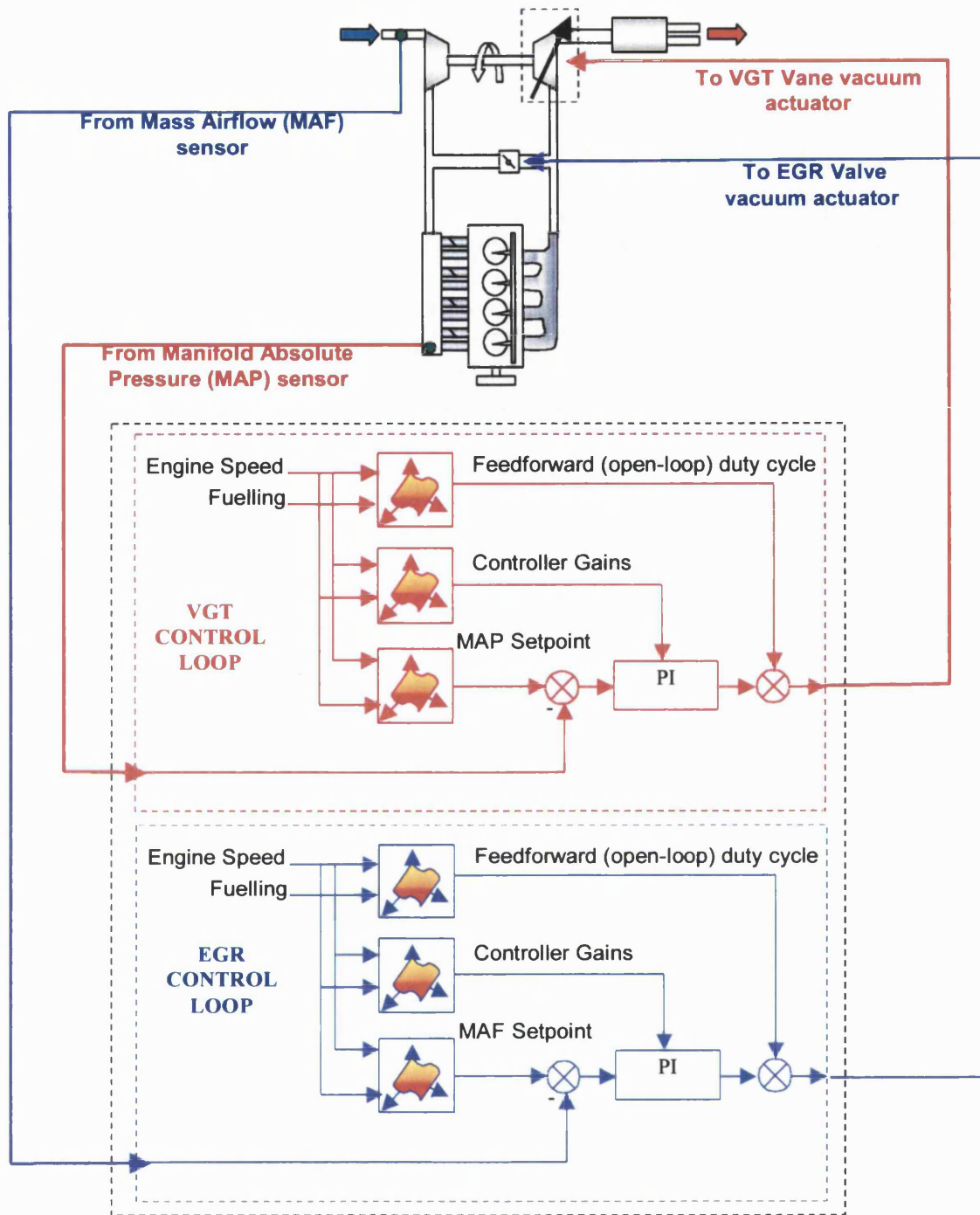


Figure 2.4 EGR and VGT standard control strategy schematic

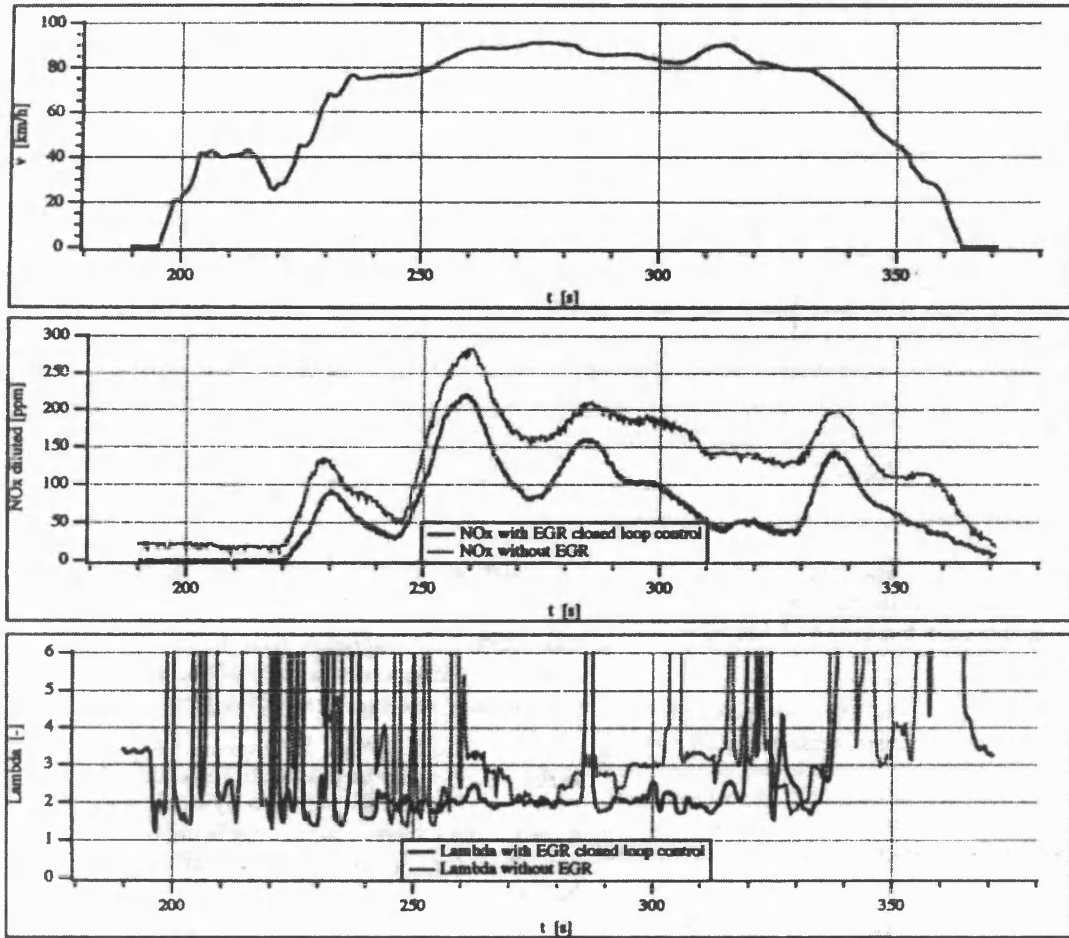


Figure 2.5 NO<sub>x</sub> reduction and Air Fuel Ratio tracking due to Oxygen Sensor feedback EGR control (Amstutz *et al* [4])

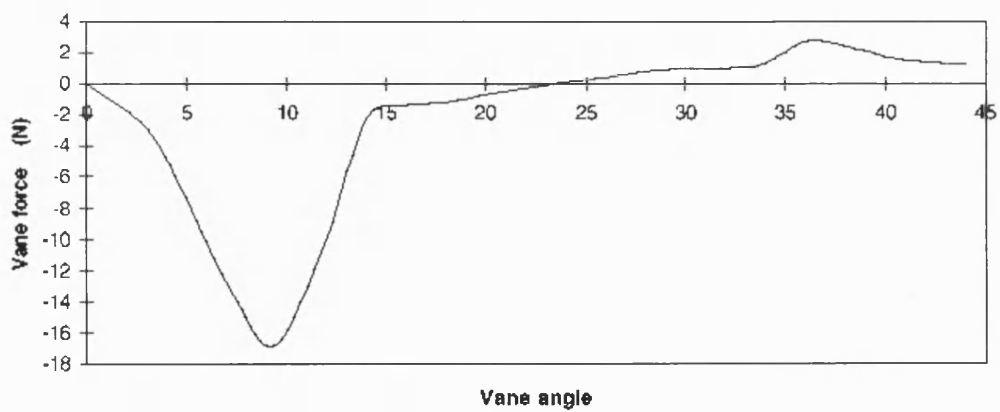


Figure 2.6 Actuation force vs. vane angle for VGT vane mechanism (Walker [7])

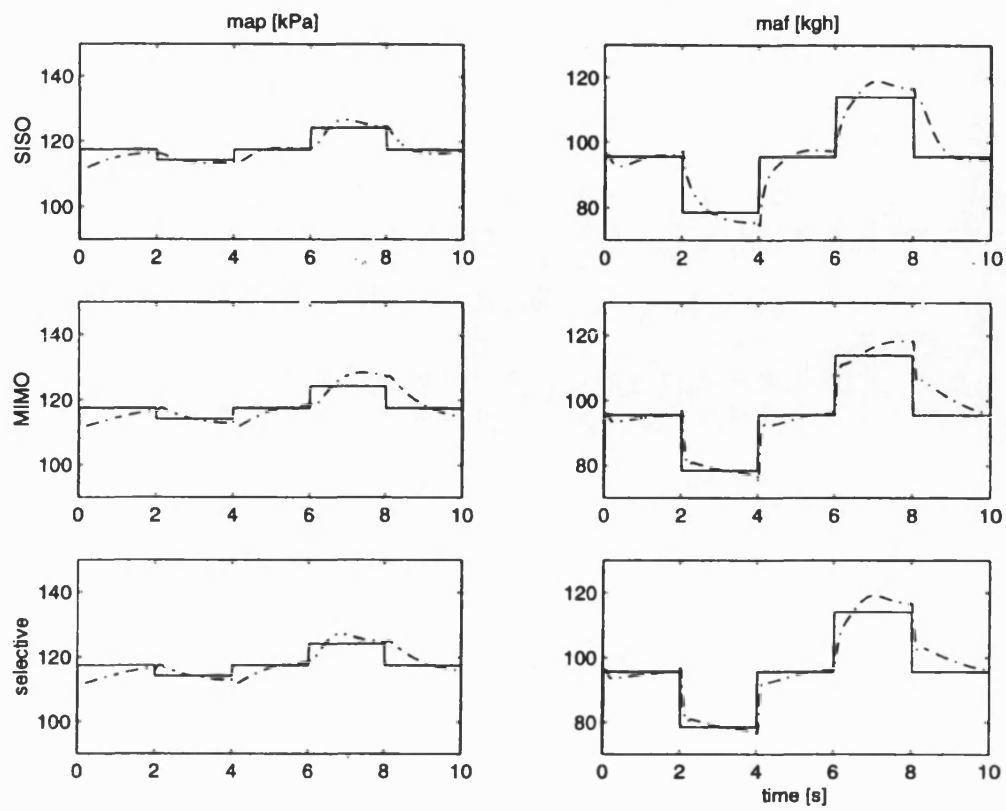


Figure 2.7 Comparison of airflow (MAF) and boost tracking(MAP) for coordinated and independent control of EGR and VGT (Van Nieuwstadt et al [16])

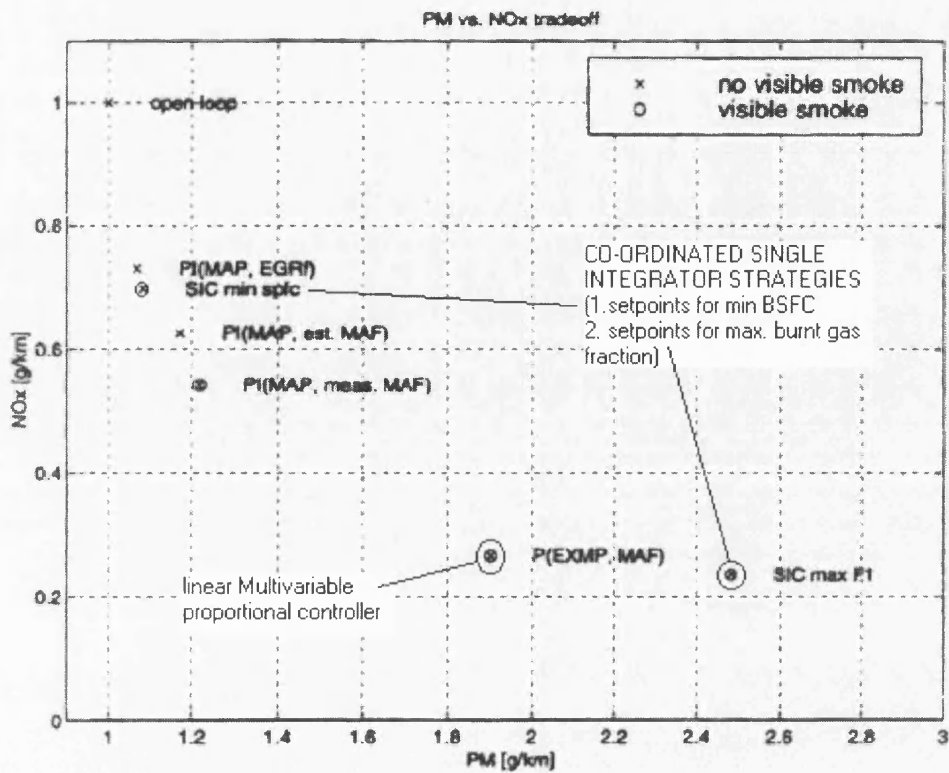


Figure 2.8  $\text{NO}_x$  / PM trade-off results for comparison between different EGR VGT control schemes (Van Nieuwstadt *et al* [17])

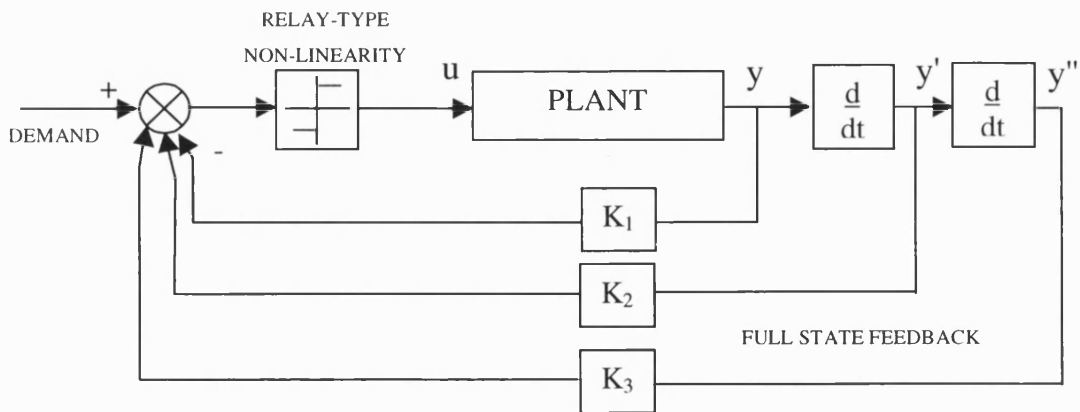


Figure 2.9 Simple sliding mode scheme

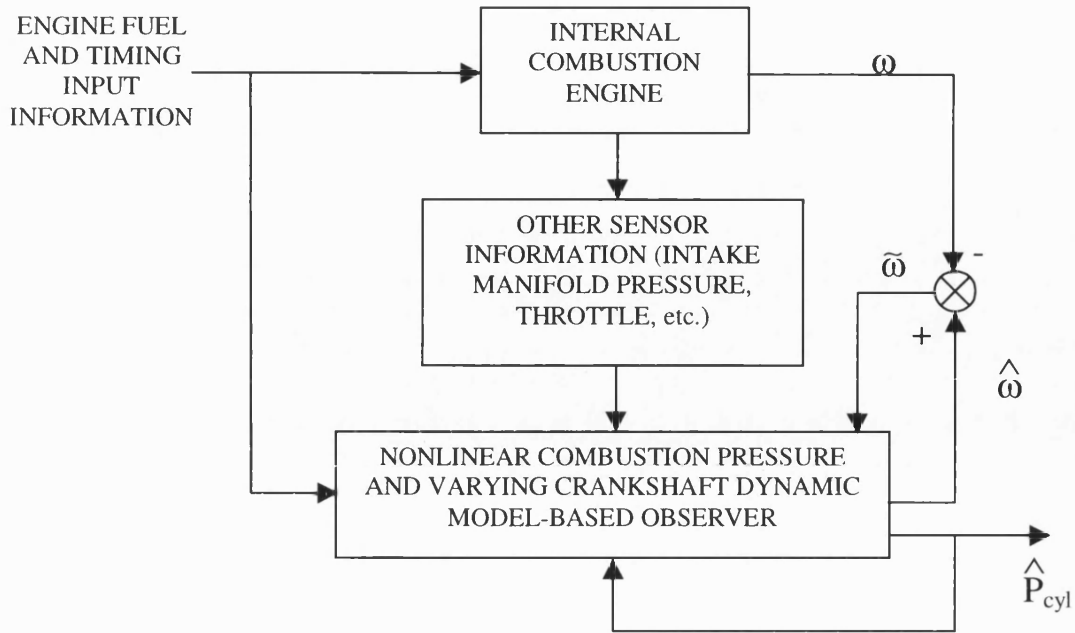


Figure 2.10 Block diagram for non-linear cylinder pressure observer (Kao and Moskwa [28])

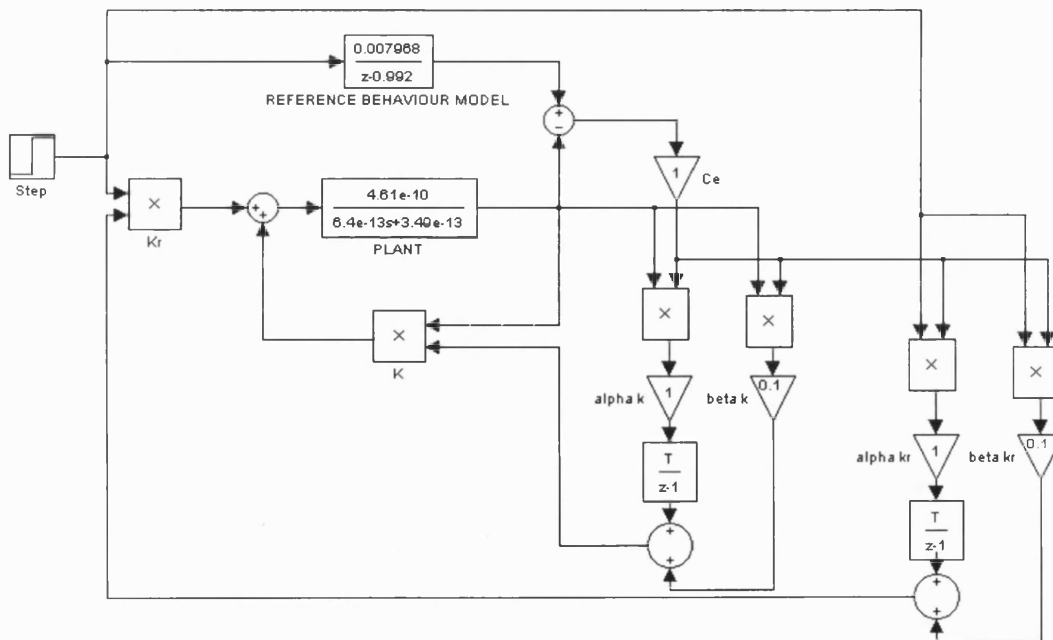


Figure 2.11 Simulink implementation of an MCS controller



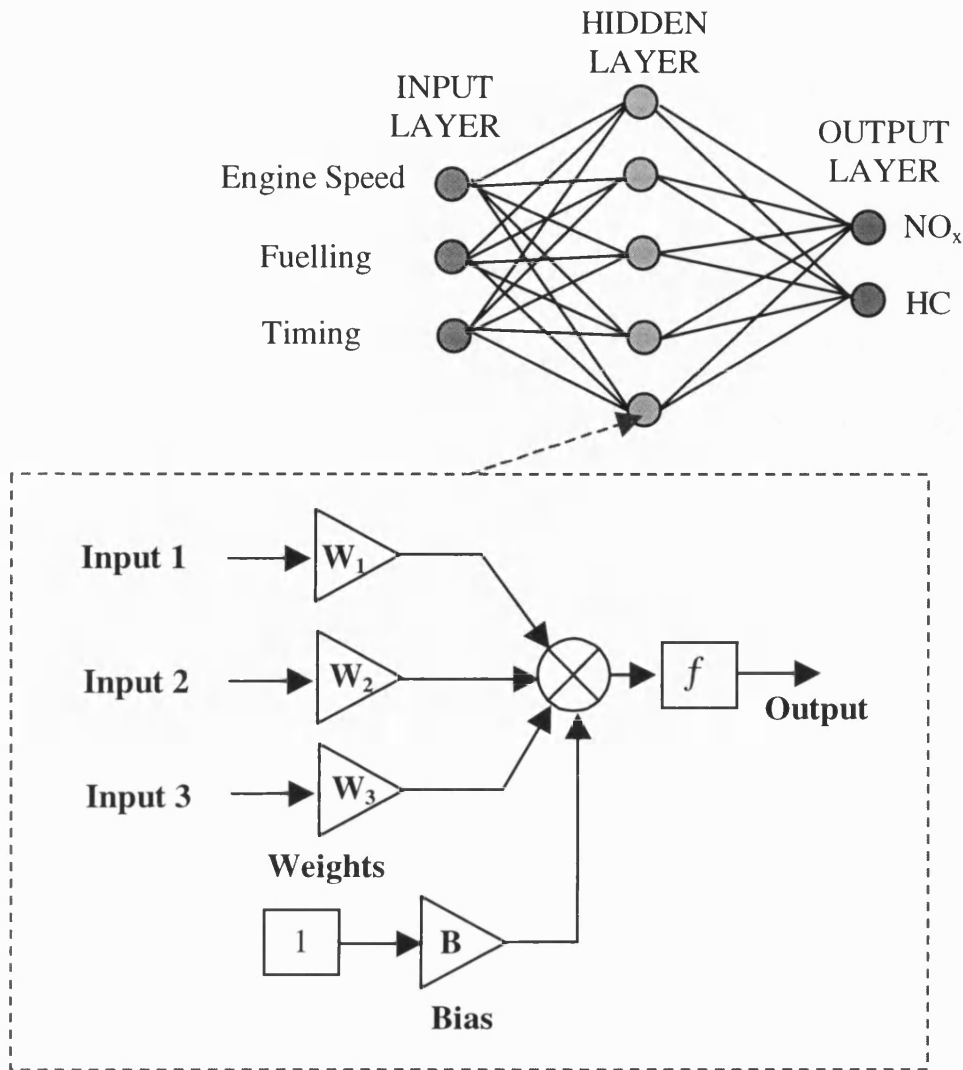


Figure 2.12 Neural Network example for automotive application (emissions mapping to engine parameters)

# Chapter 3 EXPERIMENTAL CHARACTERISATION OF THE ENGINE

## 3.1 INTRODUCTION

An extensive engine test program has been performed in order to characterise the important aspects of turbocharged Diesel engine behaviour and highlight areas where improvements can be made. In this chapter a selection of results from the steady state and dynamic testing programmes is presented and discussed.

The testing was performed on a prototype High Speed Direct Injection (HSDI) Diesel engine installed on a fully transient engine dynamometer in the dynamic test facility at the University of Bath. The test bed has an extensive array of sensors to monitor most aspects of engine performance and emissions.

Three different steady state test schedules are described; modal testing, limiting torque curves and sweeps of the Turbocharger and Exhaust Gas Recirculation system settings. The dynamic engine behaviour is investigated using fuel step transients at constant speed and legislative drive cycles. Additionally, two different types of VGT are evaluated over all the aforementioned tests to illustrate the influence on overall engine behaviour of such devices.

It is concluded that the steady state settings for the engine systems such EGR and VGT play an important role in the dynamic as well as steady state performance. The influence of actuation systems also has a dominant effect on the resulting engine dynamic behaviour and emissions. The dynamics of the fuel injection system are far faster than those of the gas charge system; this inevitably leads to dynamic emissions problems when operating the engine with EGR due to the time required to reduce EGR quantity in response to increased fuelling demands.

## 3.2 TRANSIENT TEST CELL

The transient engine test facility is shown schematically in **Figure 3.1**. The basic design was described by **Dorey and Guebeli [72]** and it was also used by **Brace et al [68]** for a research program with a continuously variable transmission powertrain. For this study the test facility configuration consisted of a Diesel engine, a 5-speed manual gearbox and clutch (standard components from a road going vehicle) and the hydraulic dynamometer.

### 3.2.1 ENGINE

The engine used in this study is a prototype 2.0 litre, 4 cylinder, 16 valve High Speed Direct Injection Diesel engine (FORD PUMA CP4 115PS, Engine No. XD66434). It is equipped with a VGT (Allied Signal VNT-25), an EGR system with an EGR cooler, charge air

intercooler, inlet port deactivation and an electronically controlled distributor pump fuel injection system. The fuel injection system has a separate controller which communicates with the main engine control unit via a Control Area Network (CAN) serial bus. The intercooler used on the test bed is a custom-built water to air heat exchanger, it has a bypass facility allowing the effectiveness of the intercooler to be varied.

The fuelling demand (accelerator pedal) input to the engine is synthesised via 2 potentiometers on a manual control panel, a toggle switch is included to allow the switching between 2 different fuel levels. The fuelling command can also be generated from the test cell control computer, allowing drive cycles to be performed under computer control.

### **3.2.2 TRANSMISSION**

The clutch and 5 speed transmission connect the engine to the dynamometer, they are operated by pneumatic actuators, either manually from the control panel or automatically from the test cell control computer.

### **3.2.3 DYNAMOMETER**

The purpose of the dynamometer is to absorb power generated by the engine and emulate the dynamic load characteristics of a vehicle when drive cycle tests are being performed. This particular system uses hydraulics in combination with a large rotating inertia to achieve this. Control is via a PC with additional I/O hardware; the system can be run in a constant speed, constant torque or vehicle emulation mode.

### **3.2.4 TEST CELL CONTROL**

Many of the automated features of the test facility are managed by the Ricardo EMPS control prototyping system. This is C-code based real-time control software environment, it provides three time scheduled tasks (at 1Hz, 10 Hz and 100Hz) that can be programmed to control any external system via analogue and digital I/O interface boards connected to the PC. Additionally any of the system variables can be logged. In this application, EMPS is used to control the engine coolant, oil and charge air (intercooler) temperatures via PID feedback control loops; these are executed in the 10Hz task.

The system also contains a complete driver emulation model for simulating drive cycles, the 100Hz task is used to control pedal position, clutch and gear selection in order to follow any given speed profile. The design and calibration of this system was the subject of much research during the initial stages of this project, however, a complete description of this work is beyond the scope of this thesis.

### **3.2.5 ENGINE CONTROL AND CALIBRATION**

The VGT and EGR are controlled from the main engine management system. The unit used here contains a prototype level strategy (PUPE1), meaning that there will be changes made to the strategy before it is released as a production code, but these are not likely to be significant.

The strategy is interrogated by a calibration tool, allowing the engineer to alter the value of parameters, acquire data and view tables and variables from within the strategy. It is also possible to download new strategies onto the EEPROM within the ECU providing the strategy is available in the appropriately compiled format. The system used here is Kleinknecht Gredi MCS 3.0. It communicates with the ECU via the CAN link, an interface box is used to connect the system to a PC via the serial link. In this work it is mainly used for data acquisition of the control strategy. The ECU also has four configurable analogue output channels that can be used to send data from the strategy to an external acquisition source.

### **3.2.6 RAPID PROTOTYPING EQUIPMENT**

The test cell is also equipped with the dSpace control system prototyping hardware. The system consists of a Digital Signal Processor (DSP) that can be programmed to run user defined code developed in and then downloaded from the Matlab / Simulink environment. The system has a variety of configurable inputs and outputs that can be used to connect the DSP to real-world signals and devices and execute control tasks in real-time. The system allows the development of control strategies in simulation and subsequent testing on real systems in very short timescales, and as such is a very powerful tool. The system used here has analogue and digital inputs and outputs and a CAN processor for communication with other devices via the Control Area Network.

### **3.2.7 EMISSIONS MEASUREMENT**

The facility is equipped with an extensive array of exhaust gas analysis equipment, the principal emissions measurement system is the Horiba MEXA 9000 system, comprising sensors for Oxides of Nitrogen (NO/NO<sub>2</sub>), Carbon Monoxide and Dioxide (CO/CO<sub>2</sub>), Oxygen (O<sub>2</sub>), and Hydrocarbons. EGR rate is determined by a separate Horiba inlet manifold CO<sub>2</sub> detector, and an AVL filter smoke meter is used to grade the density of exhaust smoke. Heated sample lines carry exhaust gases from the engine to the sensing elements of the analysers. These systems are better suited to steady state measurements as the analysers have a relatively large response times and the smoke meter takes an averaged sample over a discrete time period.

For rapid transient analysis there are principally 2 devices, the Celesco Smoke Opacimeter [73] which measures the opacity of the exhaust gases, and a Combustion FAST FID hydrocarbon analyser [74]. Both devices provide measurement response times of the order of 100ms. The latter device needs to be attached to the exhaust stream as close to the cylinder outlets as possible. It is also very difficult to set up and the sensing element tends to need regular unclogging.

### **3.2.8 FUEL FLOW**

Accurate fuel flow measurements are made with an AVL gravimetric fuel flow meter. This device determines fuel flow rate through the periodic measurement of the weight of a beaker of fuel which feeds the fuel injection pump.

### **3.2.9 IN-CYLINDER PRESSURE**

The in-cylinder pressure is monitored using the AVL Indiscop system, which uses an in-cylinder pressure transducer to give crank-angle resolved data of the in-cylinder pressure. A needle lift sensor is also included to give accurate measurement of fuel injection timing and duration.

### **3.2.10 DATA ACQUISITION**

Principal test cell data acquisition is by the HP DTVee software, using 12-bit analogue to digital conversion to log over 100 channels of temperatures, pressures, flows, positions, speeds, torques, emissions results and control signals. As previously mentioned, engine management system variables are logged using the Gredi calibration tool, and drive cycle control parameters are acquired by the EMPS software. In order to synchronise the different data streams, the fuel demand signal from the ECU is sent to the HP DTVee acquisition system via the ECU analogue outputs.

## **3.3 ENGINE TESTING**

The characterisation of engine performance and behaviour has been achieved through three different test regimes; steady state testing, constant speed fuel step testing and drive cycle testing. Through all three regimes, test results for two different types of turbocharger are discussed: the swivelling vane type (referred to as VGT) and the sliding nozzle type (referred to as VNT-O/P) introduced in **Chapter 2**.

### **3.4 STEADY STATE ENGINE TESTING**

Steady state engine testing involves measurement of engine performance once a steady state condition has been achieved. Steady state testing requires less complex dynamometer and test cell hardware which is why it is used extensively in engine test programs, the steady state conditions can give an indication of how the engine will perform under certain real life driving conditions. Due to the complex interactions between engine systems, fixing the engine speed and load also facilitates the analysis of the system by removing 2 strong dependencies allowing weaker relationships to be examined.

Three types of steady state testing are considered in this work, Modal tests, Limiting Torque Curves (LTCs), and EGR - VGT sweeps.

#### **3.4.1 MODAL TESTS**

Modal testing involves setting the engine to predefined operating points (combinations of speed and torque) and then measuring the averaged performance. During these tests the engine subsystems (e.g. EGR and VGT) are under full control of the engine management system. The test points are chosen to give an indication of how the engine will perform over the legislative ECE15 cycle. It is possible to take the steady state results from each operating point and put them into a weighted calculation to produce an estimate of the cumulative emissions performance over a drive cycle, saving time and the expense of having a fully transient test cell capable of performing drive cycles.

The mode points used for the tests are described in **Table 3.1**.

Mode	Engine Speed	BMEP	Torque
No.	rev/min	kPa	Nm
1	IDLE	34	5.4
2	1000	300	47.7
3	1000	400	63.6
4	1500	100	15.9
5	1500	500	79.5
6	1500	600	95.4
7	2000	400	63.6
8	2000	600	95.4
9	2500	500	79.5
10	2500	800	127.2

**Table 3.1 Modal test points**

A selection of the modal results are discussed here, the full results are described in [75].

These results are average values from several repeat tests.

#### 3.4.1.1 TEST RESULTS

**Figure 3.2** illustrates the evolution of engine conditions with operating point. The inlet manifold pressure can be seen to rise with increased engine loading. The control system demands unattainably high boost pressures at these operating points in order to keep the turbocharger vanes fully closed, however the VGT turbocharger gives higher boost pressures in the fully closed vane condition.

The airflow through the compressor increases with engine torque; there is very little difference between the two turbochargers for this measurement. The apparent dip at mode point 4 is due to the high EGR rates employed at this condition.

Turbocharger speed follows the trends of the boost and airflow, with the difference in boost pressure between the two turbochargers mirrored by the difference in turbocharger speeds.

The exhaust manifold pressures are similar up to mode 9, where the VNT-O/P incurs a significantly higher backpressure. This will result in greater engine pumping losses and higher specific fuel consumption.

The first frame of **Figure 3.3** shows the EGR rate (calculated from a CO<sub>2</sub> content comparison of exhaust and inlet manifolds), the idle condition and mode 4 employ extremely high EGR

rates, the higher modes show a greater EGR rate for the VGT turbocharger. The EGR valve is controlled to achieve a target compressor airflow; this is achieved by both turbochargers, however the higher inlet manifold pressure for VGT suggests that more flow is entering the cylinders since the charge will be more dense. As the compressor flows are identical the difference must come from the EGR flow, hence the higher EGR rate for the VGT turbocharger.

The large peaks in brake specific fuel consumption (BSFC) at idle and mode point 4 are due to a combination of low loads and high EGR rates, both of which reduce engine thermal efficiency. At mode point 9 the difference in fuel consumption emanates from the higher backpressure produced by the VNT-O/P turbocharger.

The smoke trace shows very little difference between the two devices, the highest smoke occurs at mode point 2, primarily because the EGR rate is high, however minimum smoke occurs at mode point 4 where the EGR rate is the highest but speed is higher and load lower. This illustrates that the relationship between smoke production and EGR rate is not a simple one.

Finally, the mass  $\text{NO}_x$  emissions shows the general trend of increasing  $\text{NO}_x$  with engine power output, the lower levels observed for the VGT at the higher modes are a direct result of the higher EGR rate compared to the VNT-O/P.

### **3.4.2 LIMITING TORQUE CURVE**

The limiting torque curve defines the peak torque that the engine will deliver for a given engine speed. The actual torque value is usually less than the maximum torque that the engine is physically capable of producing; other factors must be taken into account such as smoke production, exhaust temperature, peak in-cylinder pressure, and fuel consumption. The engine must be able to run continuously at these limiting torque conditions, therefore durability must not suffer as a result.

In these tests the engine fuelling is set at constant speed to achieve a target torque value provided by the Ford Motor Company, this process is performed across a speed range from 1000 to 4000 rev/min. The results of these tests define the operating envelope for the engine.

#### *3.4.2.1 TEST RESULTS*

**Figure 3.4** displays the performance characteristics of the engine with both turbochargers, the peak engine torque being developed around 2250rev/min, but a torque greater than 200Nm is developed from 1500 to 3500 rev/min. This characteristic is typical of modern turbocharged direct injection Diesel engines. Power grows progressively to a peak value at 3500 rev/min.



The difference between the two turbochargers becomes apparent when examining the fuel quantity plot, between 1000 and 2500 rev/min the VNT-O/P requires consistently higher fuelling levels to achieve the same torque. The higher fuel injection quantities lead to a higher smoke level in this operating region and markedly higher specific fuel consumption.

The first frame of **Figure 3.5** demonstrates how the increased fuelling for the VNT-O/P results in a lower air fuel ratio. In the region from 2500 to 4000 rev/min where the two devices elicit approximately the same fuel quantities, the lower air fuel ratio for the VNT-O/P can be linked to either a lower compressor delivery or poorer volumetric efficiency.

The VNT-O/P turbocharger generally exhibits lower in-cylinder pressures as can be seen in frame 2 of the **Figure 3.5**, the maximum permissible continuous cylinder pressure is around 140bar in order to prevent damage to the cylinder head. The exhaust manifold pressure trace shows the VNT-O/P to cause higher backpressures. This results in increased fuel consumption and reduced volumetric efficiency; it is harder to clear the residuals from the cylinder when exhaust pressure is high.

The turbocharger speed trace shows both devices to be operating at approximately the same speed across the entire engine speed range, the maximum allowable continuous turbocharger speed is approximately 210,000 rev/min.

### **3.4.3 EGR AND VGT SWEEPS**

The EGR and VGT sweeps have been the subject of a major study at University of Bath performed prior to this project, the results of which are detailed in [76], therefore the salient points of this research shall be summarised only. The tests consist of systematically varying the VGT vane position from one extremity to the other for a range of different EGR valve settings; this is performed at a series of engine speed and load points. A large number of test points are visited rendering the technique laborious, large quantities of data are produced from which optimum combinations of EGR and VGT position can be chosen for specific targets such as NO<sub>x</sub> reduction or minimum specific fuel consumption.

#### *3.4.3.1 TEST RESULTS*

**Figure 3.6** demonstrates the effect VGT position has on inlet pressure, exhaust pressure and engine torque for a variety of engine operating points when the EGR valve is closed. The trends are the same for all points, the inlet and exhaust pressures increase as the vanes are closed, the torque remains unchanged for low vanes settings then reduces towards higher vane positions as the increased exhaust backpressure saps more of the engine torque for pumping work.

**Figure 3.7** is taken from **Pease et al [76]**; it describes the Brake Specific Fuel Consumption results of a complete EGR and VGT sweep at fixed engine operating point on a 1.8 litre HSDI Diesel engine with EGR and VGT. The trend of increased fuel consumption with increasing vane closure is visible, regardless of EGR valve position. The higher EGR openings also increase BSFC through the effect that the EGR has on the combustion process.

The results of the same test on NO<sub>x</sub> emissions are detailed in **Figure 3.8**. With the EGR valve closed the NO<sub>x</sub> emissions increase gradually as the VGT is closed, due to the increased Oxygen availability in the boosted charge air. With the EGR valve open the trend is reversed, increasingly so with wider EGR openings. This is because closing of the VGT vanes increases exhaust manifold pressure and thus the pressure differential across the EGR valve, forcing more EGR flow and causing greater NO<sub>x</sub> reduction.

### **3.5 DYNAMIC TESTING**

Up until now the engine has been considered uniquely in the steady state. Dynamic testing illustrates the behavioural characteristics when changing from one of these steady states to another. The dynamic behaviour of the engine is extremely important in terms of driveability and emissions, the driver will 'feel' how the engine torque responds to their acceleration demands, and they will notice puffs of smoke from the exhaust when the car in front accelerates.

#### **3.5.1 CONSTANT SPEED FUEL STEP TESTING**

In this section, step changes in fuel at constant engine speed are applied to the engine and the resulting behaviour of engine and control system is analysed. These step changes in fuel demand are used because they are the most rapid disturbances that the EGR and VGT control systems must respond to. These types of transient correspond to the initial moments of real world driving scenarios such as overtaking manoeuvres or encountering a gradient.

The tests are performed by using the dynamometer to hold the engine speed constant, then setting two fuel levels using the two fuelling potentiometers. The fuel levels are chosen to deliver engine torque outputs of 10 Nm and 170 Nm; the step transient is initiated by a toggle switch that selects between the two potentiometers. The steps are performed at 1500, 2500 and 3500 rev/min. The EGR is active in all tests; the response of the EGR control system to the step increase in fuelling is to close the valve therefore the EGR position results have not been shown.

### 3.5.1.1 Results of Dynamic Testing

The following discussion refers to the four separate plots within in each figure as *frames 1 to 4*, *frames 1 and 2* correspond to the top two graphs and *frames 3 and 4* to the bottom two.

**10 – 170 Nm @ 1500 rev/min**

#### **Figure 3.9 – Engine Performance Parameters**

*Frame 1* shows the fuelling command sent to the fuel pump. The differences between the final fuelling quantities for each device are due to the fuelling being set to provide the same engine torque for each test (i.e. 10 & 170 Nm), the difference is of the order of 5%; this is greater than the expected variance due to test conditions. This confirms the steady state results that indicate the VNT-O/P causes increased fuel consumption at higher loads. Also of note is the effect of transient fuel limiting based on the inlet manifold air density estimate, this is performed by the fuelling control strategy to reduce transient smoke. For both devices the fuel limiting occurs at the same point but the duration of the fuel limiting is longer for the VNT-O/P as it takes slightly longer to raise the inlet density.

*Frame 3* shows the effect of the limitation on engine torque, with the VNT-O/P taking marginally longer to achieve the target value. The delay caused by the fuel limiting will be perceived as sluggish response by the driver. *Frame 4* shows the smoke opacity trace, the large spikes correspond to the initial dip in Air Fuel Ratio (*Frame 3*). For the VNT-O/P the spike is smaller due to the reduced fuelling during the limiting period (*Frame 1*), but the post transient smoke is at a higher level, in part due to the lower final Air Fuel Ratio. The preceding EGR rates will have a strong influence on the transient smoke performance. The EGR valve closes fully in response to the tip-in but the residual burnt gases in the inlet manifold will take a finite time to reduce; it will take longer to clear residuals caused by higher pre-transient EGR rates. This effect is particularly important at low engine speeds where overall cylinder throughput is low.

#### **Figure 3.10 – Turbocharger Physical Parameters**

In *Frame 1* the boost pressure dynamics are illustrated, the target values are shown as dotted lines which neither of the devices are able achieve. The boost pressure rise is notably faster for the VGT. *Frame 2* shows the same trends for the mass airflow, with a slight overshoot occurring with the VGT. The initial fast response of the mass airflow is due to the closure of the EGR valve, as the recirculated flow reduces to zero, the engine pumping rapidly draws fresh air through the compressor to replace it. This also explains the small dip in boost pressure at the start of the transient.

*Frame 3* shows that both devices remain fully closed (maximum boost position) throughout, and are therefore unable to provide further boost at this operating condition. *Frame 4* shows that the VNT-O/P creates higher exhaust back pressure than the VGT for similar levels of boost and airflow. This may contribute to the increased smoke, and in turn hydrocarbon and particulate emissions, as well as increasing pumping work and hence specific fuel consumption.

### **Figure 3.11 – Engine Control Parameters**

The plots displayed here refer to the closed-loop boost pressure control system that modulates the VGT vanes or VNT-O/P sheath. *Frame 1* shows the error between demanded and actual boost that drives the control action. The VNT-OP displays a considerably larger tracking error. The overall control action (*Frame 3*) is the sum of the individual terms shown in *Frames 2,3 & 4*. The control action tries to further shut both turbochargers to increase boost due to the continual error. Permanent steady state errors have saturated the integral terms for both devices (*Frame 4*).

**10 – 170 Nm @ 2500 rev/min**

### **Figure 3.12 – Engine Performance Parameters**

In *Frame 1* the VNT-O/P again requires slightly higher fuelling levels for the same torque. *Frame 3* shows that the VNT-O/P provides a smoother if marginally slower torque rise; with the VGT there is a small torque overshoot. This corresponds to the oscillatory behaviour of the VGT air fuel ratio (*Frame 2*), which only settles late into the transient. The VNT-O/P takes equally long to settle but the changes in air fuel ratio are smaller after the initial dip. A large smoke spike is seen initially with both devices (*Frame 4*) but the VNT-O/P peak value is lower.

### **Figure 3.13 – Turbocharger Physical Parameters.**

The boost pressure delivered by each device is shown in *Frame 1*. The VGT has a faster rise time but the overshoot is overcompensated and the subsequent convergence on the setpoint is very slow. The VNT-O/P achieves a slower boost rise but the overshoot compensation is more progressive and the boost pressure remains close to the setpoint. This behaviour is replicated in the mass airflow as shown in *Frame 2*, often the overshoot in airflow can cause the EGR valve to open slightly during the transient even though the strategy includes a feature that disables EGR on detection of significant overboost. The opening of the valve can have severe consequences to the emissions performance, although this effect is not deterministic due to valve hysteresis and does not happen in this particular test.

The root of the overcompensation experienced by the VGT is illustrated in *Frame 3*. The vanes are fully shut at the onset of the transient and remain so until the boost and airflow have overshot their setpoints. The demand signal to the actuator reduces but the vanes do not respond until a certain threshold has been passed, then the vanes suddenly flip fully open and the boost and airflow fall off dramatically as a result. Following this the control signal slowly closes the vanes down to converge on the boost setpoint. The VNT-O/P however, responds well to the control signal and progressively opens the device up to converge upon the setpoint. In *Frame 4* it can be seen that the stagnation of the VGT vanes in the closed position causes high exhaust back pressures during the transient, though again the VNT-O/P causes higher overall back pressures in the ensuing steady state.

**Figure 3.14 – Engine Controller Parameters**

*Frame 1* further illustrates the VGT tracking error, *Frames 3 & 4* show the effect this has on the control system as it tries to react to the errors. The slow recovery of boost pressure after the overcompensation is due in part to the low gain of the integral term (*Frame 4*) at that particular engine operating point.

*10 – 170 Nm @ 3500 rev/min*

**Figure 3.15 – Engine Performance Parameters**

At this engine speed there is plenty of energy available in the exhaust gases for the turbochargers to respond rapidly to changes in demand. *Frame 1* shows that very little air density limiting of the fuelling quantity is applied, with the VNT-O/P necessitating more than VGT. The torque rise (*Frame 3*) is virtually identical for both devices, as is the smoke response (*Frame 4*). The final torque from the VGT test is slightly unsteady, the air fuel ratio (*Frame 2*) is also unsteady for the VGT.

**Figure 3.16 – Turbocharger Physical Parameters**

In *Frame 1* it can be seen that the VGT boost pressure oscillates considerably whilst the VNT-OP achieves target boost with minimal oscillation. The cause of the VGT oscillations is the same as that of the overcompensation seen during the 2500 rev/min test. The response of the VGT to its control signal is highly non-linear (*Frame 3*) with small changes in demand causing large swings in vane position and hence boost. Again the VNT-O/P responds well to demand signals. In *Frame 4* the exhaust backpressures of the two devices match, though the VGT back pressure fluctuates due to the movement of the vanes.

**Figure 3.17 – Engine Controller Parameters**

As with the 2500 rev/min tests, the VGT control action is driven predominantly by the integral term (*Frame 4*) as steady state errors are slowly converged. Very little control action is applied to the VNT-O/P.

### **3.5.2 COMPARISON OF FUEL STEP RESPONSE WITH AND WITHOUT EGR**

In order to illustrate the profound effect that the initial EGR rate has on the dynamic performance of the engine in response to a step increase in fuelling, a comparison is given for the 10-170 Nm step at 2500 rev/min with and without EGR active. The EGR system can be disabled using the calibration tool to write the upper limit for the valve control signal to be zero, thus forcing the valve to be permanently closed.

#### **3.5.2.1 TEST RESULTS**

**Figure 3.18** shows the performance comparison; the airflow overshoot is still present but is much shorter in duration, the lack of initial EGR causes a much higher pre-transient airflow. The response is also slightly earlier when no EGR is present. The boost pressure does not overshoot, in fact the boost rise is halted prematurely and the subsequent convergence on the setpoint matches that of the active EGR case. The initial dip in pressure immediately after the fuel step disappears when EGR is inactive.

The transient exhaust manifold pressure is lower and shorter in duration when the EGR is inactive. The turbocharger speed unfortunately cannot be compared due to the speed sensor charge amplifier losing balance during the active EGR transient. The torque trace shows a much faster rise without the sudden jump in torque associated with the release of exhaust pressure and the smoke opacity has improved drastically due to the lack of residuals in the inlet flow immediately prior to the transient.

The EGR valve position demonstrates how the overshoot in airflow can lead to a slight opening of the valve when the EGR system is active, causing a secondary smoke peak, obviously with the EGR inactive, no valve movement occurs. The strategy feature designed to prevent this is clearly insufficient. The VGT vane behaviour is also very different, the more immediate response of inlet manifold pressure results in a faster and much more progressive vane opening. The improved boost response also reduces the fuel limiting as illustrated in the final frame.

### **3.5.3 DRIVE CYCLE TESTING**

Drive cycle tests form the basis of the emissions legislations to which production vehicles must comply. For this reason engine emissions and economy development tends to focus on the operating envelope defined by the cycle and the transient events that occur therein, even

though real world driving is more varied and, as demonstrated by **Farnlund and Bale [77]**, worse than the official fuel consumption and emissions figures suggest. Nevertheless, drive cycle tests are a useful tool in evaluation of engine, control system and component influences on overall vehicle performance.

The drive cycle tests are performed by setting the dynamometer to vehicle simulation mode and handing over clutch, gearchange and fuel control to the EMPS driver emulation system.

To address the slow response of the exhaust gas analysis equipment, a simple signal reconstruction technique has been applied that assumes the analyser response to a step change in the particular emissions species can be described by a first order lag and a time delay. This simple approximation was parameterised using test data, then the resulting equation inverted to give a reconstruction filter for that particular analyser. An example result of this process is shown for the NO<sub>x</sub> measurement in **Figure 3.19**. Other techniques for exhaust gas analysis signal reconstruction have been performed using optimal control [78] and the impulse response of the analyser signals [79].

#### 3.5.3.1 TEST RESULTS

The drive cycle performance over the urban section of the ECE15 cycle is summarised in **Figure 3.20** and **Figure 3.21**. The former describes the general engine performance; speed tracking for both tests is very similar, demonstrating good repeatability from the driver emulation model, though the VNT-O/P equipped engine appears to lag slightly when accelerating. The engine torque and fuel traces are also very similar, with big disturbances occurring at the gearchange points in the cycle.

In **Figure 3.21** the smoke opacity plot shows how smoke peaks occur with both devices around gearchanges and accelerations. The NO<sub>x</sub> concentration trace shows that the VNT-O/P test has slightly higher emissions levels, this corroborates the difference in EGR levels seen in the steady state modal tests. The VNT-O/P has a tendency to deliver slightly higher boost and airflow.

The same performance comparisons are given for the extra-urban section of the cycle in **Figure 3.22** and **Figure 3.23**. Again the vehicle speed for both tests shown in **Figure 3.22** displays good tracking behaviour. However, examining the fuel demand traces shows a difference between VGT and VNT-O/P at higher vehicle speeds (hence engine loads), the VNT-O/P requiring slightly higher fuel quantities to achieve the same torque. This can be traced back to the higher exhaust back pressure experienced with this device.

A significant difference in NO<sub>x</sub> emissions can be seen in **Figure 3.23**, the VNT-O/P generating more as a result of higher fuelling and lower EGR rates. The differences between airflows and boost pressures for the two devices also increases with vehicle speed.

### **3.6 SUMMARY OF RESULTS**

From the variety of different engine tests that have been performed a clear picture of the principal issues in turbocharged Diesel engine emissions and performance, both statically and dynamically, can be drawn. The steady state settings of system parameters such as EGR and VGT positions do not only affect the steady state engine performance but also have a strong influence on the engine behaviour as it moves between these static conditions. This is clearly illustrated by the effect that EGR levels in the steady state have on the tip-in transient performance of the engine (section 3.5.2) Careful consideration must therefore be made when designing target settings for the systems to achieve for example, NO<sub>x</sub> reduction, as high EGR rates inevitably lead to compromised dynamic performance.

These tests have illustrated how different turbocharging systems can significantly alter the performance of the engine as a whole. The swivelling vane VGT turbocharger gives better steady state emissions and fuel consumption performance when compared to the sliding nozzle VNT-O/P device, primarily due to lower exhaust backpressures and better matched compressor delivery. However dynamically the VGT suffers from a strong non-linearity in the mechanical vane-actuator system that results in poor dynamic performance and controllability as demonstrated in section 3.5.1, even though the actual turbocharger dynamics (i.e. boost and airflow response rates) are better than those of the VNT-O/P device.

The control strategy also has an important influence on the system performance, in particular, the use of independent control loops for EGR and VGT can lead to undesirable dynamic phenomenon. For example, the EGR valve opening during a large step increase in fuelling results from the EGR system being unaware that the turbocharger has overboosted in response to a large tip-in transient. Although much of the non-linearities of the engine system have been accounted for in the control strategy through gain scheduling, certain significant non-linearities are not addressed such as the VGT vane actuation mechanism response. As seen in the 2500rev/min tip-in transient scenario (section 3.5.1), the PI controller in its current configuration cannot compensate effectively the vane mechanism non-linearity and the resultant boost control is poor. It is clear that although the experimental engine tested here is a highly developed and optimised system, there is still room for improvement.



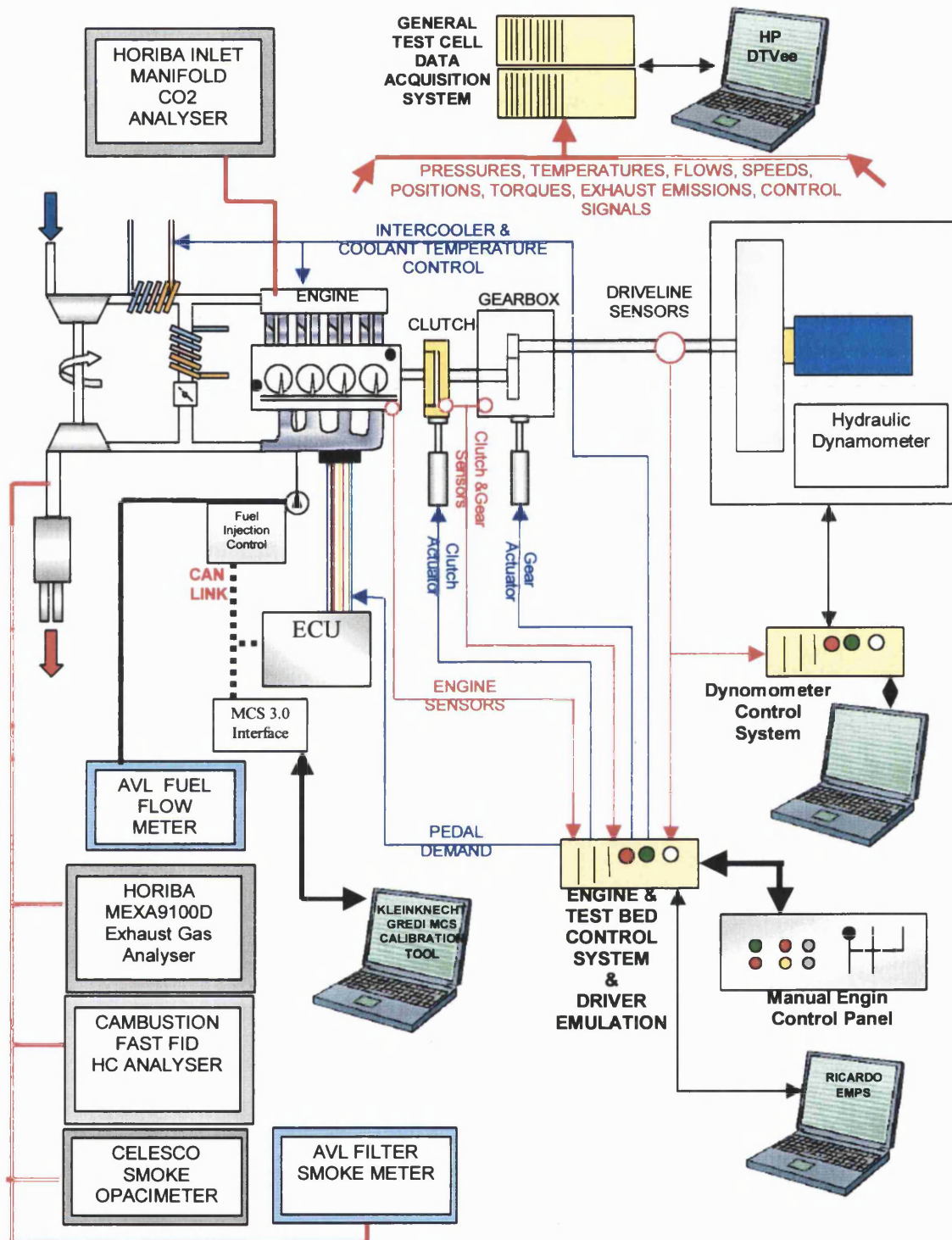


Figure 3.1 Schematic representation of dynamic engine test facility

FORD PUMA CP4 VGT / VNT-OP  
 Modal Comparison of VGT and VNT-OP

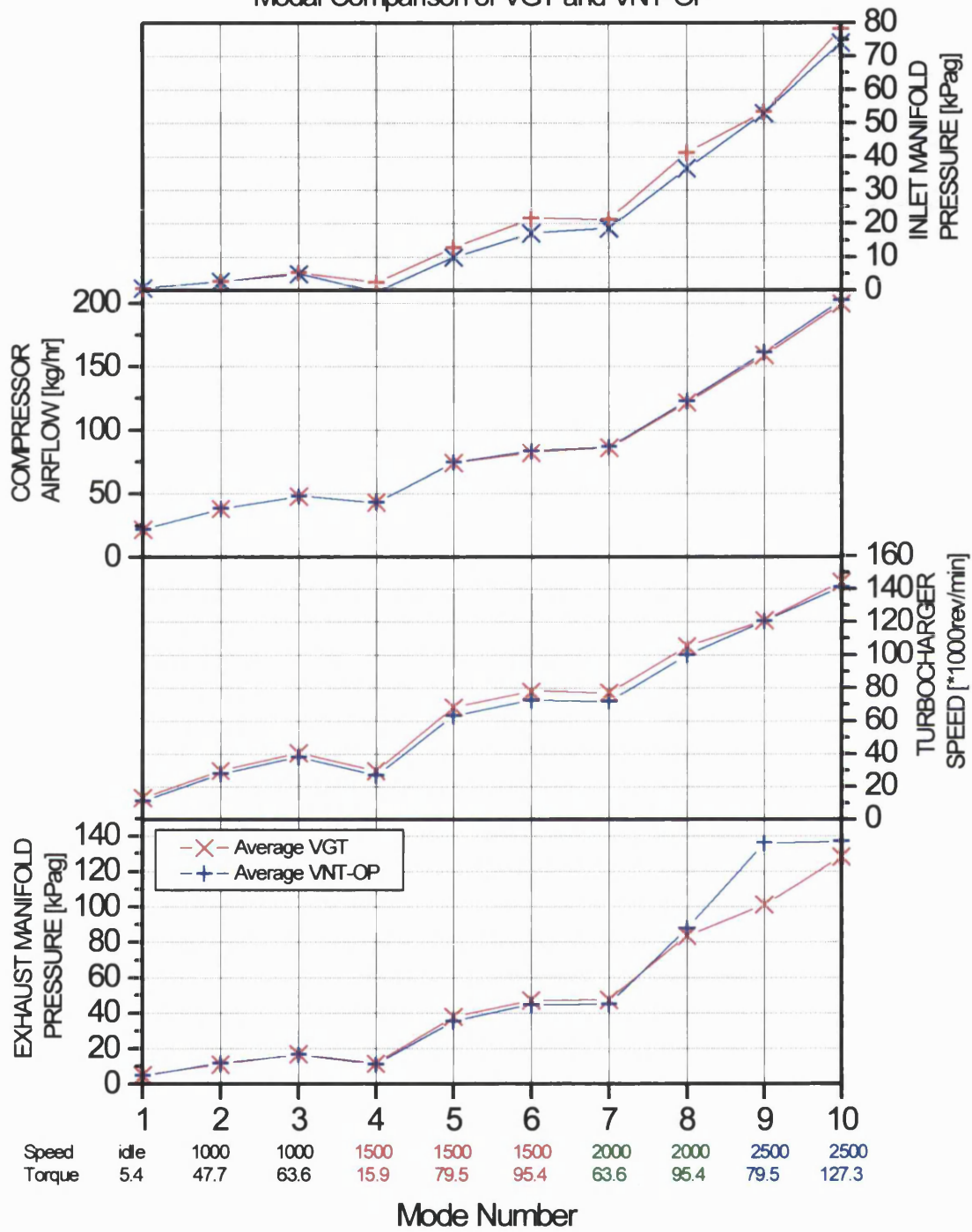


Figure 3.2 Modal test results: Boost, Airflow, Turbocharger Speed and Exhaust Pressure

FORD PUMA CP4 VGT / VNT-OP  
 Modal Comparison of VGT and VNT-OP

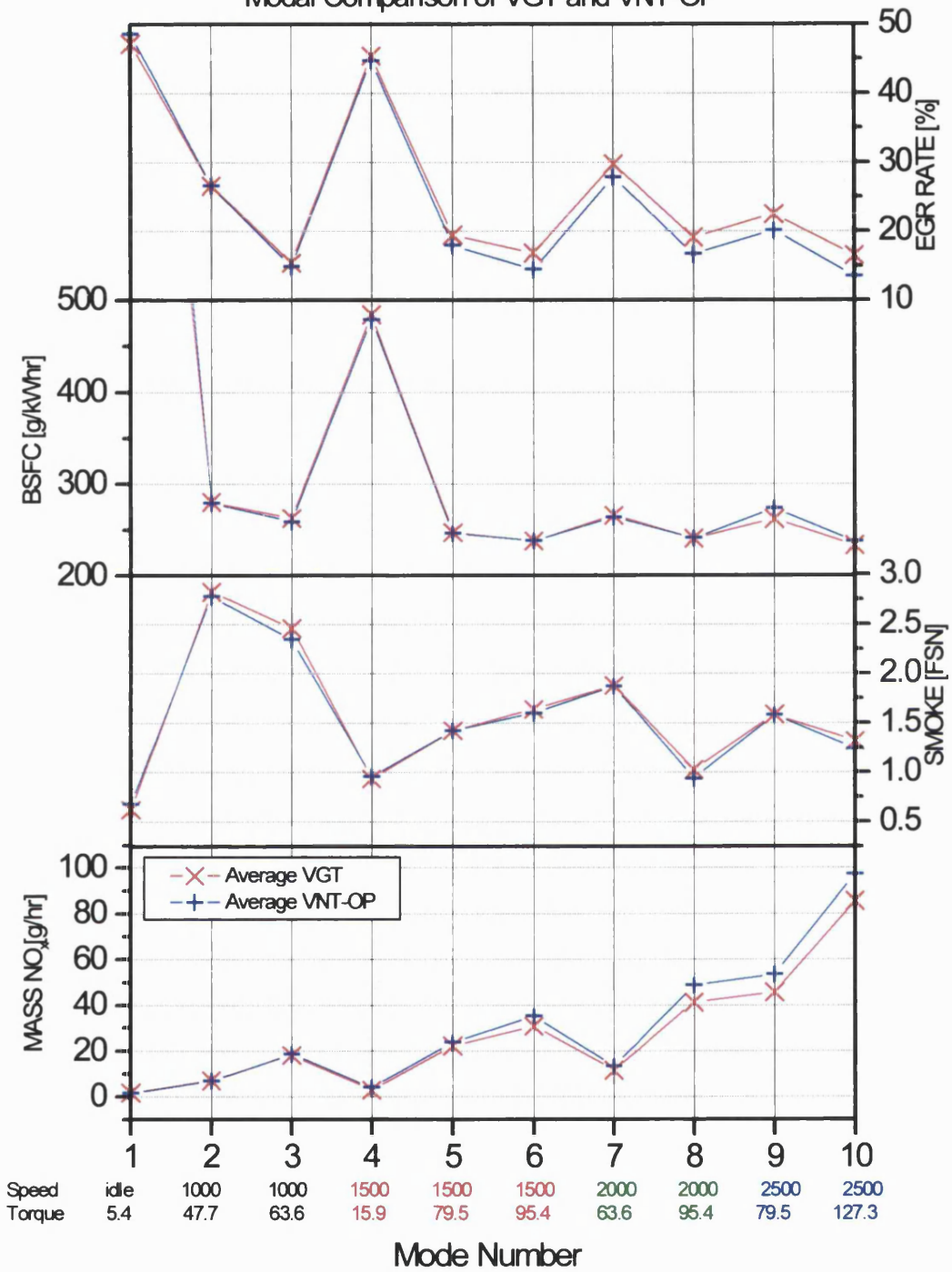


Figure 3.3 Modal test results: EGR rate, BSFC, Smoke, Mass NO<sub>x</sub>

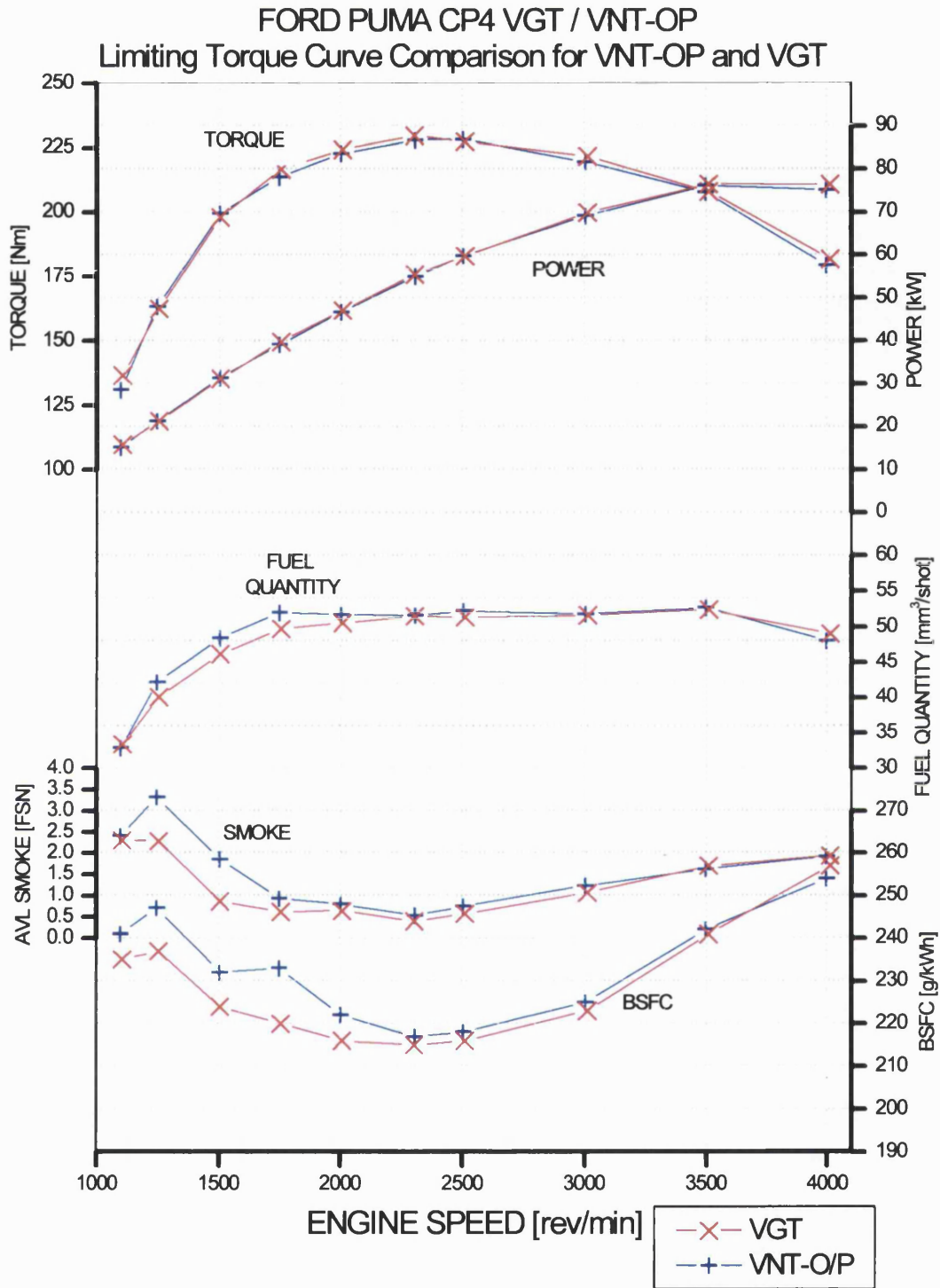


Figure 3.4 Limiting Torque Curve results: Torque, Power, Fuelling, Smoke, BSFC

FORD PUMA CP4 VGT / VNT-OP  
Limiting Torque Curve Comparison for VNT-OP and VGT

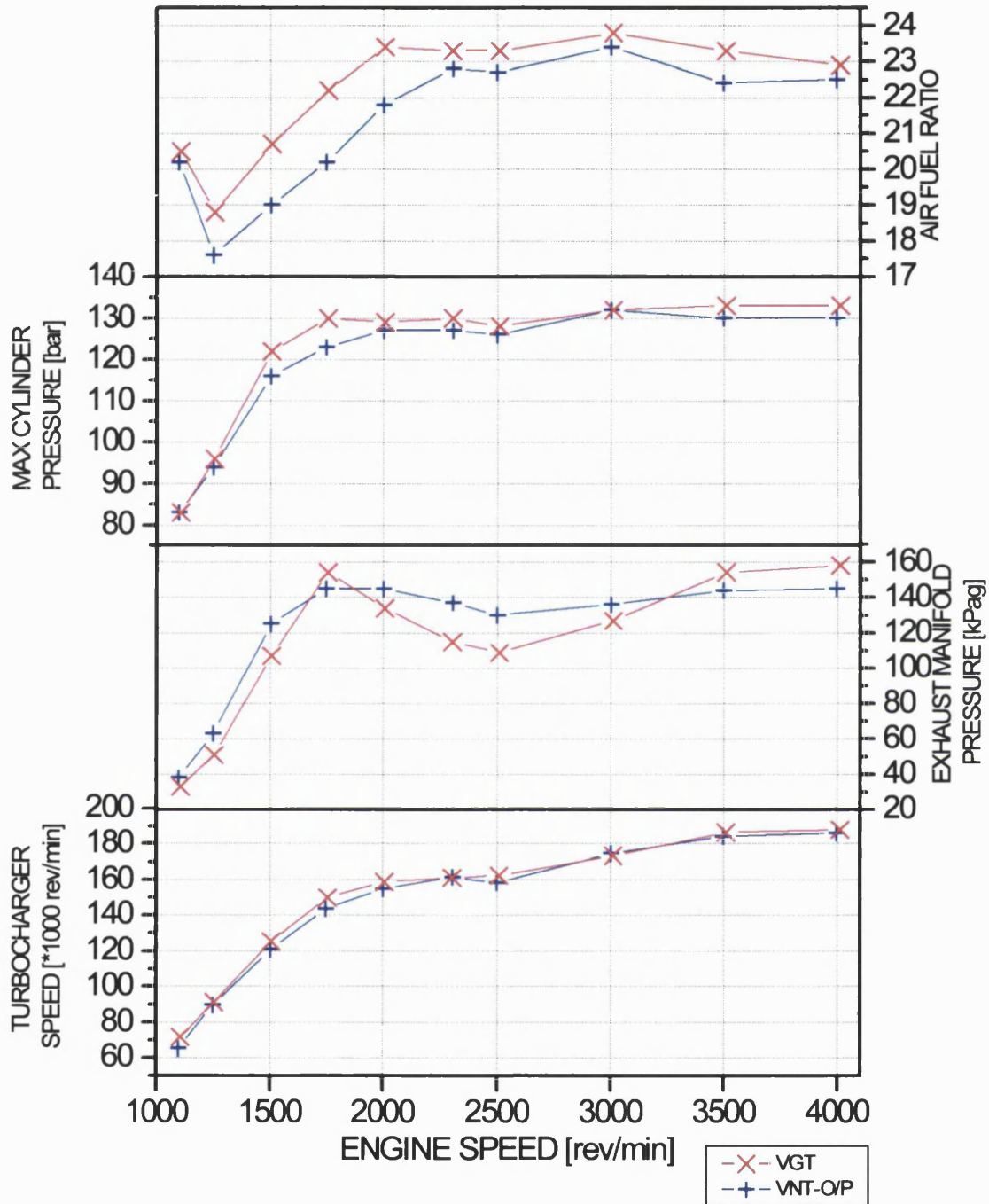


Figure 3.5 Limiting Torque Curve results: Air Fuel Ratio, Cylinder Pressure, Exhaust Pressure, Turbocharger speed

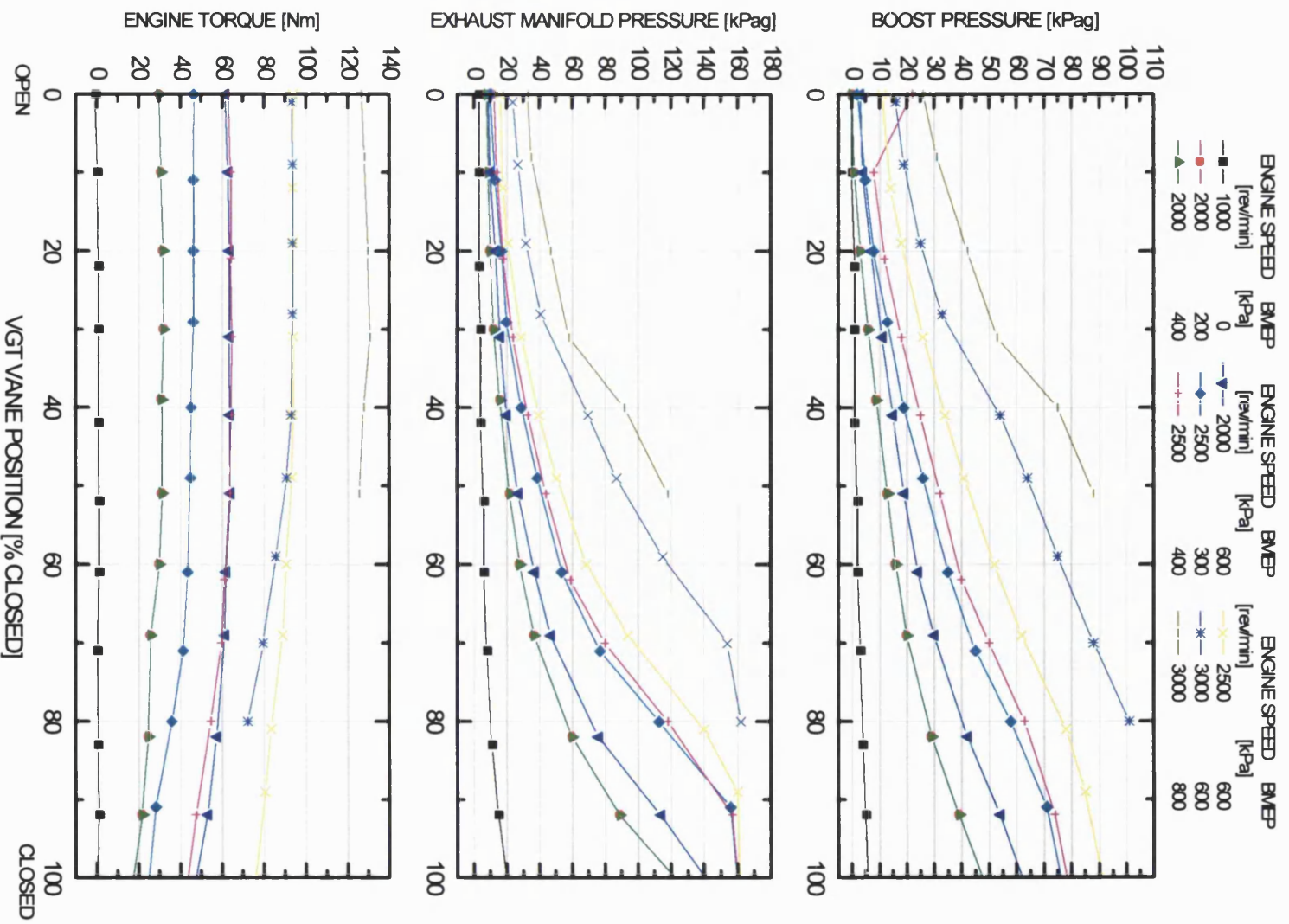
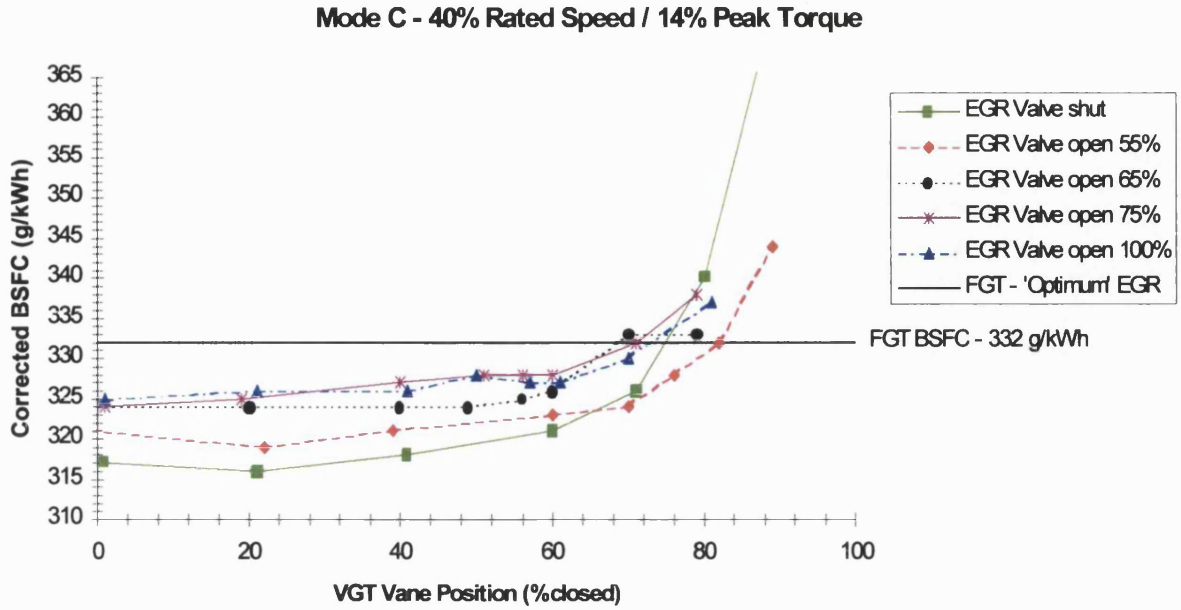
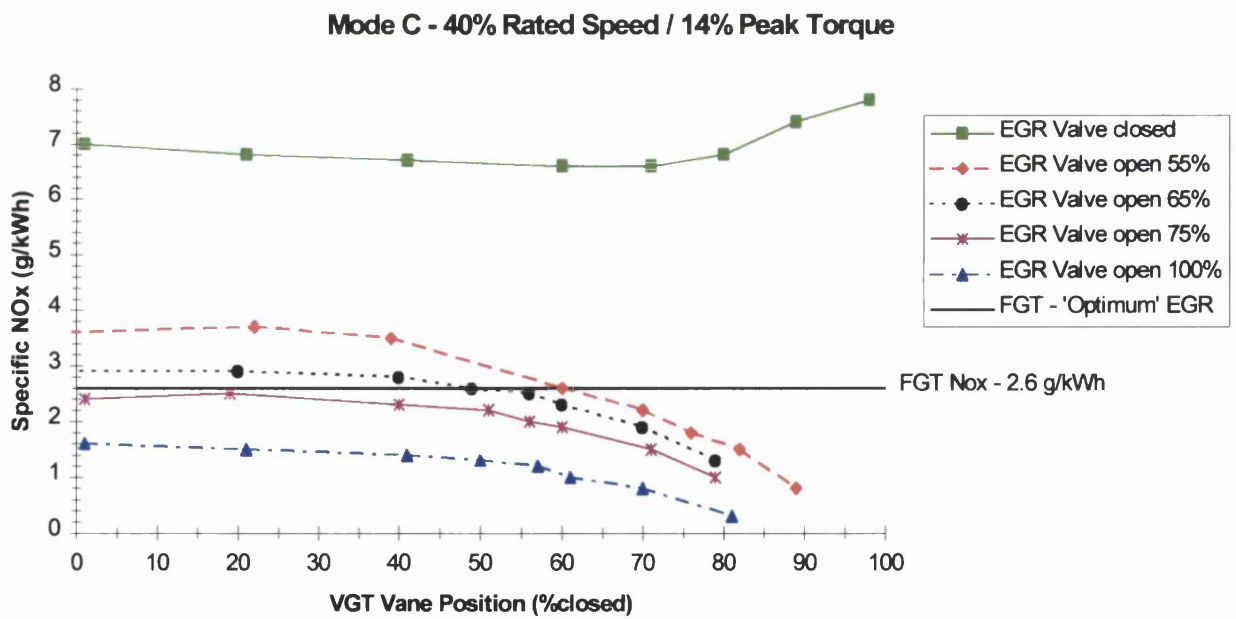


Figure 3.6 VGT sweep with EGR valve closed: Boost, Exhaust Pressure and Torque



**Figure 3.7 Brake Specific Fuel consumption variation with EGR and VGT setting**  
(Pease et al [76])



**Figure 3.8 Specific NO<sub>x</sub> emissions variation with EGR and VGT setting** (Pease et al [76])

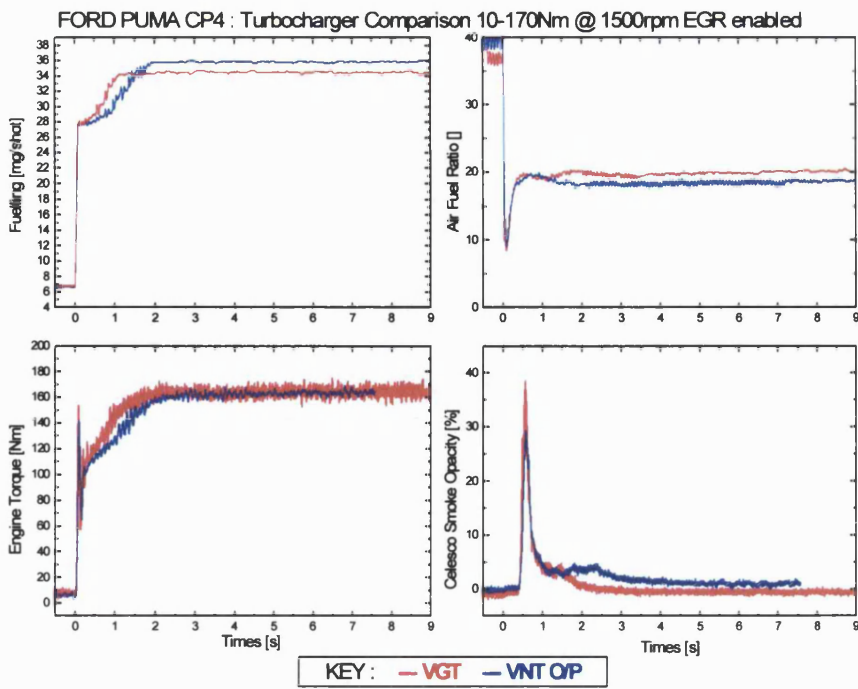


Figure 3.9 1500 rev/min fuel step transient – Engine Performance Parameters

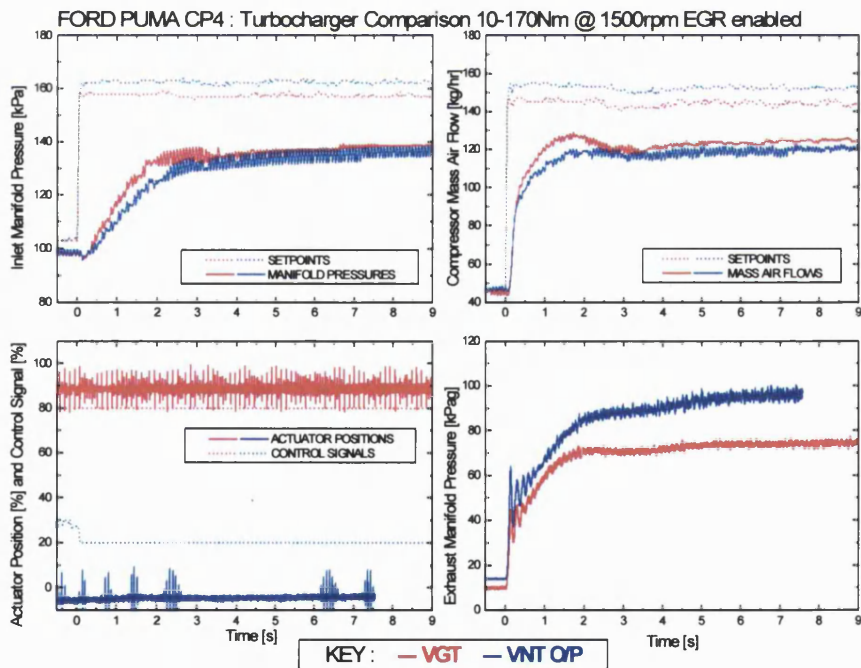


Figure 3.10 1500 rev/min fuel step transient - Turbocharger Physical Parameters



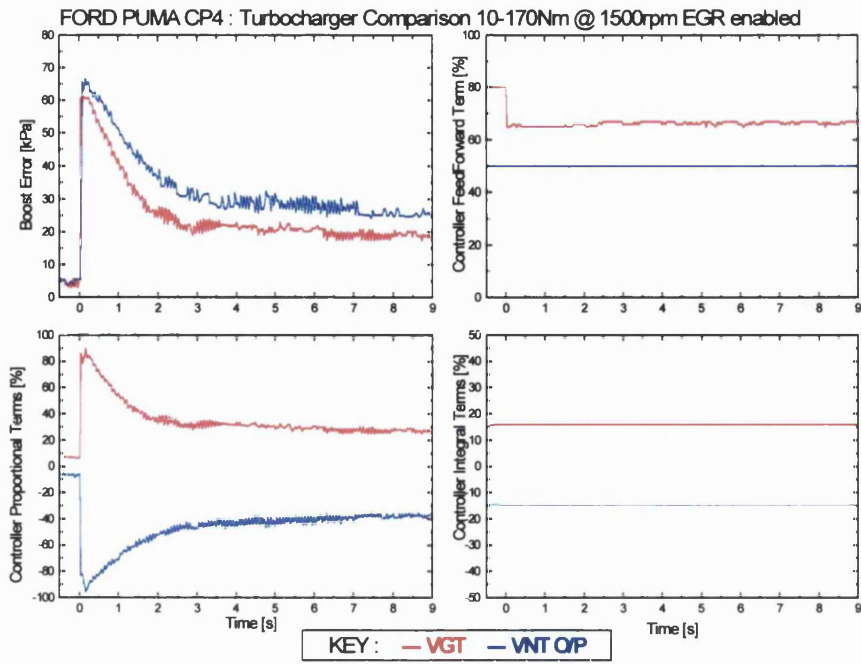


Figure 3.11 1500 rev/min fuel step transient - Engine Control Parameters

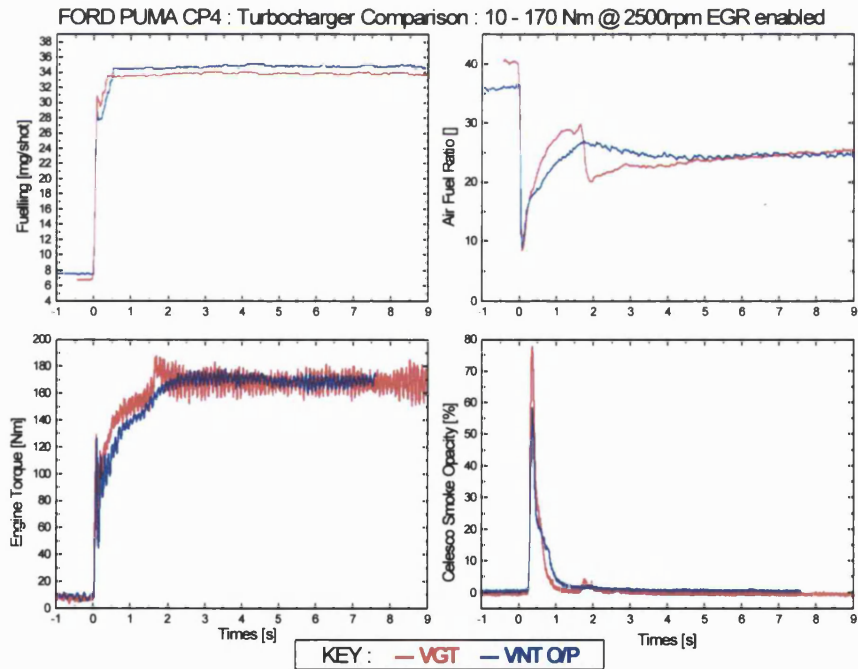


Figure 3.12 2500 rev/min Fuel step transient – Engine Performance Parameters

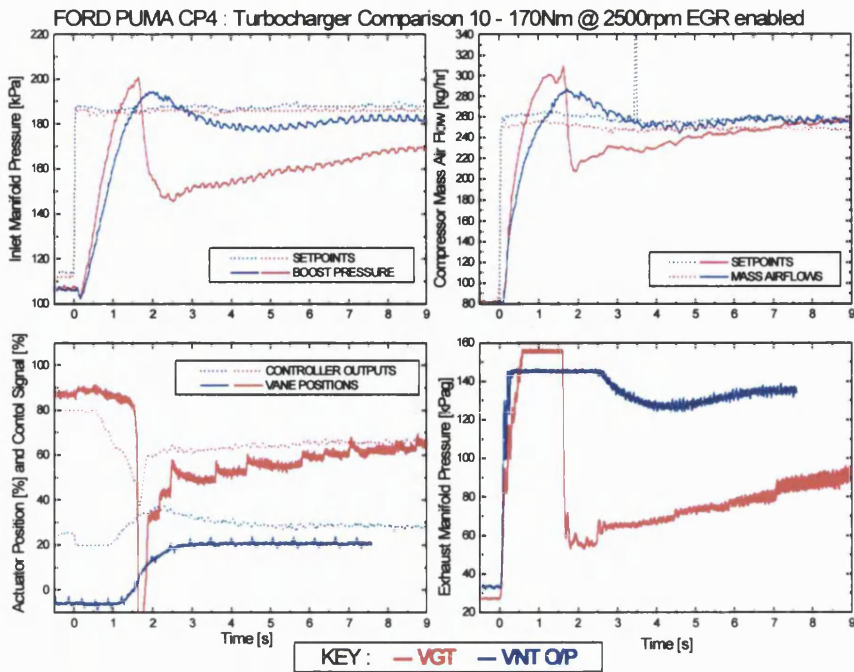


Figure 3.13 2500 rev/min Fuel step transient - Turbocharger Physical Parameters

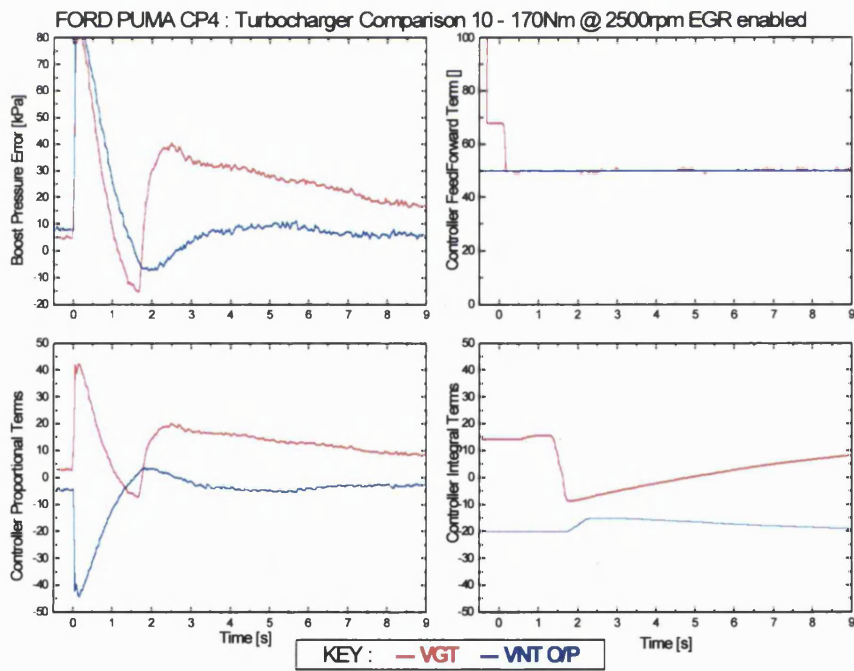


Figure 3.14 2500 rev/min Fuel step transient - Engine Control Parameters

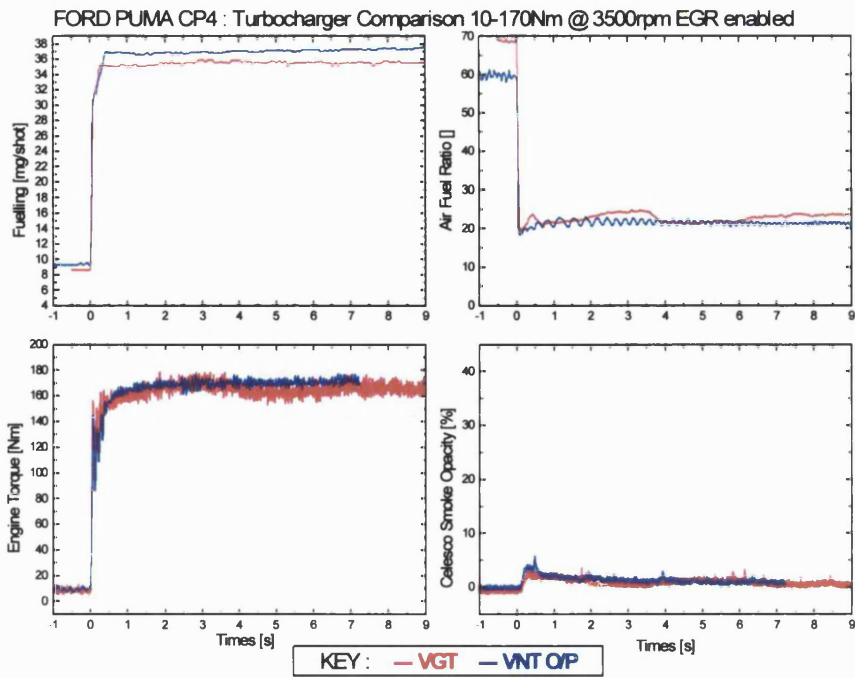


Figure 3.15 3500 rev/min fuel step transient – Engine Performance Parameters

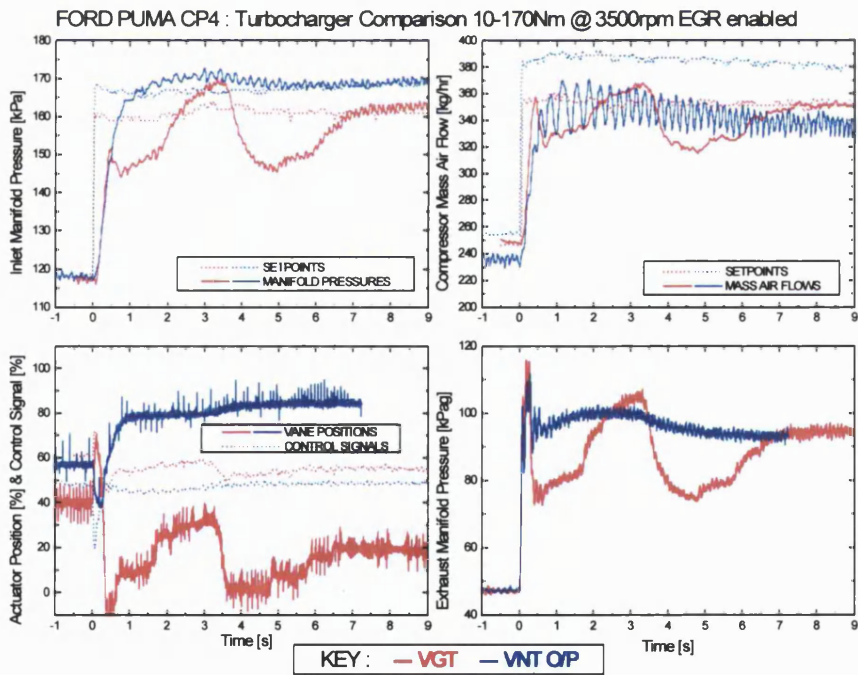


Figure 3.16 3500 rev/min fuel step transient - Turbocharger Physical Parameters

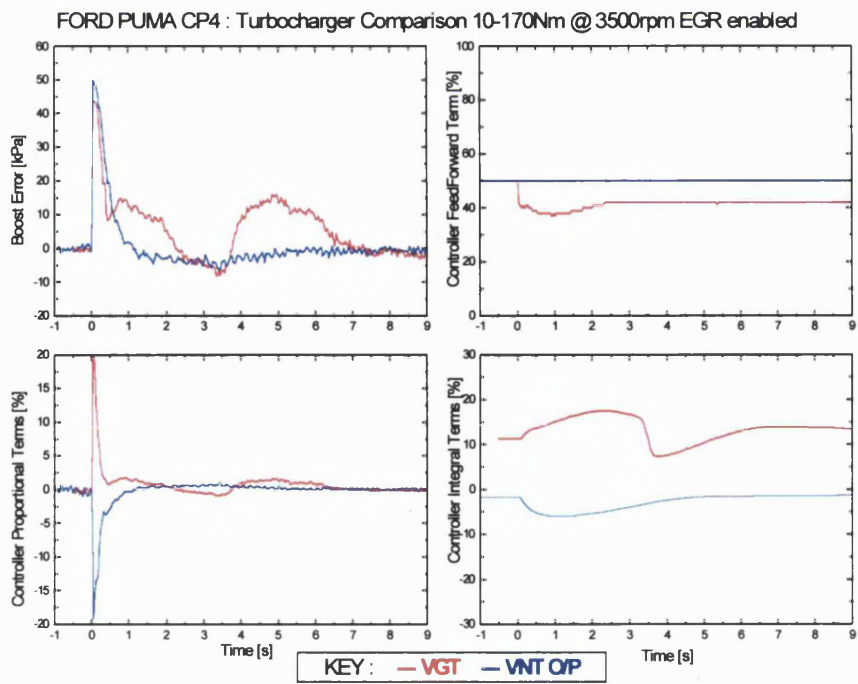
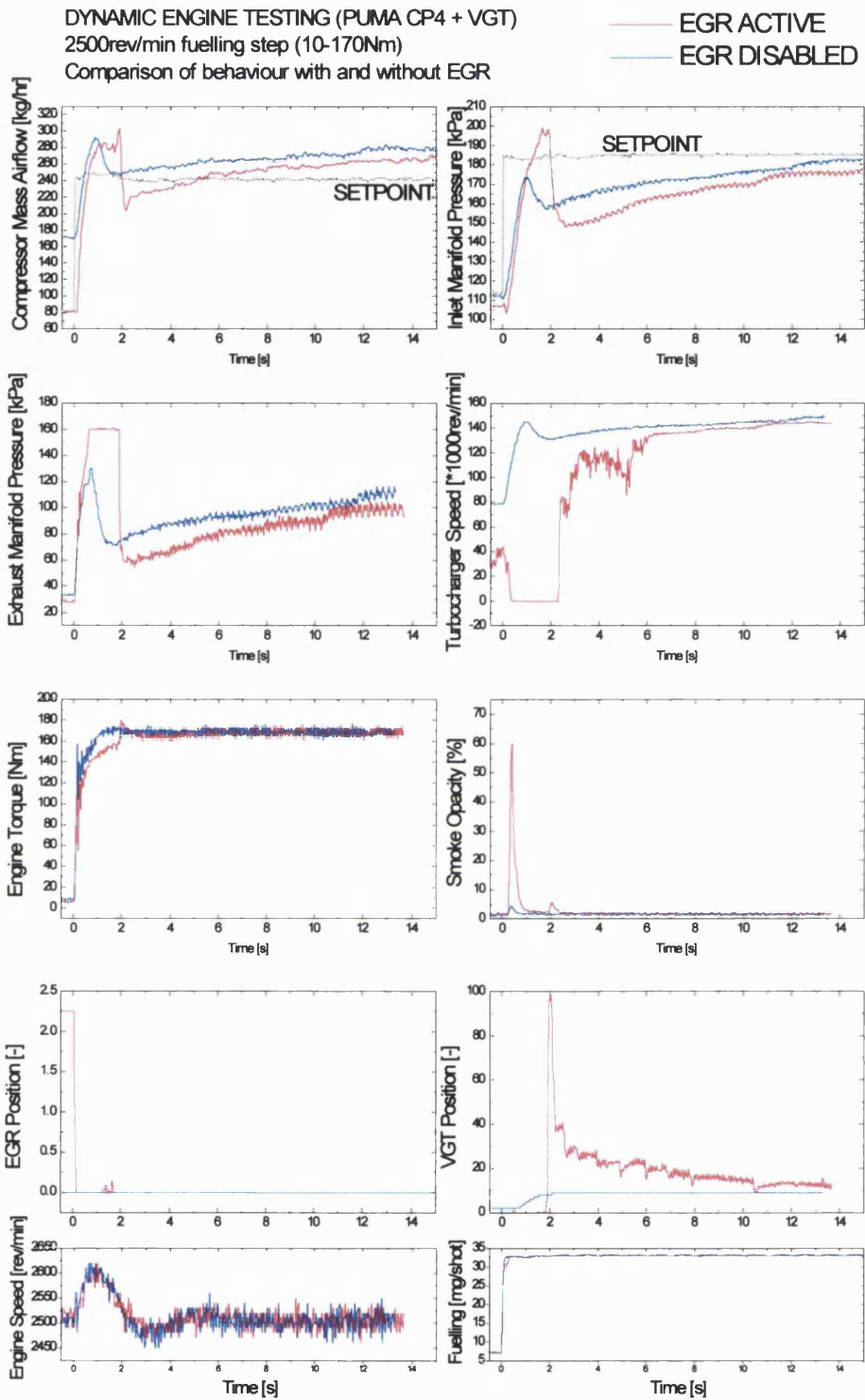
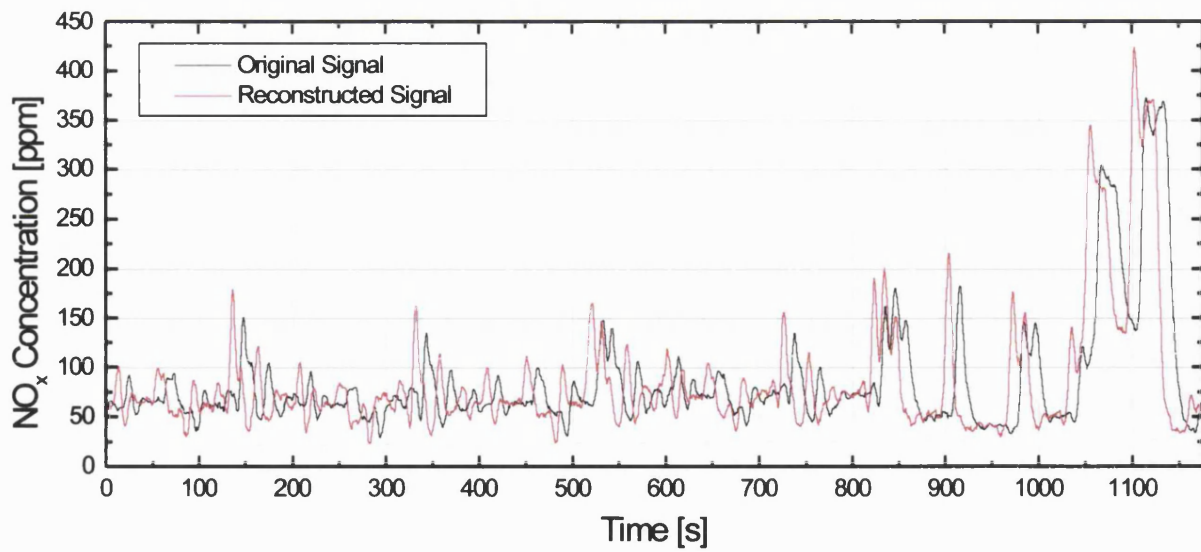


Figure 3.17 3500 rev/min fuel step transient - Engine Control Parameters



**Figure 3.18 Comparison of fuel step transient response at 2500 rev/min for VGT turbocharger with and without the EGR system active**



**Figure 3.19 Exhaust gas analyser signal reconstruction**

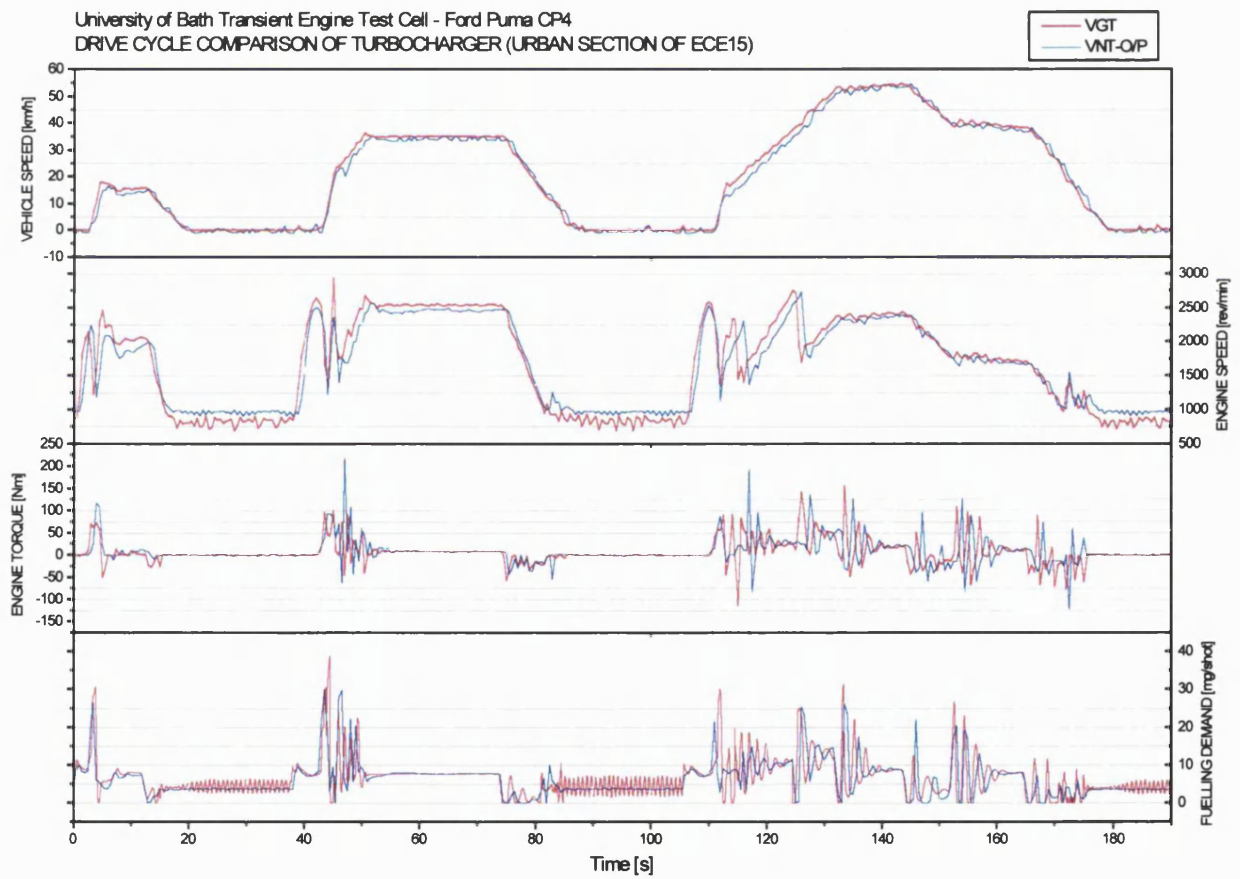


**Figure 3.20 Drive cycle performance (Urban section of ECE15 cycle)**

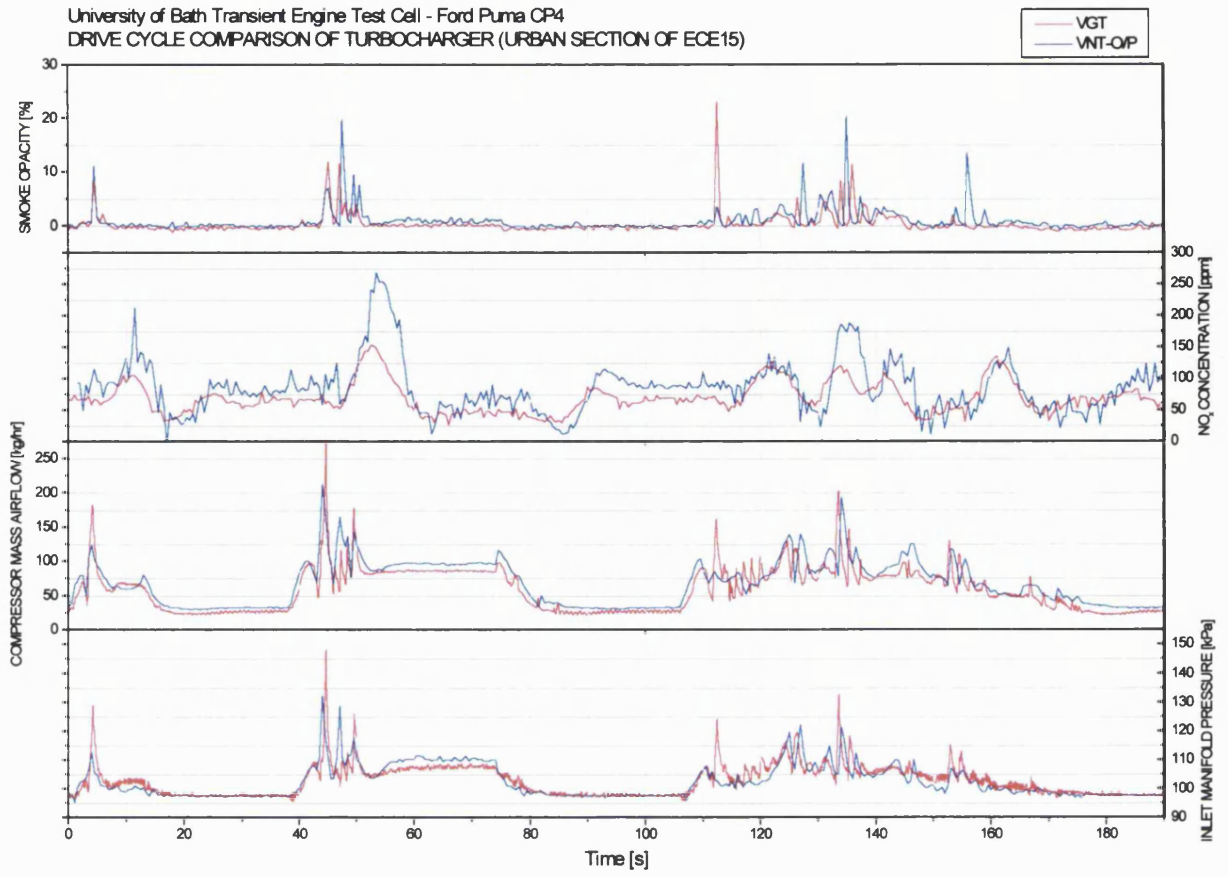


**Figure 3.21 Drive cycle performance (Urban section of ECE15 cycle)**

University of Bath Transient Engine Test Cell - Ford Puma CP4  
DRIVE CYCLE COMPARISON OF TURBOCHARGER (EXTRA-URBAN SECTION OF ECE15)

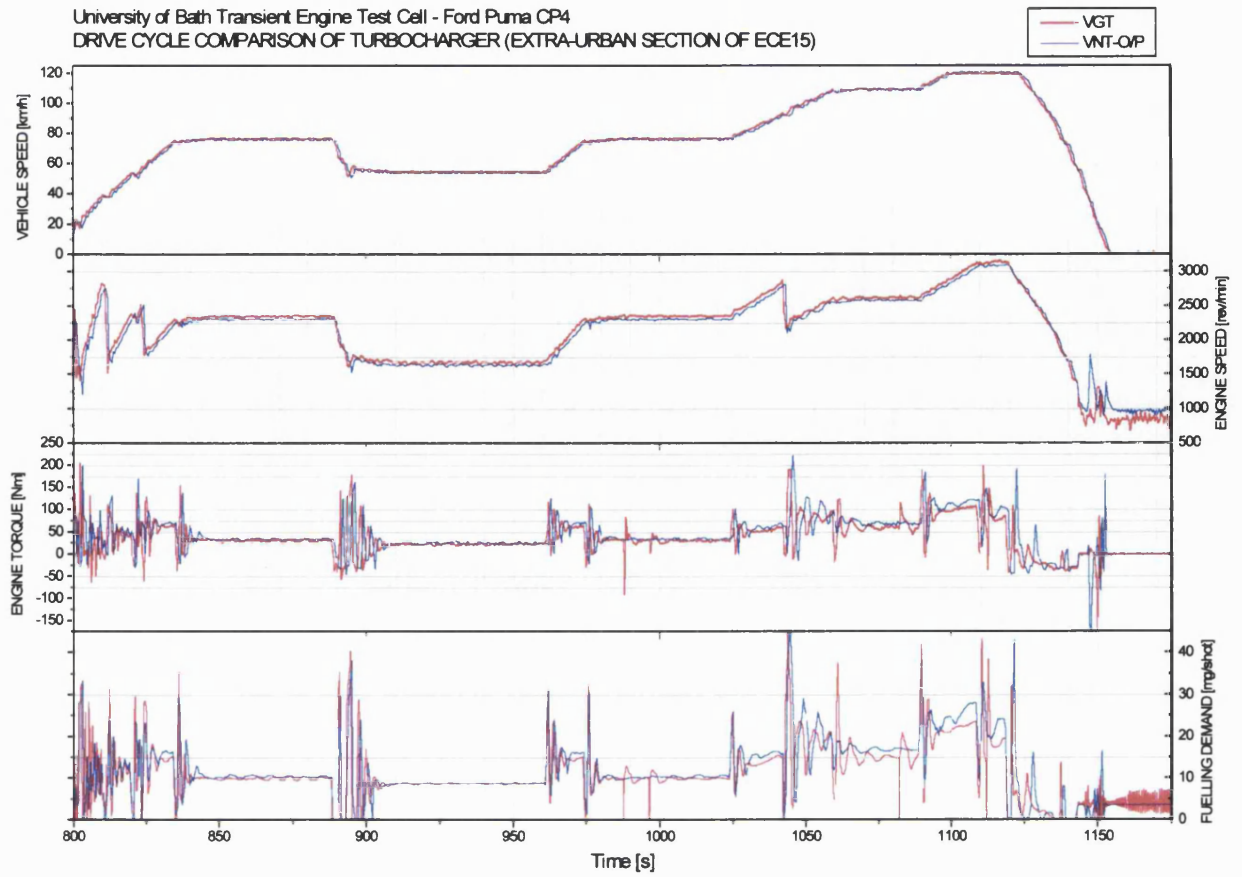
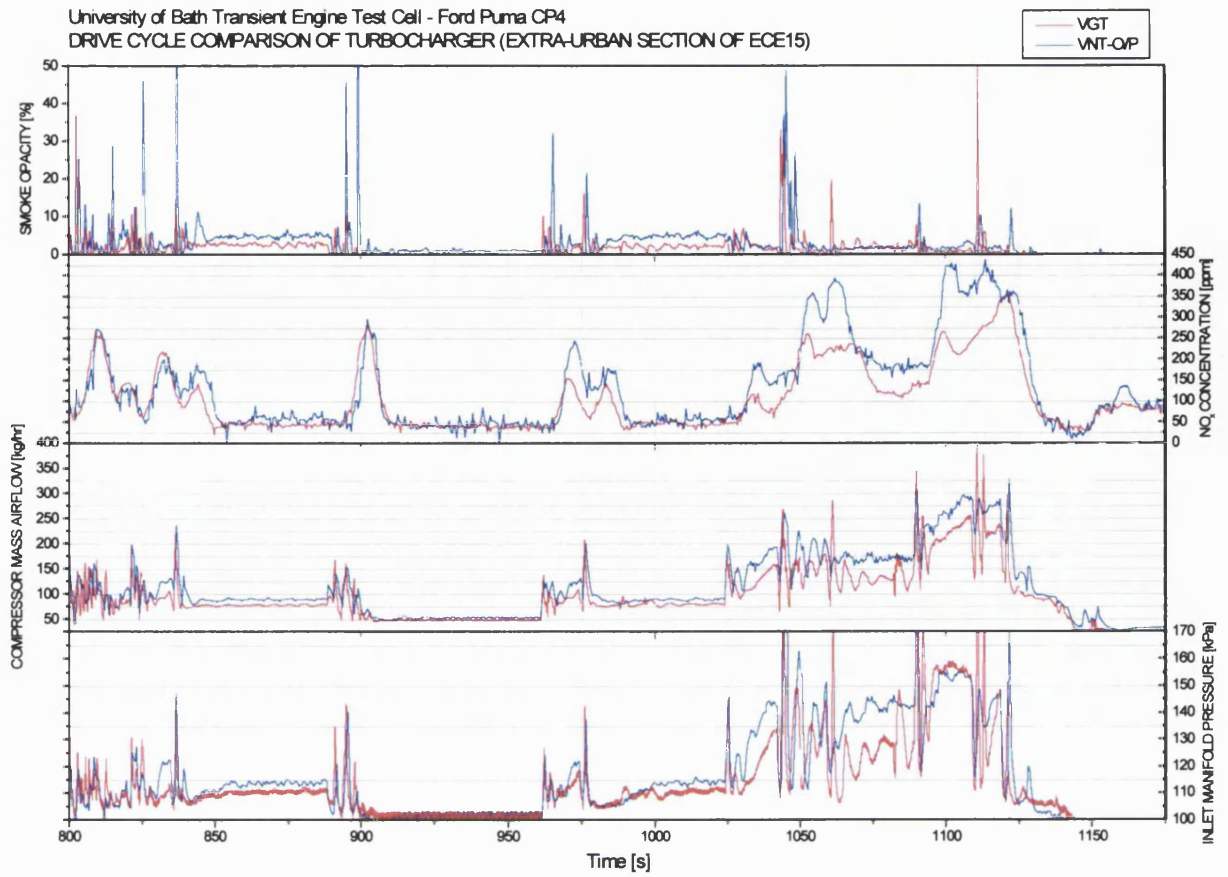


Figure 3.22 Drive cycle performance (Extra-Urban section of ECE15 cycle)





**Figure 3.23 Drive cycle performance (Extra-Urban section of ECE15 cycle)**

## Chapter 4 DYNAMIC ENGINE SIMULATION

### 4.1 INTRODUCTION

In this chapter the engine model used in this study is introduced; it was made available by the Ford Motor Company and as such has already been described in several publications. A general overview of the basic equations and modelling techniques used in its construction are given, followed by a description of additional elements developed to complement and enhance the model.

The model and its additional components are validated against transient engine test bed data outside of the range already used to validate the basic model. The general accuracy and limitations of the model are discussed and it is concluded that although certain transient phenomena can be misrepresented, in general the complete model is a very useful tool for control system design.

### 4.2 Modelling for Control

The ability to design and evaluate new control strategies in a simulation environment rather than on the physical system itself allows large savings to be made in development times and costs for new control systems. This single factor has revolutionised control system design, at least in the automotive industry, over the period of the last few years. Although engine simulations have been available since the early 1980's, it is only recently that they have arrived at a level of compactness, computational efficiency and accuracy - in combination with increased computational power from PC's - suitable for widespread use in control systems rapid-prototyping.

The models used for this purpose are principally of the Mean Value type, they simulate engine behaviour averaged over several cycles (hence the 'Mean Value'), which for most cases is sufficient resolution, however certain systems such as fuel injection controllers require cycle by cycle and even crank angle resolution. Mean Value models are compact enough to be used within control algorithms as demonstrated by **Pilley et al [80]**, it is therefore possible to model the engine and then take the model or certain elements of it to use in the control strategy itself.

The Mean Value method treats manifolds as lumped control volumes and the engine as effectively a gas pump; the manifold properties can be determined through the perfect gas relationships. The system dynamics are governed by a minimal selection of non-linear

differential equations for the physical processes that dominate engine performance; manifold filling and emptying, turbocharger rotor acceleration and crankshaft acceleration.

Due to the importance of this modelling technique to the automotive industry, Mean Value engine simulations for both compression ignition and spark ignition are well represented in the literature, the reader requiring a more in-depth analysis of such models is referred to any of the following references: general Mean Value engine models [81,82,83], Diesel engine models [84,85,86] and specifically Variable Geometry Turbocharged Diesel engine models [21,34].

Mean Value models generally do not capture wave effects in the modelling of the gas dynamics; **Chevalier et al [87]** demonstrate that such effects have important influences on transient accuracy of spark ignition throttle flow models, particularly at low engine speeds. **Fredriksson [33]** and **Payri et al [88]** introduce a pulse compensation factor for turbocharged Diesel engine models to accommodate for the fact that exhaust gas flow is not steady but pulsating. A simple modification such as this allows the model to retain a lower level of complexity whilst representing better the real-life system behaviour.

From the literature the important aspects of engine modelling that must be remembered when using such methods for control design are that the level of accuracy represented by a model is a trade-off with execution times, model development times and model complexity. The model is only as good as the validation data used to create it, and care should be taken when using the model to extrapolate engine behaviour.

### **4.3 FORD PUMA 2.0 LITRE VGT DIESEL ENGINE MODEL**

The model used in this study has been provided by the Ford Motor Company. It has been used in various forms and under different software environments in several other works [25,34,35,36,39], the version used here runs in the MATLAB / Simulink environment on a PC platform.

The design of the model is modular; this allows changes due to different engine configurations to be easily implemented. The top level of the Simulink model is shown in **Figure 4.1**, illustrating the main elements of the overall model. The model is a combination of analytical equations for the gas dynamics and mechanics of the engine system, combined with steady-state maps of the non-linearities such as the compressor and EGR valve flow characteristics. These maps are represented using polynomial regressions, which are equations that may be a function of several variables. This method is preferable to the more common (and less complex) look-up table method, as the functions are continuously

differentiable, thus free from discontinuities that will slow down the solver and even cause completely erroneous results. Each section of the model is described below.

#### 4.3.1 INLET, COMPRESSOR, INTERCOOLER AND EGR

For the sake of convenience and retaining physical correlation with the real system, the inlet manifold, compressor, intercooler and EGR valve subsystems are grouped together. The inlet manifold is described by three system states; inlet manifold gas mass, inlet manifold pressure and inlet manifold burnt gas fraction.

The inlet manifold mass is the result of a flow balance performed on the gas flows to and from the inlet manifold, given by **Equation (4-1)**. The pressure is derived from an enthalpy balance given in **Equation (4-2)**, backflow from inlet manifold to exhaust is ignored as are heat transfer effects therefore  $\dot{Q}_i=0$ . The inlet manifold burnt gas density fraction is derived from a burnt gas flow balance described by **Equation (4-3)**. Inlet manifold temperature is calculated as function of pressure and mass via the perfect gas law (see **Equation (4-4)**).

$$m_i = \int (W_{ci} + W_{xi} - W_{ie}) dt \quad (4-1)$$

Where  $m_i$  is the inlet manifold mass content  
 $W_{ci}$  is the compressor airflow  
 $W_{xi}$  is the EGR flow from exhaust to inlet  
 $W_{ie}$  is the total flow into the cylinders

$$p_i = \int \frac{\gamma R}{V_i} \left( W_{ci} T_{ci} + W_{xi} T_{xi} - W_{ie} T_i - \frac{\dot{Q}_i}{c_p} \right) dt \quad (4-2)$$

Where  $p_i$  is the inlet manifold pressure  
 $T_{ci}$  is the compressor airflow temperature  
 $T_{xi}$  is the EGR flow temperature  
 $T_i$  is the inlet manifold temperature  
 $V_i$  is the inlet manifold volume  
 $R$ ,  $c_p$  &  $\gamma$  are gas properties

$$F_i = \int \left( \frac{W_{xi} (F_x - F_i) - W_{ci} F_i}{m_i} \right) dt \quad (4-3)$$

Where  $F_i$  is the inlet manifold burnt gas fraction  
 $F_x$  is the exhaust manifold burnt gas fraction

$$T_i = \frac{p_i V_i}{m_i R} \quad (4-4)$$

The compressor is modelled as a steady state map derived from the turbocharger manufacturers' pressure versus flow data. This model is mass flow driven, that is the system pressures are calculated as functions of the mass flows, therefore the compressor model provides a mass flow output based on turbo charger speed and inlet manifold pressure. The modelling uses a technique called the Zero Slope Method (as described by **Moraal and Kolmanovsky [60]**) to represent the different regions of the compressor map with different continuous functions; the compressor characteristic is difficult to approximate with one continuous function.

The intercooler is modelled as a static function of effectiveness against the compressor delivery conditions, however due to a lack of suitable validation data the intercooler model is not used.

The EGR flow is calculated using the equation for compressible flow through an orifice, see **Equation (4-5)**. The flow is a function of inlet and exhaust manifold pressures, exhaust temperature and EGR valve position. The flow area is treated as a static function of the EGR valve position and upstream and downstream pressures. An EGR cooler is also modelled, using a static effectiveness function to calculate the temperature drop assuming constant coolant temperature.

$$W_{xi} = A_{eff}(x_{EGR}, p_i, p_x) \frac{p_x}{\sqrt{RT_x}} \Psi\left(\frac{p_i}{p_x}\right) \quad (4-5)$$

Where  $A_{eff}(x_{EGR}, p_i, p_x)$  is the effective valve area  
 $x_{EGR}$  is the EGR valve position  
 $\Psi(p_i/p_x)$  is the flow function

### 4.3.2 CYLINDERS

The engine cylinder block models the engine pumping, the combustion heat release, torque production and the exhaust emissions. The speed density relationship is used to evaluate the mass flow into the cylinders from the inlet manifold as shown in **Equation (4-6)**. The volumetric efficiency is modelled as a static function of engine speed, inlet and exhaust pressures and temperatures.

$$W_{ie} = \frac{N_{eng} * n_{cyl} * V_{swept} * \rho_{ie} * \eta_{vol}}{60 * n_{stroke}}$$

(4-6)

Where  $N_{eng}$  is the engine speed  
 $n_{cyl}$  is the number of cylinders  
 $V_{swept}$  is the swept volume per cylinder  
 $\rho_{ie}$  is the inlet manifold density  
 $\eta_{vol}$  is the volumetric efficiency  
 $n_{stroke}$  is the number of strokes per cycle

Heat release is modelled as the temperature rise due to combustion, this is a static function of engine speed, fuel flow, injection timing, exhaust and inlet flows, inlet temperature and burnt gas fraction.

The cylinder section of the model contains one state variable, engine speed. It is a function of the engine torque, load torque and the associated inertias, see **Equation (4-7)**. Engine brake torque is given by a static function of several variables, with modifiers based on air fuel ratio, engine speed and inlet manifold pressure.

$$N_{eng} = \frac{1}{(J_{eng} + J_{driveline})} \int (Tq_{brake} - Tq_{load}) dt$$

(4-7)

Where  $Tq_{brake}$  is the brake engine torque  
 $Tq_{load}$  is the engine load  
 $J_{eng}$  is the engine inertia  
 $J_{driveline}$  is the driveline inertia

A model of the exhaust gas emissions is included; the important (i.e. legislated emissions) are modelled using polynomial regressions that map in-cylinder conditions to tailpipe emissions.

### 4.3.3 EXHAUST MANIFOLD AND TURBINE

As was the case for the inlet manifold, the exhaust manifold is modelled by three system states, the manifold gas mass, pressure and burnt gas fraction. These are calculated in the same manner as for the inlet manifold as shown in **Equations (4-8) to (4-10)**. Heat transfer is ignored in the exhaust manifold, therefore  $\dot{Q}_x = 0$  in **Equation (4-9)**; this is still valid even though heat transfer is important in the exhaust manifold because the static function used to describe the exhaust temperature includes the (steady state) heat transfer taken from experimental results.

$$m_x = \int (W_{ex} - W_{xi} - W_{xt}) dt \quad (4-8)$$

Where  $m_x$  is the exhaust manifold mass content  
 $W_{ex}$  is the flow from cylinders to exhaust  
 $W_{xt}$  is the flow through the turbocharger turbine

$$p_x = \int \frac{\gamma R}{V_x} \left( W_{ex} T_{ex} - W_{xi} T_{xi} - W_{xt} T_{xt} - \frac{\dot{Q}_x}{c_p} \right) dt \quad (4-9)$$

Where  $p_x$  is the exhaust manifold pressure  
 $T_{ex}$  is the cylinder to exhaust manifold flow temperature  
 $T_{xt}$  is the turbine flow temperature  
 $V_x$  is the inlet manifold volume

$$F_x = \int \left( \frac{F_{ex} W_{ex} - F_x (W_{xi} + W_{xt})}{m_i} \right) dt \quad (4-10)$$

Where  $F_{ex}$  is the burnt gas flow fraction from the cylinders to the exhaust manifold

The turbocharger turbine is modelled as a static function of turbine mass flow against pressure ratio, turbocharger speed and VGT vane position. The equation for adiabatic nozzle flow is used, with modifications for zero flow pressure ratio and the effective flow area as a function of vane position, pressure ratio and turbocharger speed.

The post turbine pressure is a linear first order dynamic function of turbine flow and post turbine temperature; the dynamic model was derived using system identification from experimental results.

#### 4.3.4 TURBOCHARGER SHAFT

Turbocharger speed is the final state variable of the main engine model, it is calculated from the difference between the power extracted by the turbine and the power consumed by the compressor: the difference results in an acceleration or deceleration of the turbocharger shaft, illustrated in **Equation (4-11)**.

$$N_{turbo} = \frac{91.18907 c_p}{J_{turbo}} \int \left( \frac{\eta_{imech} W_{xt} (T_x - T_{postturb}) - W_{ci} (T_{ci} - T_{amb})}{N_{turbo}} \right) dt \quad (4-11)$$

Where  $N_{turbo}$  is the turbocharger speed  
 $J_{turbo}$  is the turbocharger rotating inertia  
 $\eta_{imech}$  is the mechanical efficiency of the turbocharger turbine  
 $T_{postturb}$  is the post turbine temperature  
 $T_{amb}$  is the ambient temperature

## 4.4 ADDITIONAL SUB-MODELS

### 4.4.1 VGT ACTUATOR AND VANE MODEL

From the experimental characterisation it was apparent that the dynamics of the VGT vane mechanism have an important effect on the overall engine dynamics, it was therefore necessary to develop a suitable system model to improve the fidelity of the simulation. A schematic representation of the VGT vane and actuator mechanism is given in **Figure 4.2**. The PWM signal from the engine control unit drives an Electronic Vacuum Regulator (EVR) that regulates the vacuum level provided by the engine vacuum pump. The actuator consists of a diaphragm with one side exposed to atmospheric pressure, and the other to the regulated vacuum pressure, the difference in pressure across the diaphragm produces a net force. This force is opposed by a return spring (which acts to keep the vanes open for failsafe operation), a velocity dependent friction term and also an aerodynamic term resulting from gas flow over the vanes. This last force is important as it leads to strong non-linearities in the vane behaviour, the force arises due to the exhaust gases changing direction as they travel across the vanes, producing a moment on the pivoting vane mechanism that can either oppose or reinforce the actuator effort depending on the vane position.

A force balance for the mechanism is given below;

$$m_{vgt}\ddot{x}_{vgt} = f_{act} + f_{spring} + f_{friction} + f_{aero} \quad (4-12)$$

Where  $m_{vgt}$  is the equivalent mass of moving parts in the VGT vane and actuator assembly

$\ddot{x}_{vgt}$  is the acceleration of the mechanism

$f_{act}$  is the actuator force

$f_{spring}$  is the actuator force

$f_{friction}$  is the actuator force

$f_{aero}$  is the actuator force

The forces are defined by the following equations:

$$f_{act} = p_{amb}A_1 - p_{vac}A_2 \quad (4-13)$$



$$f_{spring} = -k_1 x_{vgt} \quad (4-14)$$

$$f_{friction} = -k_2 \dot{x}_{vgt} \quad (4-15)$$

$$\begin{aligned} f_{aero} &= k_3 x_{vgt} \\ k_3 &= \varphi(x_{vgt}) \end{aligned} \quad (4-16)$$

where  $p_{amb}$  is the atmospheric pressure  
 $p_{vac}$  the vacuum pressure  
 $A_1$  and  $A_2$  are the areas on either side of the diaphragm  
 $x_{vgt}$  is the VGT position  
 $k_1$  is the spring constant  
 $k_2$  is the coefficient of friction  
 $k_3$  is coefficient for the aerodynamic force on the vanes as a function of VGT position

Substituting the above expressions into **Equation (4-12)** gives the second order non-linear equation of motion for the vane and actuator mechanism:

$$\ddot{x}_{vgt} = \frac{1}{m_{vgt}} \left[ (p_{amb} A_1 - p_{vac} A_2) + (k_3(x_{vgt}) - k_1) x_{vgt} - k_2 \dot{x}_{vgt} \right] \quad (4-17)$$

The Simulink implementation of this model is shown in **Figure 4.3**. The dynamics of the EVR have not been modelled separately but included in the parameterisation of **Equation (4-17)**, the non-linear relationship between control signal and vacuum force is encapsulated in a static look-up table. The aerodynamic force acting on the vanes is derived from a look-up table based on vane position; the data for this table was taken from work presented in [25]. As an additional feature, the backlash in the vane mechanism has been modelled as a dead-band that is only active towards the extremities of the mechanisms travel.

#### 4.4.2 EGR VALVE

Although the EGR valve has non-linear response characteristics, the mechanism that determines this response is considerably less complex than that of the VGT. It was therefore found that a first order lag in combination with a static representation of the non-linearity (in the form of a look-up table) produced representative valve performance.

### 4.4.3 DRIVER MODEL

Although a vehicle and transmission model was supplied with the engine model, it relied on time-series pedal data taken from the test rig being fed into the vehicle model in order to perform drive cycle simulations. To make the model more generic and capable of following arbitrary drive cycles automatically, a driver model was developed.

The driver model uses a proportional plus integral controller on vehicle speed, the drive cycle speed profile is used to generate speed demands, which in combination with feedback of the vehicle speed give a speed error signal. The integral term is a non-linear function of speed error and change of speed error generated by a look-up table. This arrangement was developed from a fuzzy logic feedback controller; the map for the integral action is shown in **Figure 4.4**.

A feedforward term is used which reads ahead the demanded cycle speed and generates a pedal offset proportional to this. An inverse pedal map and acceleration demand were originally implemented in the feedforward path but did not work as effectively as this more simple arrangement. The Simulink diagram for the driver model is shown in **Figure 4.5**.

### 4.4.4 STANDARD CONTROLLER

In order to emulate the performance of the engine as seen on the test facility, a controller for the EGR, VGT and fuelling features was necessary. The controller used in simulation is a simplified version of the full engine control module, the only processing performed on the fuelling quantity is to convert it from a demanded quantity per injection to a continuous fuel flow value. The smoke limited fuelling algorithm has also been reproduced, this limits the fuel flow sent to the engine on the basis of an estimate in inlet manifold gas density.

The EGR and VGT control algorithms consist of proportional plus integral feedback controllers as described in **Chapter 2**. The top level of the Simulink diagram for the controller is shown in **Figure 4.6**.

Signals used by the ECU are discretised at a 16 millisecond sampling interval, gaussian distributed noise is added to these signals to simulate the noise one would expect to find on the real-world signals.

### 4.4.5 DYNAMOMETER MODEL

In order to emulate the constant speed fuel steps used extensively in the experimental survey of the engine, the dynamometer was modelled as a very large inertia and a first order lag. The driveline dynamics were ignored for this work.

The Simulink diagram for the complete model including the additional sub-models is given in **Figure 4.7**.

## **4.5 MODEL VALIDATION**

The basic Puma engine model has been validated by the Ford Motor Company using drive cycle and steady state data: in this section the validation of the entire engine model system including the additional elements described above is discussed. It is well known to users of this model that its validity is limited to an area well away from the boundaries of the operating envelope, many of the dynamic issues uncovered in the experimental work occur during large excursions across the engine operating regime therefore the model is evaluated under the same transient conditions in order to assess its utility in these situations.

### **4.5.1 VGT VANE MECHANISM MODEL VALIDATION**

The sub-model of the VGT vane mechanism was validated using experimental data from a fuel step transient performed at 2500 rev/min between 7 and 34 mg/shot fuelling. With this particular transient, the phenomena of the VGT vanes stagnating and then suddenly opening occurs consistently, therefore it was chosen to test the model as it was exactly this behaviour that it was designed to capture. The VGT vacuum pressure data logged from the experiment was fed into the sub-model and the resulting VGT position logged, the result is shown in **Figure 4.8**. As can be seen, the model captures very well the non-linear behaviour of the real life system, most important is the dead time between the reduction in vacuum and the response of the vanes, the simulated vanes do not open quite as fast or as far as the real system, but the overall representation of the non-linearity is very good. When the turbocharger vanes are operating away from the extremities of their travel, they respond almost linearly to changes in demand, this was also observed with the model.

### **4.5.2 FUEL STEP TRANSIENTS**

For this validation, the large step increases in fuel demand (tip-ins) at three constant engine speeds were simulated using the complete engine model, controller, actuator and dynamometer combination, these results are compared to the experimental results for the same transients.

**Figure 4.9** summarises the performance comparison for a fuel step of 7 to 34 mg/shot at 1500rev/min.

#### *4.5.2.1 AIRFLOW AND BOOST PRESSURE @ 1500 rev/min*

The initial airflow response following the tip-in is slightly faster in simulation than in reality, this phase is dominated by the closure of the EGR valve and the sudden increase in fresh air to make up for the sudden decrease in EGR flow, a considerable length of tubing exists between compressor and inlet manifold on the test bed, this may explain the slower experimental rise as it creates an effectively larger manifold volume. The following slow rise is dominated by the turbocharger dynamics, showing that at this speed the turbocharger flow rise is slightly too slow. However, both simulation and reality converge after 3 seconds highlighting good steady state accuracy. The boost pressure dynamics are very close but the simulated boost pressure continues to rise well beyond the experimental pressure, the initial boost pressure is also higher.

#### *4.5.2.2 EXHAUST MANIFOLD PRESSURE AND TURBOCHARGER SPEED @ 1500 rev/min*

The simulated exhaust manifold pressure rises much faster than is seen on the test rig, this behaviour will be determined largely by the turbocharger mapping which at these low engine operating conditions are likely to be inaccurate. The turbocharger speed increase is greater than in reality, and starts at a lower level; however, the rate of increase appears to match the experimental rate very well.

#### *4.5.2.3 ENGINE TORQUE AND EXHAUST TEMPERATURE @ 1500 rev/min*

The torque rise has been captured very well by the simulation, the slow ramp in torque after the initial peak is due to the smoke limited fuelling algorithm in the fuel quantity controller, the simulated implementation corresponds well with reality. The simulated exhaust temperature appears to increase far faster than the experimental data, but account must be taken of the large rise time for the thermocouples used on the test bed. In reality, the exhaust gas temperature will respond instantaneously to the change in in-cylinder conditions, therefore the simulated temperature rise rate seen here can be expected, however dynamic heat transfer effects from the exhaust manifold will tend to reduce the exhaust temperature in the post transient period.

#### *4.5.2.4 EGR VALVE AND VGT VANE POSITIONS @ 1500 rev/min*

The EGR valve is only open before the transient, the valve position is set by the controller to achieve the target airflow rate, this has been achieved with a wider opening in the case of the simulation. From this it can be deduced that either the valve area has been modelled too small, the engine volumetric efficiency is too high (which would allow a greater EGR flow)

or that the MAF sensor on the engine is inaccurate, which has been shown to be the case at low flow rates. The VGT remains closed during this transient.

#### 4.5.2.5 *ENGINE SPEED AND FUELLING @ 1500 rev/min*

The engine speed on the test rig deviates from the constant speed target at start of the transient as the dynamometer speed control does not have the bandwidth to reject the disturbance caused by the large step increase in torque, this effect is not captured in the simulation. The deviation in speed can change the engine operating point, however as long as it remains small this effect should be negligible.

**Figure 4.10** summarises the performance comparison for a fuel step of 7 to 34 mg/shot at 2500rev/min.

#### 4.5.2.6 *AIRFLOW AND BOOST PRESSURE @ 2500 rev/min*

As for the 1500 rev/min example, the initial simulated airflow response is faster than the experimental. Additionally in both airflow and boost pressure plots a sudden speed-up in response leading to an excessive rise in airflow and pressure is subsequently observed. This is primarily the result of the mapping technique used to characterise the compressor and turbine mass flows. In reality, the lines to the left hand side of the compressor map are virtually horizontal as are those to the right of the turbine characteristic, from the point of view of a dynamic simulation this is problematic as a very small change in pressure ratio will result in a large change in mass flow, therefore the simulation will slow down tremendously as the numerical solver takes extremely small time steps throughout this region. The modelling technique used here increases the gradient of these curves away from the horizontal in order to prevent the simulation from slowing down, therefore the result is a continued increase in mass flow and pressure where the real system would choke or stagnate. When the VGT vanes open the pressure and airflow rapidly fall back to sensible values.

#### 4.5.2.7 *EXHAUST MANIFOLD PRESSURE AND TURBOCHARGER SPEED @ 2500 rev/min*

The exhaust manifold pressure behaves in the same way as the inlet manifold pressure, for the same reasons, the rise is very large, although the experimental exhaust pressure saturates the transducer before the maximum value is achieved. The simulated drop in pressure once the vanes open is well correlated to the experimental results, the faster steady state convergence is due to the differing VGT vane behaviours. Unfortunately, the turbocharger speed measurement failed during the transient, however the simulated result follows the correct trend, if somewhat greater in initial and final value.

#### *4.5.2.8 ENGINE TORQUE AND EXHAUST TEMPERATURE @ 2500 rev/min*

The variation in engine torque due to the large exhaust backpressures and associated pumping work is seen in both simulation and reality, though the simulated effect is exaggerated by much higher exhaust pressures. There appears to be a significant difference in final exhaust temperatures, suggesting that the heat release model is too generous. As previously mentioned, the lack of dynamic heat transfer effects from the exhaust manifold can cause significant differences at high temperature.

#### *4.5.2.9 EGR VALVE AND VGT VANE POSITIONS @ 2500 rev/min*

As seen previously, the initial EGR valve opening is much greater in the case of the simulation. There is a small opening of the valve in simulation during the transient when the airflow overshoots the setpoint. This can only just be seen on the experimental EGR trace, showing that the lack of hysteresis modelling for the EGR valve leads to a small discrepancy. The VGT vanes open faster in simulation than in reality, this is because the vane response will depend on the boost pressure. The simulated boost pressure rises faster and higher than the real boost pressure, therefore the simulated control signal to the vane actuator will be different to the experimental, explaining the earlier opening and better convergence.

**Figure 4.11** summarises the performance comparison for a fuel step of 10 to 35 mg/shot at 3500rev/min.

#### *4.5.2.10 AIRFLOW AND BOOST PRESSURE @ 3500 rev/min*

In this test the experimental airflow responds faster than in simulation, however the boost pressure rise rate is about the same. The fluctuations seen in the experimental results originate from the VGT vane movements which do not occur in the simulation.

#### *4.5.2.11 EXHAUST MANIFOLD PRESSURE AND TURBOCHARGER SPEED @ 3500 rev/min*

Ignoring the differences caused by the fluctuations in vane position, both exhaust pressure and turbocharger speed correlate well between simulation and experiment.

#### *4.5.2.12 ENGINE TORQUE AND EXHAUST TEMPERATURE @ 3500 rev/min*

The simulated rate of change in torque matches closely the experimental result, initial and final steady states show a reasonable discrepancy in values given that the operating point is outside of the validated region and the model is therefore extrapolating. The experimental speed excursion is very large, this is due to the inability of the dynamometer to respond rapidly enough to the change in load.

#### 4.5.2.13 EGR VALVE AND VGT VANE POSITIONS @ 3500 rev/min

No EGR is present in this test hence the complete closure of both simulated and experimental valves. The VGT behaviour is very different, much of the difference can be derived from the turbocharger model (the simulated system uses a much wider vane setting to achieve approximately the same initial boost pressure), the difference in initial conditions and the turbocharger mapping technique result in different responses. These factors all result in a different control signal driving the VGT in simulation and therefore, different responses.

### 4.5.3 DRIVE CYCLE VALIDATION

This section of the validation incorporates the driver and vehicle model into the overall simulation, the results of an ECE15+EUDC drive cycle test are simulated and compared to those measured from the transient test bed.

#### 4.5.3.1 URBAN SECTION

**Figure 4.12** shows the performance of the simulated vehicle compared to the experimental data; the correspondence between the two is generally very good. The real system has higher fuelling at idle, the modelled driver tends to apply higher fuelling levels during pullaway manoeuvres.

The torque production at idle is not well modelled, however the transient torque follows the real system results very well. The engine speed traces show where gear changes occur, there is a disparity towards the end of the test where the model tries to down shift during the last constant speed section (at approximately 163 seconds) but then aborts, the down shift is then performed on the subsequent deceleration. The experimental results show that the test bed controller holds the gear then simply declutches when the vehicle speed is low enough.

The speed trace shows how both the experimental and simulated robot drivers accurately follow the speed demand.

**Figure 4.13** illustrates key parameters relating to EGR and VGT system performance. From the inlet manifold pressure it can be seen that the simulated values are generally too high. At idle conditions the compressor mass airflow is overestimated but otherwise the correlation is very good.

As seen in the step transient validations, the EGR valve position is much higher in simulation than in reality; the VGT remains mostly closed over this section of the cycle. Towards the end of the cycle there are large spikes in boost and airflow, these occur because the EGR and VGT shut momentarily whilst the engine is at medium speed (around 2500 rev/min), this

results in the unrealistic escalations in pressure and flow also seen in the step transient validations.

#### 4.5.3.2 EXTRA URBAN SECTION

**Figure 4.14** shows the modelled vehicle performance against the measured values. The fuelling profile corresponds well to the experimental data, though as the vehicle speed increases the simulated system applies higher fuelling levels. The torque trace mirrors this, with higher torque production at speed suggesting slight differences in the road load models used in the test bed dynamometer controller and the simulation.

The engine speed corresponds well, except for one section (between 100 and 175 seconds) where the simulation has shifted down a gear and the engine speed is therefore much higher. The gearshift points on the simulation can be altered to iron out these differences. The vehicle speed tracking of both systems is again very good.

In **Figure 4.15** the EGR and VGT system performance shows similar trends to those seen in the urban section of the cycle, boost pressures in general are over-estimated in simulation, this effect being exaggerated with increasing engine load.

The EGR positions are again wider open, and both EGR and VGT actuators display less activity in simulation than in reality.

## 4.6 SUMMARY OF RESULTS

From the validations described above it can be seen that the complete system model is a good representation of the real system. Problems arise when the turbocharger static maps are forced into operating regions that cannot be modelled accurately due to the nature of the simulation technique, such as fully closed VGT at high load, this causes excessive pressures and flows throughout the engine for reasons already mentioned. These conditions tend to occur transiently, as seen by the excessive pressure and flow rises in response to the fuel step transients, the modelling of the non-linearity in VGT position serves to exacerbate this phenomenon.

Unfortunately, the rates of change of pressures and flows will alter the dynamic performance of the control strategies that use these parameters as feedback, this can have the effect of making simulated controllers seem better than they really are through improved dynamics, or worse because of instabilities.

The VGT and EGR valve sub-models do not capture the complete non-linearities of the system, in particular the experimental results showed much more activity from the actuators. This has much to do with the hysteresis of the mechanisms and also the variable sensitivity of



the actuators to the control signals. Under certain conditions a change in the control signal of a few percent can cause a large change in the actuator position, whilst in other situations the actuator will not move at all for the same signal. The non-deterministic nature of this behaviour makes it very difficult to simulate accurately. Additionally, the system response is a function of the control signal driving it. The inaccuracies present in other sections of the model such as boost pressure and airflow response will cause differences between control signals generated by the real and simulated control systems, hence different actuator behaviour.

It is possible to add more detail to the model and encapsulate more of the observed behaviour into the simulation, but as the complexity of the model increases, the execution time also increases, reducing the effectiveness of the model as a tool for the rapid prototyping of control strategies. Already the simulation can be cumbersome depending on what operating region the engine is in; certain combinations of EGR and VGT settings can cause the simulation to crash or slow down to impracticably small time steps. When simulating the drive cycles for the validation, run times of the order of two to three times slower than real-time were experienced, with large bottlenecks occurring around gearchanges and pullaway manoeuvres.

Despite the limitations, the simulation is a useful tool and can be applied to wide area of the engine operating envelope providing the above points are considered. New controller structures can be evaluated rapidly using constant speed tests, and more slowly using full drive cycle simulations, however parameters selected for controllers using the model such as setpoints and gains will be different to those on the test bed.

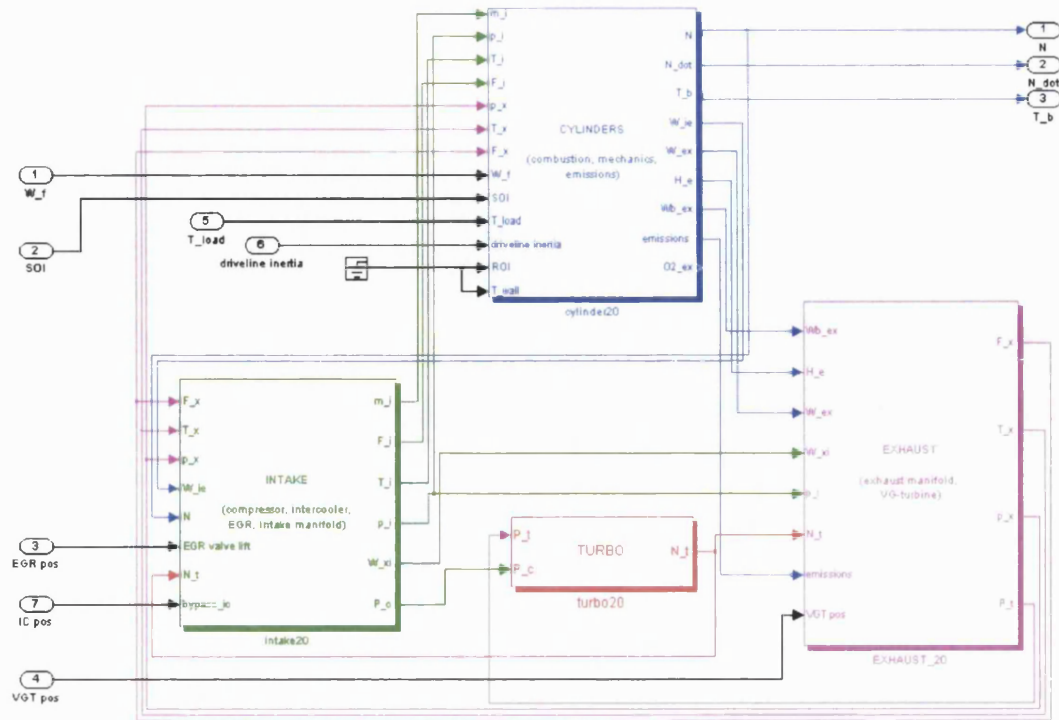


Figure 4.1 Top layer of Simulink engine model

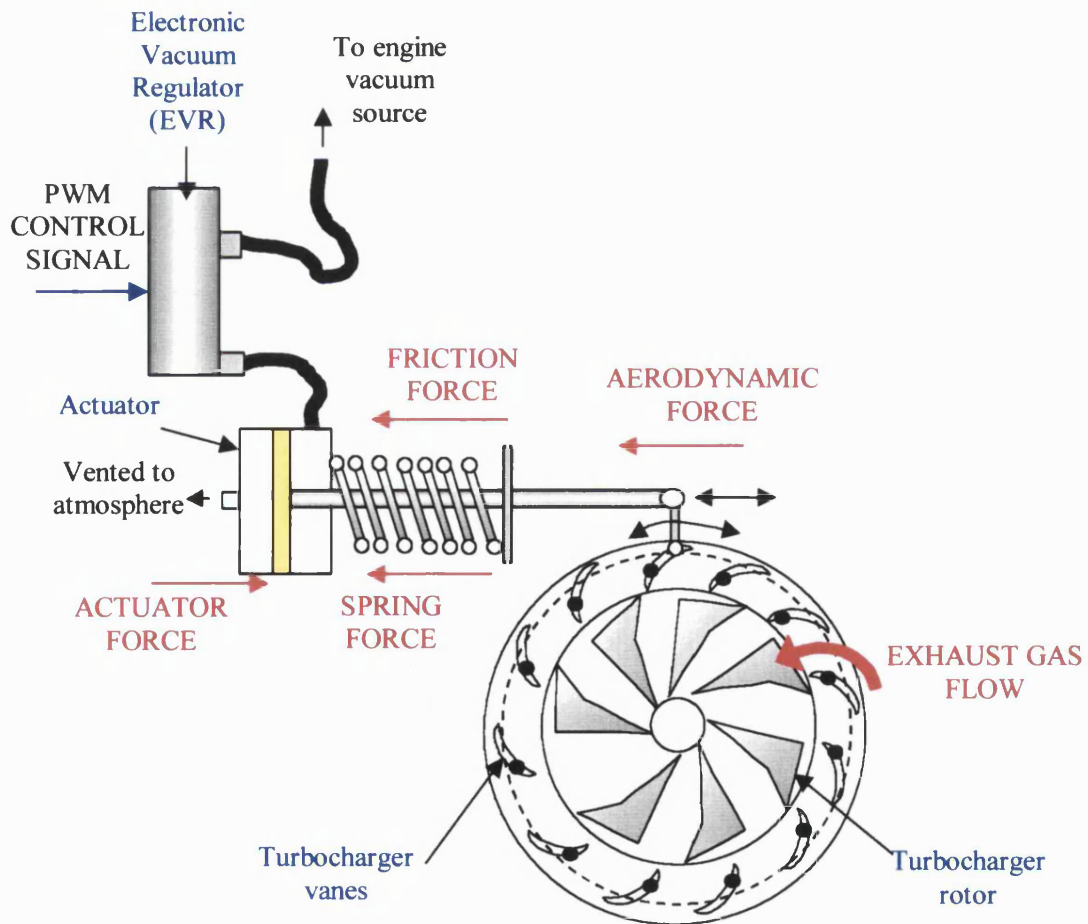


Figure 4.2 Schematic of VGT vane and actuator mechanism

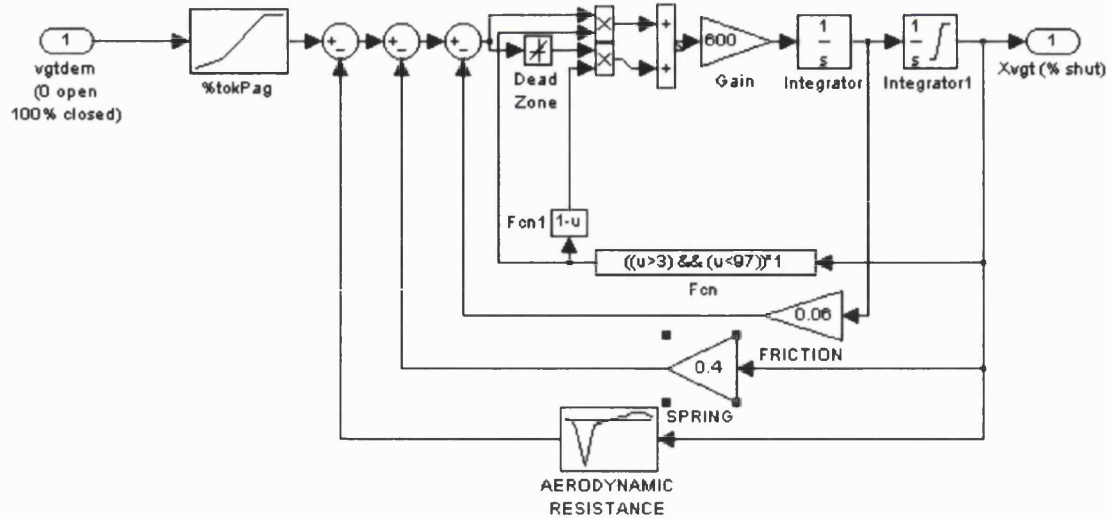


Figure 4.3 Simulink implementation of VGT actuator and vane model

DRIVE CYCLE PEDAL CONTROLLER  
NON-LINEAR INTEGRAL MAP

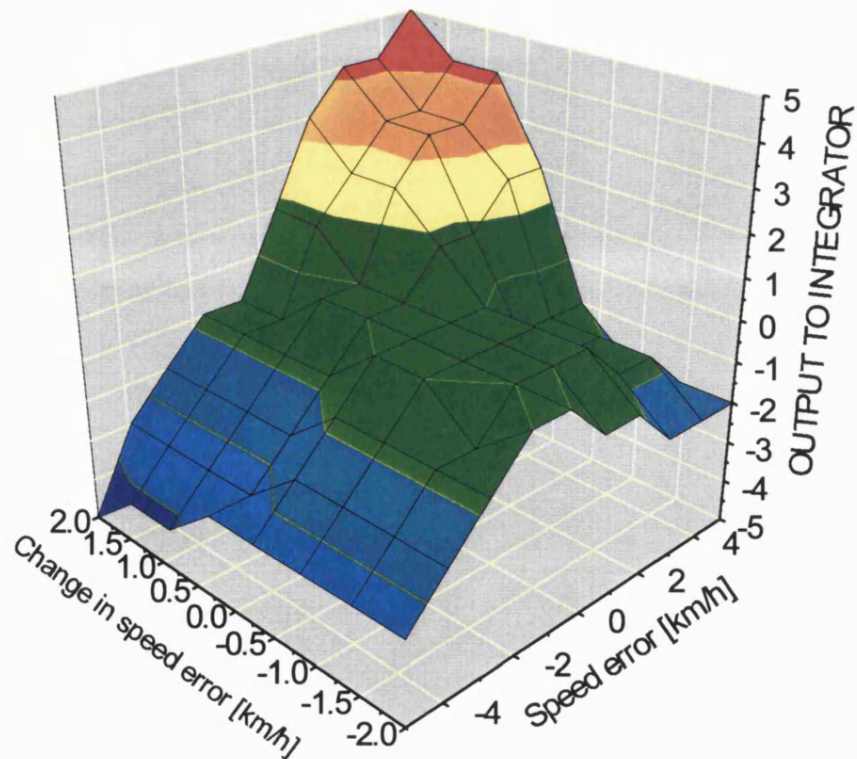


Figure 4.4 Drive cycle controller non-linear integral pedal map

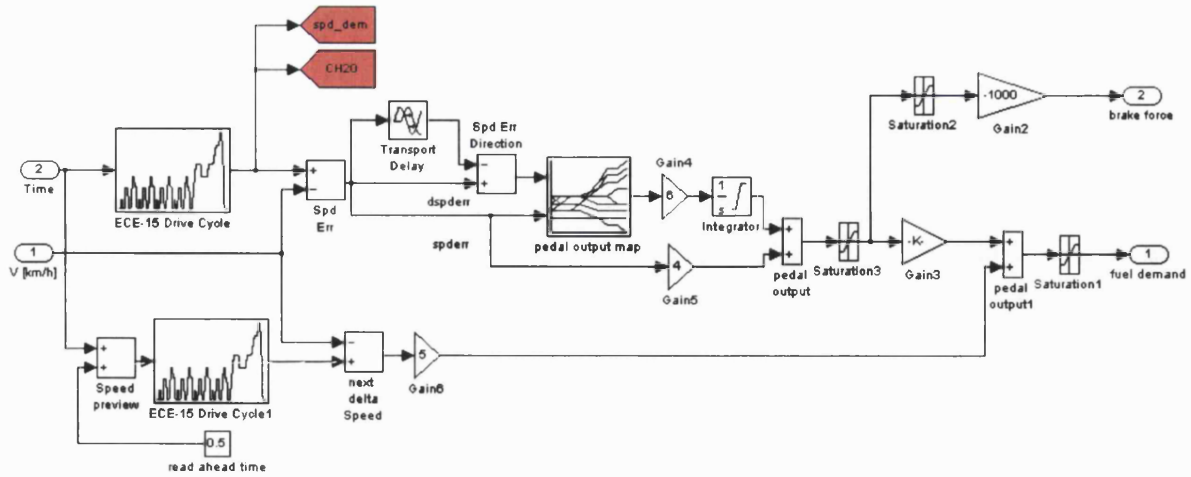


Figure 4.5 Detail of Simulink driver model

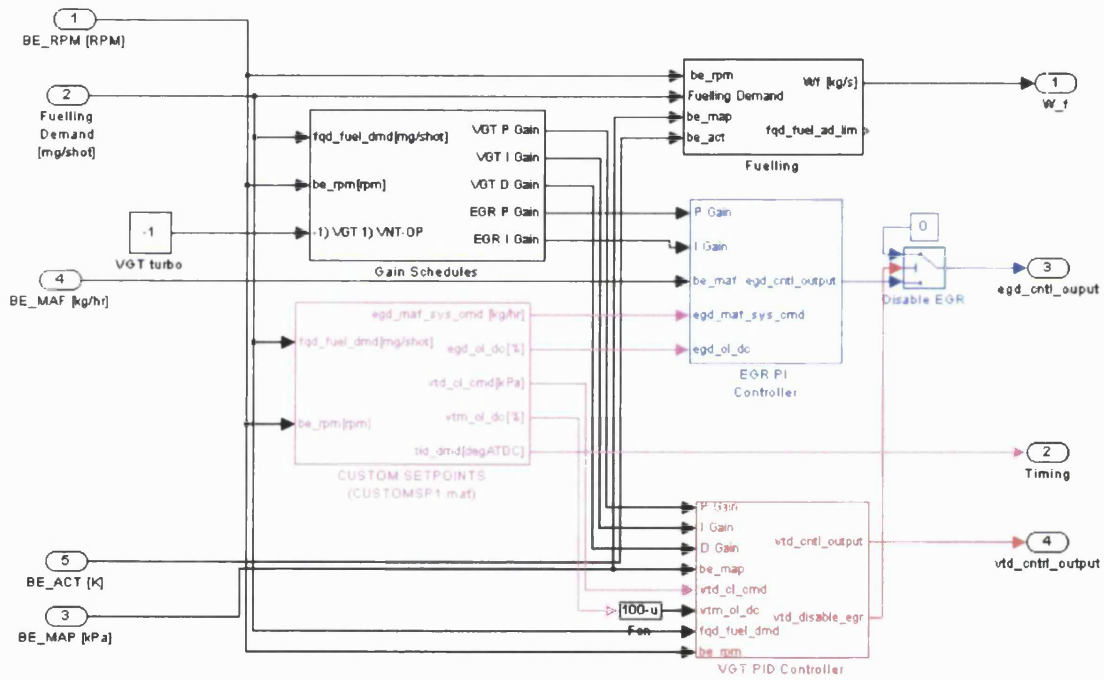


Figure 4.6 Standard Controller Simulink Implementation

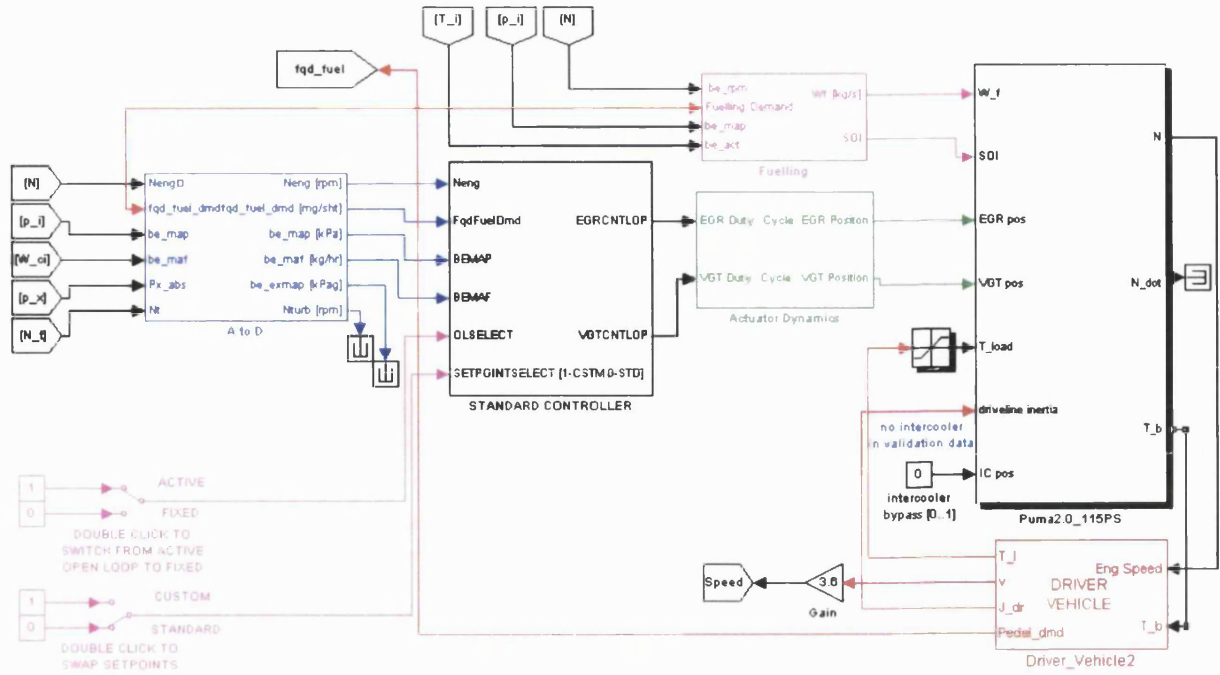


Figure 4.7 Complete engine and subsystem models

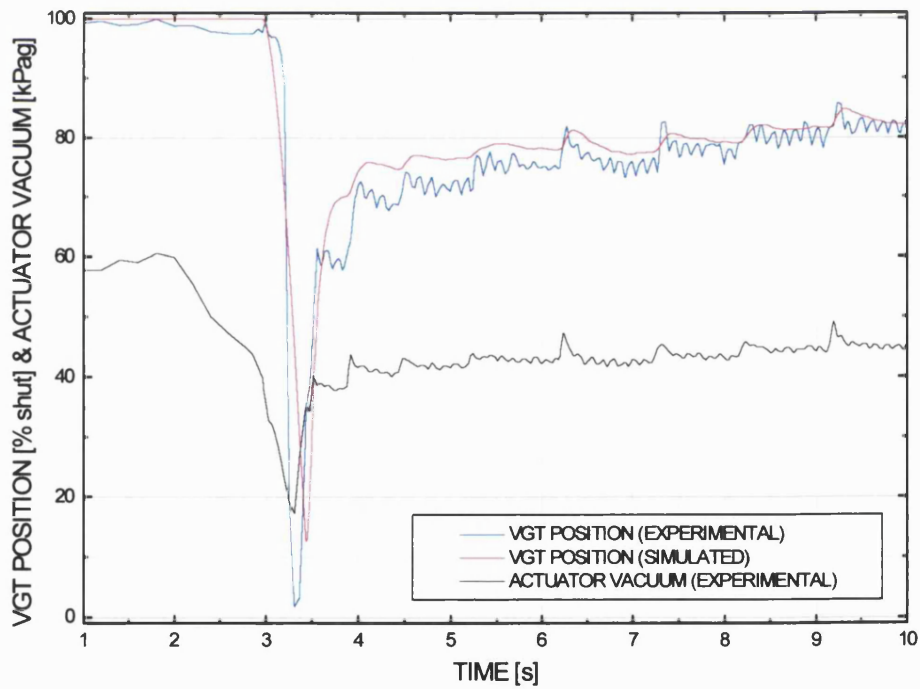
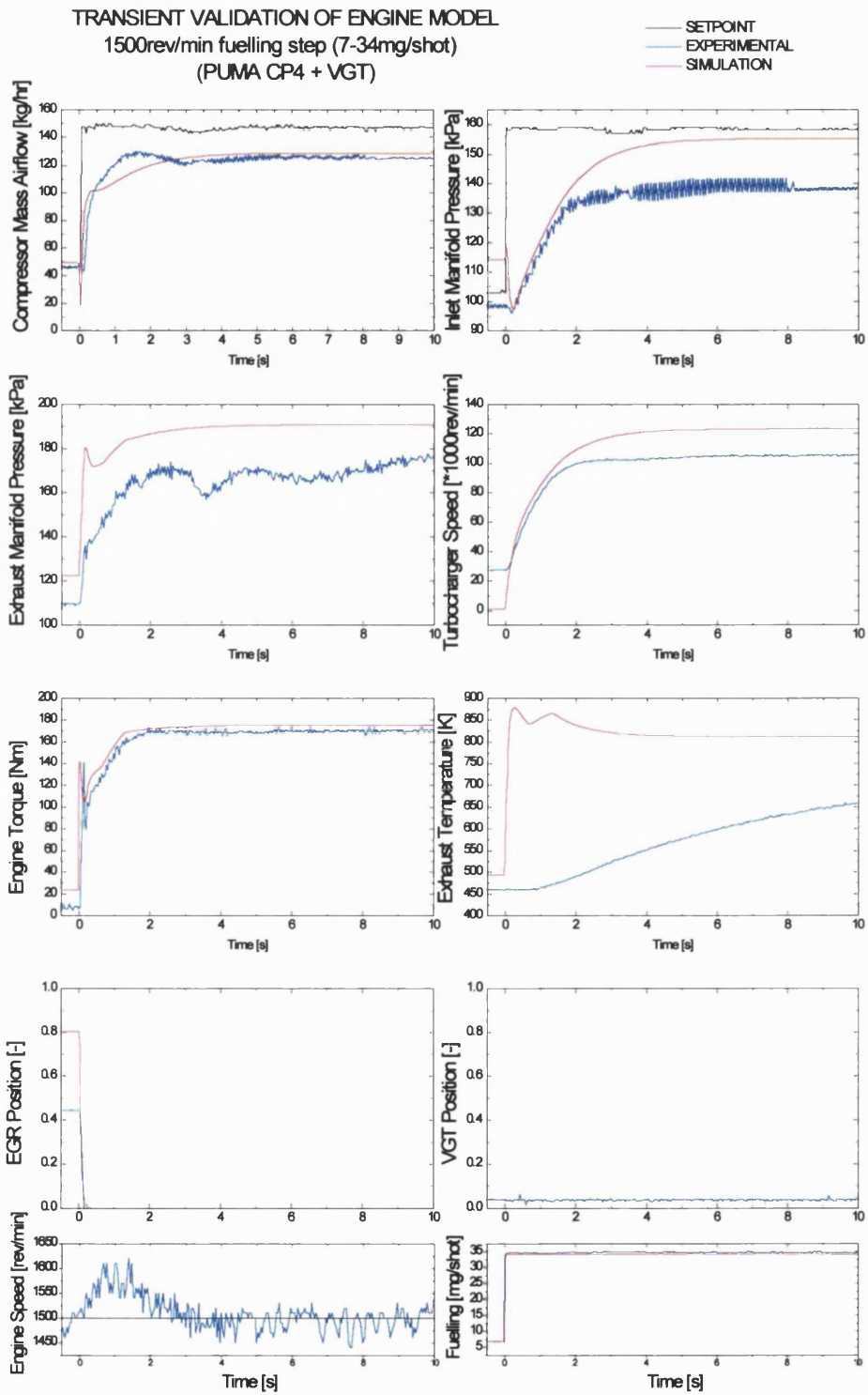
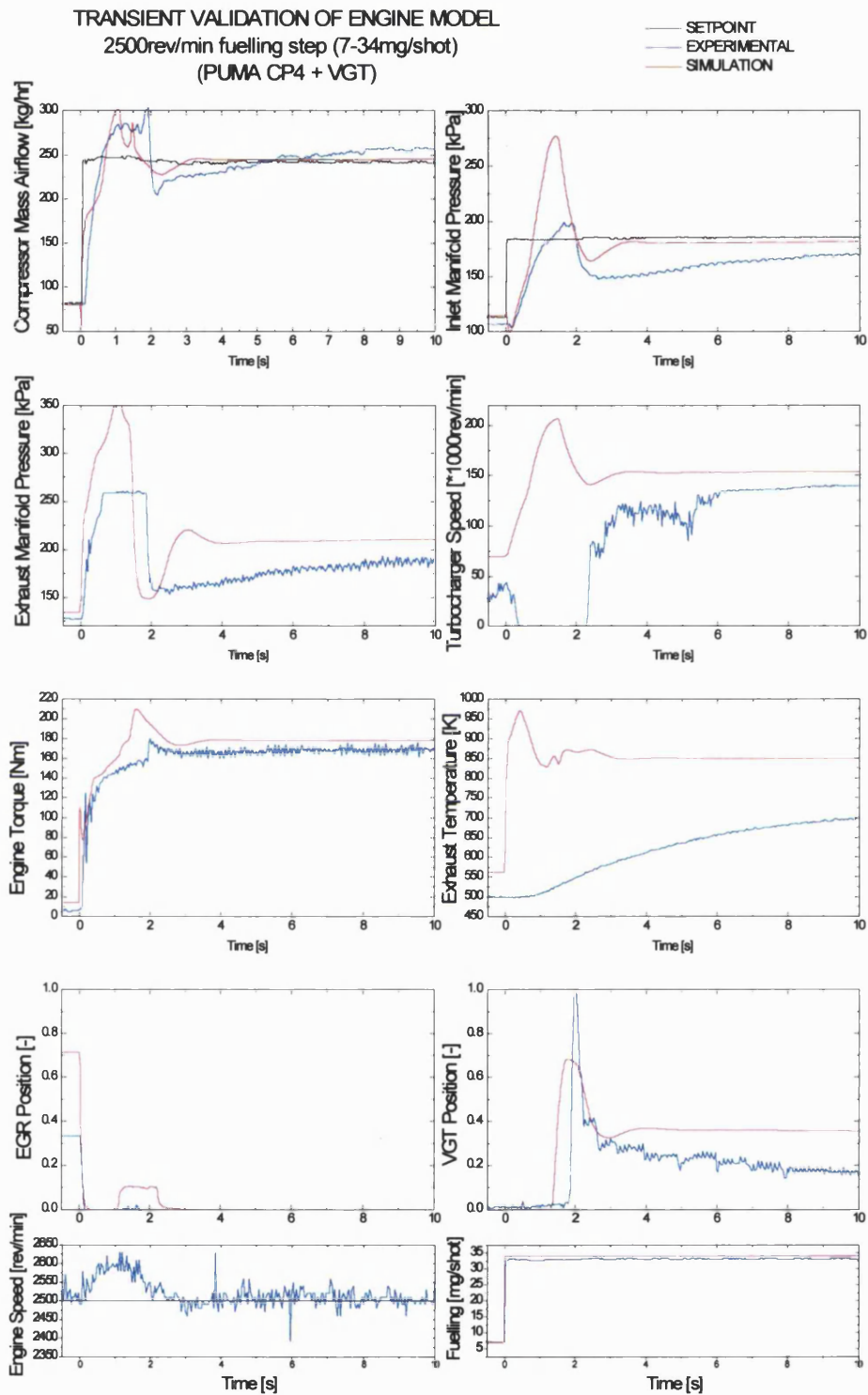


Figure 4.8 VGT Vane response, simulated and experimental



**Figure 4.9 Comparison of simulated and experimental engine behaviour for a large fuel step at 1500 rev/min**



**Figure 4.10 Comparison of simulated and experimental engine behaviour for a large fuel step at 2500 rev/min**

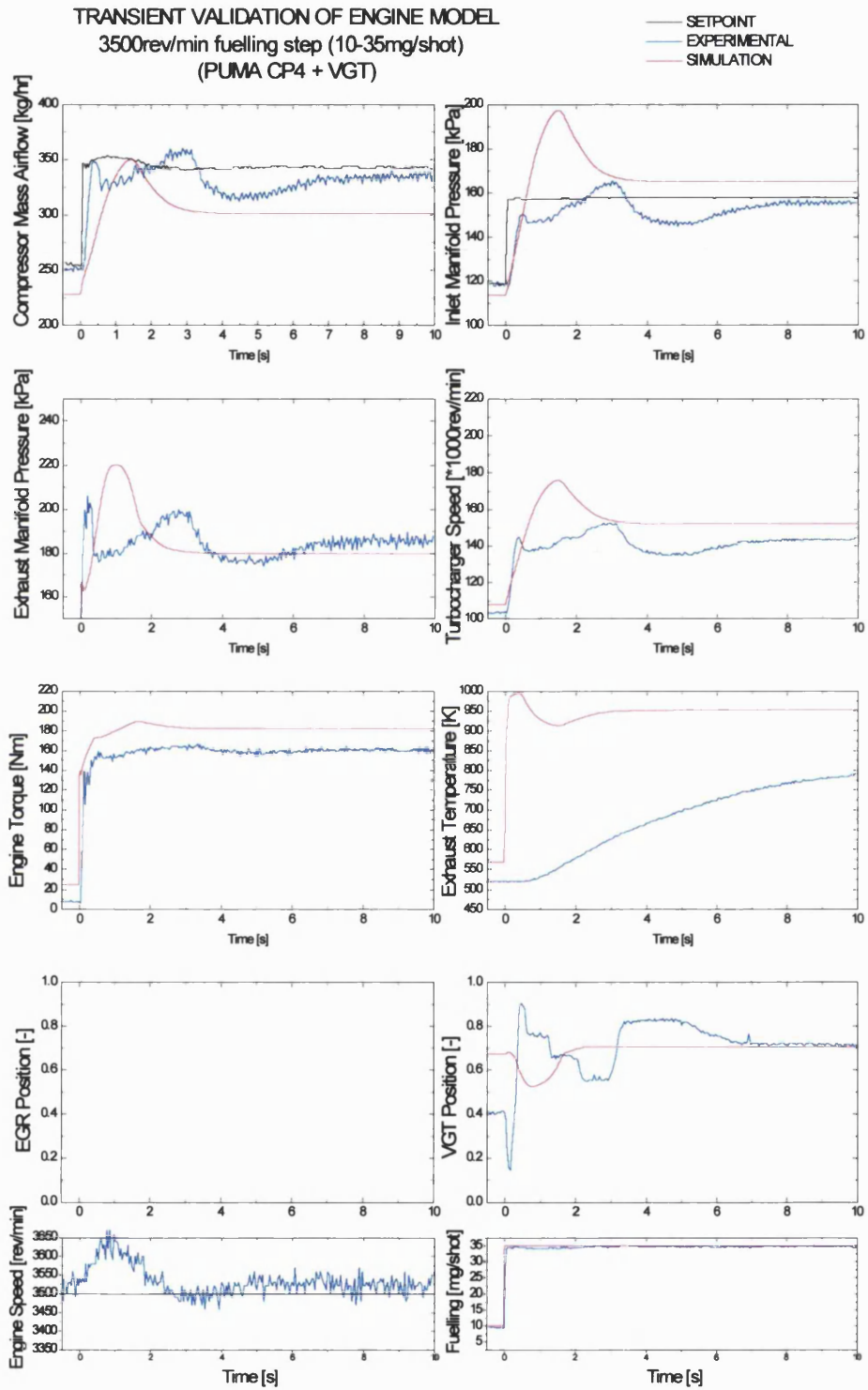


**Figure 4.11 Comparison of simulated and experimental engine behaviour for a large fuel step at 3500 rev/min**



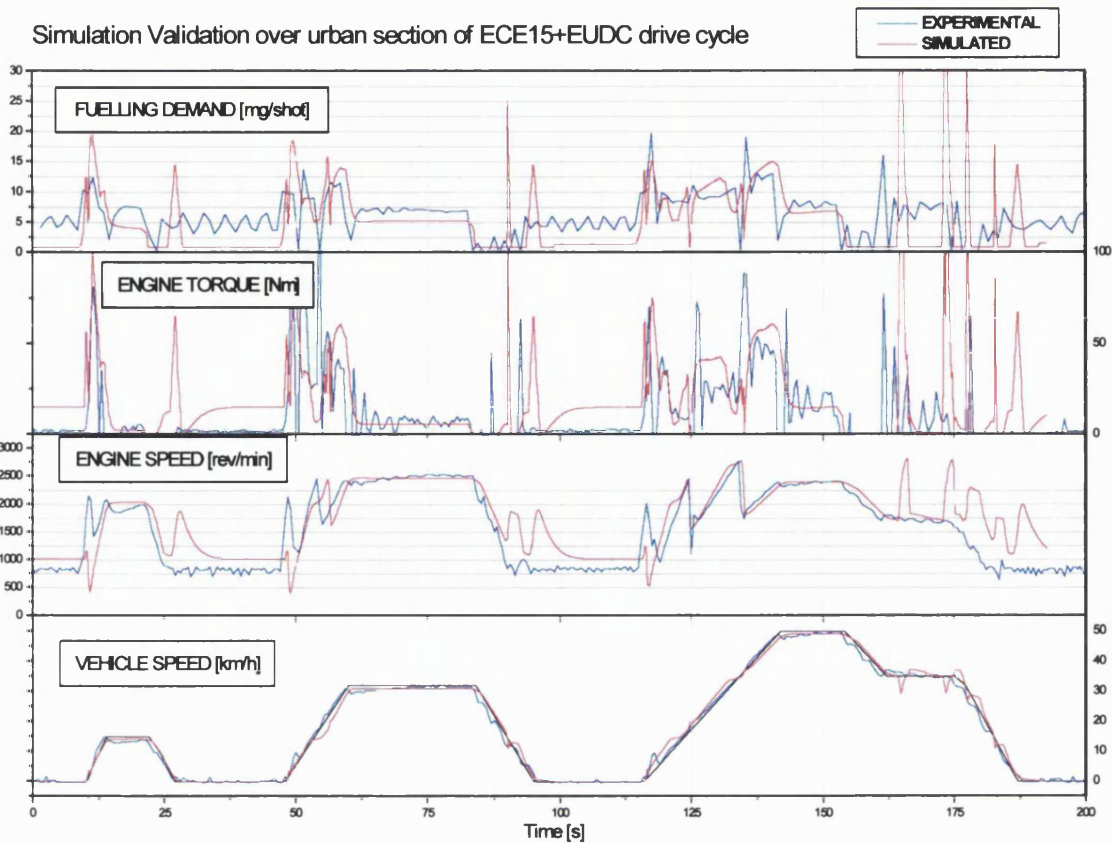


**Figure 4.12 Simulation validation over urban section of ECE drive cycle, general performance comparison**

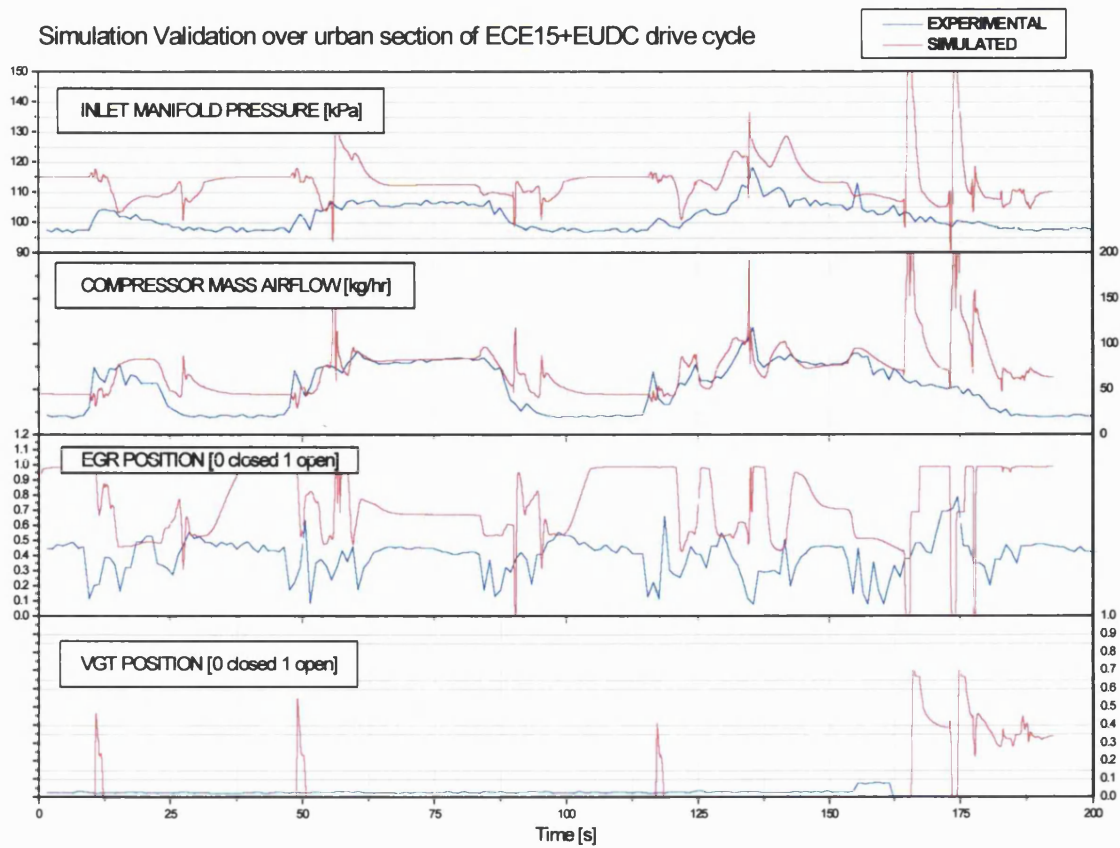


**Figure 4.13 Simulation validation over urban section of ECE drive cycle, EGR and VGT system behaviour comparison**

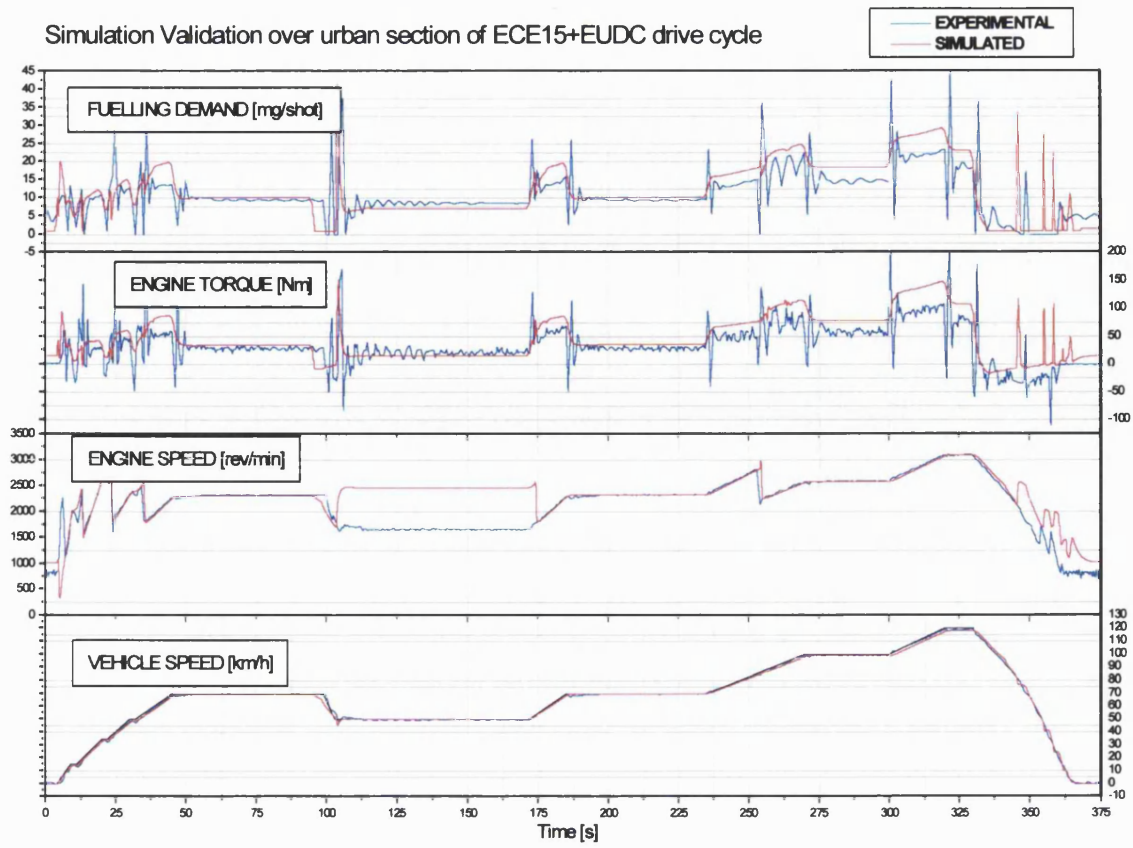


**Figure 4.14** Simulation validation over extra-urban section of ECE drive cycle, general performance comparison

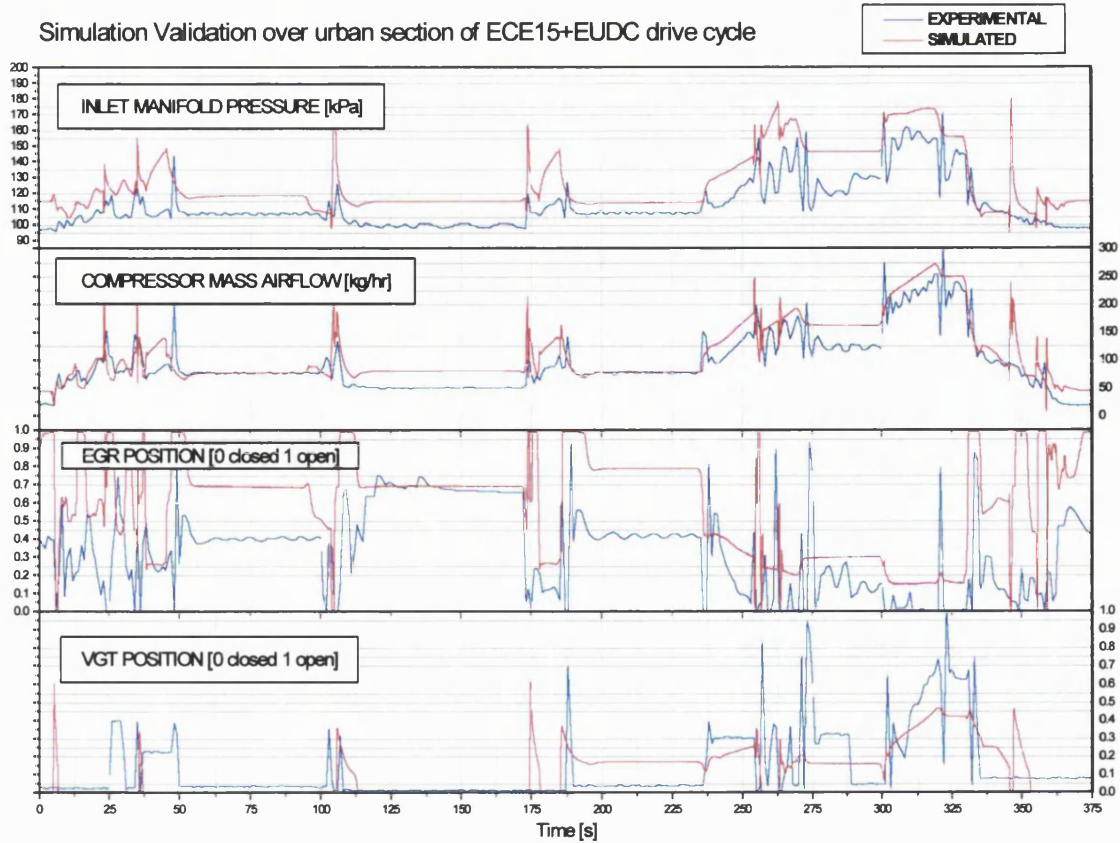


**Figure 4.15 Simulation validation over extra-urban section of ECE drive cycle, EGR and VGT system behaviour comparison**

## Chapter 5 EXHAUST PRESSURE CONTROLLER

### 5.1 INTRODUCTION

The control strategy developed in this chapter is motivated by the desire to reduce exhaust backpressures during large tip-in manoeuvres at elevated engine speeds, thus reducing transient fuel consumption and emissions, and also to improve the VGT control system tracking stability in the wake of such manoeuvres.

It has already been demonstrated in **Chapter 3** that in response to fuel step or tip-in transients, the VGT vane mechanism can stagnate in the fully closed position causing excessive exhaust pressures (see **Figure 5.1**), then open rapidly leading to a sudden loss of boost which the controller slowly compensates. Additionally, the turbocharger vane response can be oscillatory (see **Figure 5.2**), the ensuing fluctuations in the air charge pressure cause changes in the air fuel ratio which at high speed and load is already critical. These disturbances can result in increased smoke and NO<sub>x</sub> emissions depending on the leanness / richness of the ensuing charge.

During the transients, the high exhaust backpressures increase the amount of pumping work performed by the engine. This behaviour is strongly linked to the non-linear response of the VGT vane actuator, however, it is also a function of using the inlet boost pressure as a feedback parameter.

A control method is developed that uses exhaust manifold pressure measurements to control the VGT vanes during transient operation. Significant reductions in exhaust manifold pressures are achieved without degrading turbocharger response, in fact the overall engine behaviour is improved through more rapid torque delivery, lower transient smoke and improved VGT tracking stability after the transient. Control of the EGR system is not considered in the design of this controller, as the EGR valve will be closed over the operating range for which this controller is active.

### 5.2 *Transient turbine behaviour*

The existing VGT control scheme uses inlet boost pressure feedback to regulate the VGT vanes, interpreting a fuelling step / tip-in as a demanded increase in inlet boost pressure, and therefore responding by closing the vanes during a transient to increase boost. A large boost demand will cause full closure of the vanes if they are not already in this position. The system will only open the vanes when the boost pressure responds, even at elevated engine speeds where exhaust gas energy is high this can take an appreciable amount of time. The turbocharger mechanics act as a first order lag, the exhaust pressure responds almost instantaneously to the change vane position and fuelling, but the inlet boost pressure responds

more slowly due to the acceleration of the rotor. The delays inherent in the system are illustrated in **Figure 5.3**.

Considering the gas dynamics of the turbocharger system, the nozzle vanes guide exhaust gas flow onto the turbine, the VGT setting determines the gas flow area and as such dictates an upper limit for the mass flow that can pass through this opening. This mass flow limit corresponds to the critical pressure ratio across the nozzle; increasing this pressure ratio will cause only a very small increase in mass flow through the turbine. At this condition the system is said to be choked, this can be seen on the plot of turbine pressure ratio against mass flow in **Figure 5.4**; for a fixed vane position the curves are asymptotic.

During a transient the excessive exhaust backpressure can give rise to a pressure ratio greater than the critical pressure ratio, but the extra pressure does not significantly increase flow through the turbine. For optimum turbocharger response the maximum energy transfer to the turbine is required in order to accelerate it, the energy transfer rate is defined by Eulers equation and can be reduced to **Equation (5.1)**.

$$P_t = W_{xt} (h_x - h_{postturb}) \tag{5.1}$$

Where  $P_t$  is the power transfer from exhaust gas to turbine  
 $W_{xt}$  is the turbine mass flow  
 $h_x$  is the pre-turbine exhaust enthalpy  
 $h_{postturb}$  is the post-turbine exhaust enthalpy

From this equation it can be seen that in order to transfer more energy to the turbine, either the mass flow or the enthalpy change of the exhaust gases must increase. The enthalpy change is not directly controllable except through altered fuelling, either increasing the quantity or retarding the timing, but this will have a strong effect on torque and emissions, leaving increasing the mass flow as the only method of increased energy transfer.

The acceleration of the turbine depends on the balance of power extracted from the exhaust gases by the turbine with the power expended by the compressor in compressing the inlet charge. Any difference between these quantities results in either an acceleration or deceleration of the turbocharger rotor until the new equilibrium condition is attained. In order to attain maximum acceleration from the turbocharger in response to a large tip-in, the pressure ratio across the turbine nozzle should remain at or near the critical pressure ratio in order to achieve the best compromise between increased mass flow and minimal engine pumping work. There is no benefit to be gained from higher exhaust pressures at low vane openings as the increase in mass flow will be small.

The desired turbocharger behaviour can be achieved by opening the vanes to counter the rise in exhaust pressure into the region of nozzle choking, this is illustrated as a transition across the turbine operating characteristic in **Figure 5.5**. The increased opening gives the turbine a

greater swallowing capacity and this increases the mass flow over the turbine. When opening the vanes the pressure in the exhaust will initially drop due to the increased emptying of the exhaust manifold. However the increased turbine flow will augment the compressor delivery and hence inlet flow conditions, this will in turn cause the exhaust pressure to rise again as more flow enters the manifold. A reduction in backpressure will result in a reduction in engine pumping work, this can significantly reduce fuel consumption or alternatively improve torque response during the transient.

### **5.3 Exhaust Pressure Measurement**

For better control of gas flow through the turbine, it is proposed that measurement of the pressure ratio across the turbocharger nozzle is used in the VGT control strategy; this is a difficult measurement to obtain on an experimental test bed, let alone a mass-produced unit. The alternatives are either measurement of exhaust manifold pressure or estimation of the pressure ratio through the use of an on-line model. Great difficulty exists in providing an accurate model of exhaust manifold pressure, mainly due to the difficulties involved in modelling the highly non-linear turbocharger and engine system gas flows. In particular, as this is a transient phenomenon the accuracy of the dynamic model is essential to the controller performance, but as the simulation validation in **Chapter 4** shows, even a relatively complex model may not provide an accurate representation of the transient behaviour. An additional constraint is that of computational overhead, the type of on-line model required here will exert significant chronometric demands on the processor.

Exhaust *manifold* pressure measurement is straightforward, but the conditions prevalent in the exhaust manifold will necessitate a sensor more robust than those employed in the inlet manifold. The exhaust pressure signal can replace other measurements in the engine, for example the MAF (Mass Airflow) sensor could be deleted as the EGR flow can be calculated from inlet and exhaust pressures and EGR valve position (a signal already available to, but not used in the current strategy). In this manner, the EGR flow can be controlled directly as opposed to by implication from compressor flow. The work by **Van Nieuwstadt [36]** follows this approach and corroborates the production feasibility, stating that this choice of sensors is less costly than the standard combination of MAF and MAP sensors.

Exhaust manifold pressure is already monitored on the test bed engine, the sensor is not mounted directly onto the manifold but remotely via a coiled copper tube in order to reduce the gas temperature at the sensing element. The delay introduced by this arrangement was an initial concern but proved to be insignificant, however it is uncertain as to whether the pressure fluctuations observed during tip-in transients are exaggerated by this set-up.

Measurement of the exhaust manifold pressure will not provide the exact pressure ratio across the turbine nozzle, it must be noted that this will be slightly different to the pressure ratio

across the entire turbine. Choked flow in the nozzle occurs at pressure ratio defined **Equation (5.2)**

$$\frac{P_2}{P_{01}} = \left( \frac{2}{\gamma + 1} \right)^{\frac{\gamma}{\gamma + 1}} \quad (5.2)$$

Where  $p_2$  is the downstream pressure

$p_{01}$  is the upstream pressure

$\gamma$  is the ratio of specific heat capacities

This pressure ratio has a theoretical value of 0.528 but this will vary according to Air Fuel Ratio and temperature (due to the effect these properties have on  $\gamma$ ), and geometry effects. The turbine rotor chokes at a much higher pressure ratio than an adiabatic nozzle due to centrifugal effects. At high speed the centrifugal force on the gas in the turbine passage must be countered by higher inlet pressures for mass to flow in the correct direction [89]. This is why the mass flow characteristic decreases with increasing speed for fixed pressure ratio.

For the normal 50% reaction design (the ratio of isentropic enthalpy change in rotor compared to entire turbine stage) the expansion ratio across rotor will be similar, leading to a theoretical 0.285 overall ratio (3.5:1 expansion ratio) before choking [89]. However, as can be seen from the turbine flow characteristic in **Figure 5.4**, the flow is asymptotic and the turbine is almost choked at a considerably lower pressure ratio. Therefore, controlling the exhaust manifold pressure to a level corresponding to the pressure ratio where the flow characteristic becomes essentially flat will approximately achieve the maximum flow for the given vane setting. As turbocharger speed increases, the required pressure ratio increases (due to the centrifugal effects mentioned earlier), this can be accommodated by scheduling the target exhaust manifold pressure with engine speed.

## **5.4 Transient detection**

This strategy has been designed for high load transient and steady state control only because under other operating conditions the turbine flows and pressures do not drive the turbine characteristic into the choking region of the map. Usually a complete exhaust pressure based strategy will require some form of flow modelling for the turbine and EGR as in [36]. The exhaust pressure is strongly affected by EGR valve position, VGT vane position, fuelling quantity and timing, therefore the use of exhaust pressure as a control parameter for all engine conditions is more complex than the current method. Additionally, a separate operating mode for handling large transients would ensure that EGR openings due to airflow overshoots during the transient could be completely eradicated by explicitly switching the valve from airflow control to a zero duty cycle.



In order to apply this strategy to transient manoeuvres only a method of detecting the operating conditions of interest is needed. A simple transient detection routine involves comparing the fuel quantity demand signal over several samples; if a change above a defined threshold occurs then it can be deduced that the driver has instigated a transient.

The exhaust pressure control VGT strategy is only effective when the exhaust pressure is high enough to drive the turbine operating point into the choked/almost choked flow region of the turbine characteristic, therefore the strategy should only be enabled when the pre-transient pressure is approaching this region.

These two conditions will provide the enabling logic for the switch to exhaust pressure control.

## **5.5 Proposed Control Scheme**

A schematic of the proposed strategy is shown in **Figure 5.6**. The system works as follows;

Error signals are calculated for boost (MAP) and exhaust manifold pressure (Px) tracking by comparing the signals with look-up table values for desired inlet and exhaust manifold pressures. Under normal steady state and low load transients the VGT is controlled in the usual way via the MAP tracking error, the Px tracking is ignored.

The exhaust pressure controller is designed to operate when the exhaust pressure is high enough to enter the choking region of the turbine map. In order that the controller does not operate for transients below this range (where it would be of no benefit), the system is enabled only when the exhaust pressure exceeds a certain level, nominally set here for 180kPa.

When a large transient is detected and exhaust pressure is close to the choking region the error signal feeding the VGT PID compensator is switched from the boost tracking error to the exhaust pressure tracking error. Both inputs are engine gas pressures with approximately the same order of magnitude. The setpoints for boost pressure are normally scheduled with speed and fuelling, and as such are subject to almost instantaneous change due to tip-in and tip-out manoeuvres, so the fuelling-driven switching from inlet boost error to exhaust pressure error will not cause any unpredictable behaviour from the system.

## **5.6 Simulink Implementation**

The Simulink implementation of the proposed control scheme is shown in **Figure 5.7** and **Figure 5.8**. The sections of the scheme coloured blue are from the standard control scheme, and those coloured red are the additional blocks used to implement this scheme, this shows how simple a modification this strategy actually is from the original. The additional blocks are as follows:

1. An exhaust pressure tracking error calculated by subtracting the exhaust pressure from a setpoint
2. Transient fuel step detection, detailed in **Figure 5.8**, this block compares the current fuelling demand to that of 3 samples previously, if the difference is greater than a specified tolerance (10 mg/shot for this example) then a signal is sent to a 'set / reset flip-flop' block. This block has 2 stable states which can be selected by the set and reset ports. When the block is activated by a pulse to the 'set' port, its output goes high (i.e. equals 1) to indicate that a 'tip-in' transient has occurred. The 'reset' port to the 'flip-flop' needs to be sent high for the system to reset and the output to fall to 0 again.
3. Overspeed and Overboost protection, these were added for initial engine testing work as a precaution in case excessive inlet pressure or turbocharger speed occurs. Should any of these conditions arise, the output of the OR block becomes 1 (normally 0)
4. Transient control enable logic, this is the mechanism that decides when to apply transient control. The output is used as a trigger for switching the input to the VGT PID controller, it has 3 states, 1 = normal operation (boost control), 2 = transient exhaust pressure control, 3 = Overboost or Overspeed protection. The routine makes use of a feature of Simulink that allows Boolean signals to be treated as real numbers, for instance the output of the logic AND block is OFF or ON (0 or 1), the *relaxed boolean checking* option allows the output to be operated on as any ordinary number. In this model the output of an AND block has been multiplied by 2, the resultant values will be either 0 (OFF) or 2 (ON). This is a convenient way of indexing several different logical events, for example, the AND block will output HIGH when a transient has been detected and the exhaust pressure is above the lower threshold for transient Px controller operation and an overspeed or overboost has occurred. The output is multiplied by 2 and added to 1, therefore the state value is switches from 2 to 3, this is used to switch the controller section to a protection mode. The functioning of the logic is summarised in **Table 5.1**.
5. VGT control selector, this is simply a switch that routes 1 of 3 inputs to the VGT PID error input depending on the value of the trigger input from the transient control enable logic defined above. For a value of 1 the boost error is fed to the controller, for a value of 2 the exhaust pressure error is used (corresponding to transient control mode) and for a value of 3 a constant input to the controller (corresponding to overboost or overspeed) is selected; this can be chosen to drive the VGT vanes open.
6. Gain switching, this was implemented to allow different gains to be used when the exhaust pressure tracking controller is applied, this can also be used to assist the overboost protection mode by switching to a very high P gain and no I or D gains. The switching is the same as for the VGT PID input switch, using the trigger signal produced by the transient control enable logic.

The same controller implementation is used for the simulation evaluation and the on-engine evaluation.

<b>Px &gt; Threshold</b>	<b>Fuel Step Detected</b>	<b>Overboost / Overspeed</b>	<b>Trigger Value</b>	<b>Interpretation</b>
NO	NO	NO	<b>1</b>	<i>low speed / low load, small transient or steady state operation (boost control)</i>
YES	NO	NO	<b>1</b>	<i>steady state operation at higher speeds and loads, or slow transient (boost control adequate)</i>
NO	YES	NO	<b>1</b>	<i>Large transient but at low speed / low load, no need for Px control</i>
YES	YES	NO	<b>2</b>	<i>Large transient, Px control region (Px Control active)</i>
NO	NO	YES	<b>1</b>	<i>improbable operating conditon (need high exhaust pressures to overspeed turbo / over boost inlet)</i>
YES	NO	YES	<b>1</b>	<i>overboosting or overspeeding in steady state or slow / small transient conditions, (boost control should avoid this)</i>
YES	YES	YES	<b>3</b>	<i>Overboost / Overspeed during large tip-in transient at elevated speed (Overboost protection mode)</i>
NO	YES	YES	<b>1</b>	<i>improbable operating conditon, large tip-in causing overboost / overspeed should involve high backpressure</i>

**Table 5.1**Transient Control Enable Logic description

## **5.7 Comparison in Simulation of Controllers**

**Figure 5.9** compares the 2 controllers in simulation over a tip-in transient at a constant engine speed of 2500 rev/min.

### **5.7.1 INLET MANIFOLD PRESSURE**

The first frame shows the inlet manifold pressure rise in response to the tip-in, the exhaust pressure controller gives a more stable boost response, without the overshoot demonstrated by the standard controller. As discussed in **chapter 4**, these transients drive the simulation into an operating region where accuracy of the modelling technique is low, hence the exaggerated boost rise demonstrated by the standard controller.

A difference exists between the final values of boost for the 2 controllers because the Px controller does not control to an inlet manifold setpoint, it tracks an equivalent exhaust pressure setpoint. In order to achieve the same levels of inlet boost, the exhaust setpoint can be increased.

### **5.7.2 VGT VANE POSITION**

The second frame illustrates the VGT vane position. The simulated boost pressure rise is more rapid and much greater in absolute value than the real pressure as discussed in the validation of the simulation, therefore the vane mechanism is prompted to open much earlier than it would in reality due to the larger control signal.

The vane response of the exhaust pressure controller also is more oscillatory, although only a rudimentary gain tuning procedure was performed and a more thorough attempt may reduce these oscillations. In real life these oscillations may not be of such high amplitude as they originate from the exhaust pressure which is greater and faster in simulation.

### **5.7.3 EXHAUST MANIFOLD PRESSURE**

The modelled exhaust pressure also rises too quickly compared to the real pressure in much the same way that the simulated inlet pressure rises. The exhaust pressure controller responds almost instantaneously because the exhaust pressure itself responds almost instantaneously, however the standard controller has to wait until the inlet pressure has increased sufficiently before it acts.

The reduction in exhaust pressure during the transient is highly evident, this will reduce the pumping work performed by the engine and thus increase the transient torque output. This can be seen in the torque trace, there is a significant difference between the 2 controllers, the lower backpressure allows the exhaust pressure controller to deliver a higher torque level earlier in the transient. The standard controller torque output only reaches the target value when the VGT vanes open in response to the overboost.

### **5.7.4 FUELLING**

The final frame shows the fuelling demands for the different controllers during the transient, the experimental results include the effect of smoke limited fuelling (seen as the deviation of the fuelling profile from a step demand). The results displayed are of the pedal demand only, although smoke limited fuelling is implemented in the model and can be seen by the initial dip in the torque rise. The turbocharger speed trace illustrates the continued acceleration of the turbocharger as the vanes remain closed.

Despite the discrepancies between simulation and experimental performance, the benefits of the transient exhaust pressure control method are evident; An experimental investigation was therefore motivated.

## 5.8 Exhaust Pressure Controller Experimental Evaluation on Test Bed

The new controller scheme was evaluated over a series of extreme fuel step scenarios performed at a range of engine speeds as described by **Table 5.2** (also illustrated in **Figure 5.10**). These transients represent acceleration manoeuvres as experienced during overtaking or encountering a sudden gradient. The standard controller was evaluated over the same manoeuvres for the purposes of comparison. At each test condition the exhaust pressure controller was tested with a range of target transient exhaust pressures, from 190kPa to 220kPa in 10kPa increments. The test procedure used here is the same as that for the constant speed fuelling step transients described elsewhere in this thesis.

ENGINE SPEED (rev/min)	FUELLING STEP (mg/shot)	TORQUE STEP (Nm)
2000	25 - 45	120 - 227
2500	25 - 45	110 - 220
3000	15 - 40	55 - 190
3500	15 - 35	55 - 155

**Table 5.2 Testing schedule**

### 5.8.1 Implementation on test bed using dSpace

The exhaust pressure controller was implemented on the engine test bed using the dSpace rapid prototyping hardware. The same Simulink model of the controller developed in simulation was used in the experiments, the only difference being that the strategy inputs and outputs were connected to the relevant dSpace blocks to allow use of the systems analogue and digital I/O. The input variables to the strategy were provided by the existing ECU using the CAN bus. The additional measurement of exhaust pressure was taken from the test bed instrumentation, the signal was low pass filtered and sampled at 0.016s to comply with the execution rate of the controller. Output is via PWM signals driving the EGR and VGT electronic vacuum regulators in place of the existing ECU outputs. Considerable development time was spent on the researching of this rapid-prototyping method, further details of the controller implementation are given in **APPENDIX A**.

### 5.8.2 Comparison of controllers over 2500 rev/min tip-in response

The results for the transient Px controller with an exhaust pressure target of 200 kPa are summarised in **Figure 5.11** to **Figure 5.13**. The trends displayed in the results are representative of all tests, the same holds true for the baseline transient performed with the standard controller. The plots compare the standard controller (blue lines) to the Px controller (red lines).

### 5.8.2.1 *Figure 5.11 Engine performance*

Comparing the torque response of the 2 controllers, the improvements in behaviour are obvious. The initial peak torque value is higher than that achieved with the standard controller; this is due to the lower back pressure at this instant in time. The subsequent torque rise is of the same rate as the standard controller but achieves the target torque when the standard controller has reached only 90% of the demanded change. The improvement in response can be compared in terms of  $T_{90}$  times, the time it takes to achieve 90% of the required change in value. The standard controller has a torque  $T_{90}$  of 0.68s whilst the Px controller more than halves this value to 0.32s. Additionally, the Px controller provides a more stable torque response, there is a slight upwards drift in torque over the proceeding seconds but not as marked as the drop in torque experienced with the standard controller.

The smoke response comparison is also in favour of the Px controller, the initial smoke spike in response to the tip-in is almost halved in magnitude, this can be explained by the lower transient exhaust backpressure reducing the amount of trapped residuals in the cylinder, thus increasing in-cylinder air fuel ratio. A secondary smoke spike is observed for the standard controller due to the fractional opening of the EGR valve when the airflow overshoots its setpoint, however it is not observed for the exhaust pressure controller as no airflow overshoot occurs. The smoke levels in the seconds following the tip-in are also noticeably lower. As can be seen in the fuelling results the Px controller has undergone the same tip-in but does not experience the fuel limiting between 2 and 4 seconds as applied to the standard controller.

### 5.8.2.2 *Figure 5.12 Turbocharger and Engine Pressure Behaviour*

Examining the turbocharger and engine pressure behaviour it can be seen how the above improvements in torque and smoke are made possible by the improved engine backpressure. The pressure initially peaks at the same value as the standard controller, but instead of increasing in magnitude it converges on the target level of 200 kPa, albeit with several oscillations. It is uncertain if the oscillatory nature of the exhaust pressure is a real effect or a result of the measurement arrangement. As mentioned previously, a coiled pipe is used to divert gas from the manifold to the sensor, it is possible that the sudden increase in pressure may excite pressure waves in this pipe. A test was performed to ensure that the oscillations were not the result of aliasing due to the acquisition rate, but at 10kHz sampling the pressure signal exhibited identical behaviour. These oscillations will not be carried through to the inlet manifold due to the filtering effect of the turbocharger dynamics. The inlet manifold pressure is displayed in the frame below, the difference in response rate between exhaust and inlet pressure can clearly be seen, the exhaust pressure controller responds to the exhaust pressure error and hence responds faster than the standard controller on inlet boost error.

The air fuel ratio trace confirms that the smoke reduction during the initial tip-in corresponds to a slightly higher in-cylinder air fuel ratio for the exhaust pressure controller. The improvement in post transient smoke is validated by the higher and more stable air fuel ratio for the exhaust pressure controller.

Comparing turbocharger speeds it can be seen how significant the overshoot in turbocharger speed actually is. The Px controller provides an equally rapid acceleration to the standard control system as is illustrated by the turbocharger acceleration trace, but for a much shorter time period. A slow drop off in turbocharger speed can be noticed, this is eventually corrected at around 4.5s. The delay is due to the hysteresis in the vane mechanism. The VGT position remains constant after the initial part of the transient, however the exhaust pressure error increases slightly leading to a gradual increase in controller output in an attempt to close the vanes to track the target exhaust pressure. As the change in control output is gradual, the turbocharger vanes do not respond initially, only when the output has changed by a certain amount do they actually move. There is slight undershoot in exhaust pressure before the tracking error is brought back down to zero.

#### 5.8.2.3 *Figure 5.13 VGT Vane Position and Controller Terms*

The plot of VGT vane position shows that for the exhaust pressure controller the vanes respond much earlier in the transient before settling rapidly to an intermediate position. The VGT does not instantaneously 'flip' open to its end-stop as is the case for the standard controller.

It can be seen from the decomposition of the control signal that the proportional (P) term is doing most of the work. The control system response is oscillatory which suggests that the gains are too high, provision was made in the strategy for different gains to be used during transient control but overall the system works well with the gains unaltered from the original calibration. The vane mechanism and actuator vacuum dynamics tend to attenuate the oscillations in the control signal, this can be seen in small disturbances to the vane position before settling.

#### 5.8.2.4 *Figure 5.14 TURBINE FLOW vs. PRESSURE RATIO*

The two transients have been plotted across the turbine flow characteristic; the turbine flow is not directly measured but estimated from other measurements (see **Appendix B**). The exhaust pressure controller guides the transient away from the choked region of the turbine map following the 'ideal' trajectory defined previously as in **Figure 5.5**. Each data point on this plot represents 1 controller timestep (16milliseconds) therefore the difference in time spent in the choking region between the 2 controllers is very clear.

### 5.8.3 Summary of performance at different engine speeds

**Figure 5.15** to **Figure 5.18** summarise the testing at all engine speeds, the black lines show the behaviour of the standard controller whereas the coloured lines represent the exhaust pressure controller with various setpoints as defined in the legend.

#### 5.8.3.1 *Figure 5.15 Exhaust Manifold Pressure*

This figure describes the exhaust pressure tracking at four engine speeds, for the first three the improvement in exhaust backpressure behaviour is clear, all plots show the pressure controller to reduce drastically the time spent at excessive exhaust pressures. All controllers display a certain amount of steady state tracking drift, this follows the explanation given for the detailed discussion of the 2500 rev/min test. In the first frame (2000 rev/min) the exhaust pressure controller with a setpoint of 120 kPag appears to give worse performance than the baseline strategy. This is the result of inappropriate settings for the safety monitoring routines designed to prevent overspeeding of the turbocharger or overboosting of the engine. In the final frame (3500 rev/min) it appears that the exhaust pressure controller is not tracking setpoints at all. This is the case but is caused by operator error, the control signal lower saturation limit was set too high, therefore although the control action is trying to track the exhaust pressure, the output signal is being held at the lower saturation limit and no movement of the vanes occurs.

#### 5.8.3.2 *Figure 5.16 TURBOCHARGER SPEED*

A clear relationship between exhaust pressure setpoint and resultant turbocharger speed can be seen except during the 3500 rev/min test, but this does not count as the controller did not have authority over the vane mechanism.

#### 5.8.3.3 *Figure 5.17 INLET MANIFOLD PRESSURE*

The inlet manifold pressures achieved by the controllers are described in **Figure 5.17**, a simple monotonically increasing relationship between exhaust pressure setpoint and the resultant inlet manifold pressure is observed, this allows the inlet pressure setpoints from the boost control strategy to be translated into exhaust pressure setpoints.

#### 5.8.3.4 *Figure 5.18 VGT VANE POSITION*

The VGT vane position for all tests is illustrated in **Figure 5.18**, in general the delay between the fuel step occurring and the response of the vanes by the standard strategy reduces with increasing engine speed. This follows as the inlet boost pressure rise time reduces with increasing engine speed. The exhaust pressure controllers do not show such a variance, the setpoint has an effect on when the vanes open, but because the exhaust pressure dynamics are much faster, the vane response is generally much faster than for the standard controller. In the



third frame (3500rev/min) the effect of the control signal output saturation on the vane position is clear, no movement occurs for any of the exhaust pressure controllers, whereas the standard controller manages to over-open the vanes.

#### 5.8.3.5 *Figure 5.19 TURBINE PRESSURE RATIO vs. EXHAUST MANIFOLD PRESSURE*

The turbine pressure ratio is plotted against the exhaust manifold pressure for all tests. This illustrates that the turbine pressure ratio has a linear relationship with the exhaust manifold pressure and therefore the exhaust manifold pressure can be confidently used as a setpoint for a target for turbine pressure ratio. The relationship seems to be altered slightly in gradient with increasing engine speed, although for the actual amount of scatter shown it may be possible to ignore this trend and keep a simple relationship between pressure ratio and pre-turbine pressure.

## **5.9 SUMMARY OF RESULTS**

Exhaust manifold pressure offers significantly reduced delays as a feedback variable for the VGT vane mechanism. The delay in the response of the vane mechanism still applies but the small volume of the manifold ensures a near instantaneous response in pressure to a change in vane settings or cylinder-out conditions.

The overall transient behaviour has been significantly improved by the simple strategy alteration. From the point of view of calibration, the additional elements require minimal effort, the exhaust pressure setpoints need to be chosen and scheduled; the simple relationship with inlet conditions allows the inlet setpoints to be translated directly to exhaust setpoints. Different gains can be chosen however the existing gains are shown to perform adequately. The new strategy is also no less transparent than the standard strategy, contributing to the ease of calibration. In terms of computational requirements, the additional blocks incur only a marginal increase in controller execution time.

2500 rev/min tip-in transient (7-34 mg/shot fuel step)

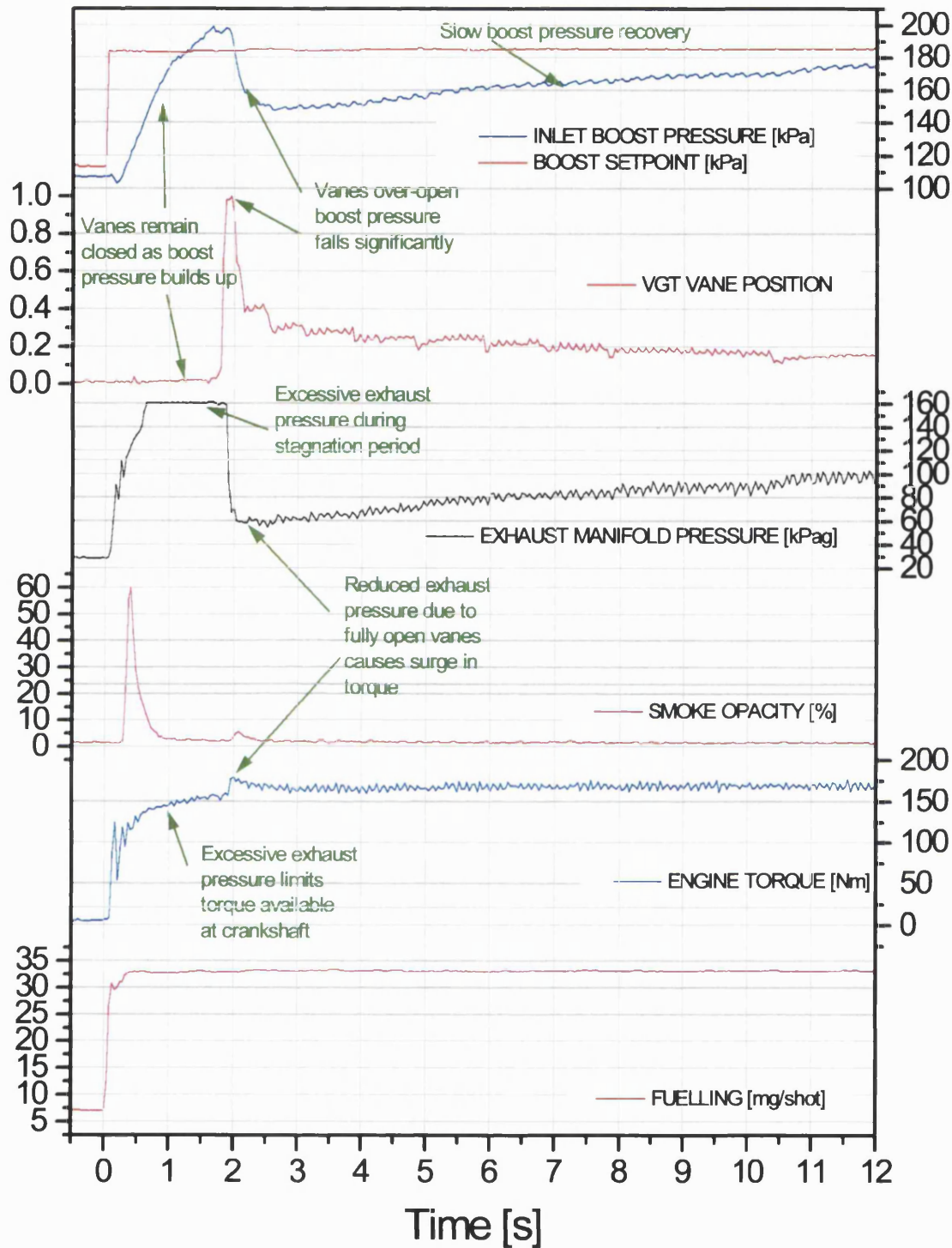


Figure 5.1 2500 rev/min tip-in transient

3500 rev/min tip-in transient (10-35 mg/shot fuel step)

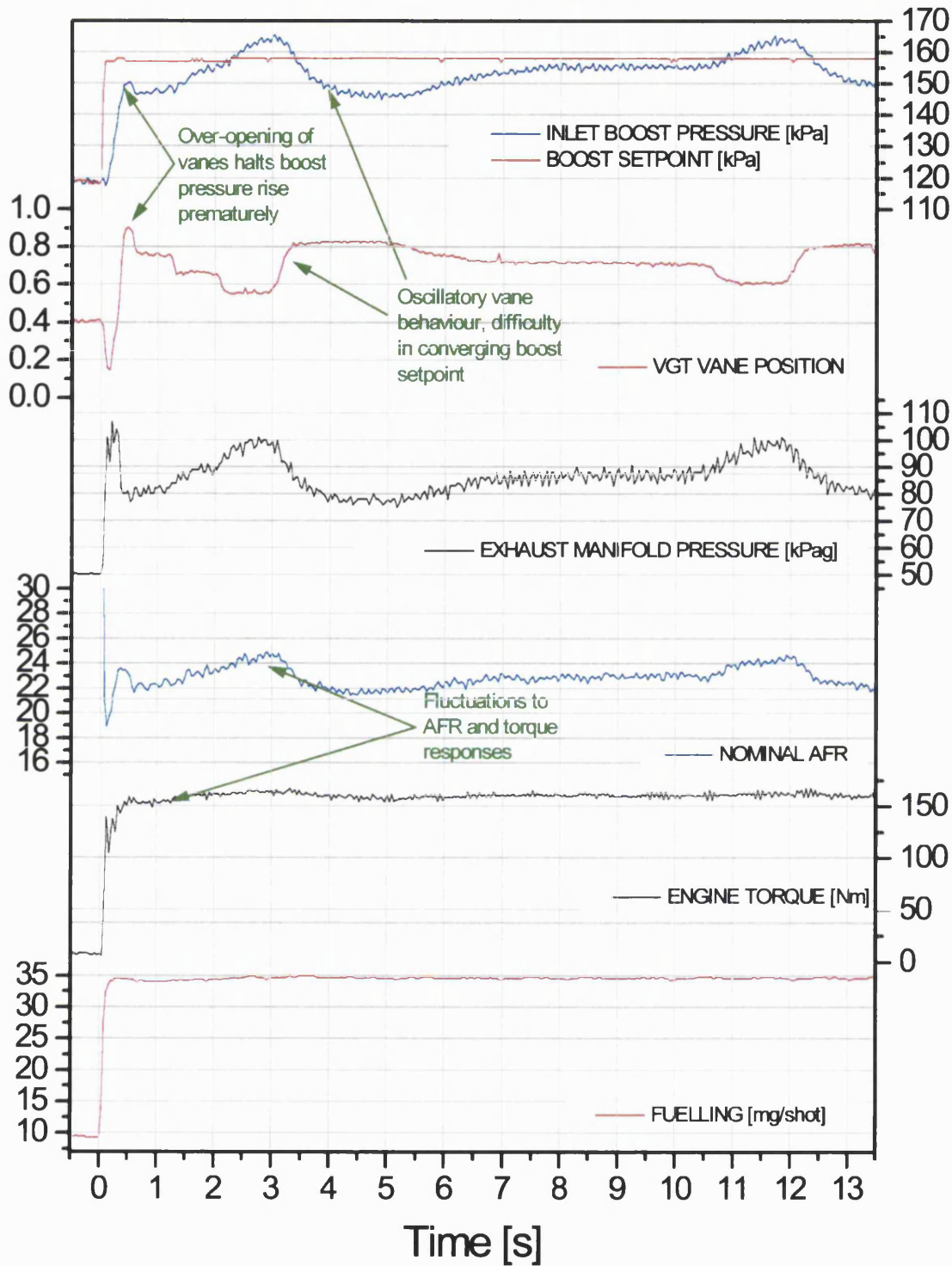


Figure 5.2 3500 rev/min tip-in transient

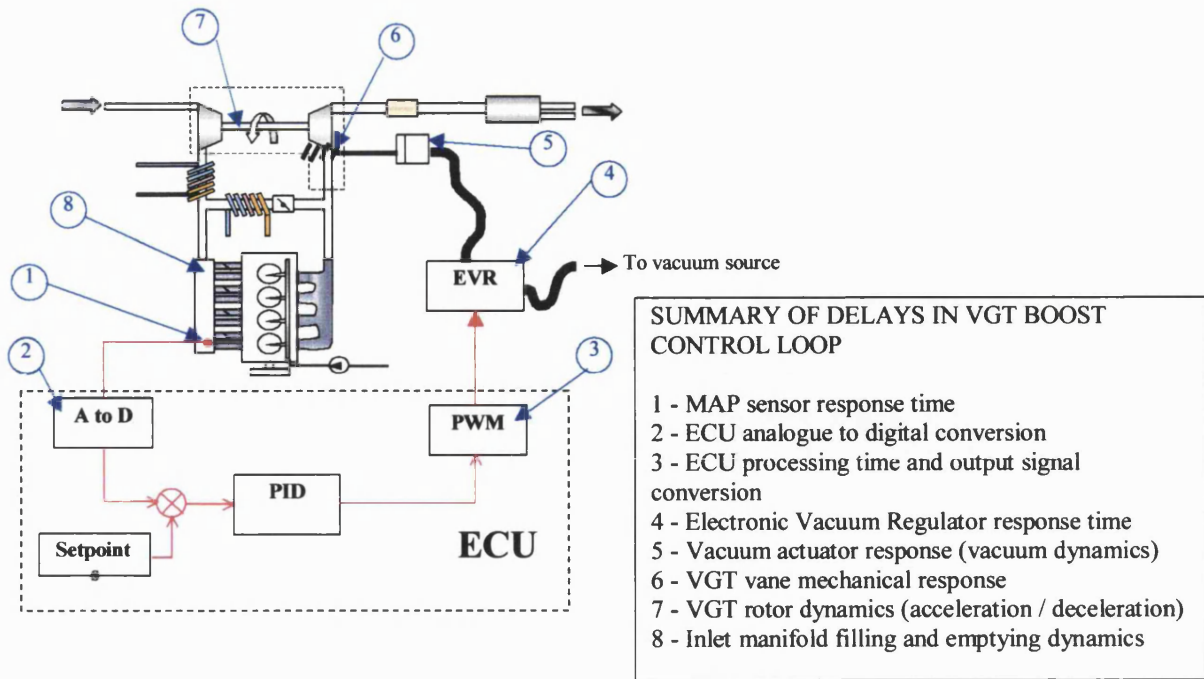


Figure 5.3 VGT boost control loop system delays

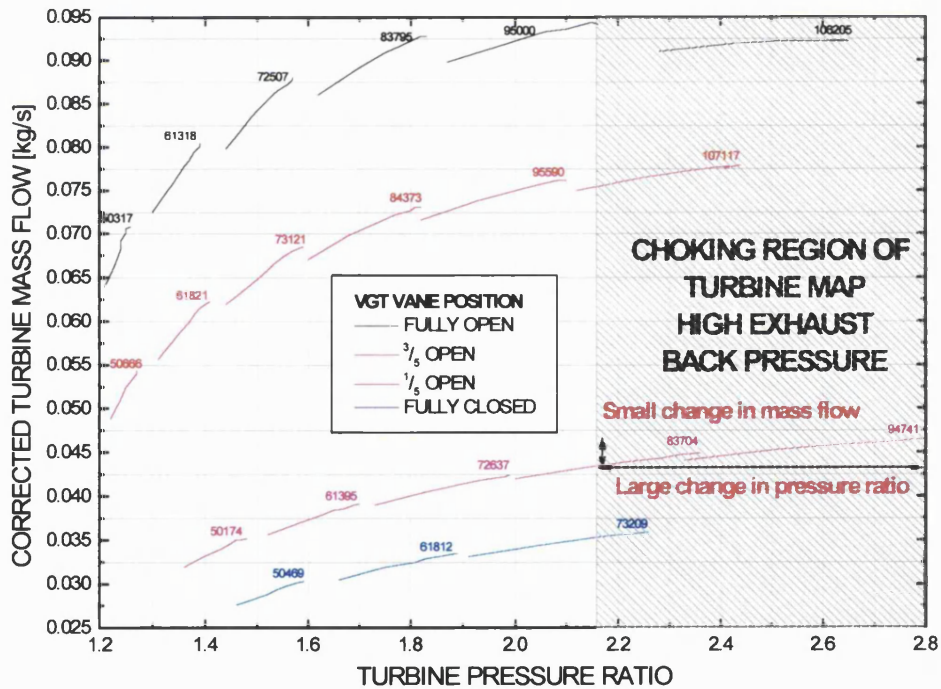


Figure 5.4 Turbine characteristic indicating choking region

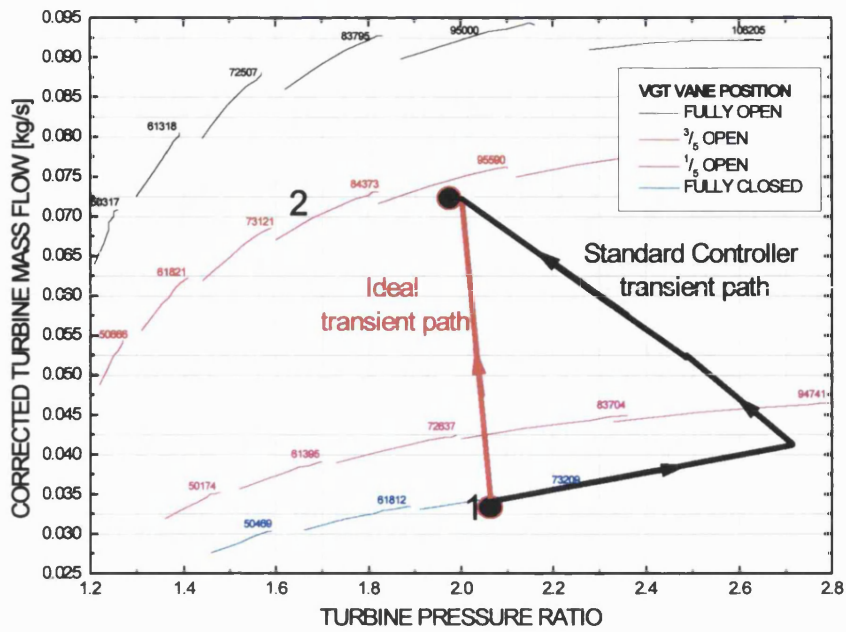


Figure 5.5 Turbine characteristic with actual and ideal transient trajectories

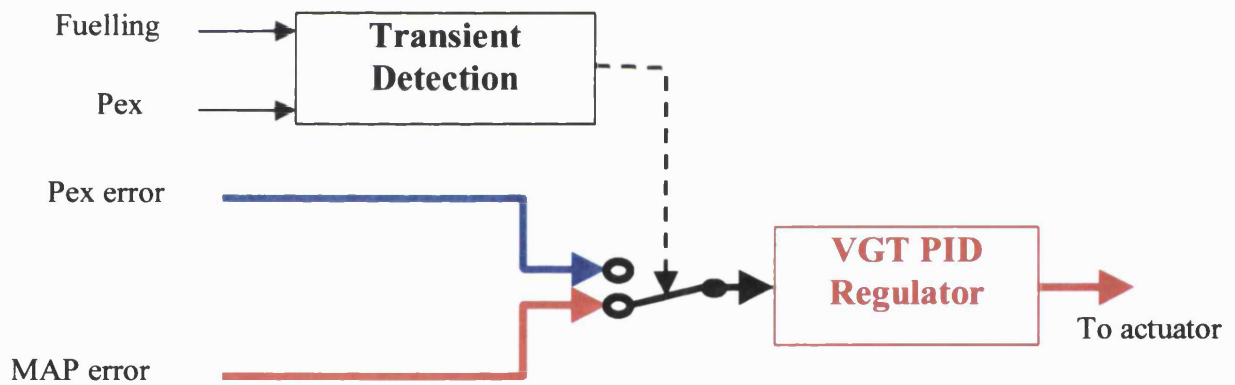


Figure 5.6 Schematic representation of control strategy

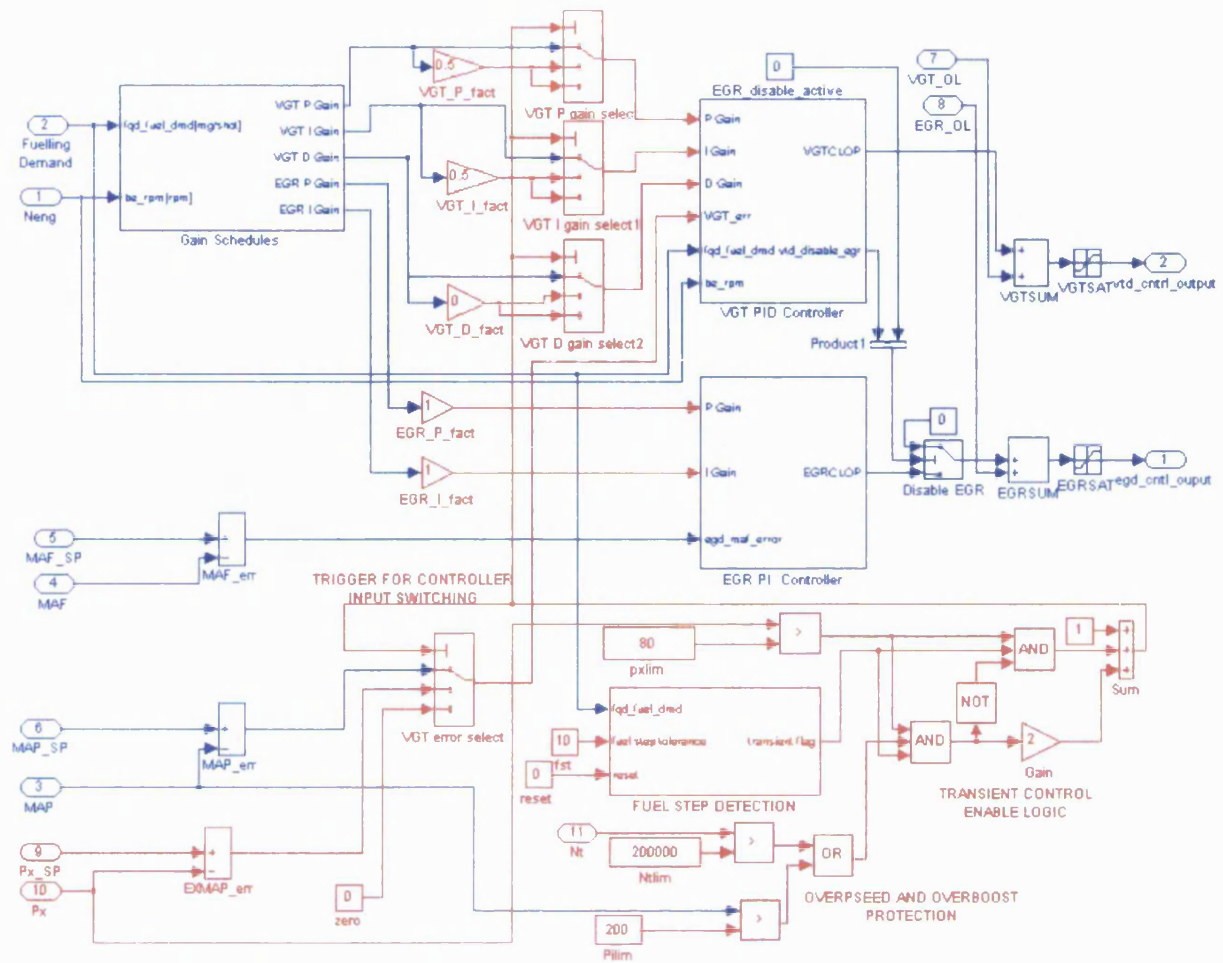


Figure 5.7 Simulink implementation of Exhaust Pressure Controller

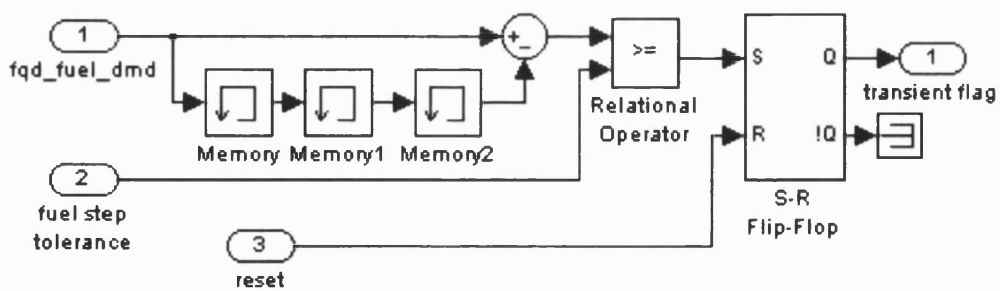
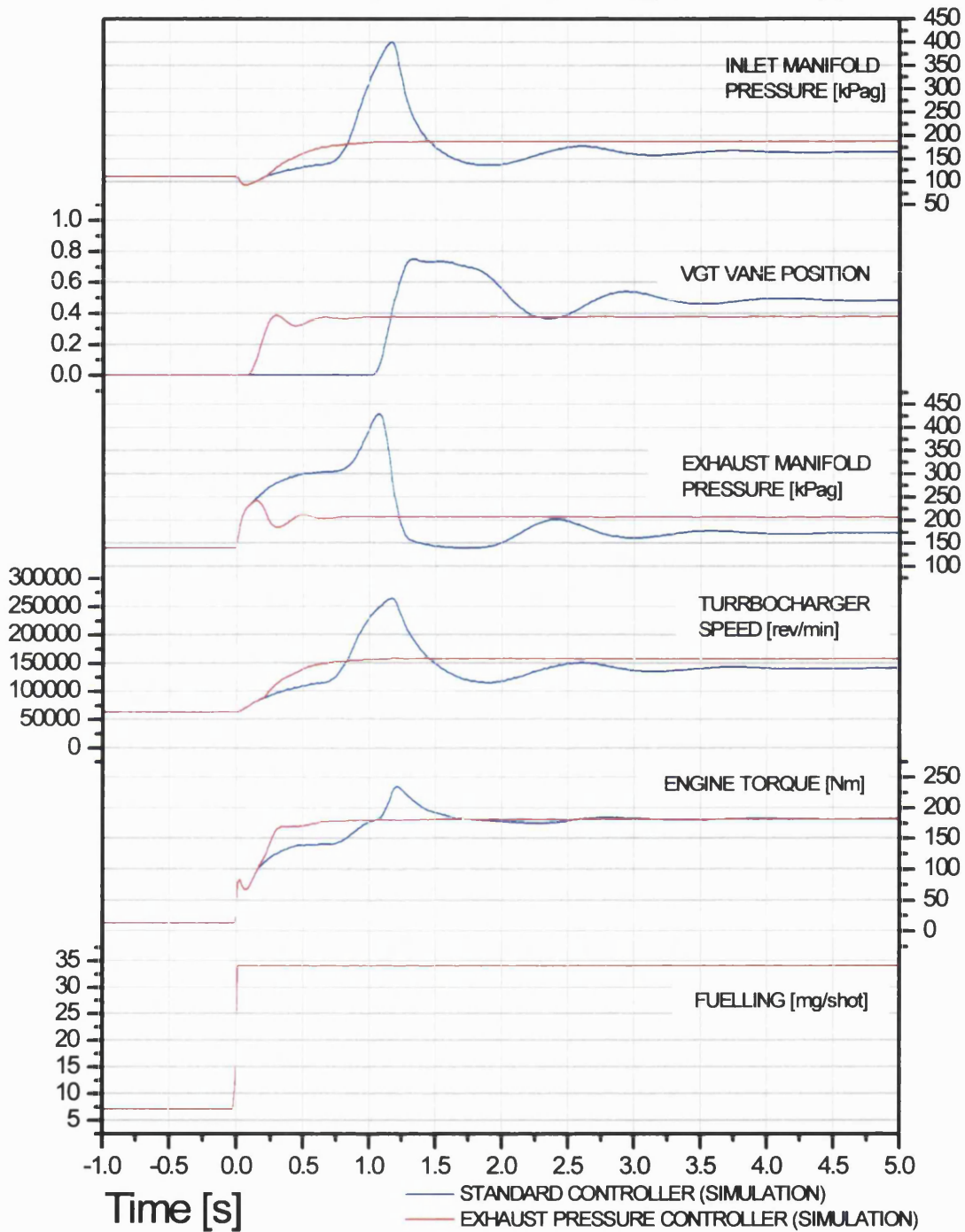


Figure 5.8 Transient detection routine

SIMULATION (DEVMODEL\_Px.mdl)  
 WITH NON-LINEAR ACTUATOR DYNAMICS  
 2500 rev/min tip-in transient (7-34 mg/shot fuel step)



**Figure 5.9 Simulation of the exhaust pressure controller compared with standard controller**

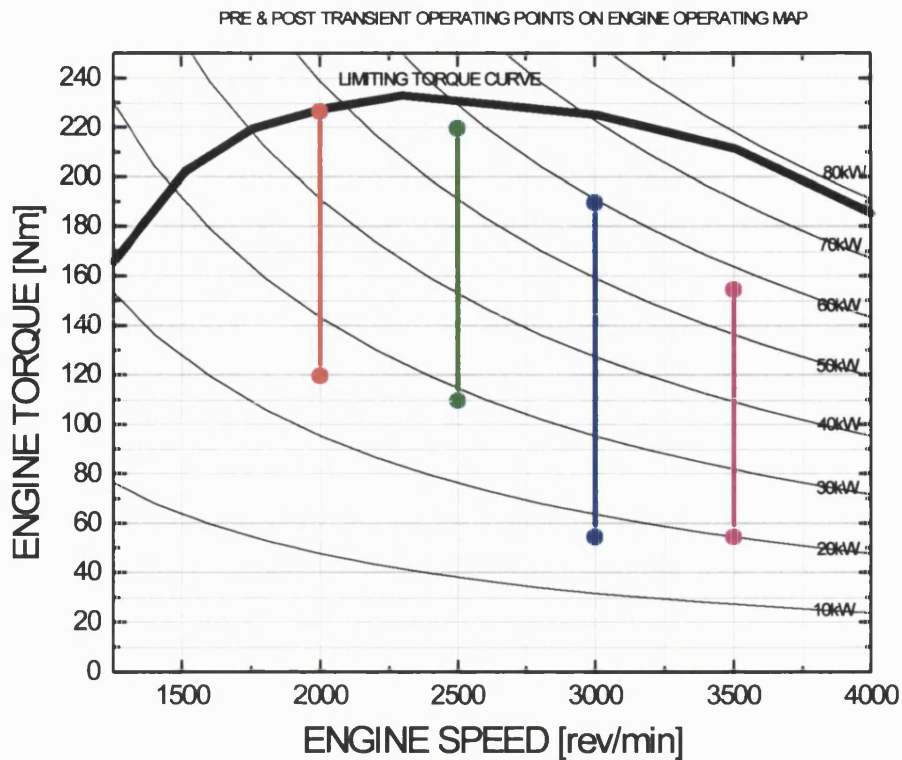


Figure 5.10 Engine operating conditions covered by the exhaust pressure controller

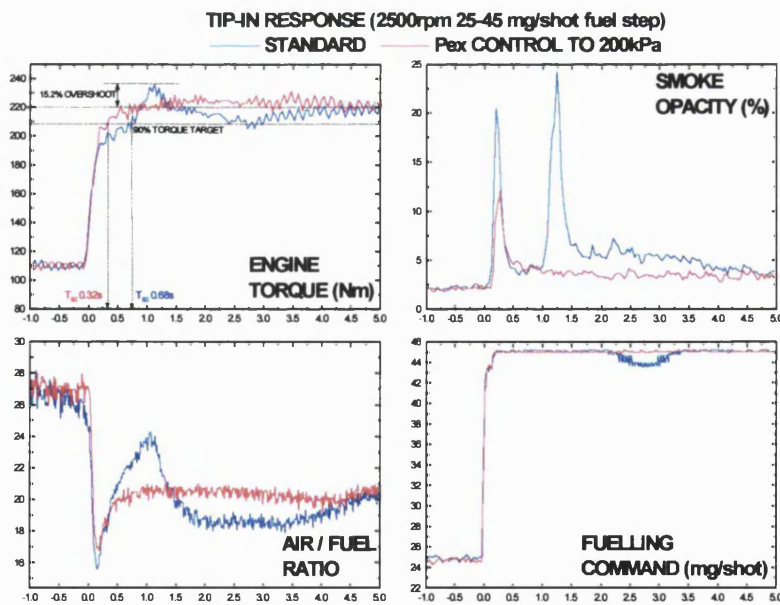
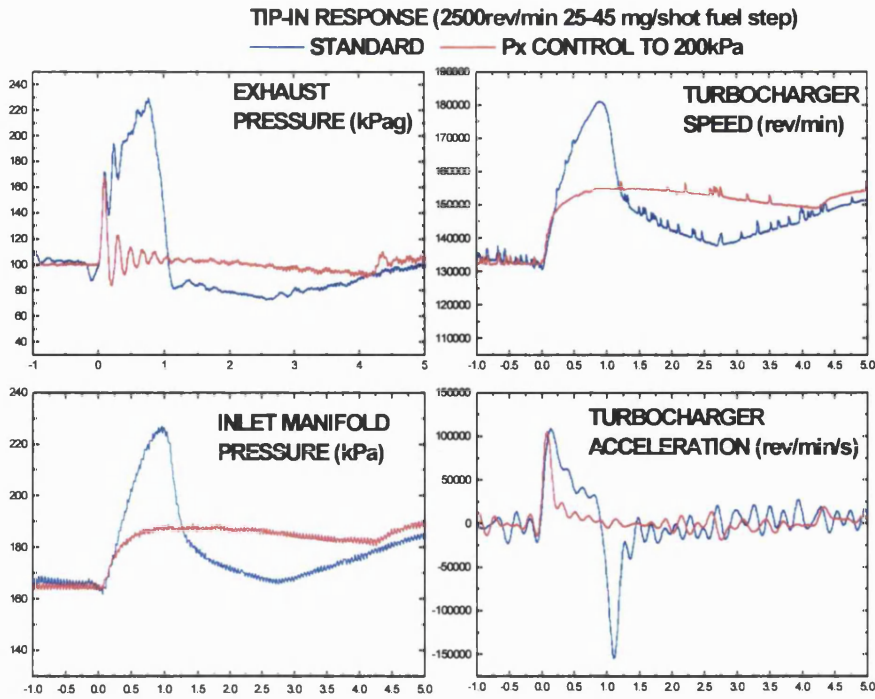
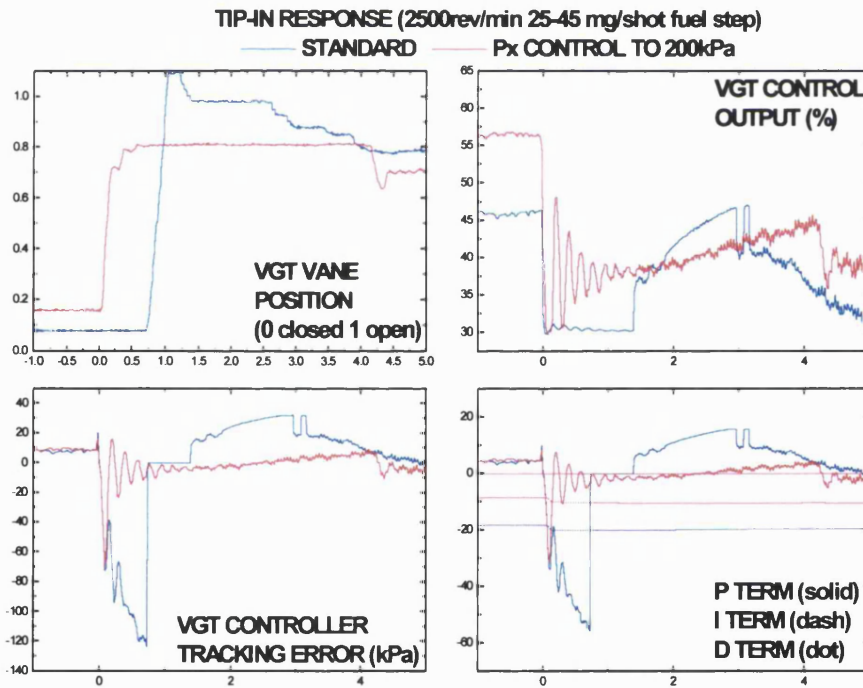


Figure 5.11 Experimental comparison of controllers: Engine Performance





**Figure 5.12 Experimental comparison of controllers: Turbocharger and Engine Pressure Behaviour**



**Figure 5.13 Experimental comparison of controllers: VGT Vane Position and Controller Terms**

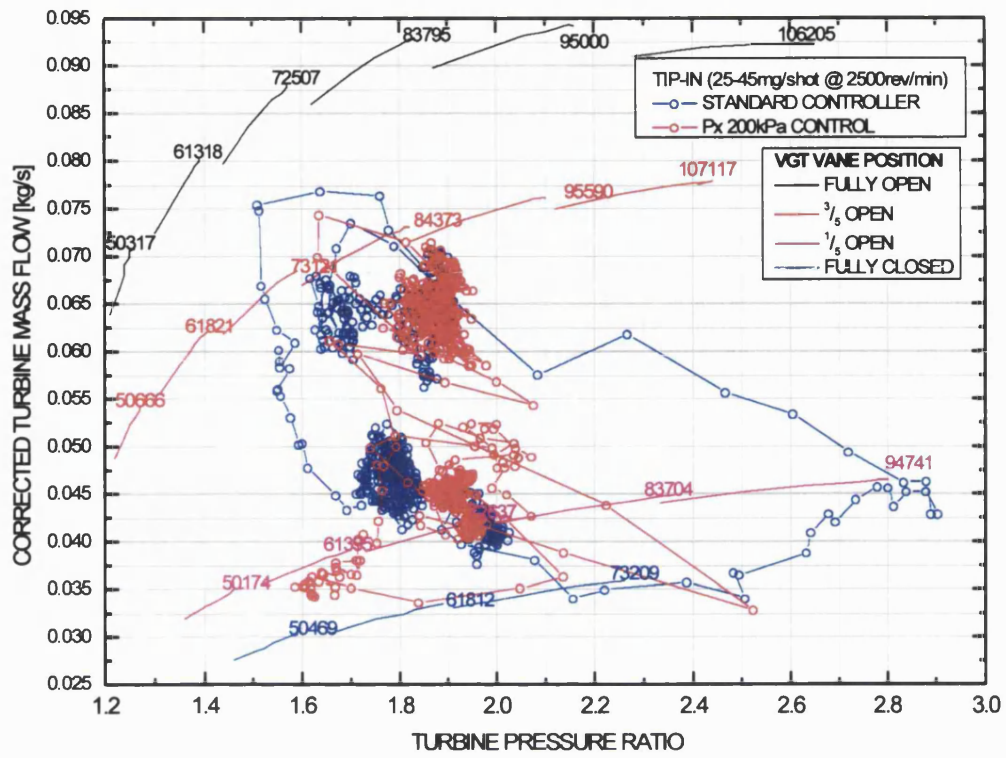


Figure 5.14 Turbine Flow versus Pressure Ratio

PX\_2.mdl TRANSIENT EXHAUST PRESSURE CONTROLLER  
 Comparison of exhaust pressure behaviour at different engine speeds

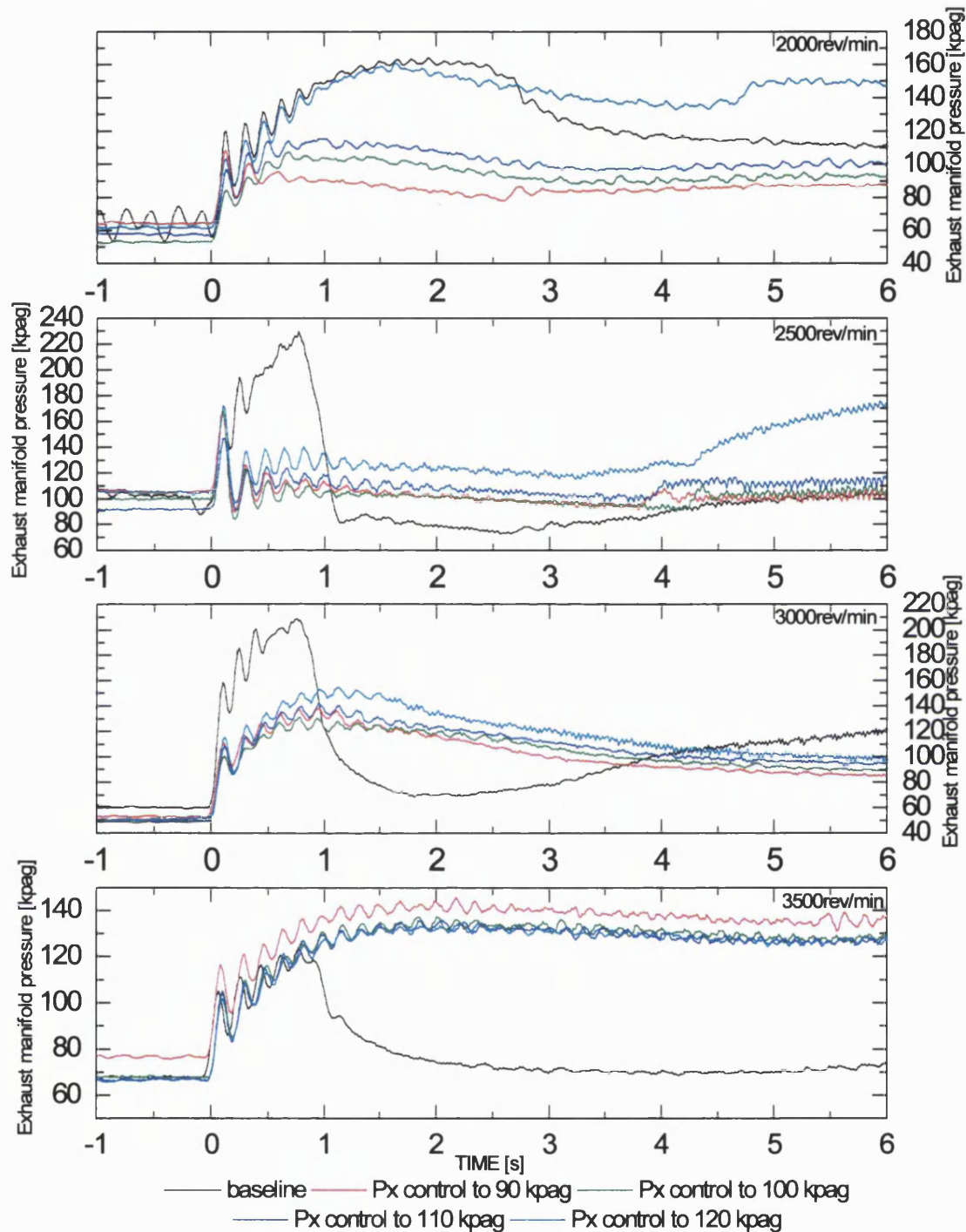
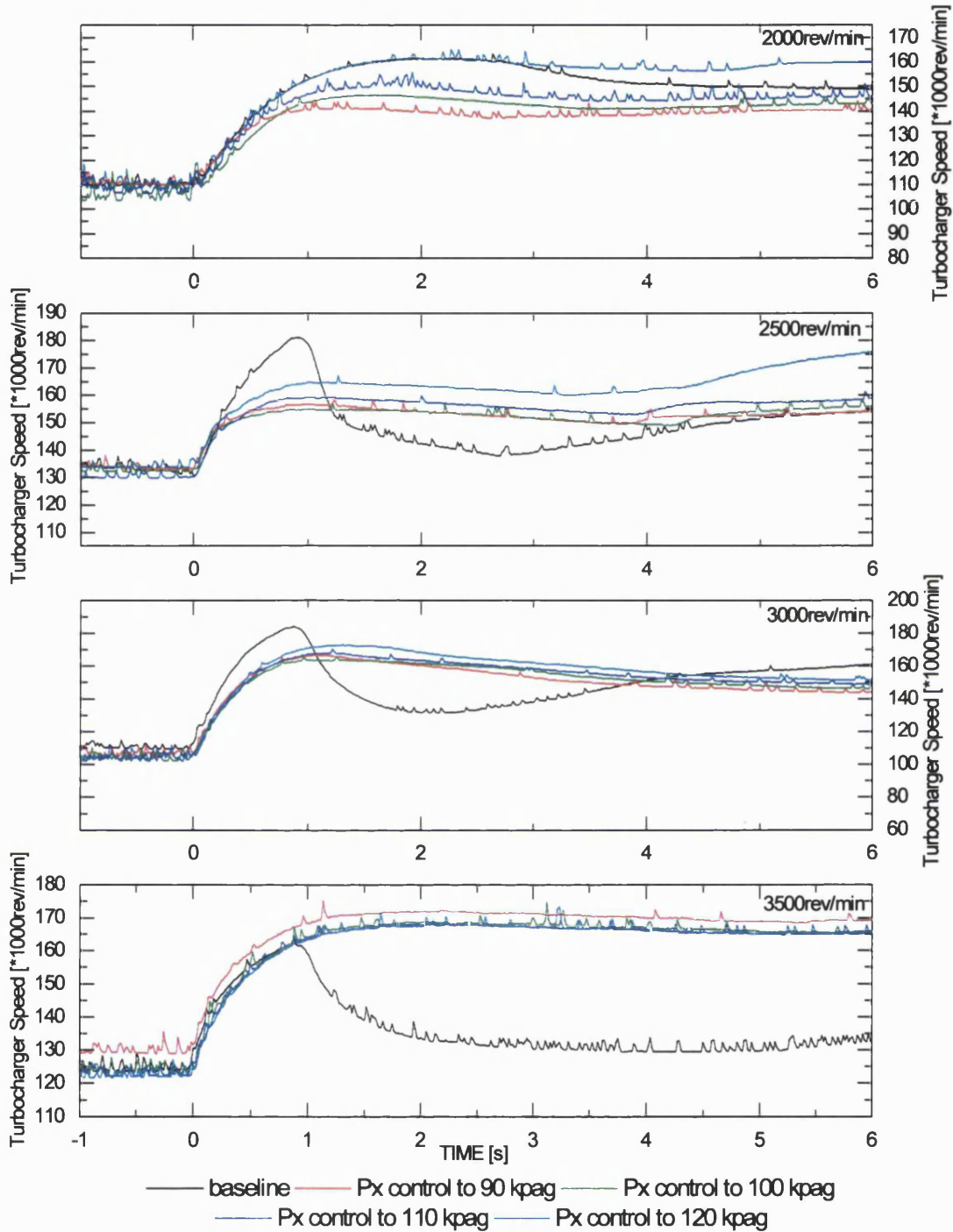


Figure 5.15 Comparison of controller performance at different engine speeds: Exhaust Manifold Pressure

PX\_2.mdl TRANSIENT EXHAUST PRESSURE CONTROLLER  
 Comparison of turbocharger speed behaviour at different engine speeds



**Figure 5.16 Comparison of controller performance at different engine speeds:  
 Turbocharger Speed**

PX\_2.mdl TRANSIENT EXHAUST PRESSURE CONTROLLER  
 Comparison of Inlet Manifold Pressures at different engine speeds

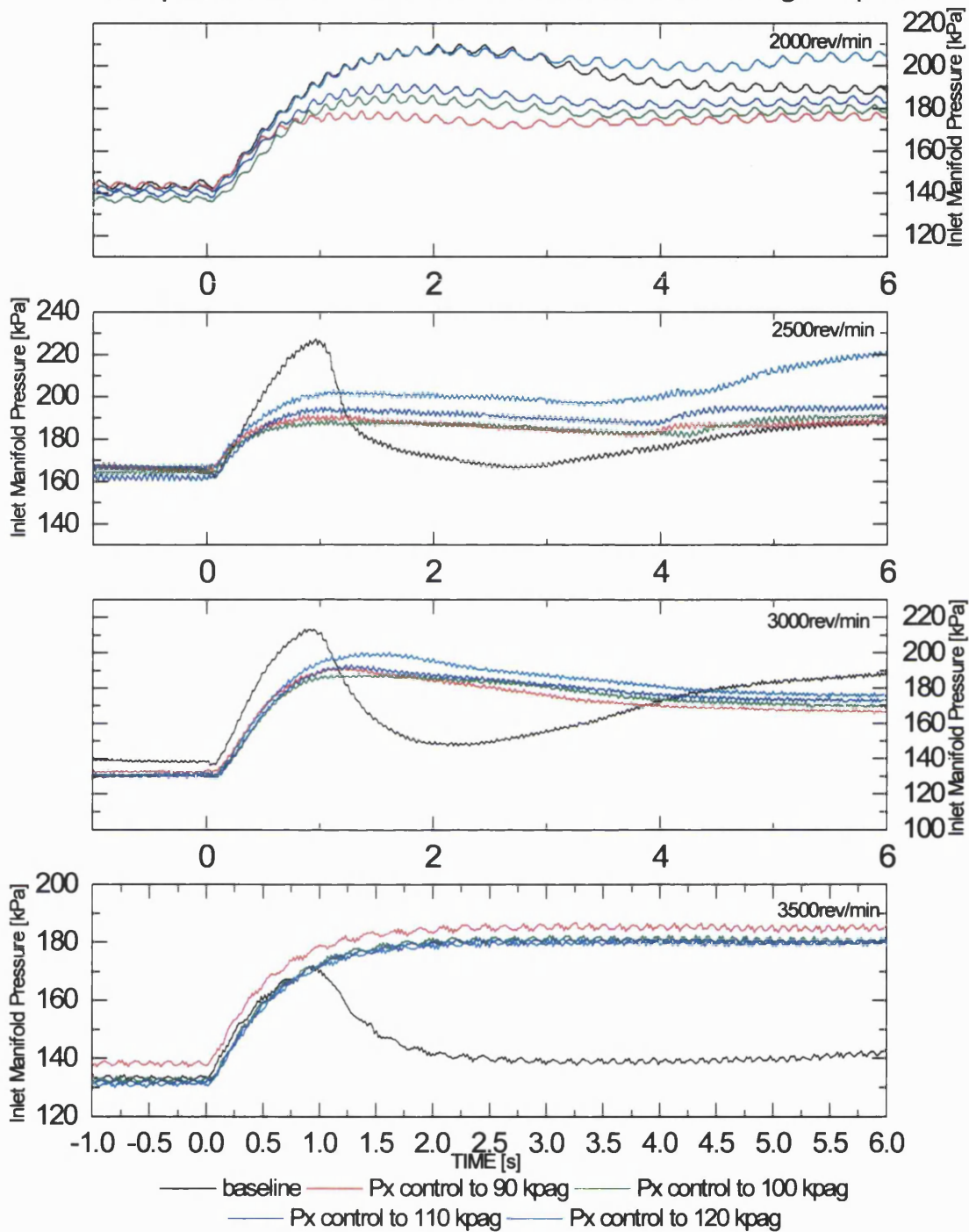


Figure 5.17 Comparison of controller performance at different engine speeds: Inlet Manifold Pressure

PX\_2.mdl TRANSIENT EXHAUST PRESSURE CONTROLLER  
 Comparison of VGT vane position at different engine speeds

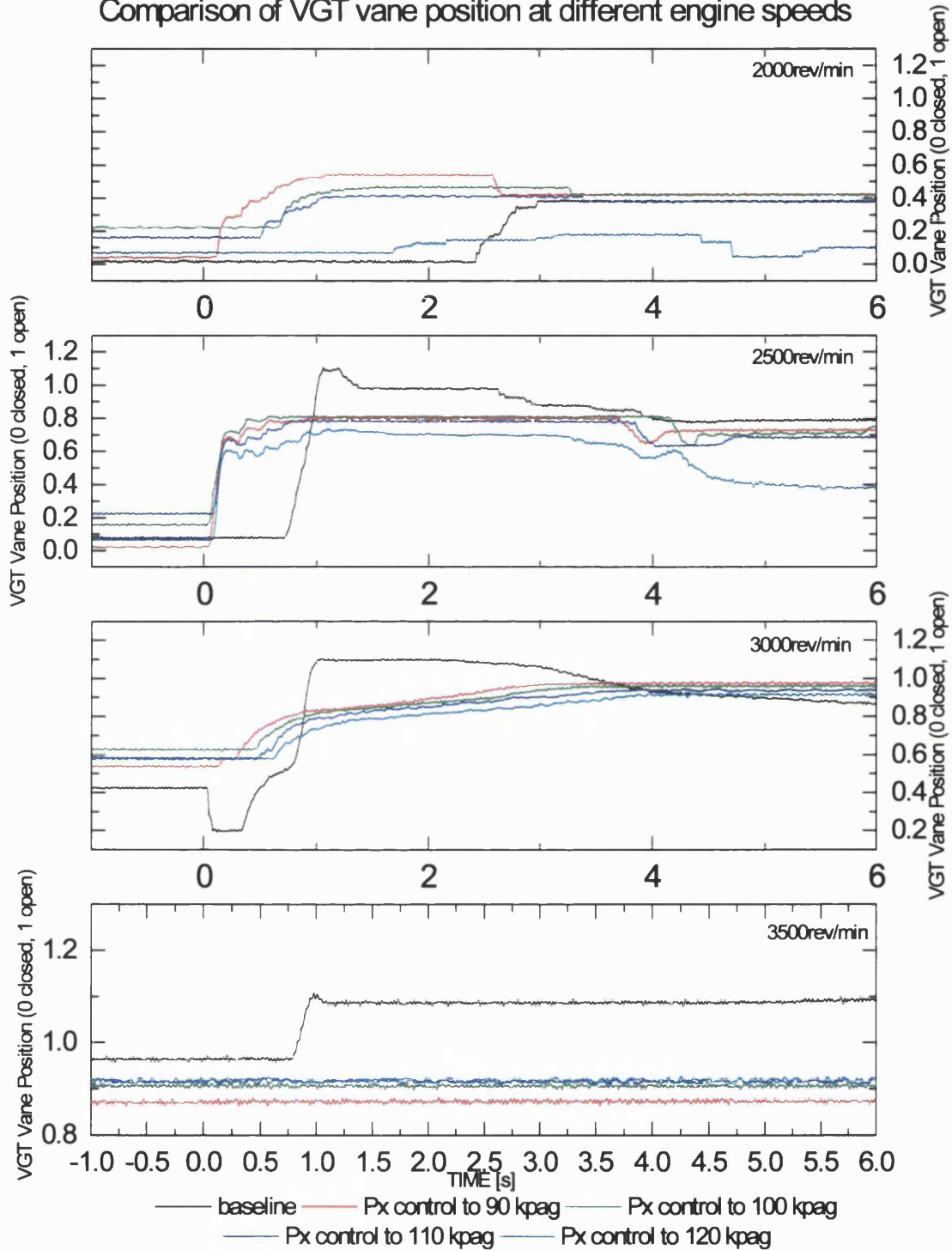


Figure 5.18 Comparison of controller performance at different engine speeds: VGT Vane Position

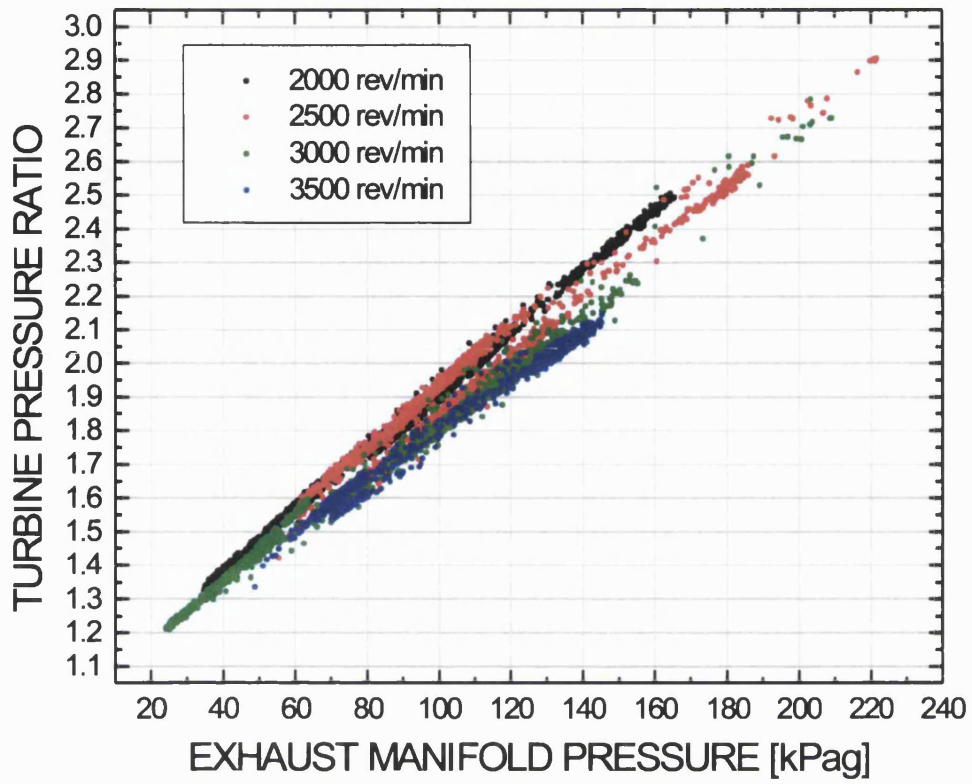


Figure 5.19 Turbine Pressure Ratio vs. Exhaust Manifold Pressure

## **Chapter 6 COORDINATED EGR VGT CONTROL 1**

### **6.1 INTRODUCTION**

In several recent publications, coordinated EGR and VGT controllers are proposed as a means of extracting improved dynamic airflow response from the engine. A strong coupling exists between the two systems due to the exhaust manifold, causing changes to the setting of one system to alter the conditions of the other.

Most of the previous attempts at coordinated control have used complex control techniques, usually incorporating linearised system models. In this study fuzzy logic is proposed as a control method to achieve a more simple and transparent strategy. In particular, the identification of the operating region where coordinated control should be used is readily encapsulated in the simple heuristic rule structure of fuzzy logic.

An EGR-VGT controller which tracks compressor airflow and inlet manifold boost pressure is synthesized, using fuzzy logic to provide the control law. The controller is developed in simulation and on the dynamic engine test facility, using constant speed fuelling step changes to evaluate the airflow response.

The controller was initially developed without including the proportional action into the fuzzy logic rule base of the controller, but this was found to produce poor performance. A version of the same controller with the proportional term integrated into the rule base was tested in simulation and showed much improved response and tracking behaviour.

Although the fuzzy controller represents an improvement over the standard control strategy, the large computational demands of a full fuzzy logic controller reduce the overall benefit of such a controller when considering the limited processor resources of a production engine management system.

### **6.2 MOTIVATION FOR COORDINATED EGR AND VGT CONTROL**

Because of the coupling of EGR and VGT through the exhaust manifold, coordinated action of these systems can improve the dynamic response of the EGR and fresh airflows into the engine. The ability to reduce and increase exhaust gas recirculation levels more rapidly has beneficial consequences on both driveability and emissions. The coordination of the devices can also prevent one system reacting to changes made to the setting of the other. A simple method of obtaining such improvements is highly desirable.



### 6.2.1 EGR FLOW BEHAVIOUR

**Equation (6-1)** describes the mass flow through the EGR valve, it is derived from the expression for compressible flow through an orifice.

$$W_{xi} = A_{eff}(x_{EGR}, p_i, p_x) \frac{p_x}{\sqrt{RT_x}} \psi\left(\frac{p_i}{p_x}\right) \quad (6-1)$$

where  $W_{xi}$  is the EGR flow

$A_{eff}(x_{EGR}, p_i, p_x)$  is a non-linear expression for the flow area

$p_i, p_x$  are inlet and exhaust manifold pressures respectively

$R$  is the Universal Gas Constant

$T_x$  is the exhaust temperature

$\psi\left(\frac{p_i}{p_x}\right)$  is a non-linear flow function of the pressure ratio acting across the valve

From this expression it is clear that the EGR flow is a strong function of pressure ratio, upstream pressure and valve position.

For a step increase in fuelling (tip-in), a rapid reduction in EGR flow is required in order not to compromise the air fuel ratio of the cylinder charge. For a step reduction in fuelling (tip-out) the EGR flow must be increased rapidly to minimise  $\text{NO}_x$  emissions.

### 6.2.2 EGR BEHAVIOUR UNDER THE STANDARD CONTROL SCHEME

Under the standard control scheme, the response of the EGR system to a tip-in is to close the EGR valve. By examining **Equation (6-1)** it is clear that this will reduce EGR flow by reducing the flow area, however the reduced exhaust gas flow path presents a greater flow restriction and as a result, the exhaust manifold pressure increases. This increase in exhaust manifold pressure acts to increase the EGR flow via the upstream pressure ( $p_x$ ) and pressure ratio ( $\Psi$ ) terms of the flow equation. The rise in flow effect is not strong enough to counter the reduction in flow due to closing the valve, but it does slow down the overall rate of reduction in EGR flow.

In response to the tip-out manoeuvre the standard control scheme opens the EGR valve, this will rapidly increase the flow through the EGR circuit, however, opening the valve has the effect of reducing exhaust pressure, this will slow down the rate of change in EGR flow.

In both of the above cases, the standard control scheme controls the EGR valve independently of the VGT vane mechanism, the VGT vanes will respond to boost pressure targets that typically change in the same sense as the airflow setpoints governing the EGR behaviour, i.e.

for a tip-in the boost pressure demand increases, and for a tip-out the boost pressure demand decreases.

In response to a tip-in the control system reduces the flow areas of both devices, this will further increase exhaust manifold pressure. The increased pressure upstream of the valve will reduce the rate at which EGR flow decreases. Similarly, a tip-out results in reduced boost and airflow demands, therefore both EGR valve and VGT vanes are opened. This action results in a rapid reduction of exhaust pressure, thus reducing the driving pressure differential for EGR flow and hindering the EGR flow response.

### **6.2.3 OPERATING REGION DEPENDENCY**

Due to the highly non-linear nature of the engine-EGR-turbocharger gas dynamics, it is not surprising to find that this behaviour does not apply to all engine operating conditions (i.e. combinations of engine speed and fuelling quantity). The standard control scheme was designed around the fact that for a large region of the engine operating map, the airflow to EGR valve position loop and boost pressure to VGT vane position loop are reasonably well decoupled and can therefore be treated as independent control problems. Only in the regions where exhaust gas energy is low does the behaviour change such that both EGR and VGT position have a dominant effect over airflow.

As a physical interpretation of this behaviour, consider exhaust gas leaving the cylinders and entering the exhaust manifold, once in the manifold it has a choice of two paths to take, through the EGR circuit or through the turbocharger. At low speeds and loads exhaust gas energy is low and the turbocharger presents the more resistive of flow paths as it will attempt to extract more energy from the gases. Therefore the gas will flow more readily through the EGR circuit as it offers less resistance.

The energy available to accelerate the turbocharger increases with exhaust gas energy, thus the turbocharger flow path becomes more receptive to flow. As more energy is extracted by the turbocharger, more energy is put into the inlet air charge by the compressor, hence the increase in inlet manifold boost pressure. At a certain exhaust gas energy level, the consequence of altering the turbocharger vane position will be a stronger effect on the inlet manifold pressure than on the EGR flowrate, this is the point where a crossover occurs.

The standard control scheme is configured to avoid the problems associated with this reversal in behaviour; the open-loop controller terms and boost pressure setpoints are chosen such that throughout the strongly coupled region the VGT vanes remain fully closed. In this manner the VGT acts as a backpressure source to provide high EGR flow for a given EGR valve opening.

Once the engine operating condition is well clear of the coupled region, the VGT is allowed to open and modulate boost pressure.

### **6.3 COORDINATED EGR AND VGT CONTROL**

It is now clear why improvements in EGR flow response are possible through the coordinated control of the EGR and VGT actuators. In the case of a tip-in, as well as closing the EGR valve, opening the VGT vanes will counter the rise in exhaust manifold pressure thus help to reduce EGR flow more rapidly. This will also have the effect of reducing the turbocharger pressure ratio and as a consequence the inlet boost pressure, however this is of little consequence for the low speed and low load engine operating range as the boost pressures are very low anyway. For the case of a tip-out, closing the VGT vanes whilst opening the EGR valve will help maintain the exhaust backpressure and thus increase the EGR flow response.

As investigated in the literature study Van Nieuwstadt et al [35,36] have developed at least 3 schemes to achieve coordinated control. The H-infinity approach appeared most successful but was the only controller to be tested over a constant speed fuelling profile, thus showing clearly any improvements in airflow response. The other controllers were evaluated over drive cycles and therefore it is difficult to ascertain to what extent they improve airflow response. Judging by the cumulative drive cycle emission results presented in [36], the performance is strongly affected by the choice of setpoint, both coordinated controllers use different setpoints and both achieve higher smoke and lower NO<sub>x</sub> than the standard control scheme. The H-infinity approach is a powerful controller synthesis tool, however the resulting strategies utilise linearised plant models and the overall scheme is computationally intensive.

### **6.4 FUZZY LOGIC FOR COORDINATED CONTROL**

The change in the VGT to airflow behaviour with engine operating point is a big obstacle when designing a coordinated controller, it is imprecise as to where exactly the VGT influence on airflow becomes negative. For this reason, a fuzzy logic approach is proposed due the simple incorporation of such imprecision offered by the method. Fuzzy logic allows the use of linguistic rules to construct control laws, from this point of view it can be seen that a rule of the sort "*if AIRFLOW ERROR is POSITIVE and ENGINE SPEED is LOW and FUELLING is LOW then CLOSE EGR and OPEN VGT*" can be used to achieve the necessary control action under the specified operating condition.

### 6.4.1 FUZZY LOGIC

Fuzzy Logic has been introduced briefly in **Chapter 2**. A detailed explanation of its workings are clearly beyond the scope of this thesis therefore the reader is referred to the references given in the literature review for more detail; an overview is however given in **Appendix C**. Fuzzy Logic was first introduced by Zadeh in 1965, but Mandani implemented the first practical controller in 1974. Today fuzzy logic is commonplace in a wide variety of applications from domestic appliances to aerospace control systems. Fuzzy logic control is cited as useful for control problems where a qualitative model is available and the control strategy is formulated and executed on the basis of a set of linguistic rules.

A typical fuzzy logic feedback control arrangement is given in **Figure 6.1** showing the main elements of a fuzzy controller; the *fuzzification interface*, the *rulebase* and *inference engine*, and the *defuzzification* interface, these terms are explained in **Appendix C**.

## 6.5 FUZZY CONTROLLER DESIGN

It is very difficult to identify a universally adopted design procedure for controllers using fuzzy logic, the literature can offer useful guidelines and pointers but the designer ultimately has a great deal of freedom, and often as a result difficulty when it comes to establishing an effective control law.

In [90] some of the design issues of fuzzy logic controllers are considered from static and dynamic performance perspectives. Static considerations that must be addressed in the design are:

*The completeness of the control rules* : Ensuring the rules cover all possible input scenarios.

*Consistency of control rules* : There should be no conflicting rules that produce opposing outputs, such conflicts will be masked by the defuzzification process and are therefore difficult to detect from the output alone.

*The interaction of control rules* : The effect of interactive rules or rules based around similar conditions must be carefully checked.

*The robustness of the rules* : How will the rules stand up to possible variations in system behaviour?

The fuzzy logic structure allows a range of hybrid combinations with PID controllers, models and predictive elements to create a good tracking controller based on fuzzy logic.

In [91] several hybrid controller configurations based on the PID controller are proposed:

*Fuzzy proportional* where the output is simply a non-linear function of input error.

*Fuzzy Proportional + Derivative* uses rules based on the rate of change of input error in addition to the proportional function.

*Fuzzy Proportional + Derivative + Fuzzy Integral* is proposed as it has been shown that it is not straightforward to write integral action rules, also, a rule base simultaneously involving 3 control terms is very large. Therefore, an independent I controller is used.

In [68] **Brace et al** use a fuzzy inference engine to generate rates of change for demanded speed and torque of an integrated Diesel and CVT powertrain. The generated increments are integrated to create the demand values, this is a straightforward approach to implementing integral action into the controller.

## **6.6 PROPOSED CONTROLLER**

### **6.6.1 OVERVIEW**

The proposed controller is a multivariable fuzzy proportional plus integral controller that tracks setpoints for airflow and boost pressure by modulating the PWM demands to the EGR and VGT actuators. The controller was designed in the Matlab / Simulink environment using the Fuzzy Logic Toolbox, the software provides a flexible and user-friendly graphical interface for building fuzzy inference systems. The controller evolved through several successive iterations; in simulation, on the test rig and in simulation once again when it was no longer possible to make use of the engine test facility.

The desired control action is embodied in a set of rules that map the inputs to the outputs. For coordinated action this requires using both the EGR valve and the VGT vanes to track airflow setpoints when in the low speed low load operating region. Outside of this region the system is to behave as independent feedback loops from airflow to EGR setting and boost to VGT setting. In the coordinated region the VGT vanes will move in the opposite direction to the EGR valve, i.e. EGR opens and VGT closes, EGR closes and VGT opens. A schematic representation of the controller is given in **Figure 6.2**.

### **6.6.2 CONTROLLER DESIGN**

The first stage of the fuzzy controller design was to decide on a structure. As the controller is to track target airflows and boost pressures, the airflow and boost errors are required as inputs to the inference engine. The behaviour of the system will change depending on the engine operating point, therefore the engine speed and fuelling demand must also be included.

VGT and EGR position inputs to the controller were initially investigated. Although the effectiveness of coordination varies to some extent with valve and vane settings, the benefits

of including them in the inference did not outweigh the additional complication and enlargement to the rule base they caused.

Controller outputs are the rate of change of EGR and VGT duty cycles. These are scaled then integrated and added to open-loop and proportional terms to give a duty cycle demand for the actuators.

The proportional terms were kept independent from the fuzzy logic, the sign of the control loop does not change for the EGR valve, i.e. EGR is always driven by the airflow error regardless of engine operating point. However the VGT will change the sign of its loop gain when operating under coordinated conditions as opposed to independent ones; when tracking airflow error the gain is positive, when tracking boost error the gain is negative. In the first instance this was achieved by using the magnitude of the boost pressure error to generate the VGT proportional term, then using the sign of the VGT fuzzy output to dictate the sign of the proportional term. This method maintains the good tracking control of boost pressure outside of the coordinated control region.

Including the proportional term in the fuzzy inference decouples the proportional term from the size of input error, thus rendering it no longer proportional. The additional rules and Membership Functions required increases significantly the controller computational demand, which although not a problem in simulation does cause problems with the real-time implementation on the test bed and reduces the benefit of such a scheme.

### **6.6.3 CONTROLLER INPUT AND OUTPUT CLASSIFICATION**

The four inputs to the control strategy were 'fuzzified' using the Membership Functions described in **Figure 6.3**. Airflow and boost pressure errors are evaluated by three Membership Functions: positive (P), zero (Z) and negative (N). Initially the positive and negative errors were further subdivided into sets for large and small magnitudes, leading to five functions for each input error. This was found to be excessive and also increased significantly the number of control rules required.

Triangular Membership Functions were adopted because they are the most simple and hence least computationally intensive functions to use in the inference. The apexes of the P and N Membership Functions represent the maximum input errors to the controller. The Z Membership Function was necessary as all possible input values to the system must be classified, otherwise this particular fuzzy inference system will take the average value of all the outputs and produce undesired responses. Saturation limits were placed on the error signals before they entered the fuzzy controller, these limit the maximum errors to correspond with the apex values of the P and N Membership Functions. The reason for this is that above a

certain size of error, the maximum control action will be necessary, this method guarantees such a response without having to use additional Membership Functions to grade the error magnitude.

The fuelling quantity demand input uses only 1 Membership Function which defines the low (LO) fuelling condition. A particularly attractive aspect of fuzzy logic is that this function can be visually shaped to match the qualitative description of low fuelling. As can be seen in **Figure 6.3** the low fuelling region has been defined as definite between 0 and 15mg/shot, then the certainty that fuelling is low tapers away until 25 mg/shot where it can be said that fuelling is definitely not low. The same reasoning applies to the engine speed fuzzification, which uses one Membership Function to define the low speed range of the engine.

The two controller outputs were classified using the similar Membership Functions to the input error signals. The magnitudes of the outputs are different as can be seen in the figure, the apexes of the Membership Functions correspond to 1 for P, 0 for Z and -1 for N, giving an output range of -1 to 1.

#### **6.6.4 CONTROLLER RULE BASE**

The rule base for this controller initially used six rules, but this was found to be insufficient to cover the complete range of operating conditions. After several iterations the minimum number of rules that could cover all operating conditions and provide the required performance was determined to be twelve. **Table 6.1** lists these rules.

Rule Number	Airflow error	Boost error		Engine speed		Fuel Demand	EGR output	VGT output
1	P						N	
2	N						P	
3		P	AND			NL		N
4		N	AND			NL		P
5	P		AND	L	AND	L		P
6	N		AND	L	AND	L		N
7	Z		AND	L	AND	L	Z	Z
8	Z						Z	
9		Z	AND			NL		Z
10		Z	AND	NL				Z
11		N	AND	NL				P
12		P	AND	NL				N

**Table 6.1 Rules for the coordinated EGR VGT fuzzy logic controller**

An explanation for each rule is given as follows:

1. *When the airflow error is positive (i.e. less than the setpoint), close the EGR valve (reduce controller output). This rule is valid for all engine operating conditions.*
2. *When the airflow error is negative, open the EGR valve to reduce fresh airflow. As with rule 1 this rule is active throughout the engine operating regime.*
3. *If the boost pressure error is positive (i.e. less than the setpoint) and the fuelling demand is not low, close the VGT vanes to increase boost. This is the independent boost control loop for the VGT, valid for any condition where Fuelling Demand is not low.*
4. *If the boost pressure error is negative and Fuelling Demand is not low, then open the VGT vanes to reduce boost pressure. As for rule 3 this rule represents independent VGT to boost pressure control for conditions where the Fuelling Demand is not low.*
5. *If the airflow error is positive and both engine speed and fuelling demand are low, then open the VGT. This is a coordinated rule, it is only active in the low speed and low fuelling region of the operating envelope, it works in conjunction with rule 1 to provide coordinated EGR and VGT action to increase fresh airflow.*



6. *If the airflow error is negative and the engine speed and fuelling demands are both low then close the VGT.* This is a coordinated rule, it is active only at low speed and fuelling levels and works in conjunction with rule 2 to provide coordinated action to reduce fresh airflow.
7. *If the airflow error is zero and both engine speed and fuelling are low, then the output increments to VGT and EGR actuator are both zero.* This rule applies the zero airflow tracking error condition at low speed and fuelling. As both actuators are being used to track the airflow demands, an explicit definition of the zero tracking error action is necessary for the low speed and load operating region.
8. *If the airflow error is zero then the EGR valve increment is zero.* This applies the zero airflow tracking error condition to the entire engine operating range, the behaviour of the EGR valve does not change with engine operating point therefore a ‘global’ rule can be defined.
9. *If the boost pressure error is zero and the fuelling demand is not low then the VGT increment is zero.* This rule corresponds to the independent boost to VGT vane setting control loop, and is only active when the fuelling demand is not low. Because the VGT behaviour changes depending on operating region, a global zero tracking error rule cannot be defined as different tracking parameters apply depending on operating point.
10. *If the boost pressure error is zero and the engine speed is not low then the VGT increment is zero.* As for rule 9, this rule addresses the fact that outside of the low speed region, the VGT tracks boost pressure, and therefore provides the explicit zero tracking error condition.
11. *If boost pressure error is negative (i.e. greater than the setpoint) and engine speed is not low then open the VGT.* This rule forms part of the independent boost pressure control loop from VGT vane setting. Rule 4 addresses the case of the same tracking error but for fuelling conditions outside of the low region, this rule is only active for engine speeds outside of the low region.
12. *If boost pressure error is positive and engine speed is not low then close the VGT.* As for rule 11 this rule is part of the independent VGT to boost pressure control loop active outside of the low speed and fuelling operating regime.

#### **6.6.5 EXAMPLE INFERENCE OPERATION**

In order to understand the behaviour of the rule system it is useful to ‘walk through’ an example. **Figure 6.4** is taken from the ‘Rule View’ function of the Matlab Fuzzy Logic

Toolbox, this allows the user to simulate inputs to the system and analyse the behaviour of the inference engine on a rule-by-rule basis. In the figure each row represents a rule, the rule is described by the Membership Functions it uses, the first four columns are the inputs and the last two columns the output actions. The vertical lines intersecting all rules over the first four columns represent the system input values, this allows the user to see how much a particular input activates a particular rule. In the bottom right hand corner the two graphs represent the aggregate output of the system. The input conditions are as follows;

*Airflow error = -41.6 kg/hr      Boost pressure error = -16.8 kPa*

*Fuelling Demand = 15.2 mg/shot      Engine speed = 1340 rev/min*

This corresponds to too much fresh airflow and boost pressure in the low speed and low fuelling region. The desired operation is that of coordinated action to reduce fresh airflow, to be achieved by opening the EGR valve whilst closing the VGT vanes.

*Rule 1* is inactive as it applies to positive airflow errors only.

*Rule 2* is activated by the negative airflow error, it contributes an activation of the positive EGR valve increment (P) Membership Function.

*Rule 3* is inactive as it applies to positive boost pressure errors.

*Rule 4* is slightly activated as the boost error is negative and the fuelling is on the limit of being 'NOT LO', the resultant output is a low activation of the increase VGT position (P) Membership Function.

*Rule 5* is inactive as it applies to positive airflow errors, even though the low speed and low fuelling Membership Functions are fully activated, the output is the result of an AND operation therefore no output activation takes place.

*Rule 6* is active because the airflow error is negative and the engine speed and fuelling are both low, the result of the rules is to activate the reduce VGT vane position (N) Membership Function.

*Rule 7* is inactive as the airflow error is non-zero.

*Rule 8* is active but only marginally so, the boost pressure error is at the limit of the zero error (Z) Membership Function, and the fuelling only just activates the 'NOT LO' condition, therefore the output is a small activation of the zero VGT increment (Z) Membership Function.

*Rule 9* remains inactive as it addresses positive boost errors.

*Rule 10* is activated very slightly, the negative boost error combined with a very low activation of the 'NOT LO' engine speed condition produces a very small 'P' output for VGT.

*Rule 11* is inactive as the airflow error is too large to activate the zero error membership (Z) function.

*Rule 12* is only just active, the boost error activates the 'Z' Membership Function, and the engine speed is at the lower limit of the 'NOT LO' Membership Function, the resulting output is a very small activation of the 'Z' function for VGT.

The aggregate output is given below the last rule, all the output Membership Functions are summed using a maximum value operation. The output values which are sent to the integrators for EGR and VGT demand are derived by centre of mass calculations on the aggregate output. For the EGR valve output only one Membership Function was activated, the positive increment function. This is an isosceles triangle so the centre of mass lies along the axis of symmetry, i.e. the output will be the value over which the axis of symmetry has been aligned, in this case 1.

For the VGT vane output, rules 4,6,8,10 and 11 contribute to the output, but the most significant contribution comes from rule 4, this is reflected in the output which is heavily weighted toward the close VGT increment. The resultant centre of mass lies closer to zero due to the 'Z' and 'P' Membership Function contributions, hence the output value of  $-0.841$ .

## **6.7 COORDINATED CONTROLLER PERFORMANCE TESTING**

Due to the iterative development of this control scheme, it would be impractical to provide all the simulation and test results for the preceding versions of the controller. Each iteration of the control scheme highlighted new issues in the design of fuzzy systems, particularly with respect to the rulebase and the interaction of the rules. For this reason the data presented here represents the experimental evaluation of the final build of controller as described in the previous sections.

The controller was tested over a constant engine speed using a fuelling step profile that simulates step increases and decreases in fuelling demand of increasing magnitude. The steps were performed at 1500 rev/min with both fixed and active open-loop term demands to gain an understanding of how robust the controller could be.

The Simulink implementation of the controller is shown in **Figure 6.5**. This model was used for the real time implementation with dSpace (see **APPENDIX A**). All inputs to the strategy were taken from the original ECU via the CAN link, no additional sensor inputs were required. The controller was run at a 16 milliseconds sample interval.

## 6.7.1 1500 rev/min fuelling profile with active open-loop

### 6.7.1.1 AIRFLOW AND BOOST TRACKING

Figure 6.6 summarises the controller performance at 1500 rev/min. The 2 plots in the first row describe the airflow and boost pressure tracking performance over the fuelling profile. Airflow tracking appears to be fast and stable with good steady state error performance, however, the response rates do not represent any improvement over those achieved under the standard control scheme.

### 6.7.1.2 ACTUATOR POSITIONS AND CONTROL OUTPUT

The reason for the unexceptional airflow and boost behaviour can be determined from the plot of EGR and VGT actuator positions on the second row. The VGT actuator does not move for most of the test duration, remaining at a mid-open position until just before the final tip-out / tip-in sequence. By examining the controller output plot in the adjacent frame, it can be seen that the VGT control output does not change in magnitude that much over the first 15 seconds of the test, the small changes that do occur are insufficient to move the turbocharger vanes.

### 6.7.1.3 FUZZY OUTPUT

The fuzzy logic controller output can be seen in the third row, the desired response from the inference engine is achieved as demonstrated by the symmetrical outputs for EGR and VGT. The opposite motions of the EGR and VGT output represent coordinated action to increase and decrease airflow. For the final fuelling step up at approximately 25 seconds into the test, the controller tracks airflow and boost independent of each other, therefore the output of the fuzzy logic block travels in the same direction for both EGR and VGT outputs.

### 6.7.1.4 OPEN-LOOP TERM

The open-loop term is active in this test and can be seen on the second plot of the third row. The open-loop term does not initially assist in achieving coordinated action, for the first step up in fuelling at around 5 seconds, the open-loop demand for the VGT increases corresponding to action to close the vanes, and the EGR demand decreases corresponding to action to close the valve.

### 6.7.1.5 CONTROLLER PROPORTIONAL AND INTEGRAL TERMS

In the fourth row of the figure the EGR and VGT proportional and integral terms are shown. Of note here is the minimal contribution to the VGT control output made by the proportional term. This is the key reason for the unsatisfactory performance, the proportional term is generally very low as it is responding to boost pressure error, and at these operating

conditions the boost pressure targets are low therefore the errors will be small in magnitude. Although the integral terms are responding well and in the desired directions, they cannot be relied on for good dynamic response, this is the role of the proportional term.

### **6.7.2 Summary 1500 rev/min fuelling profile with fixed open-loop**

**Figure 6.7** summarises the controller behaviour for the case of a fixed 50% open-loop term. The airflow tracking is worse than for the active open-loop case, longer rise and fall times and greater steady state errors. The VGT actuator opens the vanes in response to the first tip-in whilst closing the EGR as desired, however the EGR valve motion is now marginally slower as the system relies on the closed-loop control, this results in slower airflow response. After opening in response to the initial tip-in, the VGT remains at a wide setting until the final tip-in of the sequence where it is forced to close. The wide openings result in poor boost pressure behaviour. The fuzzy logic controller output can be seen in the third row, the output is more active than for the active open-loop case, signifying more closed-loop action to compensate for the fixed open-loop term.

## **6.8 EXPERIMENTAL RESULTS DISCUSSION**

### **6.8.1 GENERAL PERFORMANCE**

The testbed results highlight the poor performance offered by this controller, although airflow tracking at low speed and load is good, it is in general no better than the standard control scheme except with respect to steady state performance, and more importantly, achieves this with a more complicated controller structure. The main limitation for this controller is that the VGT proportional control term is determined by the boost pressure error, this produces low VGT response in the coordinated region as boost errors are low. The use of the sign of the VGT fuzzy integral increments to dictate the sign of the proportional term encounters problems when the fuzzy output is near zero and noisy, resulting in oscillations in the sign of the Proportional term, this is clearly unacceptable.

### **6.8.2 PROPORTIONAL TERMS**

The proportional terms of the controllers were kept outside of the fuzzy logic in order to simplify the controller implementation. As previously mentioned, once included within the fuzzy inference, the proportional term is no longer proportional to the loop error and as such it becomes a non-linear function of the input error. The proportional term will normally require additional Membership Functions and rules, this will increase the already near critical computational burden significantly.

An implementation that included the proportional terms within the inference was tested, but would not execute within the 16 millisecond timestep used by the controller. The new controller required 6 new Membership Functions for EGR and VGT proportional terms, and the existing rules were merely adjusted to include the proportional output (the same rules apply as for the integral terms).

The proportional gain can be increased but at the expense of stability, another possible approach would be to increase the boost pressure setpoints for the coordinated operating region. This is feasible as the pressure targets are not being tracked in this operating regime, but may be problematic on the boundary regions where control transfers from coordinated to independent and boost is subsequently tracked by the VGT.

### **6.8.3 FUZZY INFERENCE**

The actual fuzzy inference section of the controller works well, generating the required control actions to achieve coordinated movements of EGR and VGT systems in response to fuelling changes. Using a fuzzy inference system of this size exerts a large penalty on the real time processor resources. The execution rate for 1 cycle of the control code was in the order of 12 milliseconds, this is very close to the overall execution interval for the controller which was set to 16 milliseconds. This figure also varied greatly when rules and Membership Functions were added or removed from the inference engine.

The fuzzy logic code used in the real time application was generated as C-code from the Matlab system using a standard template. This is unlikely to be optimal for all applications, i.e. the structure of the resulting code may not be the most computationally efficient for the given fuzzy system, therefore it is envisaged that execution times could be reduced through implementation of hand-written code for the fuzzy logic.

The interface for designing rules does not permit combinations of different logical operators, each rule could only make use of the same logical operator which limits the efficiency of the rulebase. Again, custom encoding of the fuzzy logic would avoid such issues, for example, significant simplifications to the rule base could be made if the use of rules such as :

“If BOOSTERROR is POSITIVE AND (ENGINE SPEED is NOT LOW OR FUELLING is NOT LOW) then CLOSE VGT”

## **6.9 REVISED CONTROL SCHEME**

A revised version of the Fuzzy Controller was designed in the light of experience gained from the testing and development of the original controller. The new controller keeps the same basic structure, the inference engine is the same and the rules are the same. The 'proportional'

terms for the new controller are derived from the existing outputs of the fuzzy inference, these outputs range from  $-1$  to  $1$  and need to be scaled by 'proportional' gains. This does increase the calibration effort as the selection of these gains is a non-trivial task, the normally easy interpretation of the proportional term is distorted by the non-linearity introduced by the fuzzy logic.

Problems relating to stability and robustness are difficult to assess, judging from previous experimental work, for small outputs from the fuzzy inference, noise can be significant leading to oscillations about zero, these oscillations will be carried through to the actuators via the proportional term.

The schematic of the revised controller is shown in **Figure 6.8** and the Simulink implementation in **Figure 6.9**, the less complex nature of the 'proportional' term arrangement is evident. It was not possible to test this controller on the test bed due to the decommissioning of the test facility, however the simulation can be used to demonstrate its performance.

### **6.9.1 REVISED FUZZY CONTROLLER SIMULATED PERFORMANCE EVALUATION**

The revised fuzzy controller is compared with the standard control scheme. Both controllers use custom setpoints designed for coordinated action, in order to allow the controller tracking performances to be compared with each other, however it must be noted that the setpoint choice will have a large effect on the dynamic performance of the controller, from this point of view the standard controller can perform worse than it does when using appropriate setpoints.

#### **6.9.1.1 AIRFLOW TRACKING AT 1500 rev/min COMPARED TO STANDARD CONTROL SCHEME**

**Figure 6.10** shows the airflow tracking for both standard control and the revised fuzzy control scheme. The new strategy shows a clear improvement over the standard control scheme with faster response to both tip-in and tip-out and better steady state error due to the fuzzy integral action and increased actuator authority. The fuzzy proportional terms now permit the system to respond rapidly in a coordinated manner to the changes in fuelling demand. Frames 2 and 3 of the figure show the EGR and VGT positions for both standard and coordinated control, the EGR positions for both controllers are very similar, although the standard controller tends to open the EGR further to reduce fresh airflow. This is because it does not have the additional command over airflow offered by the VGT as can be seen in the final frame by the coordinated movements of the VGT.

### 6.9.1.2 CONTROLLER DETAIL

**Figure 6.11** describes the performance in simulation of the revised fuzzy coordinated controller in detail. The first row of the figure illustrates the airflow and boost tracking performance. As seen previously, the airflow tracking is very good and the boost tracking has deteriorated, this is expected as the tracking emphasis is on airflow. The second and third tip-in events at time  $t=15$ seconds and  $t=25$  seconds take the fuelling into the uncoordinated operating region where boost and airflow are tracked independently, this accounts for the better boost pressure tracking at these test points.

The second row of **Figure 6.11** illustrates the EGR and VGT positions and the respective control signals. The VGT control action is reversed due to the fail-safe design of the mechanism, i.e. for zero control input the VGT is fully open whereas the EGR is fully closed. The third row shows the fuzzy logic output, the symmetry of the EGR and VGT outputs represents coordinated action. The two instances where control becomes independent can be seen in the loss of symmetry in the outputs. The open-loop term is given in the adjacent frame, illustrating the lack of assistance to the controller action due to a fixed 50% open-loop demand. This illustrates good robustness from the controller in response to open-loop inaccuracies.

The fourth row of the figure shows the controller terms for both EGR and VGT loops. Compared to the first version of this controller, the VGT proportional action is much greater and is largely responsible for the good dynamic response of the system to changes in demand.

The final row describes the fuelling profile applied and the engine speed for the test.

## 6.10 REVISED CONTROLLER DISCUSSION

### 6.10.1 GENERAL PERFORMANCE

The revision to the original controller shows good performance in simulation, providing better tracking of airflow through coordinated control action. The fuzzy integral terms and increased actuator authority from the VGT also give much better steady state airflow error performance. The fuzzy 'proportional' gains are likely to change throughout the operating region owing to the non-linear nature of the system.

### 6.10.2 STABILITY

One aspect of fuzzy logic that dissuades many people from applying it is the difficulty involved in establishing formal stability proofs for the system. Simulation can be used to demonstrate stability of the controller around the plant operating envelope but this will



depend greatly on the accuracy of the simulation. In this study, the fuzzy controller has demonstrated stable operation at the test points visited without the assistance of an open-loop controller term. However, a formal survey of the controller performance across the entire engine operating range would need to be performed in order to guarantee global stability.

## **6.11 SUMMARY OF RESULTS**

A fuzzy logic controller has been developed that achieves coordinated EGR and VGT action selectively at low load and low speed, resulting in improved airflow response. The use of fuzzy logic has allowed the information that traditionally would be derived from several linearised plant models to be encapsulated into a compact and transparent form.

Although the strategy is effective, the computational demands incurred by the fuzzy inference system limit the practicality of such an approach, at least under current engine management system restrictions. Should there be a more efficient method of implementing the fuzzy scheme then it would offer a more attractive alternative to the current EGR VGT control strategy.

The actual design and optimisation of the fuzzy inference requires considerable initial effort. The systems presented in this chapter were the result of a series of iterations of the rules, Membership Functions (shape and number) and calculation methods. There are many degrees of freedom available to the designer for optimisation, and this tends to complicate the task. However, once the rules are established, the system is generic and requires only 4 gains to be tuned. The controller has also shown itself to be fairly robust to large inaccuracies in the feedforward path, therefore a reduced calibration could be applied without incurring deteriorated performance.

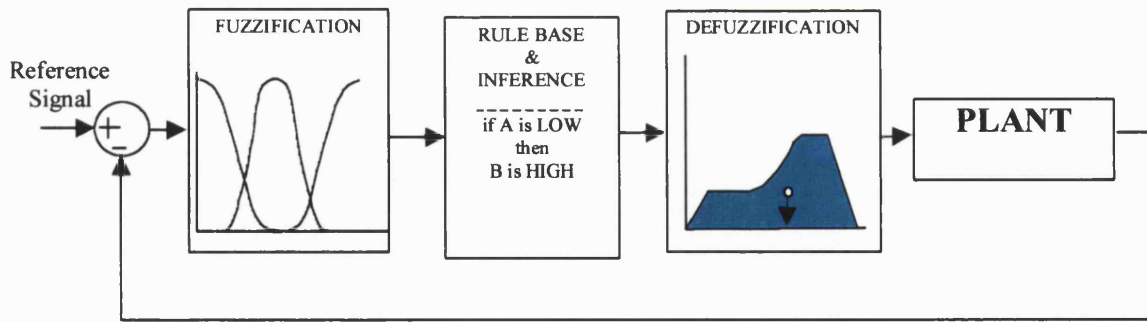


Figure 6.1 Typical arrangement of a fuzzy feedback control scheme

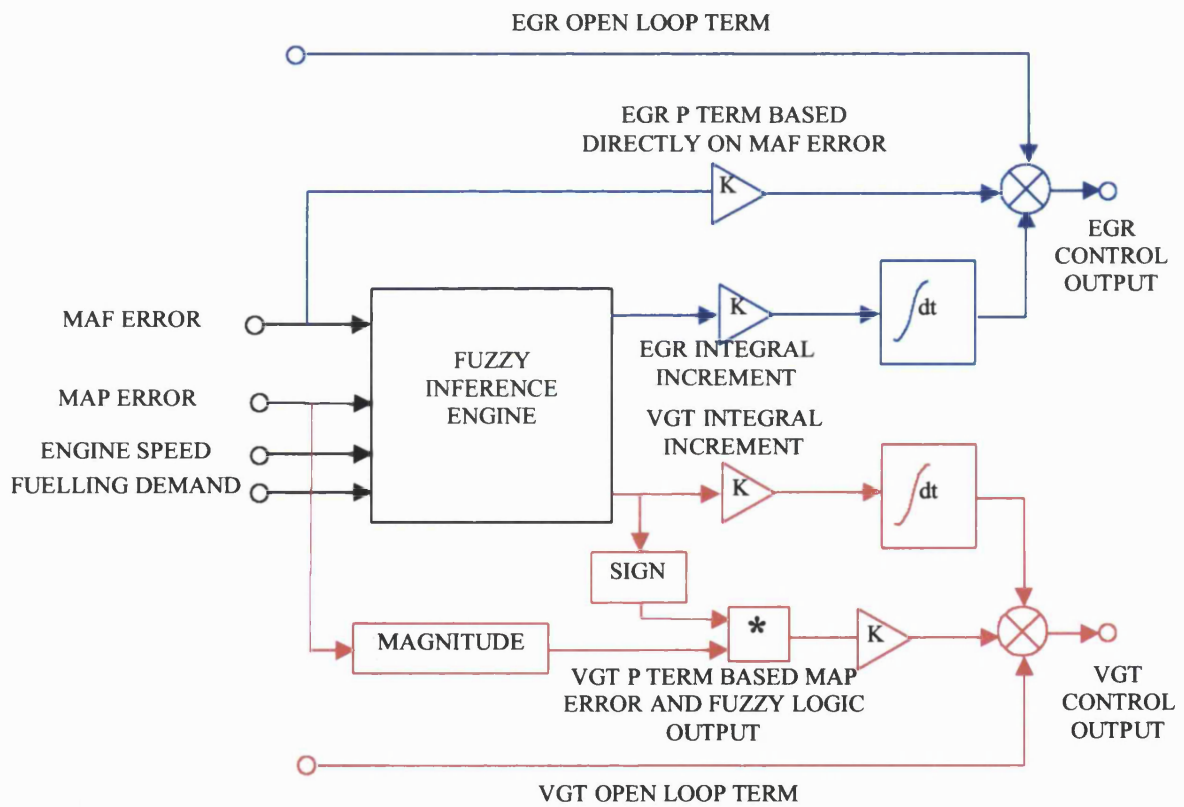
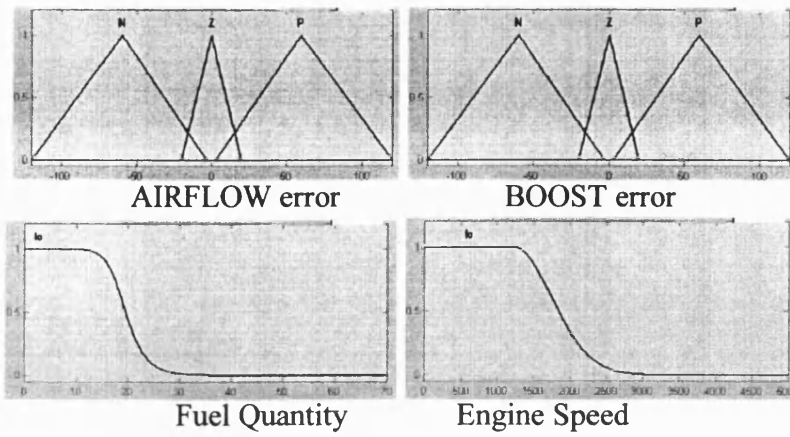


Figure 6.2 Schematic representation of controller

INPUTS



OUTPUTS

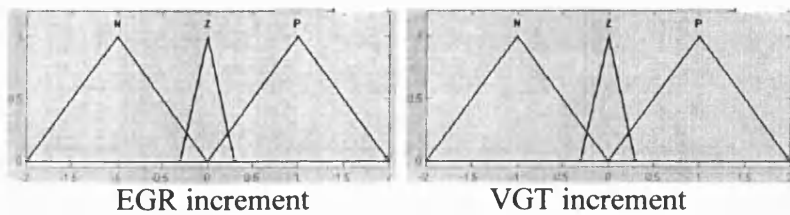


Figure 6.3 Membership functions for Fuzzy Controller inputs and outputs

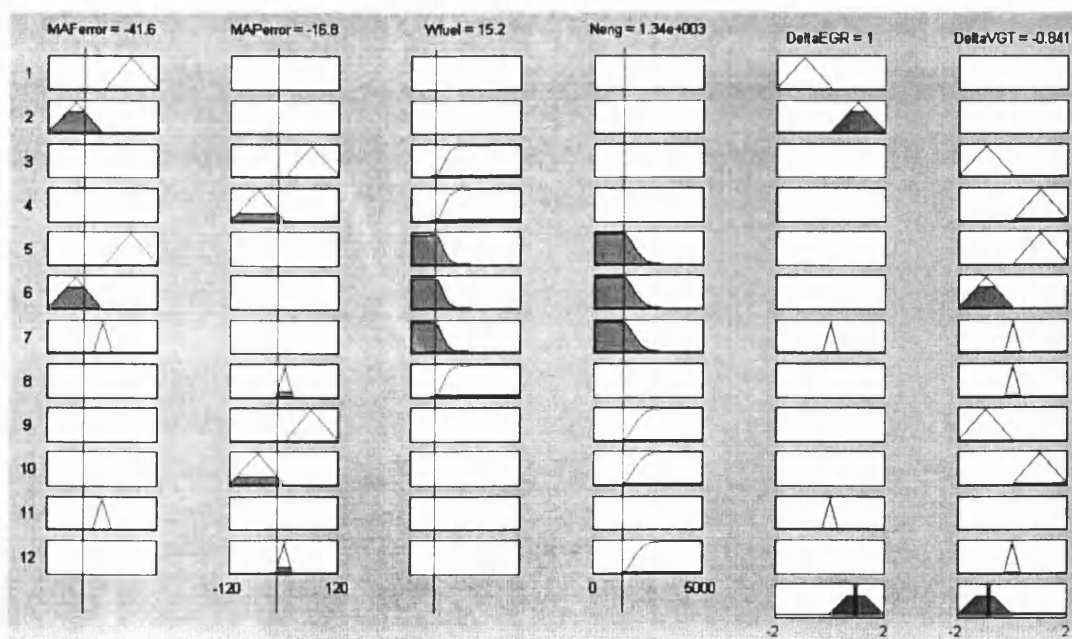
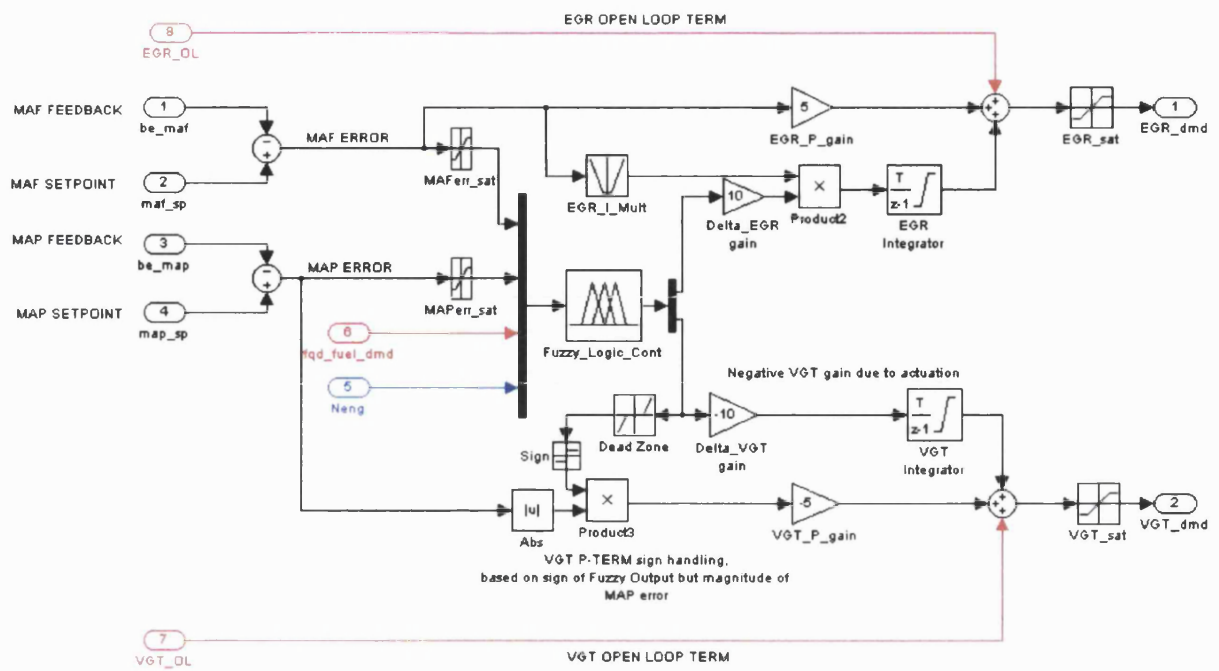


Figure 6.4 Example of fuzzy inference engine



FUZZY LOGIC CO-ORDINATED EGR VGT CONTROLLER FOR MAF AND MAP

Figure 6.5 Simulink implementation of fuzzy controller

DYNAMIC ENGINE TEST FACILITY : TEST RESULTS (FORD PUMA CP4 + VGT)  
 FUZZY LOGIC CO-ORDINATED CONTROLLER ACTIVE OPEN LOOP TERMS  
 DAT FILE I.D.: 21jul\_fuz001.mat , 00072101.dyn

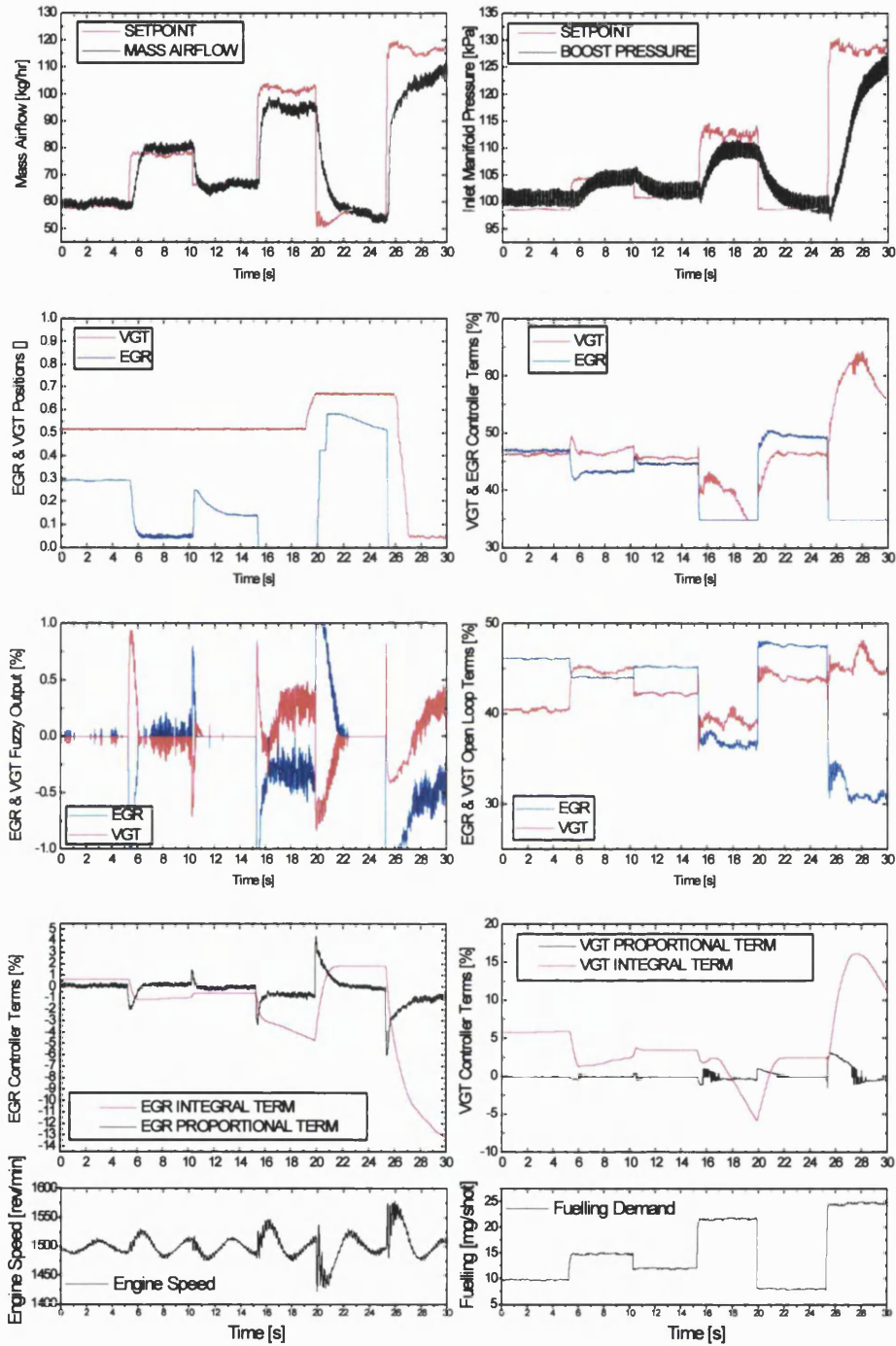


Figure 6.6 Experimental evaluation of Fuzzy Controller

DYNAMIC ENGINE TEST FACILITY : TEST RESULTS (FORD PUMA CP4 + VGT)  
 FUZZY LOGIC CO-ORDINATED CONTROLLER FIXED OPEN LOOP TERMS  
 DAT FILE I.D.: 21jul\_fuz002.mat , 00072102.dyn

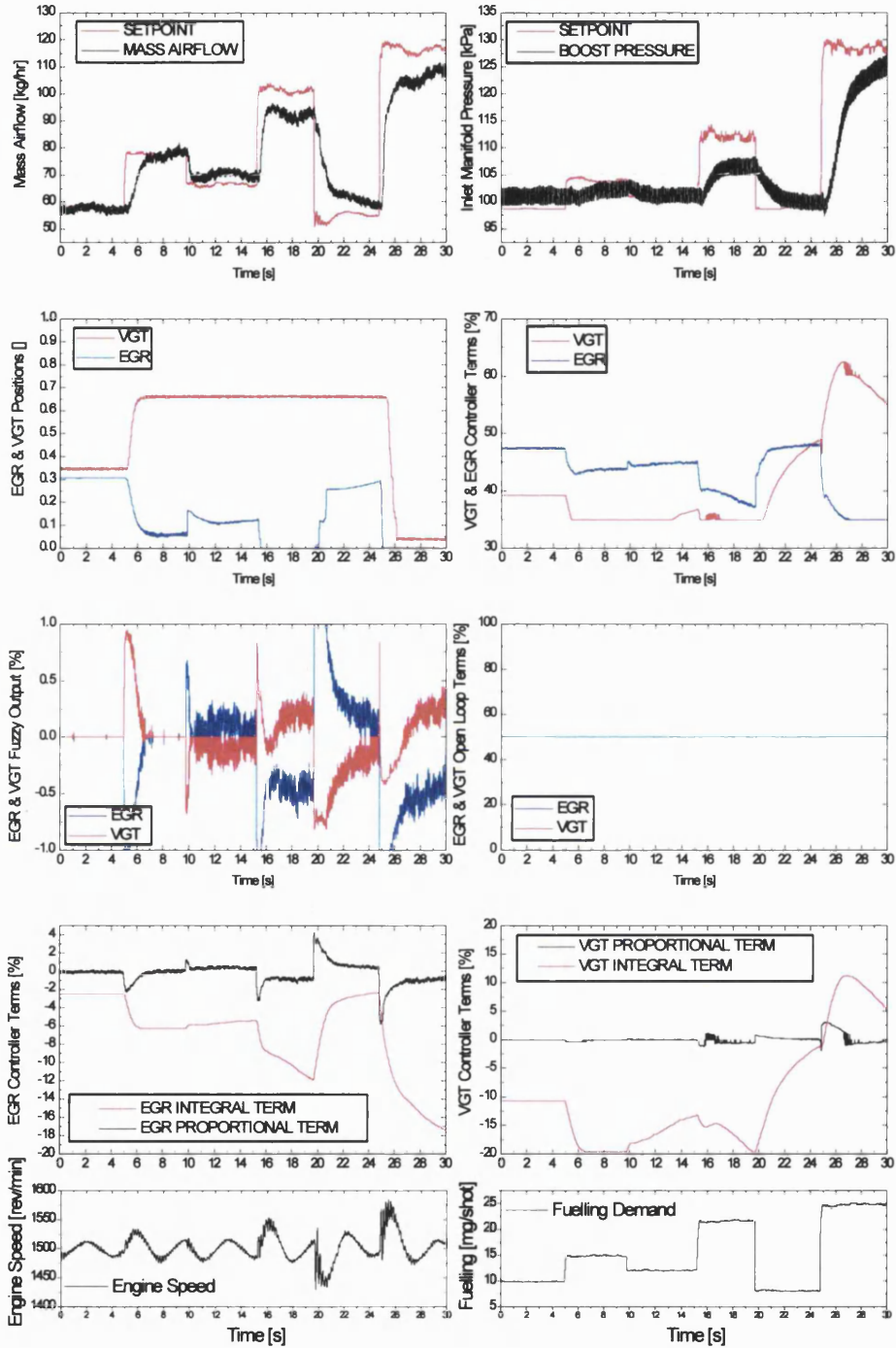


Figure 6.7 Experimental evaluation of Fuzzy Controller (Fixed 50 % Open-loop Term)

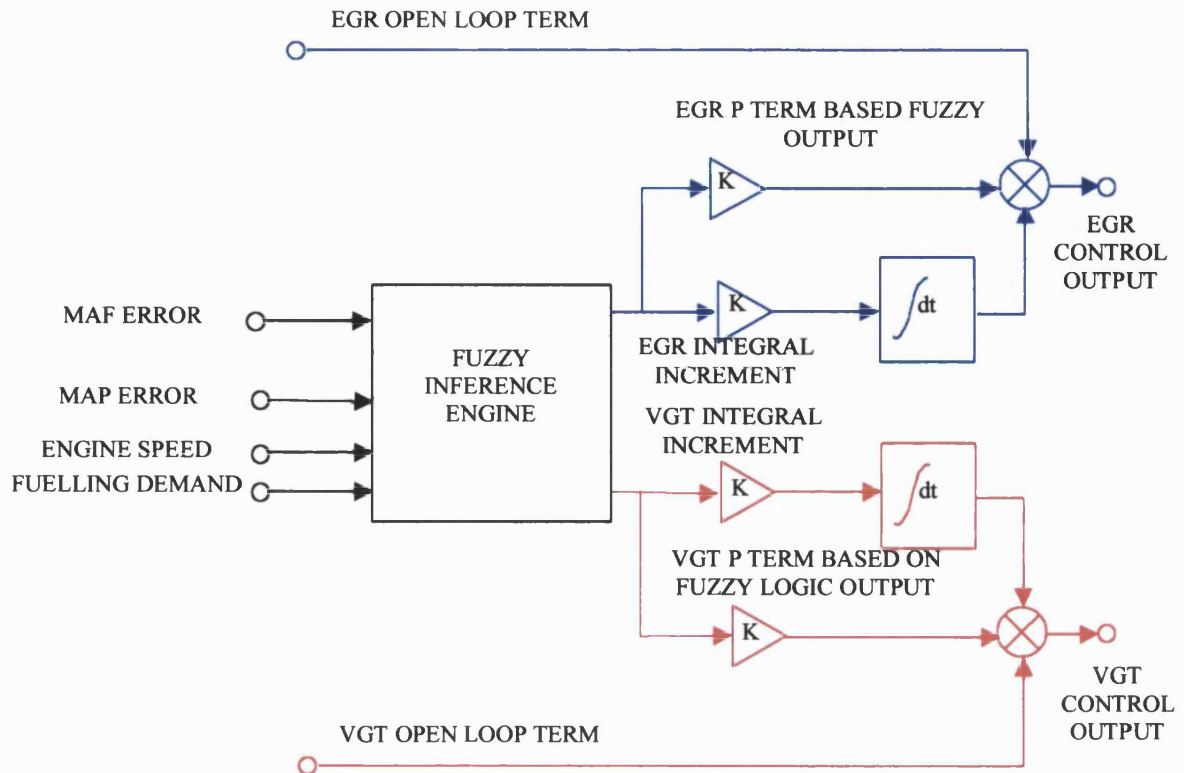


Figure 6.8 Schematic of revised fuzzy controller

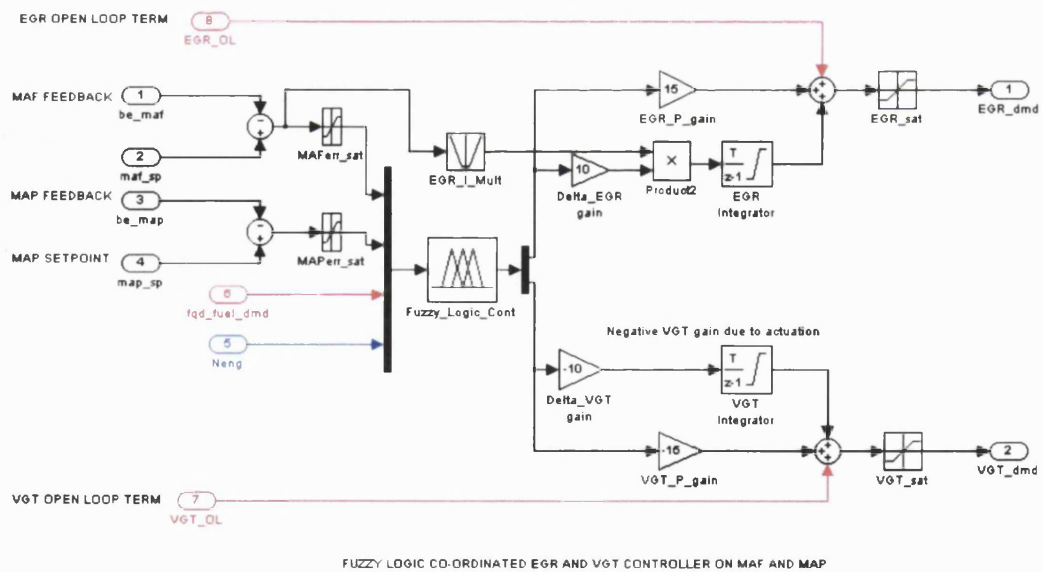
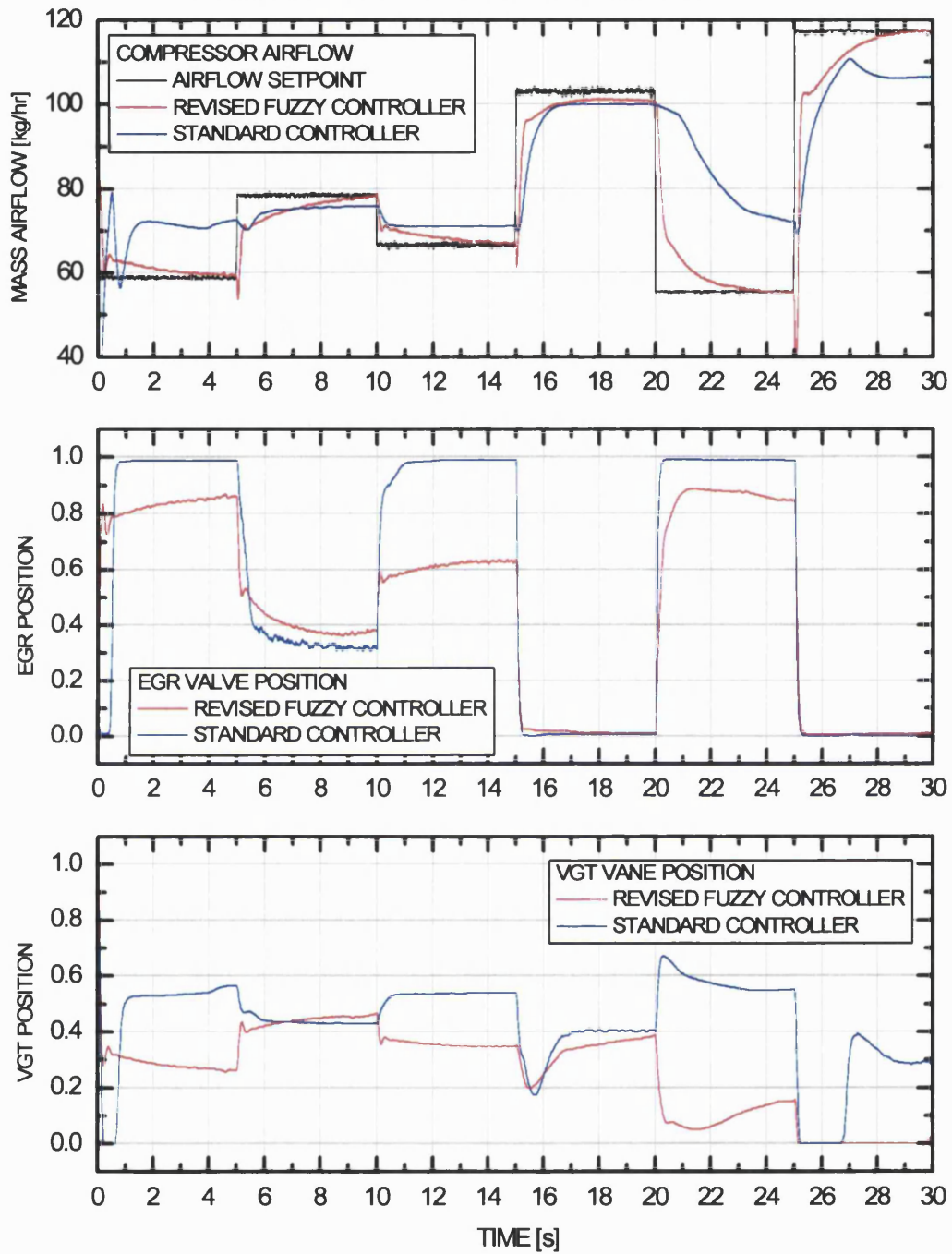


Figure 6.9 Simulink implementation of revised fuzzy controller

SIMULATION RESULTS (FORD PUMA CP4 + VGT)  
 COMPARISON OF REVISED FULL FUZZY CONTROLLER  
 AGAINST STANDARD CONTROLLER OVER 1500 rev/min FUEL PROFILE



**Figure 6.10 Simulated comparison of revised fuzzy controller with standard controller over 1500 rev/min fuelling profile**



SIMULATION RESULTS : FORD PUMA CP4+VGT  
 DETAIL OF REVISED FULL FUZZY CONTROLLER  
 OVER 1500 rev/min FUEL PROFILE

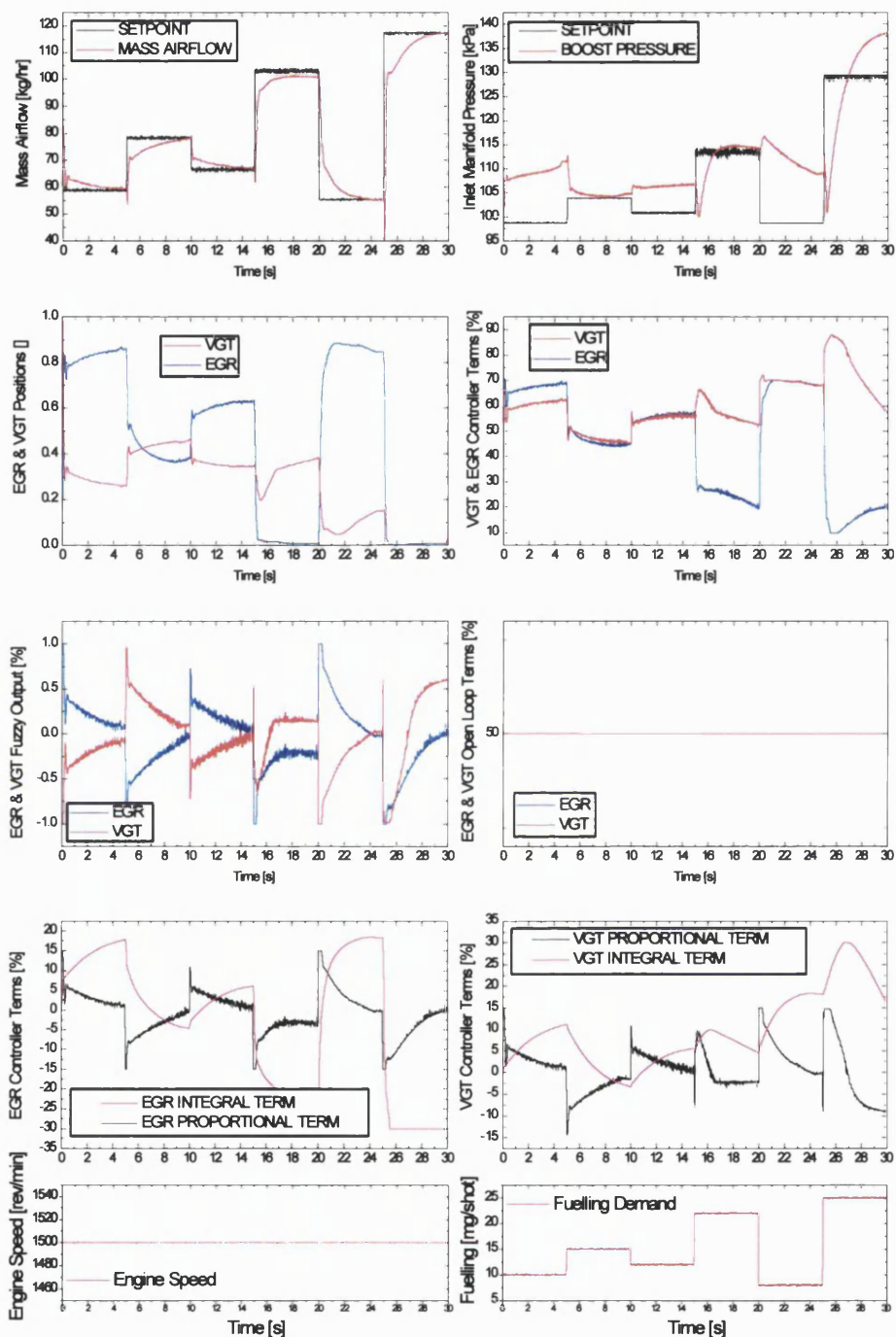


**Figure 6.11** Detail of simulated performance of revised fuzzy controller over 1500 rev/min fuel profile

## **Chapter 7 COORDINATED CONTROL USING CROSS-COUPLED INDEPENDENT CONTROLLERS**

### **7.1 INTRODUCTION**

In this chapter an alternative approach to obtaining coordinated EGR VGT control is investigated. Although a method for coordinated control has already been presented in Chapter 6, the performance benefits were offset by the computational requirements for a fuzzy logic controller with large number of rules and Membership Functions, as well as the associated calibration issues. Therefore an alternative, simpler strategy is proposed.

Selective coupling of the existing independent EGR and VGT control loops during low speed and low engine operation is investigated as a method of obtaining coordinated EGR and VGT control. Different methods of implementing such a coupling are discussed, and a technique is presented that achieves the desired system behaviour using a very simple implementation.

The new strategy uses a compact fuzzy inference system to channel the airflow tracking error into both the EGR and VGT feedback control loops when in the low speed and low load operating region, and attenuate the boost tracking error signal normally fed to the VGT control loop. Outside of the low speed and load operating range, the controller behaves identically to the independent loop controller (standard control scheme).

The new strategy is demonstrated in simulation as an effective coordinated controller that yields faster transient airflow response than the standard independent controller scheme. This is then confirmed through experimental investigation on the dynamic engine test facility. The new strategy retains the computationally efficient implementation and transparent nature of the existing strategy.

### **7.2 COORDINATED CONTROL REVISITED**

The motivation for coordinated control has already been discussed in detail in the previous chapter in *section 6.2*. The need to achieve such control action through a simple strategy that can be readily calibrated and understood is paramount for a massed produced automotive control feature. For this reason, an investigation into a less computationally demanding method of obtaining coordinated control was pursued.

### **7.3 CROSS-COUPLED APPROACH**

The independent feedback control loops from airflow to EGR valve PWM duty cycle, and from boost pressure to VGT vane PWM duty cycle perform adequately, if not optimally, over

the entire engine operating envelope. The PID control structure is well understood and does not require particularly specialist knowledge to calibrate, and in addition it is chronometrically very efficient. Clearly, retaining these features in a coordinated controller would be desirable. One way of achieving this would be to couple the independent control loops together throughout the coordinated control region, and use both EGR and VGT control loops to track airflow errors. Two variations on this theme were investigated, the first involved coupling the outputs of the independent controllers such that the output of the airflow tracking EGR loop is added to the output of the VGT loop (Output Coupling). The second method involves channelling the airflow tracking error into the VGT control loop (Input Coupling) when in the coordinated operating region, this allows both actuators to be used to track airflow demands and improve the airflow response.

The first configuration (Output Coupling, see **Figure 7.1**) will cause problems when the system changes from coordinated to independent control, this is because the VGT loop will still track boost error and the output will simply be replaced with the EGR control loop output. This means that the integrator in the VGT control loop will saturate as the system tries to track boost error but has no actuator authority to do so. Therefore the second configuration (Input Coupling) is the better approach as throughout all operating regimes the VGT control loop will be active, this method was therefore adopted and is described in the following sections.

## **7.4 PROPOSED CONTROL SCHEME**

### **7.4.1 OVERVIEW**

The proposed method switches the tracking error signal feeding into the individual feedback controllers. The EGR control loop behaviour remains unchanged throughout the engine operating range, as the action to reduce EGR flow will always be to close the EGR valve. The VGT control loop behaviour must change with operating point to achieve coordinated action. In the low speed and load operating region, the airflow tracking error is channelled into the VGT and EGR compensators, outside of this region the VGT controller will independently track the boost demands exactly as in the standard configuration.

### **7.4.2 SWITCHING MECHANISM**

The switching of the tracking error signal between airflow and boost at the input to the VGT compensator must be determined by a function that recognises the engine operating point. The switchover can be binary, where the VGT tracks either airflow or boost error alone; for

this case a dead zone should be implemented to prevent rapid switching from airflow to boost tracking when the engine is operating on the boundaries of low load and low speed.

Alternatively, a gradual transition from airflow to boost tracking can be implemented, where the VGT uses airflow error in the low load and speed region, then as the operating point moves towards high speed and/or high load, the input to the VGT becomes a blend of airflow and boost tracking errors until it is eventually tracking boost pressure only.

Because of the uncertainty in determining the point where VGT influence over airflow reverses, the gradual transition method is more appropriate than a binary switching from one control mode to another. Also, the transition in engine behaviour is a gradual one, not an instantaneous one so this method is better suited to the problem.

The transition region will be defined by a band of fuelling quantities and engine speeds within which the VGT input will be a blend of boost and airflow errors. These two error signals will elicit opposing control actions from the VGT. A step up in fuelling will cause increased airflow and boost demands resulting in positive tracking errors, however the gain from airflow error to VGT command will be negative as the desired action will be to open the VGT (reduce controller output). The gain from boost pressure error to VGT command will be positive, acting to close the VGT. The blended errors may cancel each other out resulting in no VGT action, but this is not likely to be problematic. The transition region shall be small, therefore any changes in setpoint within the transition region will also be small resulting in small changes in demanded boost and airflow values that generally will not require significant change in VGT position. The VGT control will be biased towards whichever operating region is nearer to the current operating point, any large changes in demand will be instigated by large changes in operating point that will switch the control from definitely coordinated to definitely independent or vice-versa.

Fuzzy logic is proposed as the switching mechanism; it has been shown to work well in the previous chapter as the basis for deciding whether or not to coordinate the EGR and VGT systems, therefore it was chosen for use in this application. It is possible to use other mathematical functions to define the low speed and load regions, but the fuzzy logic allows a very simple and intuitive implementation, particularly through the use of the Matlab graphical user interface. The Membership Functions can be manually shaped to match the operators interpretation of low load and low speed. Although fuzzy logic incurred large computational overheads in the application in the previous chapter, in the proposed system only a very small inference engine is required therefore the processor resource demands will be low.

## 7.5 FUZZY OPERATING POINT IDENTIFICATION

A schematic of the control system is shown in **Figure 7.2**, the fuzzy logic block takes inputs of engine speed and fuelling quantity and outputs the gain from airflow tracking error to VGT compensator input. The inverse of this output is applied to the boost tracking error and the two errors are summed and fed into the VGT compensator.

The fuzzy logic block must output a value of -1 when inside the coordinated operating region, signifying a gain of  $-1$  from airflow error to VGT control action, and 0 outside of this region to ensure no airflow tracking action is taken by the VGT. To achieve this the system uses two inputs, two rules and one output.

The inputs are engine speed and fuelling quantity, each are classified with one Membership Function, 'LOW', illustrated in **Figure 7.3**. As was the case for the fuzzy logic controller discussed in **Chapter 6**, the Membership Functions are shaped to approximate the certainty in identifying the low load and load speed operating region for the engine.

The output is the gain from airflow error to the VGT compensator input, it is classified with two triangular Membership Functions, 'ON' and 'OFF' (see **Figure 7.4**).

The two rules used for the fuzzy inference are illustrated in **Table 7.1**.

Fuelling		Engine Speed		MAF to VGT error term
LOW	AND	LOW		ON
NOT LOW	OR	NOT LOW		OFF

**Table 7.1 Fuzzy inference rules for coordinated control action**

### 7.5.1 EXAMPLE INFERENCE

Examples of the inference output are shown in **Figure 7.5** and **Figure 7.6**, the first figure shows the fuzzy logic activation for an engine operating point of 13.3mg/shot fuelling and 1700 rev/min engine speed. This operating point falls well within the bounds of low speed and low load, therefore the output of the inference is -1. The second figure shows the fuzzy logic activation for an operating point on the boundaries of coordinated control, the output is closer to 0 and therefore biased towards independent control.

## **7.6 SIMULINK IMPLEMENTATION**

The Simulink implementation of the controller is given in **Figure 7.7**, the blocks in red are the additional elements to the existing strategy, illustrating how the new controller is derived from only a small modification of the standard scheme. The coordinated controller makes use of an integral gain multiplier based on the magnitude of the incoming error signal, when the error signal is large the integral gain is scaled up. When the error signal approaches zero, the integral gain is left unaltered so as not to compromise steady state stability. This is implemented with a simple one dimensional look-up table, the standard controller already uses this on the VGT control loop, but not for the EGR. It is used on both control loops for the coordinated controller.

## **7.7 SIMULATED PERFORMANCE**

The controller implementation was tested in simulation using the engine model. The controller update rate remained the same as for the standard scheme (16 milliseconds). A fuelling profile was applied to the engine model at constant engine speed as described in the previous chapter, the controller was tested with various combinations of 'as supplied' and custom airflow and boost pressure setpoints, and active and fixed open-loop terms (fixed at 50% term). The results shown here are a selection from these tests and compare the performance of the coordinated controller against the standard controller.

### **7.7.1 1500 rev/min FUELLING PROFILE FIXED OPEN-LOOP TERM**

**Figure 7.8** illustrates the simulated controller performance comparison at 1500 rev/min with the open-loop term fixed at 50%. The first frame shows the airflow tracking, the initial steady state error is significant for both standard and coordinated controllers and is a function of the low integral gains used in the compensation scheme. The EGR valve under coordinated control is still in the process of opening by the time the first step change occurs at  $t=5$  seconds and therefore it will eventually converge on the target airflow. However, the standard controller has a fully open EGR valve, the only way it can increase EGR flow and reduce the error is to close the VGT but it will not do this as the VGT is tracking the boost pressure error.

In response to the first tip in, the airflow demand steps up, the coordinated response of the new controller can clearly be seen in the plots of EGR and VGT position, the VGT opens whilst the EGR closes. Although the target value is not achieved, the response is notably more rapid than the standard controller.

The subsequent tip-out is accompanied by a reduction in demanded airflow, the coordinated controller closes the VGT to drive more EGR and rapidly reduces the fresh airflow into the engine. The same behaviour can be seen for the tip-out at 20 seconds test time, the fresh airflow reduction is significantly faster under coordinated control.

The next fuelling step up is large enough to leave the low load operating region, this is why the response of both controllers is practically identical, the coordinated controller should behave in exactly the same manner as the standard controller. This is also the case for the final tip-in at 25 seconds test time.

The sudden opening of the VGT at around 21 seconds into the test is due to the non-linear vane mechanism response. The control signal is reducing as the error reduces, but the vanes do not move until a certain threshold has been passed, where upon they respond suddenly causing a sharp increase in fresh airflow.

### **7.7.2 1500 rev/min FUELLING PROFILE ACTIVE OPEN-LOOP TERM**

**Figure 7.9** shows the same test as above but repeated with the open-loop term active. There is very little difference in the behaviour of the coordinated controller, suggesting good robustness to changes in plant characteristics. The active open-loop term helps the standard controller converge, but in general the coordinated controller still has the performance advantage.

## **7.8 ENGINE-BASED CONTROLLER EVALUATION**

### **7.8.1 ENGINE IMPLEMENTATION**

The control scheme developed in simulation was transferred to the test rig for development and evaluation using the dSpace hardware. No additional measurements were needed by the strategy other than those taken from the existing ECU via the CAN link as described in **Appendix A**.

### **7.8.2 TEST PROCEDURE**

Controller performance was evaluated using a constant speed fuelling profile as in the simulated tests. These were performed at 1500 rev/min under standard and then coordinated control, the open-loop terms were fixed at 50% demand to determine whether or not the feedback control method was as robust as simulation suggested.

The fuelling profile had to be applied manually, investigations were made into automating the pedal demands using dSpace which would greatly improve repeatability and consistency, but

much work was needed in overcoming the ECU safety routines associated with the drive-by-wire pedal system. Within the limited timescale of the experimental phase of this work there was no scope to pursue this further.

The fuelling profile was applied using the two fuel demand potentiometers and toggle switch described in **Chapter 3** under *section 3.4.1*. The six fuelling levels were set sequentially before the test and the potentiometer positions noted. The test then was performed by setting one potentiometer to the current fuelling value and the other to the next fuelling level using the noted positions, and switching from one to the other at five second intervals. Once the step has taken place, the potentiometer not being used is set to the subsequent fuel demand and the next step instigated with the toggle switch five seconds later; this is repeated until the profile is complete. Clearly there is room for inaccuracy in this method, the operator has to dial in the new fuel value within five seconds and this will lead to a certain amount of scatter in fuelling results. Also, the time at which the steps occur varies making it necessary to synchronise each individual event for comparison purposes when post-processing the data.

Data from the control strategy was acquired using the dSpace hardware at the control update rate (16 milliseconds or 66.67Hz), and all engine performance variables were logged on the main test cell acquisition system at 25Hz.

### **7.8.3 TEST RESULTS**

The results shown here are from two tests, one for the standard controller and one for the coordinated controller, the fuelling profile has been broken down into individual step change events.

It should be noted that the following individual figures comprise four separate plots, for convenience these are referenced as frames one to four, *frame 1* corresponds to the upper left hand graph, *frame 2* to the upper right hand graph, *frame 3* to the lower left hand and *frame 4* to the lower right hand graphs respectively.

#### *7.8.3.1 Figure 7.10 to Figure 7.12 Tip-in 1*

The first tip-in of the fuelling sequence is described by **Figure 7.10** to **Figure 7.12**. The airflow and boost pressure tracking and corresponding EGR valve and VGT vane movements are given in **Figure 7.10**. In *frame 1* the difference in airflow response between the two controllers indicates a clear improvement for the coordinated controller. The final airflow setpoints are slightly different (by approximately 5 kg/hr), this is due to the inaccuracy involved in manually setting and instigating the fuelling profile, although the effects of this discrepancy are negligible. The degradation in boost pressure response is visible in *frame 2*, with virtually no change in inlet boost under coordinated control.



The cause of the improvement in airflow response is demonstrated by the EGR and VGT positions (*frames 3 and 4*), the EGR valve trajectory is identical for both controllers, but the coordinated controller opens the VGT whilst the EGR closes, whereas the standard controller keeps the vanes in the fully closed position. There is a slight difference in the initial VGT vane positions, this causes the modest difference in initial airflow by driving slightly less recirculated gases. The coordinated controller achieves better steady state error performance, this is due to the extra control authority available from the VGT actuator and the use of the integral gain multiplier based on error magnitude as described in *section 7.6*.

The difference in the fuelling levels can be seen in **Figure 7.11 frame 1**, as can the subsequent difference in final torque output (*frame 2*). The smoke opacity (*frame 3*) for the two controllers is virtually irresolvable, but the difference between control methods in terms of their effect on exhaust manifold pressure can clearly be seen (*frame 4*). This difference is the key to the improved airflow response of the coordinated controller, as the higher transient exhaust backpressure in the case of the standard system will continue to drive the recirculated flow against the fresh airflow response.

**Figure 7.12** summarises some of the controller parameters, the first frame describes the signals entering the VGT PID compensator for each controller. The coordinated controller uses the airflow error signal passed through a gain of -1, this gives the reverse input to the boost pressure error as is illustrated by the blue line for the standard controller. The resultant controller output is shown in the second frame, the airflow derived coordinated signal acts to open the vanes whilst the boost pressure derived standard controller output attempts to close the vanes. It is interesting to note that for control signal output of little over 50%, the VGT vanes are fully closed, once again illustrating the strong non-linearities within the system.

The third frame shows the fuzzy logic output that determines if coordinated action is to be applied, this measurement is not applicable to the standard control scheme and hence is not shown for this case. The dotted line is the gain from boost pressure error to VGT controller input, and the solid line is the gain for airflow error to the VGT controller input. As the fuelling transient is well within the boundaries defined for the coordinated operating region, the boost pressure error input gain is zero and the airflow error gain is -1 signifying only airflow error is driving the VGT control loop. Finally, the turbocharger speed is illustrated in the *frame 4*, there is little discernible difference in response but the final speed for the standard controller is slightly higher, this is consistent with the slightly higher boost levels.

#### 7.8.3.2 *Figure 7.13 to Figure 7.15 Tip-in 2*

The second tip-in in the fuelling profile is shown in isolation in **Figure 7.13 to Figure 7.15**. In **Figure 7.13** a sudden dip in the transient airflow response for the standard controller

(*frame 1*) is shown, this is caused by the EGR valve opening during the transient (*frame 3*). The non-linear EGR valve and actuator dynamics are responsible for this as the EGR valve 'over-responds' to the increase in controller output and opens the valve, causing a sudden drop in fresh airflow. This does not occur for the case of the coordinated controller as the setpoint is slightly higher, this translates to a higher error signal to the EGR valve controller which keeps the EGR valve closed. Due to the unpredictable nature of the EGR valve non-linearities it is difficult to establish whether or not this would happen were the error signals to be identical for both controllers.

There is a slight opening of the VGT vanes at the very start of the transient illustrated by *frame 4*, this is because the fuelling step does not occur instantaneously, but over several controller cycles. This results in coordinated action initially until the fuelling level exceeds the boundaries of coordinated operation, when this occurs the VGT control reverts back to boost pressure feedback control and the vanes close. This by-product of the control scheme may help the actuator performance by overcoming any backlash in the system.

As seen in the previous tip-in, steady state airflow error is much better with the coordinated controller, although coordinated action is not used in the post-transient state.

In **Figure 7.14** *frame 1* a slight variance in fuelling levels between the two tests can be seen resulting in a slightly higher torque production (*frame 2*) for the coordinated controller. Marginally more smoke (*frame 3*) is produced by the standard controller though this is due to the opening of the EGR valve during the transient. In *frame 4* the exhaust pressure trace shows the dip in pressure where this valve opening occurs, it also shows a slight delay in pressure build up for the coordinated controller, caused by the initial opening of the vanes. The standard controller begins the transient with the vanes closed, this will allow backpressure to build up more rapidly.

In **Figure 7.15** the controller responses are compared, the initial coordinated action can be seen in the controller input and output. The non-instantaneous nature of the switch from airflow to boost pressure driven VGT action can be seen in the input error gain plot, this is responsible for the coordinated action at the start of the transient. The turbocharger response is initially faster for the standard controller until the EGR valve opens and reduces the pressure ratio over the turbine. The coordinated controller has a slight overshoot but this is converged by the boost pressure driven independent action from the VGT controller.

### 7.8.3.3 *Figure 7.16 to Figure 7.18 Tip-in 3*

Tip-in 3 is the largest step increase in fuelling of the profile. In **Figure 7.16** *frames 1* and *2* the airflow and boost pressure responses for both controllers are similar, although the

standard controller starts with a slightly reduced EGR rate (i.e. higher airflow) than the coordinated controller. The poor steady state airflow error for the standard strategy is again due to low EGR integral gain causing a slow convergence on the setpoint. The boost pressure response appears marginally worse for the coordinated controller though it does start from a lower boost pressure and the rate of increase looks to be identical to that of the standard controller.

Examining the EGR and VGT positions in *frames 3 and 4*, both controllers close the EGR valve rapidly, although the coordinated controller takes fractionally longer as it has further to travel, the standard controller also opens the EGR slightly during the transient, resulting in the undershoot in airflow shown in the previous trace. Again the 'spike' of coordinated action can be seen in the VGT position.

The fuelling traces in **Figure 7.17** show a slight disparity, confirmed by the minor variance in torque output. There is a large difference in smoke, the coordinated controller gives worse transient smoke, this is due not to the control action but to the initially higher EGR level and the slightly higher fuelling.

In **Figure 7.18** the controller details are given, the input to the VGT compensator first swings negative for the coordinated controller before returning to a positive error input as the control action transfers from airflow tracking to boost pressure tracking. The resultant output shows an initial swing towards opening the vanes before closing them. The control output saturation limits were set lower for the coordinated controller and as a consequence the VGT control signal becomes saturated before the vanes can be completely closed. In the turbocharger speed trace, the faster exhaust pressure response of the standard controller results in earlier acceleration of the turbo, but the open EGR valve ultimately reduces the response to below that of the coordinated controller.

#### 7.8.3.4 *Figure 7.19 to Figure 7.21 Tip-out 1*

The airflow and boost pressure tracking comparison for the first step down of the fuelling profile is given in **Figure 7.19 frames 1 and 2**. There is a clear difference to the initial airflow levels which affects the response, however the coordinated controller gives a very sharp reduction in airflow, resulting in an undershoot which is rapidly converged to the desired value. This is achieved through a combination of coordinated action and better EGR integral response. The EGR valve opens (*frame 3*) whilst the VGT closes (*frame 4*) driving more EGR into the inlet manifold, then due to the airflow undershoot the EGR valve closes whilst the VGT vanes open. The EGR valve closure is much faster for the coordinated controller, this is because the tracking error during the undershoot is large and the error based I gain multiplier increases the integral action accordingly.

In **Figure 7.20** the performance comparison for the tip-out shows a difference in torque production (*frame 2*) due to the fuelling (*frame 1*), the smoke responses are indistinguishable (*frame 3*) but the exhaust manifold pressures show a difference (*frame 4*). The coordinated controller gives lower initial backpressure as it has opened the VGT in response to the previous tip-in. However, the closure of the vanes during this tip-out causes the exhaust pressure to rise to drive more EGR where the standard controller opens the vanes, reducing the pressure and hence EGR flow; the opposite effect to that which is desired.

A break down of the control system behaviour is given in **Figure 7.21**, the first frame illustrates again the opposing nature of the VGT compensator inputs for standard and coordinated controllers. The resultant controller outputs follow the inputs closely, due to dominant proportional action. From the error gain it can be seen that co-ordination was completely active throughout the entire transient. There is minimal change in turbocharger speed at this condition, the standard controller has a slightly faster initial condition due to the higher exhaust pressure.

#### 7.8.3.5 *Figure 7.22 to Figure 7.24 Tip-out 2*

The second fuelling step down is described in the **Figure 7.22 to Figure 7.24**. The airflow and boost pressure tracking are described in *frames 1 and 2* of **Figure 7.22**. As was the case for the previous tip-out the coordinated controller gives a much better dynamic response, even though the initial airflow level is higher, the increase in EGR rate is considerably more rapid and converges with the new setpoint. The standard controller initially increases the airflow due to the opening of the turbo charger vanes in response to the reduced boost pressure setpoint. The proceeding fall in airflow is slower and does not achieve the steady state target. The coordinated action is seen in the EGR and VGT position frames as the opposing movements. The standard controller reacts strongly to the overshoot in boost pressure and fully opens the VGT, this is the principal reason for the slow response of the airflow.

**Figure 7.23** shows that the fuelling and torque levels for both controllers are approximately the same, and the smoke opacity is again indistinguishable from the measurement noise. The exhaust manifold pressure illustrates the sharp decrease in backpressure experienced when the standard controller opens both VGT vanes and EGR valve. In the same trace it can be seen that the coordinated controller maintains enough backpressure to rapidly increase the EGR flow before settling at a lower steady state level.

**Figure 7.24** describes controller input and output, the opposite nature of the controller inputs is reflected in the outputs, the coordinated controller output saturates with the vanes almost fully closed. It is very difficult to calibrate this saturation limit due to the vane mechanism

hysteresis. The error gains illustrate how this transient begins in the uncoordinated control region then switches with the step-decrease in fuel to coordinated operation.

## **7.9 SUMMARY OF RESULTS**

Although inaccuracies in the test procedure make it difficult to distinguish the improvements in performance due to coordinated control and due to differing initial and final conditions, it can still be seen that the cross-coupled control strategy proposed in this chapter offers improvements in transient airflow response. The improvement for step increases in fresh airflow demand seem small but the testing only encompassed one such demand, the improved response to step reductions in airflow demand is much more apparent and should result in better overall transient NO<sub>x</sub> performance as EGR levels are increased more rapidly.

For the case of step increases in fuelling that commence within the coordinated control region and finish outside of this region, the controller initially applies coordinated action, then switches to decoupled operation. This does not appear to have compromised the performance of the system.

It can be concluded that this approach to coordinated control achieves improved airflow tracking performance using a very simple implementation. The transparency and interpretation of the original control scheme has been maintained and the calibration effort is no different, once the fuzzy logic has been defined and tuned (which is not a particularly demanding task). The use a small fuzzy inference system will not cause computational difficulties, and the fuzzy logic can always be replaced by other mathematical functions. Indeed a look up table may even achieve the same results, but it would have to be very detailed for a smooth transition in operating characteristic.

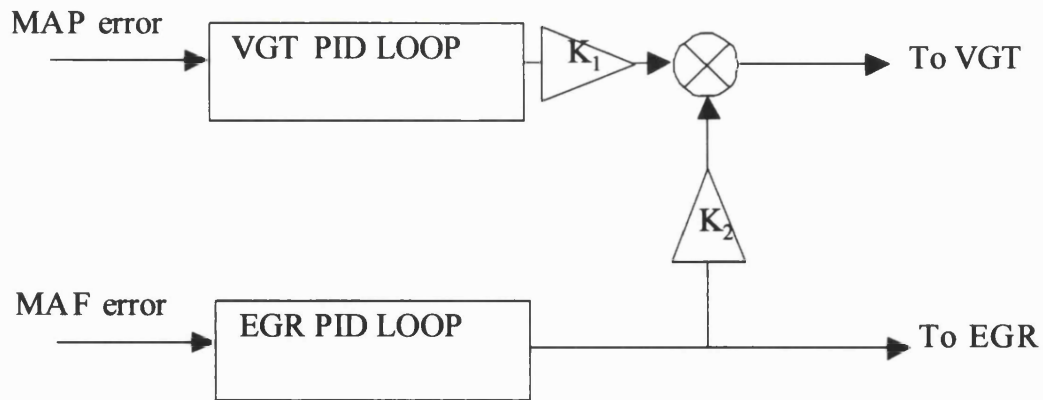


**Figure 7.1** Coupling of the independent control loop outputs to achieve coordinated control action

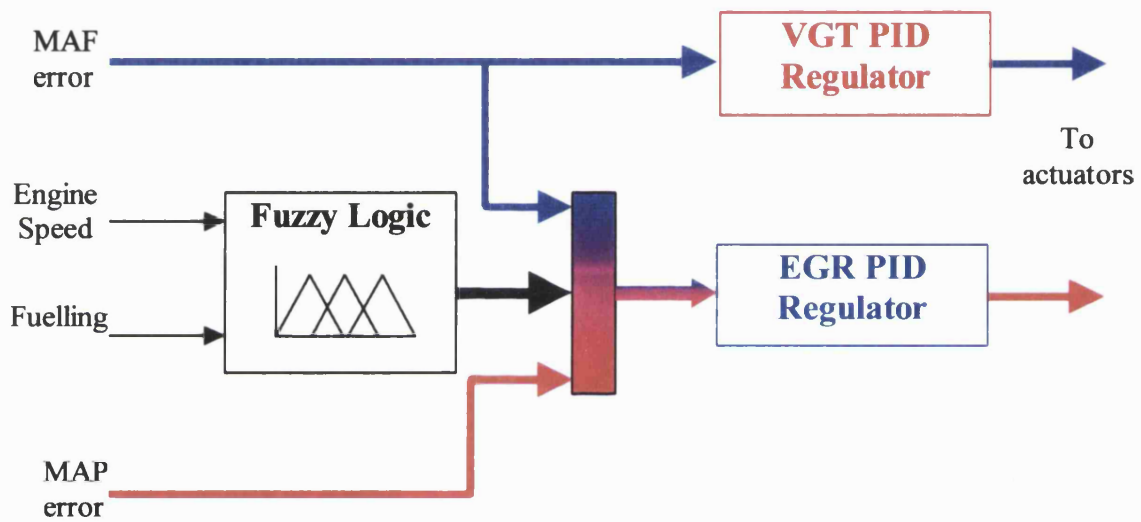


**Figure 7.2** Coupling of the independent control loop inputs to achieve coordinated control action

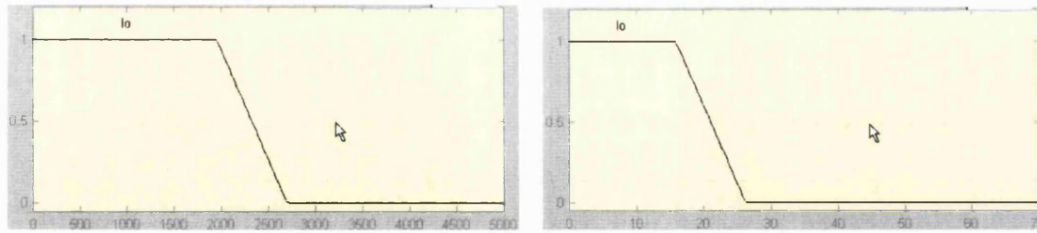


**Figure 7.3 Input Membership Functions (Engine Speed and Fuelling Demand)**

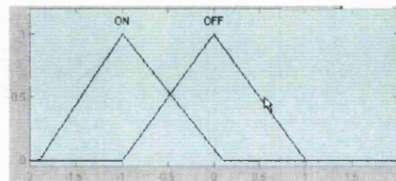


**Figure 7.4 Output Membership Functions (Airflow error to VGT loop input gain)**

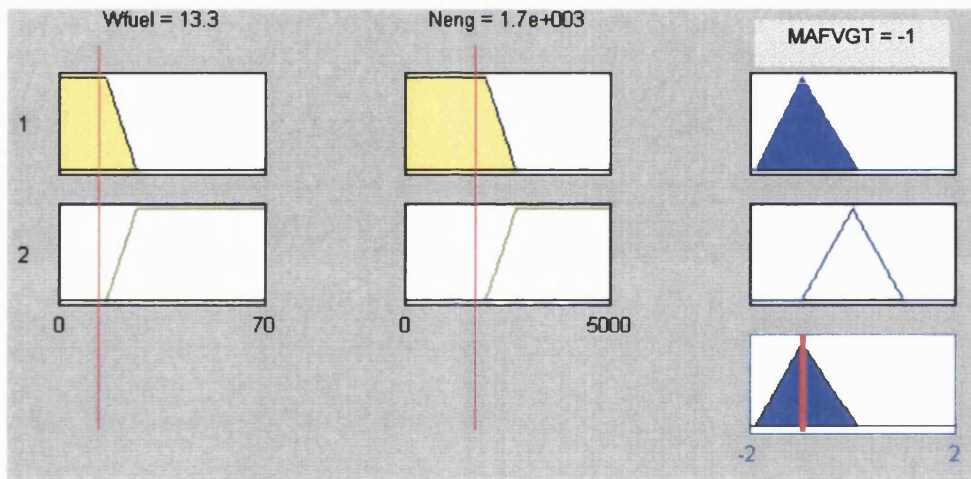


**Figure 7.5 Example of fuzzy inference in operation in the low speed and low load engine operating range**

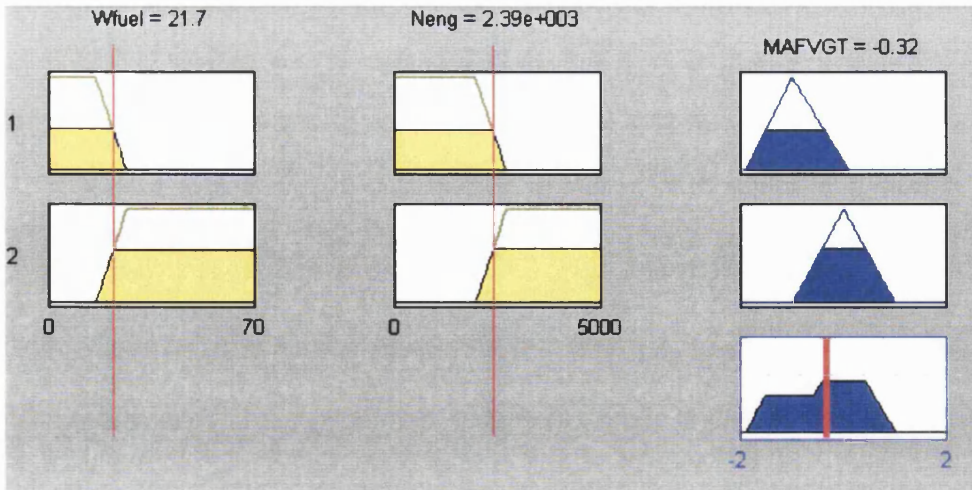


**Figure 7.6 Example of fuzzy inference in operation in the transition region from low speed and load to high speed and load**

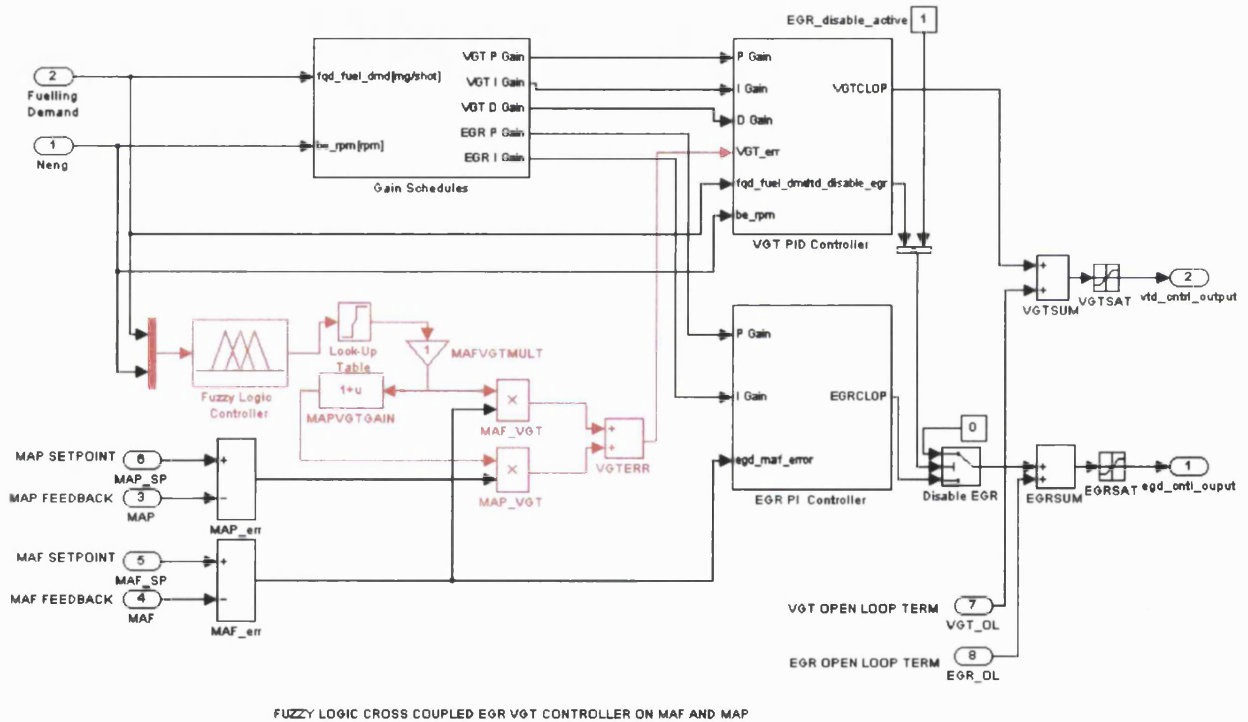


**Figure 7.7 Simulink implementation of cross-coupled controller (Additional elements shown in red)**



SIMULATION RESULTS (FORD PUMA CP4 + VGT)  
 COMPARISON OF FUZZY CROSS COUPLED CONTROLLER  
 WITH STANDARD CONTROLLER OVER 1500 rev/min FUEL PROFILE

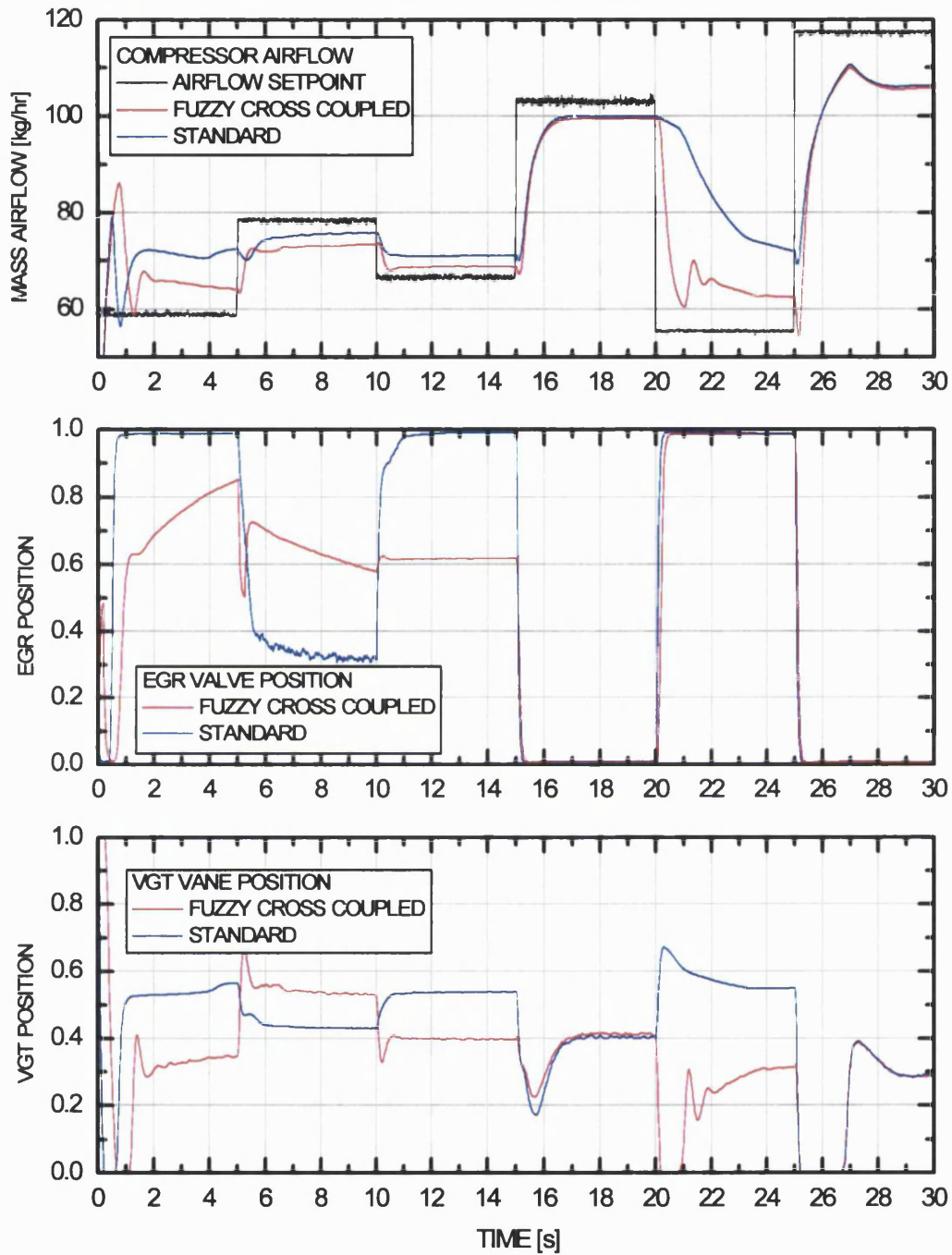


**Figure 7.8 Simulated fuel step response at 1500rev/min (Custom Setpoints and Fixed Open-loop)**

SIMULATION RESULTS (FORD PUMA CP4 + VGT)  
 COMPARISON OF REVISED FUZZY CONTROLLER #1  
 WITH STANDARD CONTROLLER  
 CUSTOM SETPOINTS AND ACTIVE OPEN LOOP

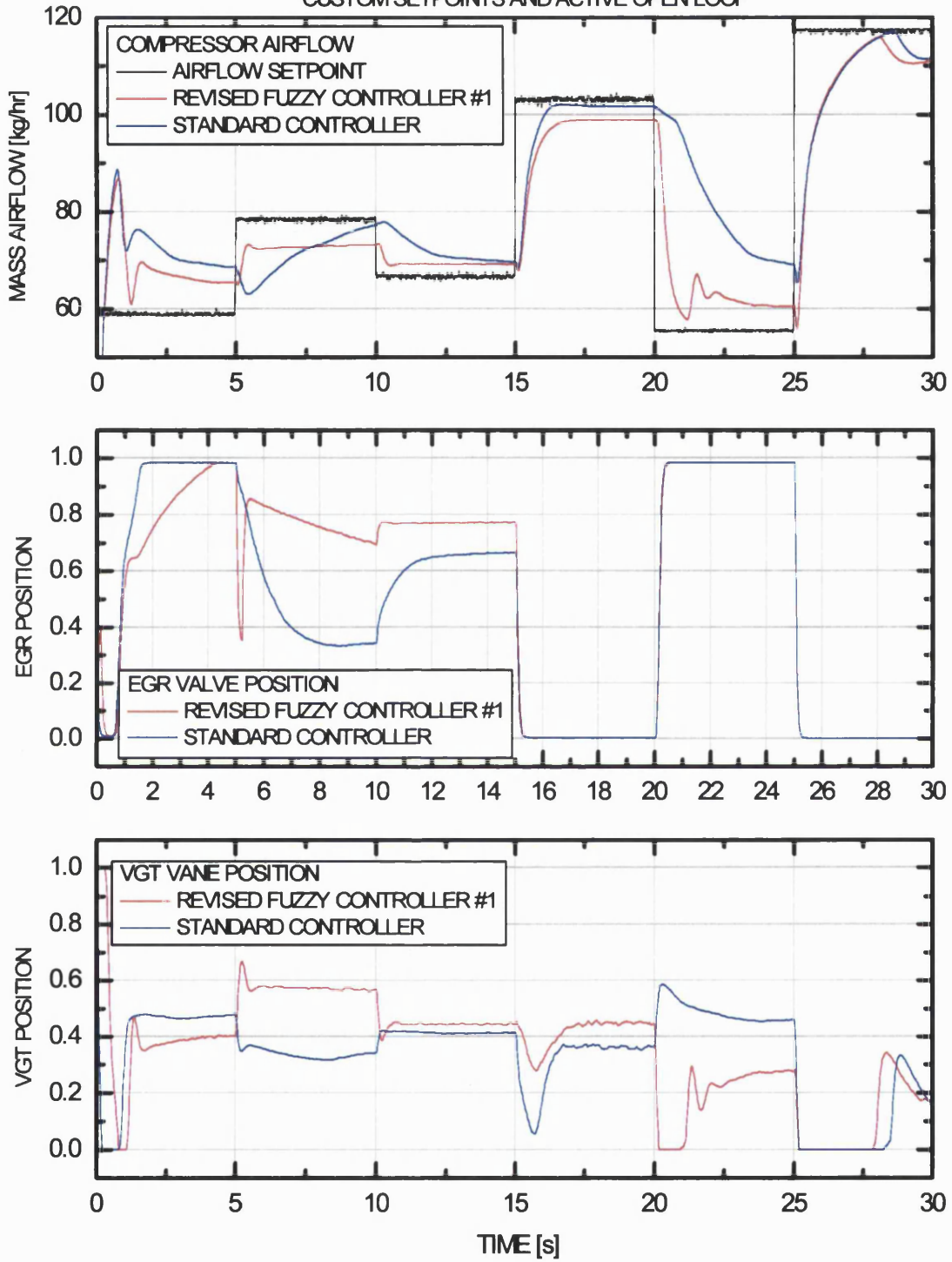


**Figure 7.9 Simulated fuel step response at 1500 rev/min (Custom Setpoints and Active Open-loop)**

CO-ORDINATED EGR VGT CONTROL COMPARED TO STANDARD CONTROL STRATEGY  
(TIP-IN 1 : 1500rev/min fuelling staircase profile, fixed 50% open loop duty cycle)

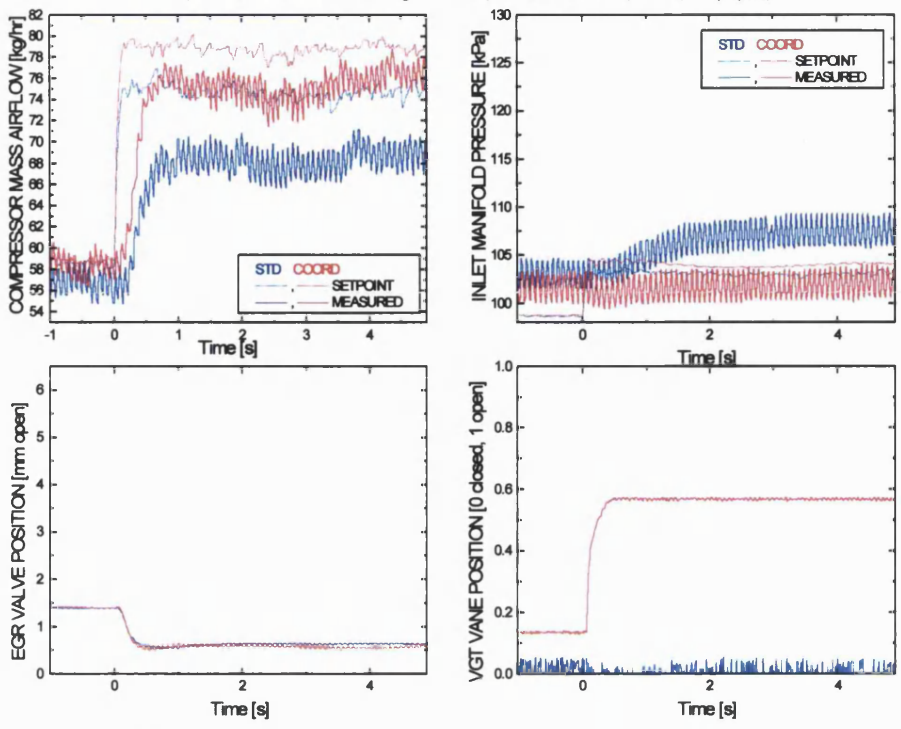


**Figure 7.10 Tip-in 1 Airflow and Boost tracking details**

CO-ORDINATED EGR VGT CONTROL COMPARED TO STANDARD CONTROL STRATEGY  
(TIP-IN 1 : 1500rev/min fuelling staircase profile, fixed 50% open loop duty cycle)

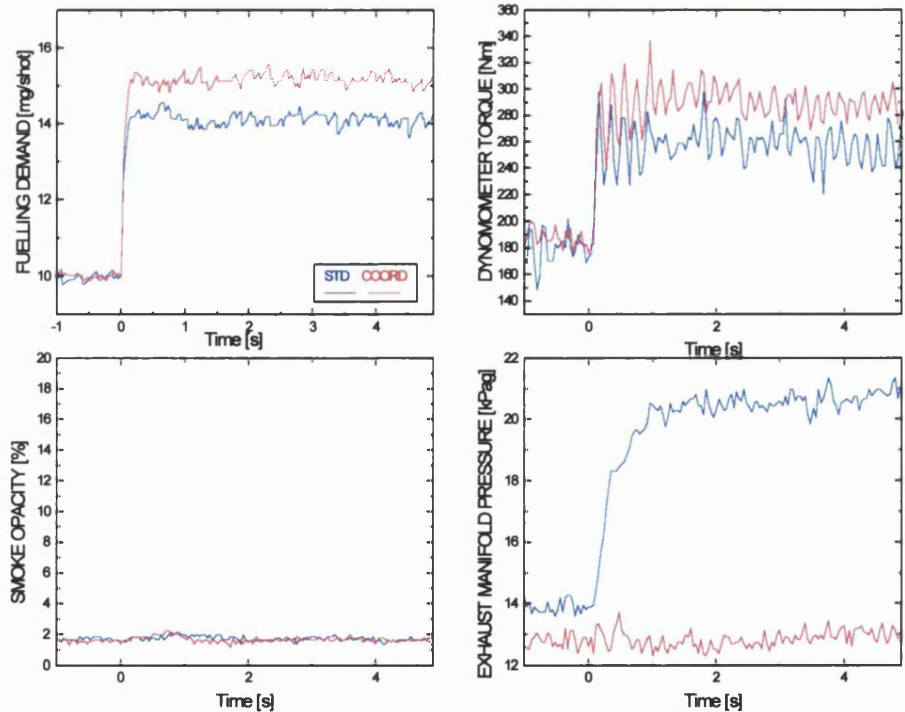


**Figure 7.11 Tip-in 1 Performance details**

CO-ORDINATED EGR VGT CONTROL COMPARED TO STANDARD CONTROL STRATEGY  
(TIP-IN 1 : 1500rev/min fuelling staircase profile, fixed 50% open loop duty cycle)

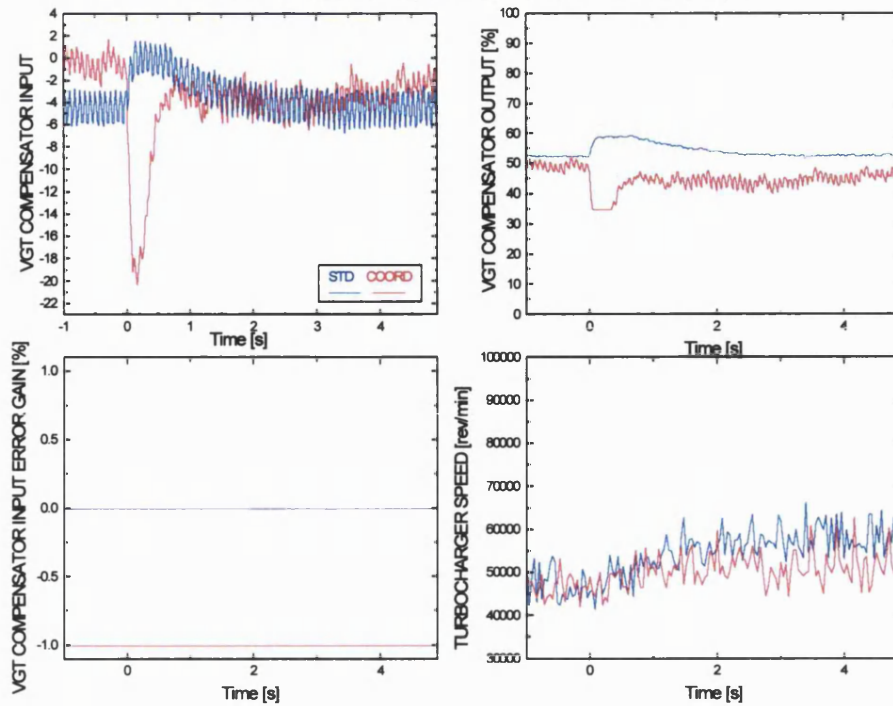


**Figure 7.12 Tip-in 1 Control detail**

CO-ORDINATED EGR VGT CONTROL COMPARED TO STANDARD CONTROL STRATEGY  
(TIP-IN 2 : 1500rev/min fuelling staircase profile, fixed 50% open loop duty cycle)

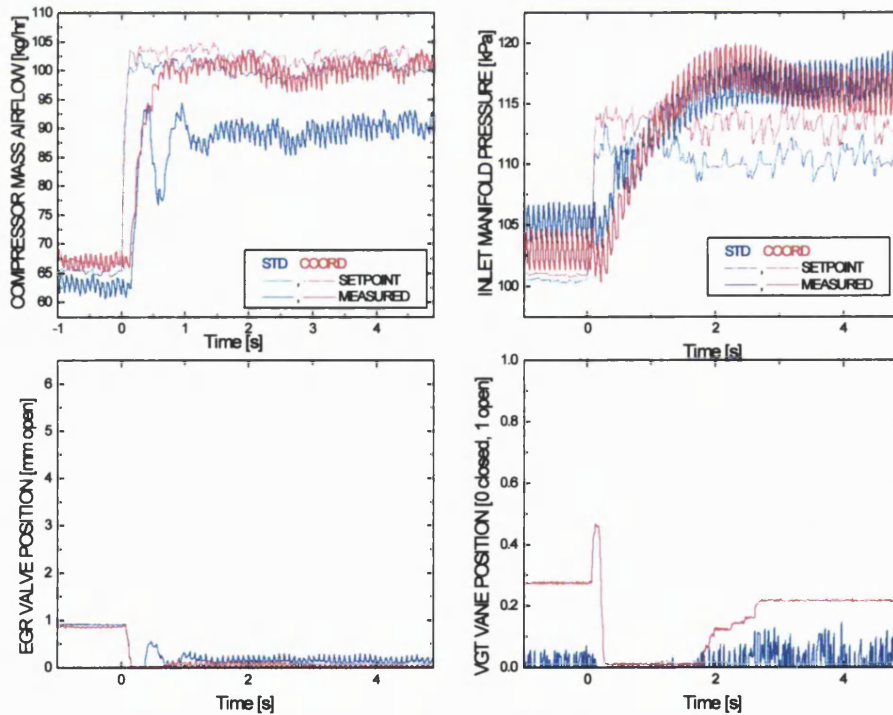


**Figure 7.13 Tip-in 2 Airflow and Boost Pressure tracking**

CO-ORDINATED EGR VGT CONTROL COMPARED TO STANDARD CONTROL STRATEGY  
(TIP-IN 2 : 1500rev/min fuelling staircase profile, fixed 50% open loop duty cycle)

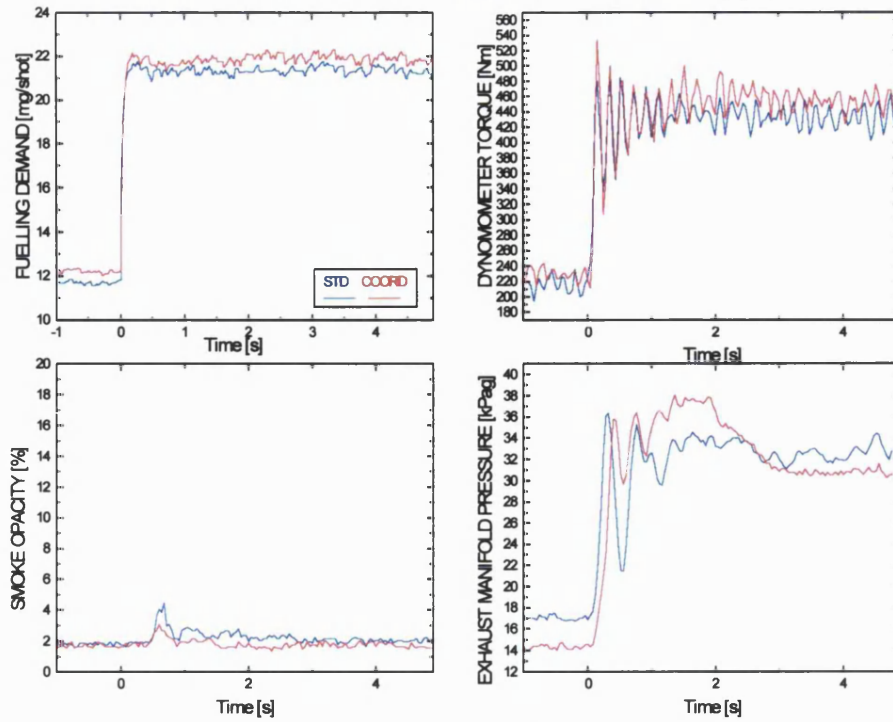


**Figure 7.14 Tip-in 2 Performance Detail**

CO-ORDINATED EGR VGT CONTROL COMPARED TO STANDARD CONTROL STRATEGY  
(TIP-IN 2 : 1500rev/min fuelling staircase profile, fixed 50% open loop duty cycle)

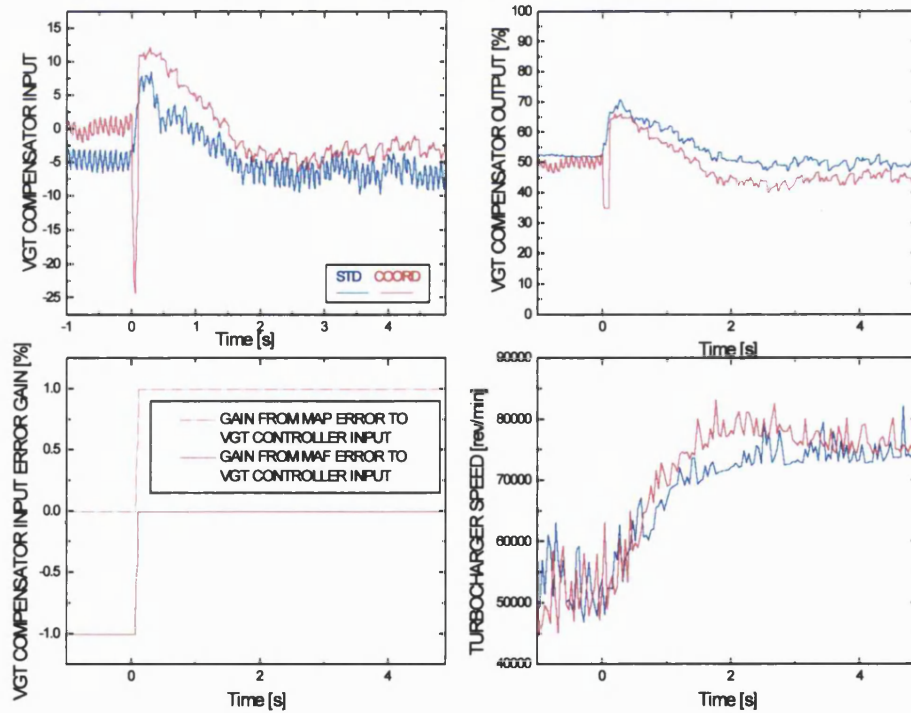


**Figure 7.15 Tip-in 2 Control Detail**

CO-ORDINATED EGR VGT CONTROL COMPARED TO STANDARD CONTROL STRATEGY  
 (TIP-IN 3 : 1500rev/min fuelling staircase profile, fixed 50% open loop duty cycle)

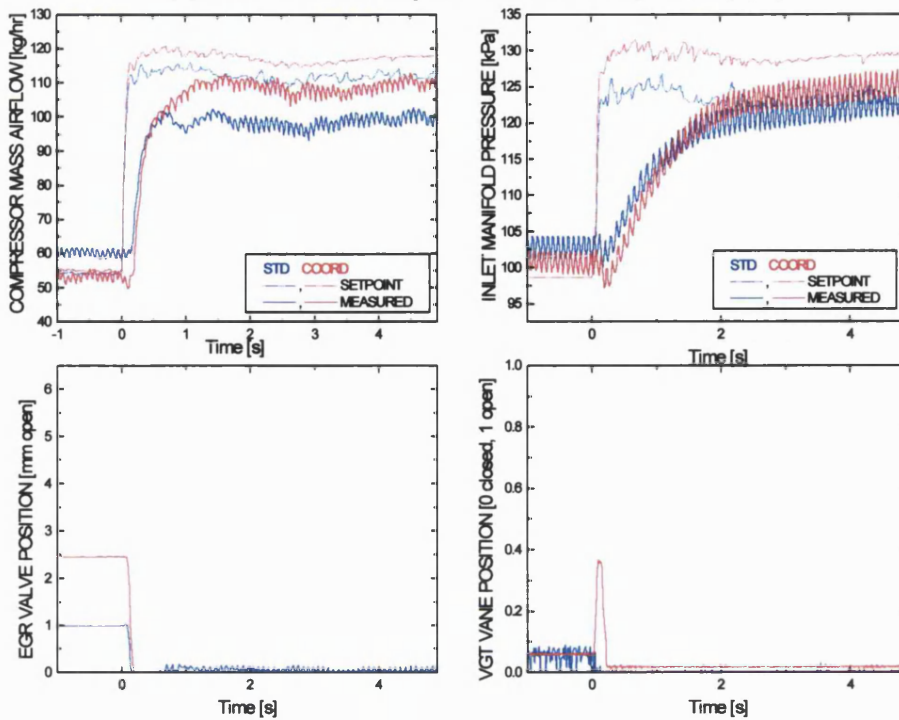


**Figure 7.16 Tip-in 3 Airflow and Boost Pressure tracking**

CO-ORDINATED EGR VGT CONTROL COMPARED TO STANDARD CONTROL STRATEGY  
 (TIP-IN 3 : 1500rev/min fuelling staircase profile, fixed 50% open loop duty cycle)

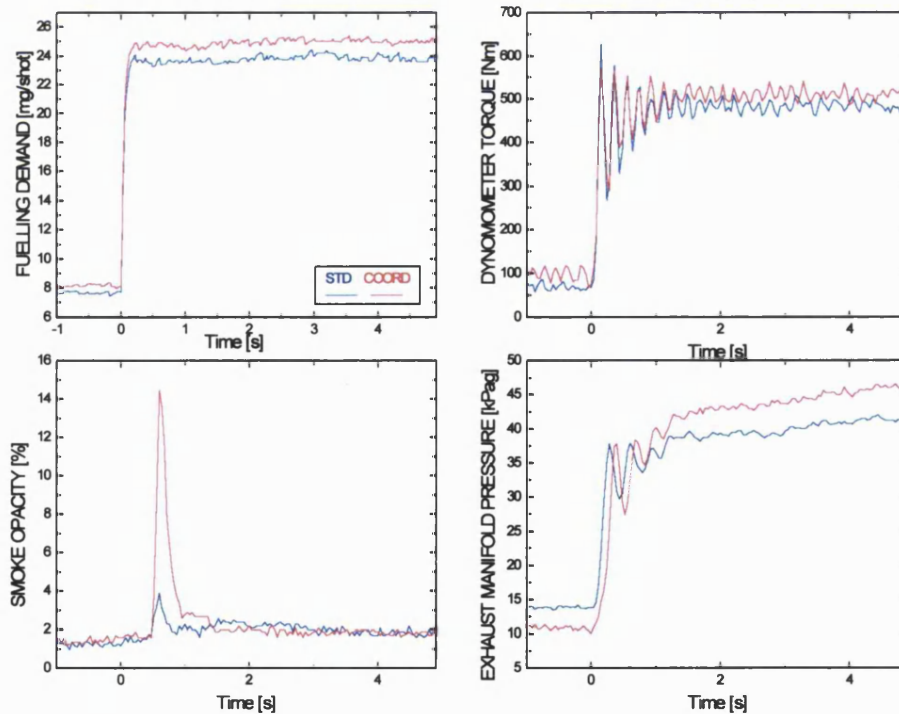


**Figure 7.17 Tip-in 3 Performance Detail**

CO-ORDINATED EGR VGT CONTROL COMPARED TO STANDARD CONTROL STRATEGY  
(TIP-IN 3 : 1500rev/min fuelling staircase profile, fixed 50% open loop duty cycle)

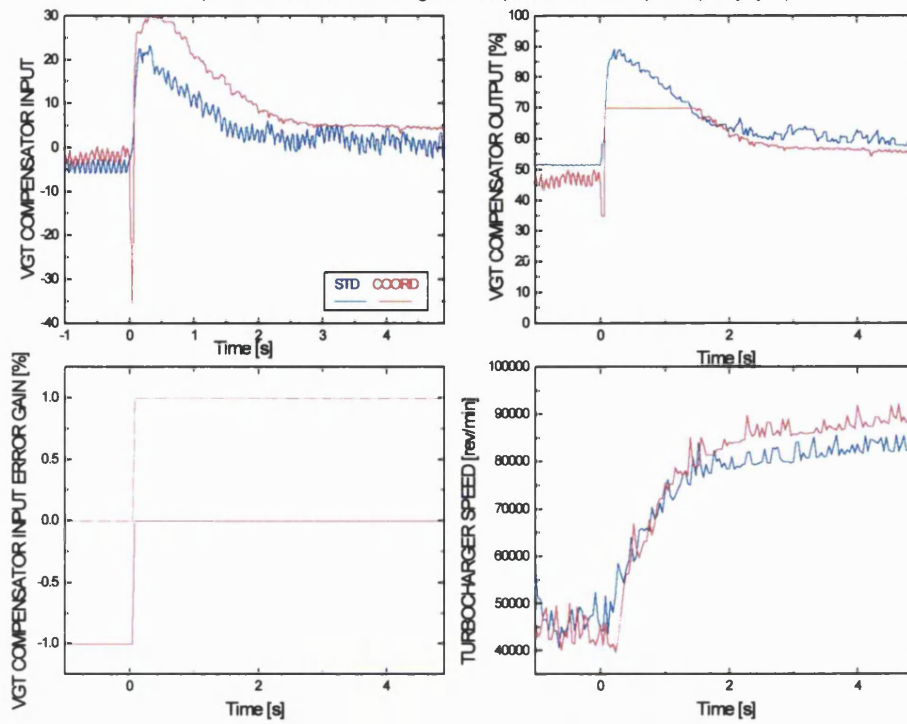


**Figure 7.18 Tip-in 3 Control Detail**

CO-ORDINATED EGR VGT CONTROL COMPARED TO STANDARD CONTROL STRATEGY  
(TIP-OUT 1 : 1500rev/min fuelling staircase profile, fixed 50% open loop duty cycle)

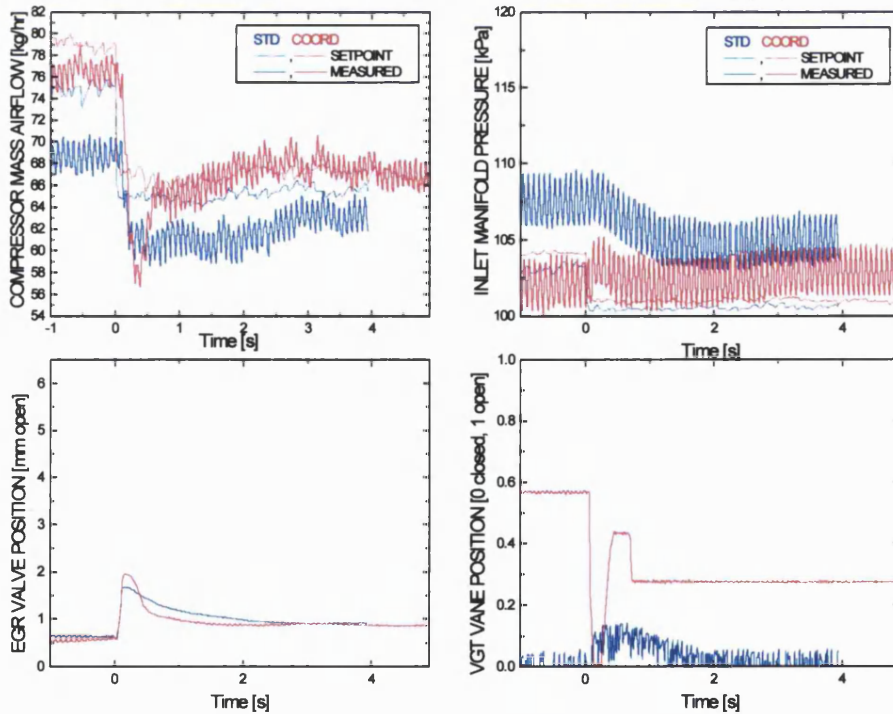


**Figure 7.19 Tip-out 1 Airflow and Boost Pressure tracking**

CO-ORDINATED EGR VGT CONTROL COMPARED TO STANDARD CONTROL STRATEGY  
 (TIP-OUT 1 : 1500rev/min fuelling staircase profile, fixed 50% open loop duty cycle)

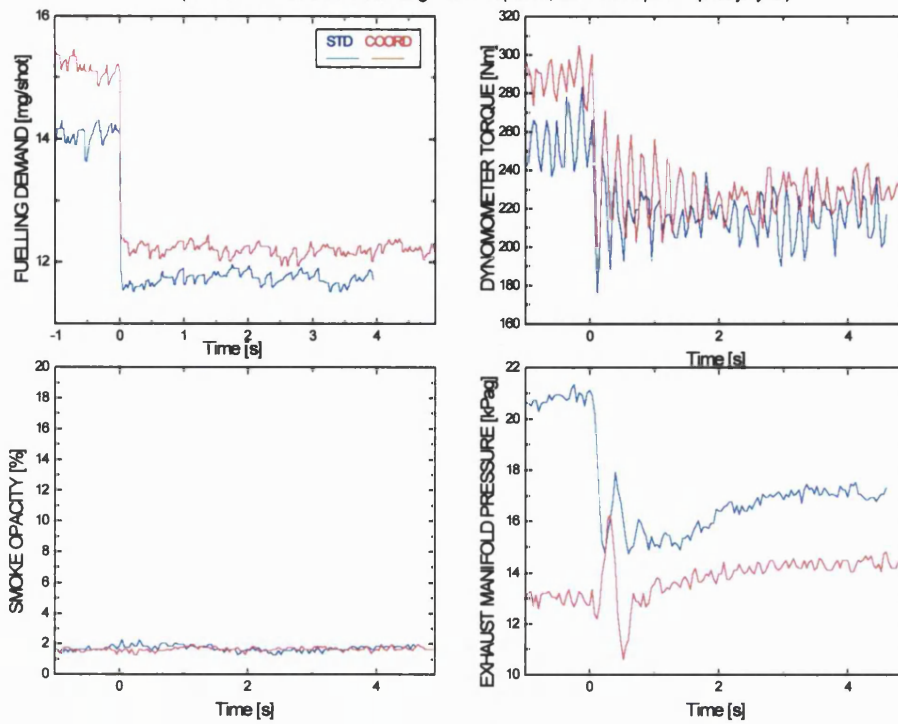


**Figure 7.20 Tip-out 1 Performance Detail**

CO-ORDINATED EGR VGT CONTROL COMPARED TO STANDARD CONTROL STRATEGY  
 (TIP-OUT 1 : 1500rev/min fuelling staircase profile, fixed 50% open loop duty cycle)

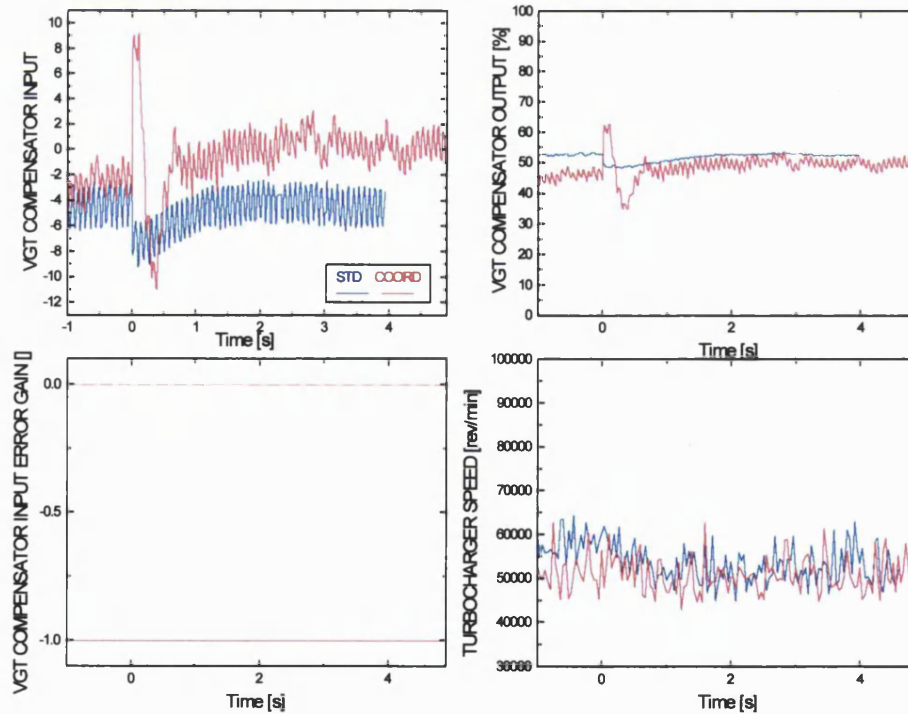


**Figure 7.21 Tip-out 1 Control Detail**



CO-ORDINATED EGR VGT CONTROL COMPARED TO STANDARD CONTROL STRATEGY  
 (TIP-OUT 2 : 1500rev/min fuelling staircase profile, fixed 50% open loop duty cycle)

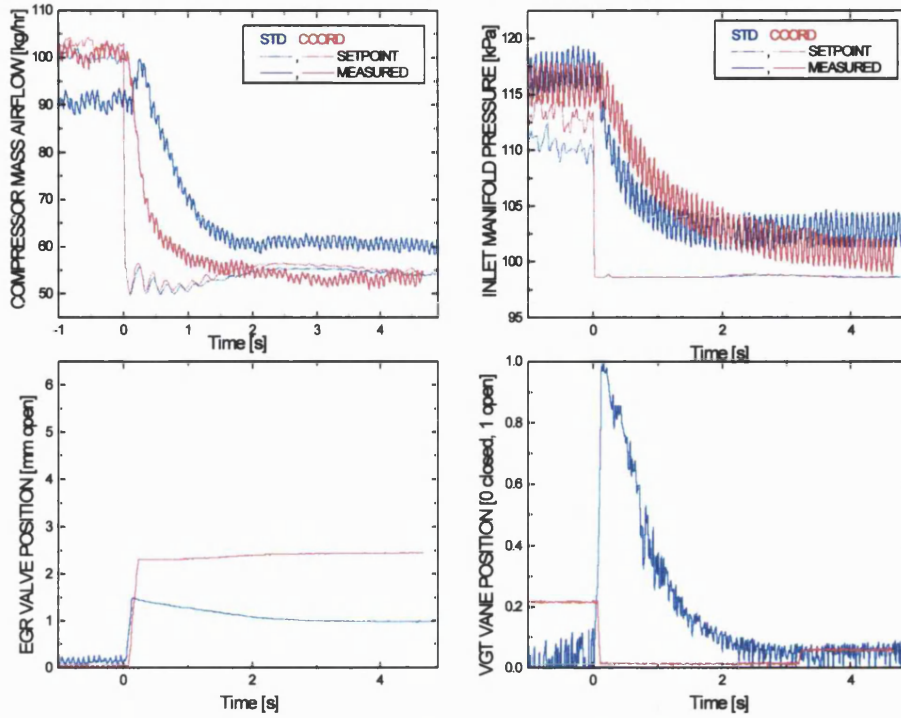


**Figure 7.22 Tip-out 2 Airflow and Boost Pressure tracking**

CO-ORDINATED EGR VGT CONTROL COMPARED TO STANDARD CONTROL STRATEGY  
 (TIP-OUT 2 : 1500rev/min fuelling staircase profile, fixed 50% open loop duty cycle)

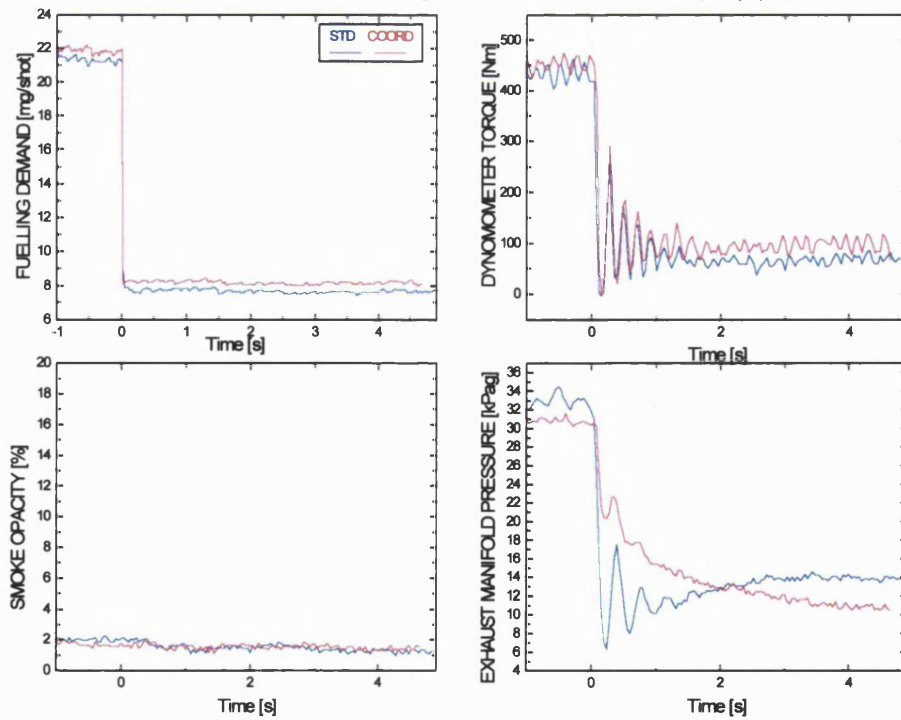


**Figure 7.23 Tip-out 2 Performance Detail**

CO-ORDINATED EGR VGT CONTROL COMPARED TO STANDARD CONTROL STRATEGY  
 (TIP-OUT 2 : 1500rev/min fuelling staircase profile, fixed 50% open loop duty cycle)

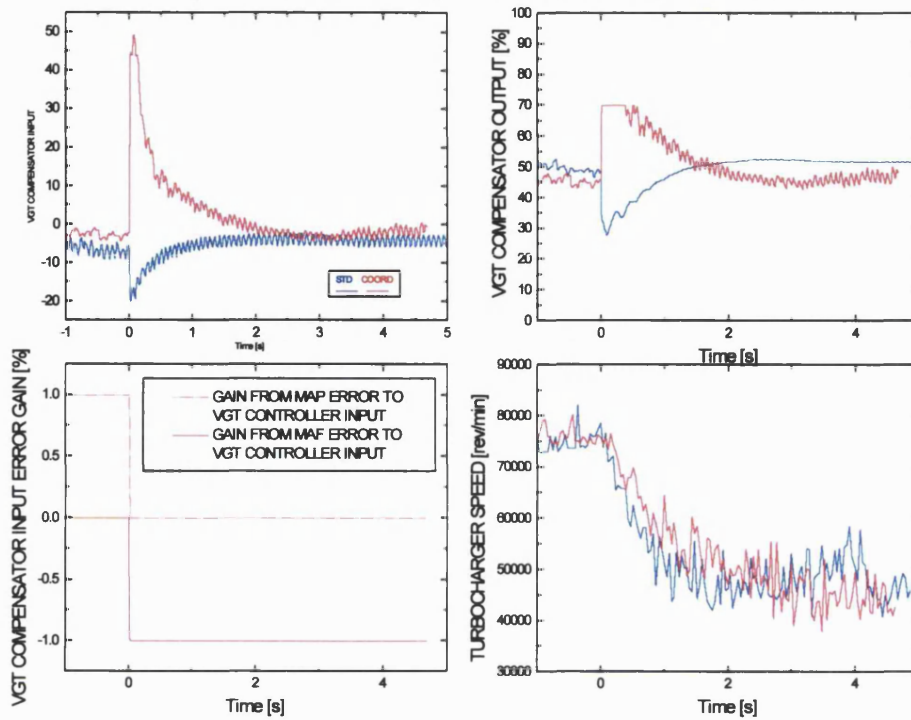


Figure 7.24 Tip-out 2 Control Detail

# Chapter 8 EXHAUST OXYGEN FEEDBACK CONTROL

## 8.1 INTRODUCTION

Universal Exhaust Gas oxygen (UEGO) sensors are widely employed in spark ignition engines for the closed-loop control of fuel injection, but their application to the Diesel engine has generally received little interest. The measurement of engine gas composition is potentially very useful for closed-loop control of the exhaust gas recirculation and turbocharging systems commonly found on modern Diesel engines. In this chapter the viability of EGR VGT control schemes based on oxygen concentration feedback are investigated.

The various options for sensor location are discussed and the exhaust downpipe is chosen as the most suitable of these. Various techniques for dealing with the feedback information are discussed. The exhaust gas oxygen concentration itself is motivated as a feedback control parameter due to the lack of modelling and additional measurements necessary in order to implement a strategy based on this variable.

In the first instance the sensor is used as a direct replacement of the Mass Airflow (MAF) sensor in the existing strategy, the EGR valve is used to track a target exhaust oxygen content whilst the VGT control loop is left unaltered to independently track inlet manifold boost pressure. This method demonstrates unsatisfactory performance including large fluctuations in exhaust oxygen levels due to the EGR valve oscillations. It is evident that disturbances to exhaust oxygen concentration caused by the fuel injection process are impossible to completely reject by the EGR and VGT due to the difference in system dynamics. In an attempt to address this, a coordinated controller is applied in order to exploit the faster airflow response rates available with this scheme.

The same technique for achieving EGR and VGT coordination as developed in **chapter 7** is used, but using exhaust oxygen concentration in place of airflow. An experimental investigation shows this controller to offer improved, if not completely satisfactory performance.

Due to the limited period available for experimental work on the engine test facility, further controller development was continued in simulation. In order to improve the disturbance rejection of the UEGO feedback controller, a model based feedforward term is developed. A linear model of the fuel disturbance to oxygen concentration is used predictively in the feedforward path, this adjusts the EGR and VGT actuators in advance of the feedback control in response to fuelling changes.

It is concluded that an exhaust gas oxygen sensor can be incorporated into an effective and relatively simple feedback EGR-VGT control scheme providing good feedforward augmentation is available for disturbance rejection. The resulting strategy has a simpler interpretation and slightly easier calibration requirements than the standard control scheme as the oxygen concentration relates directly to the combustion process.

## **8.2 Motivation for Feedback EGR control**

The use of an oxygen sensor for feedback control of EGR equipped engines has already been suggested in the literature review in **Chapter 2**; the study performed by **Amstutz et al [23]** demonstrates the potential for this method. Under the standard control scheme, the in-cylinder air charge conditions are inferred from compressor airflow and inlet manifold boost pressure, and the conditions are set from steady state schedules of these parameters. Feedback of the exhaust oxygen concentration gives a direct measurement of these conditions, allowing more accurate control of the combustion process, particularly during transients. As a control parameter such information is easier to interpret and more generic, scheduling the exhaust or inlet composition with engine operating point allows an intuitive interpretation of the controller setpoint design and this will greatly simplify the calibration process.

Direct feedback of the oxygen content will automatically compensate for changes in engine behaviour over time. For example, the standard control scheme uses airflow and boost pressure targets, these are chosen from experimental results that achieve certain conditions such as desired air fuel ratio and burnt gas fraction. Should the engine volumetric behaviour change, the same boost and airflow targets will cause different air fuel ratios and inlet burnt gas concentrations.

oxygen concentration feedback also offers potential to extend the operating envelope over which EGR is applied, achieving further  $\text{NO}_x$  reductions. As the current method implies the EGR rate, a certain safety margin must be included to ensure that combustion quality is not deteriorated, this will mean the EGR rates employed are potentially lower than they could be if the combustion conditions were known.

## **8.3 Oxygen Sensors for Automotive Diesel Application**

### **8.3.1 Operating Principle**

The oxygen sensor measures the partial pressure of oxygen in the exhaust gases, one electrode is in the exhaust stream and the other is exposed to air. The difference in partial oxygen pressures leads to a flow of electrons between the two electrodes [92]. Most sensors for stoichiometric engines give an essentially binary output to indicate rich or weak mixture,

however lean burn sensors need to evaluate the partial pressure of the gas to give an actual oxygen concentration. The sensing mechanism only works at temperatures above 300°C, requiring an in-built heater for use when the exhaust gas is cool (at part load, or highly lean mixtures).

### **8.3.2 Requirements for Application to Diesel Engines**

In order to use oxygen sensing for a Diesel application, the following requirements must be met:

1. Wide measurement range, from stoichiometric (0%) to very lean (17% +).
2. Fast dynamic response, of the same order as the MAF sensor for good EGR dynamics.
3. When employed in the exhaust manifold a wide operating temperature range is necessary, as Diesel exhaust can vary from 200 degrees C up to 900 degrees, the sensor will need its own heater to prevent cooling by the exhaust gases at low load.
4. Resistance to soot, as the Diesel exhaust is a much harsher environment from the point of view of contamination than the gasoline exhaust. Even if the sensor were mounted in the inlet manifold, it would be exposed to soot due to the presence of EGR.

Although a large number of oxygen sensors are available, very few will fulfil the criteria specified above. Of the major automotive suppliers contacted, only NTK NGK could supply a suitable sensor. Interestingly, they are also developing a combined NO<sub>x</sub>/O<sub>2</sub> sensor, the NO<sub>x</sub> sensing being a by-product of the oxygen sensing mechanism.

### **8.3.3 Sensor**

The chosen sensor is a TL-7111-W1 UEGO, the equipment is supplied as a complete in-vehicle system, with sensor, controller/signal conditioning and wiring harness. The total cost of the equipment was £710 which is expensive compared to lower measurement range sensors, however the system is a low volume product and would undoubtedly become more competitively priced with increased volume.

## **8.4 Possible Sensor Installation Configurations**

### **8.4.1 INLET MANIFOLD INSTALLATION**

Ideally, the sensor would be located in the inlet manifold, in this manner it would give a direct measurement of the inlet manifold burnt gas fraction or EGR rate and allow precise control of the inlet charge. Unfortunately, the nature of the sensor itself prohibits this type of installation as is explained by the following derivation.

The sensor is calibrated to read air fuel ratio from an oxygen concentration measurement. Considering exhaust gases leaving the engine, under lean combustion conditions there will be a flow of burnt gases ( $W_{b\_ex}$ ) and a flow of unburnt air ( $W_{a\_ex}$ ), these are given by **Equations (8.1) and (8.2)**:

$$W_{a\_ex} = W_{a\_ie} - (W_f * AFR_{stoich}) \quad (8.1)$$

$$W_{b\_ex} = W_f + (W_f * AFR_{stoich}) \quad (8.2)$$

Where  $W_{a\_ie}$  is the flow of fresh air into the cylinders  
 $W_f$  is the fuel flow rate  
 $AFR_{stoich}$  is the stoichiometric air fuel ratio

$W_{a\_ie}$  can be expressed as:

$$W_{a\_ie} = W_f * AFR \quad (8.3)$$

Where  $AFR$  is the actual in-cylinder air fuel ratio

Total exhaust gas flow ( $W_{ex}$ ) will be the sum of the two exhaust flows:

$$W_{ex} = W_{a\_ex} + W_{b\_ex} \quad (8.4)$$

By substituting **Equations (8.1), (8.2) and (8.3)** into **(8.4)** and rearranging, the following expression for total flow is derived:

$$W_{ex} = W_f * (1 + AFR) \quad (8.5)$$

The fraction of this total flow that is air ( $F_{a\_ex}$ ) can be calculated by dividing **Equation (8.1)** by **Equation (8.5)** :

$$F_{a\_ex} = \frac{W_{a\_ex}}{W_{ex}} = \left( \frac{AFR - AFR_{stoich}}{1 + AFR} \right) \quad (8.6)$$

This is then converted to an oxygen concentration ( $X_{O2\_ex}$ ) by multiplying by 0.21, and assuming a stoichiometric air fuel ratio of 14.4, the following expression is obtained:

$$X_{O_2_{ex}} = \frac{0.21AFR - 3.024}{1 + AFR} \quad (8.7)$$

**Equation (8.7)** gives the relationship between the quantity measured by the oxygen sensor (oxygen concentration) and the air fuel ratio. This relationship is plotted in **Figure 8.1**, it can be seen that as the oxygen concentration gets higher (more and more lean) the air fuel ratio increases more steeply.

For application to the inlet manifold, typical EGR levels will result in an inlet manifold burnt gas fraction of 0.3, or an air flow fraction of 0.7, converting this to an oxygen concentration gives a value of 0.147. By rearranging **Equation (8.7)** and substituting in an oxygen concentration of 0.147, the corresponding air fuel ratio will be of the order of 54, this value lies on the upper limit of measurement for most lean burn air fuel ratio sensors.

**Figure 8.2** shows the output current versus air fuel ratio for the sensor used in this work, clearly the sensor is only useful from stoichiometric to approximately 40 AFR, and therefore is unsuitable for use in the inlet manifold.

#### 8.4.2 EXHAUST MANIFOLD INSTALLATION

The more usual location for an oxygen sensor is in the exhaust path, in this arrangement the sensor will measure the exhaust gas oxygen concentration. The relationship between oxygen concentration and air fuel ratio varies with the rate of EGR employed, therefore it is not feasible to use the UEGO sensor as a direct air fuel ratio feedback source without additional measurements. This is because the oxygen sensor compares the concentration of oxygen in the exhaust gas with the concentration of oxygen in the atmosphere, when EGR is being used, the inlet air charge will have a concentration of oxygen lower than that of the atmosphere. **Figure 8.3** illustrates the effect of EGR rate on the relationship between oxygen concentration and air fuel ratio.

#### 8.4.3 EXHAUST MANIFOLD MOUNTING DETAILS

For the reasons described above, the sensor was fitted to the exhaust manifold. Ideally the sensor needs to be mounted close to the cylinder outlets for rapid response, however the exhaust manifold of the Puma engine is a highly optimised casting with an integral turbine housing; this leaves very little pre-turbine space for the sensor. There is sufficient space near the EGR tapping before the EGR cooler and valve, but when the valve is closed this will be a dead volume and therefore not a good location for dynamic measurement. The other suitable locations on the pre-turbine side had already been used by other test cell instrumentation

(pressure sensors, thermocouples), leaving the exhaust downpipe just after the turbine as the only feasible mounting location. This position was also recommended by the sensor supplier as good gas mixing is achieved by this point. Detail of the mounting can be seen in **Figure 8.4**, an M18 nut was welded onto the down pipe into which the UEGO sensor was threaded.

## **8.5 Initial Investigation**

The first phase of the oxygen concentration feedback work focused on setting up the sensor and verifying its suitability for this application. Fuel step transients were performed between various engine operating conditions (at constant speed) to determine the sensor response, one such transient is illustrated in **Figure 8.5**, this was conducted at 2500 rev/min between torque output levels of 10 and 170 Nm. The grey data set was captured at 10kHz, in a control system application this will be impractical and therefore a resampled data set at 100Hz is also shown in black. Noise is significant on the sensor output, examining the Fourier analysis of the signal frequency content (**Figure 8.6**) shows that a significant low frequency noise signal occurs around 27Hz for all tests. This can be adequately attenuated through low pass filtering leaving the signal shown in **Figure 8.5** (red line) as a useable control signal. Although filtering will reduce the bandwidth of the sensor, the EGR and VGT actuators have a very limited bandwidth and will not benefit from a faster response from the sensor.

**Figure 8.7** displays the oxygen concentration response to the fuel steps at various engine speeds with the standard EGR-VGT control scheme active. The fuel steps were chosen to achieve a 10Nm to 170Nm torque transient at each speed condition.

The transient behaviour of the oxygen concentration can be classified into three distinct phases:

1. The steep initial descent of the exhaust oxygen concentration corresponds to the fuelling increase. The fuel step occurs at time  $t=0$  seconds; the delay between the fuel step and the minimum exhaust oxygen level represents the delay between the change of in-cylinder air fuel ratio and the measured change in oxygen concentration at the sensor. This time lag includes the transport delay from cylinder to the turbine outlet and the response time of the sensor. This phase is invariant with engine speed, although the 1500rev/min case appears to descend marginally more slowly, this is due to the fuel limiting to reduce transient smoke rather than slower transport from cylinder to sensor.
2. The following phase is characterised by a sharp rise in oxygen concentration, this corresponds to the clearance of EGR residuals from the system. In all the transients EGR was initially present, but the size of the step increase in fuel dictates that no EGR will be present in the post transient condition. For speeds below 2000 rev/min the residuals take longer to



clear and the oxygen concentration takes longer to recover, this will be affected by the amount of recirculation being employed immediately before the transient.

3. The final phase is dominated by the turbocharger, as it accelerates, the inlet air charge density increases and the in-cylinder air fuel ratio increases, resulting in an increased exhaust gas oxygen concentration.

From this initial analysis it can be seen that the sensor has suitable response rate and range to capture the important exhaust gas composition dynamics. It is also clear that the response of the exhaust oxygen concentration varies greatly depending on the source of the disturbance, changes caused by fuelling are considerably more rapid than those caused by EGR and VGT changes. From the control system point of view, fuelling is considered as an external disturbance, which must be rejected by the EGR and VGT system, the difference in response rates will make this difficult.

## 8.6 UEGO APPLICATIONS FOR CONTROL

There are a number of possible methods in which the information made available by the UEGO sensor can be integrated into a control scheme, some of these are discussed in the following section.

### 8.6.1 RECONSTRUCTING INLET MANIFOLD BURNT GAS FRACTION

The UEGO sensor can be used to derive the inlet manifold burnt gas fraction, which in turn can be used as a control parameter, this is illustrated in the following derivation.

From **Equation (8.8)** the following expression for oxygen concentration can be derived

$$X_{O2\_ex} = \frac{0.21 * W_{a\_ex}}{W_{ex}} \quad (8.8)$$

Expanding the numerator of Equation (8.8) yields:

$$X_{O2\_ex} = \frac{0.21 * (W_{ex} - W_{b\_ex})}{W_{ex}} \quad (8.9)$$

When EGR is present, the expression for burnt gas flow in the exhaust is given by **Equation (8.10)**

$$W_{b\_ex} = W_f + (W_f * AFR_{stoich}) + W_{b\_ie}$$

$$W_{b\_ex} = W_f + (W_f * AFR_{stoich}) + F_{b\_ie} * W_{ie} \quad (8.10)$$

Where  $F_{b\_ie}$  is the fraction of burnt gas entering the cylinders

Substituting **Equation (8.10)** into **(8.9)** gives:

$$X_{O2\_ex} = \frac{0.21 * (W_{ex} - (W_f + (W_f * AFR_{stoich}) + X_{b\_ie} * W_{ie}))}{W_{ex}} \quad (8.11)$$

The total exhaust flow  $W_{ex}$  is the sum of the flow into the cylinders and the fuel flow:

$$W_{ex} = W_{ie} + W_f \quad (8.12)$$

Where  $W_{ie}$  is the total flow into the cylinders

By substituting **Equation (8.12)** into **Equation (8.11)** and rearranging to make  $F_{b\_ie}$  the subject of the equation, the relationship between inlet manifold burnt gas fraction and exhaust oxygen concentration is arrived at:

$$F_{b\_ie} = \left[ \frac{(X_{O2\_ex} * (W_{ie} + W_f) + 0.21 * W_f * AFR_{stoich})}{0.21 * W_{ie}} - 1 \right] \quad (8.13)$$

Clearly , in order to evaluate the inlet burnt gas fraction the fuelling quantity and total gas flow into the engine are required. The fuel flow can be derived from the fuelling demand sent to the fuel injection equipment and the inlet gas flow to the cylinders can be estimated using the speed-density relationship given by **Equation (8.14)**:

$$W_{ie} = \frac{N_{eng} * n_{cyl} * V_{swept} * \rho_{ie} * \eta_{vol}}{60 * n_{stroke}} \quad (8.14)$$

Where  $N_{eng}$  is the engine speed  
 $n_{cyl}$  the number of cylinders  
 $V_{swept}$  the swept cylinder volume  
 $\rho_{ie}$  the inlet manifold gas density  
 $\eta_{vol}$  the engine volumetric efficiency and

$n_{stroke}$  the number of intake strokes per revolution

The inlet manifold density requires a pressure and temperature measurement, but the greatest difficulty is that posed by the estimation of the volumetric efficiency,  $\eta_{vol}$ . This quantity is difficult to measure accurately on the test bed, and is even harder to predict, particularly on an engine with EGR and VGT. Many estimates make use of exhaust and inlet manifold density measurements as the volumetric efficiency varies strongly with these properties, however the exhaust density requires either measurement or modelling, both of which begin to offset any benefits that could be gained from using the oxygen sensor both in terms of cost and computational requirements.

The measurements/estimations of fuel flow and inlet gas flow introduce a large degree of uncertainty into the calculation of inlet manifold burnt gas fraction, reducing the efficacy of this approach.

### **8.6.2 MODELLING INLET BURNT GAS FRACTION**

An alternative approach would be to model the EGR flow into the inlet manifold, the information from the oxygen sensor will yield the burnt gas flow fraction into the inlet manifold, the manifold can then be modelled to obtain the actual inlet burnt gas fraction. However accurate EGR flow modelling requires exhaust pressure and temperature, and a good description of the valve flow non-linearity. Were this approach to be adopted, it may be more effective to model the entire airflow circuit and not use the oxygen sensor.

### **8.6.3 CONTROL TO AN EXHAUST GAS OXYGEN CONCENTRATION**

For a given fuel level and engine speed, altering the EGR rate alone will cause the exhaust oxygen concentration to vary. This can be used as a means of feedback control for the EGR system. By scheduling the target exhaust oxygen concentration with engine speed and fuelling, the problem of completely characterising the inlet charge is addressed implicitly.

For a fixed exhaust oxygen target concentration, the amount of EGR that can be used reduces as the fuelling level rises, this is illustrated in the contour plot in **Figure 8.8**. This can be used to automatically schedule the EGR rate according to engine operating regime.

This method is also the least complex of all the approaches discussed, requiring no system models or additional measurements/estimations; it was therefore chosen for further investigation.

## **8.7 FEEDBACK CONTROLLER DEVELOPMENT 1**

In the first instance, the existing strategy was adapted for UEGO feedback by directly replacing the MAF sensor input with that of the UEGO sensor. The setpoints for the EGR were converted to target Exhaust Gas oxygen Concentrations for the given fuelling and speed levels, these were selected with the aid of plots similar to that of **Figure 8.8**. For the fuelling profile used in the tests, the chosen setpoints request EGR rates of approximately 10 to 15 %. The EGR control loop gains also needed adjustment to cater for the different control parameter, these were simply scaled up.

### **8.7.1 TEST RESULTS FOR FEEDBACK CONTROLLER 1**

The results of the initial testing can be seen in **Figure 8.9**, they are not particularly encouraging as the control system is shown to have great difficulty tracking the target exhaust concentrations in the wake of a change in fuelling. The first step up in fuelling causes oscillatory response from the EGR valve, which is only stabilised towards the end of the proceeding step down in fuelling. The proportional term of the EGR is highly active, suggesting that the proportional gain for the EGR control loop was too high.

The VGT was operating independently on boost pressure, it also experiences difficulty tracking its own boost setpoints, the fluctuations caused by the EGR will interfere with VGT flow and inlet boost, compounding the tracking problems experienced by both loops.

From this testing it can be concluded that using the EGR valve alone with a proportional plus integral UEGO feedback control scheme cannot provide acceptable exhaust gas oxygen concentration tracking.

## **8.8 FEEDBACK CONTROLLER DEVELOPMENT 2**

With the experienced gained from the initial controller development, a new control scheme was proposed that makes use of both EGR and VGT actuators to track the oxygen concentration (whilst in the low speed and low load operating regime). This is based on the coordinated airflow and boost control developed in **Chapter 7**. It was anticipated that the more rapid response of the EGR flow to the coordinated action of EGR and VGT systems would yield a more rapid oxygen concentration response. This could be used to improve the rejection of disturbances caused by changes in fuelling level.

The theoretical improvement in response of oxygen concentration to coordinated EGR and VGT action is illustrated in **Figure 8.10**, this is a simulated step response plot comparing independent EGR and VGT control (blue line) with coordinated control (red line). The response to a fuel step is also shown to give an indication of relative response rates.

Coordinated action offers a considerably faster exhaust oxygen response when compared to independent (i.e. EGR valve only) control, however, the response to fuelling is still significantly faster.

In the new controller, the UEGO signal replaces that of the MAF sensor and the controller distributes the exhaust oxygen concentration tracking error between EGR and VGT proportional plus integral control loops (depending on engine operating point). In the low speed and low load region, negative oxygen concentration tracking errors (too much oxygen in exhaust) will be compensated by opening the EGR valve whilst closing the VGT vanes and vice versa. The controller also incorporates anti wind-up of the EGR control integrator output based on the EGR valve position, and an additional EGR disabling function which is activated when the exhaust oxygen content drops below a certain threshold.

### **8.8.1 TEST RESULTS FOR FEEDBACK CONTROLLER 2**

The coordinated controller was implemented on the test rig and evaluated over a constant speed fuelling profile, the results of this investigation are summarised in **Figure 8.11**. The initial 5 seconds or so before the first tip-in shows that the system has managed to converge on the target exhaust oxygen content, the first tip-in results in a drop in oxygen levels, the controller closes the EGR whilst opening the VGT in response to this, and the oxygen concentration eventually begins to rise quite rapidly as the EGR flow falls. It then overshoots and undershoots, the magnitude of each successive deviation decreases slightly suggesting an under-damped response, it is likely the system would have converged in the fullness of time, however the proceeding step down in fuelling occurs before it has the opportunity to do so.

The response to the tip-out in fuelling is better than that of the previous tip in, with a small undershoot followed by slow monotonic convergence. The VGT remains static during this transient, although its control signal is changing in response to the changing exhaust oxygen error.

The following tip-in (at approximately 15 seconds into the test) causes a large enough drop in exhaust oxygen content to trigger the 'EGR disable' mechanism, this can be seen by the sudden dip in the EGR controller output signal. However, when the oxygen content recovers, the EGR is re-enabled and the control signal resumes its closed-loop tracking, resulting a sudden opening of the EGR due to hysteresis in the mechanism.

The large increase in exhaust oxygen content at approximately 20 seconds into the test corresponds to a tip-out manoeuvre, here full coordinated action is used to try and reduce the deviation. The proceeding tip-in results in both EGR and VGT actuators closing fully.

In general, it appears that the system gains are set too high in an effort to minimise tracking error, resulting in oscillatory behaviour. However, with a stable choice of gains the system response would be lethargic, this leads to the inevitable conclusion that feedback control alone is insufficient for tracking the exhaust oxygen concentration using the EGR and VGT actuators to reject disturbances brought on by changes in fuelling.

## **8.9 FEEDFORWARD CONTROLLER DEVELOPMENT**

Up until this point the research has focused on feedback as the primary means of control. In many problems, particularly ones like this where large external, measurable disturbances (fuelling) are present, a feedforward control strategy can be employed with success. There are many techniques on offer, the most useful tend to be computationally intensive, such as General Predictive Control. With this technique system models are used to predict how a change in input will affect the plant output, control action is then decided by the minimisation of some cost function based on predicted performance.

A formulation for an optimisation based scheme is shown in **Figure 8.12**. A model is identified from the fuelling input to the exhaust oxygen concentration. It is used to predict the disturbance to the oxygen concentration due to a change in fuel demand, which is then set as a target for which the EGR and VGT systems must compensate. Using models of the EGR and VGT to oxygen concentration and optimisation techniques, a trajectory for the actuators can be predicted that rejects the disturbance as quickly as possible.

Whilst this approach is in theory very attractive, the practical aspects of such an implementation are difficult. The technique relies on plant models, if linear models are used then they will only be valid in highly localised operating regions, for the case of the Diesel engine with EGR and VGT the non-linearities extend in the dimensions of engine speed, fuelling, EGR position and VGT position, resulting a large number of linear models to consider. Non-linear models can be used but this increases the controller computational demands, particularly if the strong non-linearities associated with EGR and VGT gas flows need to be included in the actual models.

For these reasons, techniques such as the aforementioned have largely been avoided in this work due to the impracticalities associated with their implementations given the constraints of the automotive processor environment. However, without delving into optimal control, the use of predictive models can still be applied with relative simplicity to the feedforward path of the controller structures tested up to now, and these can alleviate many of the performance problems that have been observed.

### **8.9.1 FEEDFORWARD COMPENSATION OF FUELLING DISTURBANCE**

The change in fuelling quantity will cause a disturbance to the exhaust gas oxygen concentration, if this disturbance were known then the control system could use the EGR and VGT systems to compensate in advance instead of waiting for the oxygen concentration to change and then react to this change. This is the premise behind the following control scheme, this work was performed in simulation due to the limited time available on the dynamic engine test facility.

The controller makes use of the same coordinated feedback structure used previously in this chapter, where fuzzy logic is used to channel the oxygen concentration tracking error to both EGR and VGT proportional plus integral control loops when the engine is operating in the low speed and low load region. The new strategy uses a model of the disturbance to the oxygen concentration caused by the change in fuelling, the output of the model is scaled via two gains (one for EGR, one for VGT) and added to the closed-loop control outputs for EGR and VGT (see **Figure 8.13**).

### **8.9.2 OXYGEN DISTURBANCE MODEL**

The model in the feedforward path predicts the disturbance to the oxygen concentration caused by the fuelling change. This model is a linear second order model that was derived by performing a system identification procedure on the non-linear engine model.

### **8.9.3 MODEL IDENTIFICATION**

The model identification was performed by perturbing the non-linear engine model fuel quantity about a nominal value using a Pseudo Random Binary Sequence (PRBS), this is used as it excites the full bandwidth of the system. The resulting variations in exhaust oxygen concentration were recorded and the input and output data used for the system identification procedure. The perturbation testing was performed at various combinations of fuel quantity, EGR and VGT positions as the response was expected to vary with these conditions, engine speed was fixed at 1500 rev/min for this particular investigation.

The system identification procedure was performed using the Matlab System Identification Toolbox running in the same software environment as the engine model, a graphical user interface greatly simplifies the task. The principal of system identification involves choosing a model structure (i.e. order, delays, noise model etc..) and then iterating the model coefficients such that the model best fits (in a least squares manner) the input output data from the perturbation tests, further explanation of the procedure can be found in [93].

Through trial and error, the best compromise between model order and modelling accuracy was found to be a second order Box-Jenkins type model. **Figure 8.14** and **Figure 8.15** show the frequency and step responses respectively for some of the models identified at different operating points, the closeness of the responses suggest that for the operating points chosen the non-linearities have little effect on the fuel to oxygen concentration response. This means that only one model may suffice for the wide range of fuel, EGR and VGT settings, though scheduling may be necessary with engine speed.

The model used here was derived from the following operating point:

Engine Speed	:	1500 rev/min
Fuel Demand	:	15mg/shot
EGR position	:	0.5
VGT Position	:	0.5

The discrete time transfer function for the model is given by **Equation (8.15)**:

$$\frac{y(t)}{u(t)} = \frac{-0.0004221z^2 - 0.0006739z}{z^2 - 0.7606z - 0.04987} \quad (8.15)$$

For a sample frequency of 0.016 seconds (corresponding to the current controller update rate).

The equation can be arranged recursively so that the current output is expressed as a function of the current and previous two inputs, and the previous two outputs. Once in this recursive form it is easy to generate an equation that predicts the output of the system  $n$  steps ahead by back substituting the original expression  $n$  times, this is shown in **Appendix D**. The Simulink implementation of this prediction model is shown in **Figure 8.16**. Each of the main blocks is a symbolic interpretation of the recursive equation (shown in **Figure 8.17**). The prediction assumes that the new fuel value remains constant for the following two time steps; this is a reasonable assumption considering the prediction horizon is very short.

**Figure 8.18** shows the output of the linear model compared to that of the full non-linear engine model for a series of step changes in fuelling within the range of 5 to 20 mg/shot. The prediction model output has been delayed by two time steps in order to coincide with the output of the full engine model. Clearly the model gives a very good representation of the 'real' output.

The output of the model is scaled via gains to generate open-loop demand signals for the EGR and VGT actuators. This does assume that the relationship between the disturbance to oxygen concentration and the required EGR and VGT offsets to compensate for this are linear and



static. This is not strictly true, however identifying the inverse plant model of oxygen concentration to EGR and VGT position and implementing this in-line with the oxygen model is a non-trivial task which is shown from the results to be unnecessary.

## **8.10 SIMULATED CONTROL SYSTEM PERFORMANCE**

The new control scheme was tested in simulation over a constant speed fuelling step profile and fuelling ramp profile. The performance of the combined feedforward and feedback strategy was compared to that of the feedback strategy alone with fixed feedforward terms.

### **8.10.1 FUEL STEP PERFORMANCE**

**Figure 8.19** illustrates the oxygen concentration tracking performance of the new controller (red line) compared to feedback control alone with a fixed 50% open-loop term (blue line). The improvement in tracking obtained with the active feedforward scheme is clear, the oxygen concentration disturbances caused by the fuel steps are compensated very rapidly, whilst the tests with feedback only control show a slow response often without convergence within the five seconds between each fuel step.

**Figure 8.20** gives a detailed breakdown of the performance of the new control scheme compared to that of the fixed 50% open-loop case. The fuel step profile remains within the low load operating region therefore coordinated EGR and VGT action is used throughout by both controllers. The assistance of the model-based open-loop term significantly reduces the activity of the closed-loop control terms, having the effect of offsetting the control output by the approximate amount required to reject the disturbance. The closed-loop control therefore only needs to trim the control output to converge on the target oxygen concentration.

### **8.10.2 FUEL RAMP PERFORMANCE**

A fuelling ramp profile was also used to compare the tracking performance of the model-based feedforward control scheme with the fixed 50% open-loop demand feedback scheme. This is illustrated in **Figure 8.21**. In both cases the tracking performance is worse than for the step profile used previously, though the test is more difficult as the disturbance to the oxygen content changes continuously. The active feedforward controller does perform noticeably better, maintaining the oxygen concentration to the target over most of the profile, except for the spike at 20 seconds into the test which corresponds to a sharp step up in fuelling.

A breakdown of the controller performances is given in **Figure 8.22**, as was seen in the previous fuel step testing, the active open-loop term has significantly reduced the work performed by the closed-loop section of the controller, resulting in faster and closer tracking.

## **8.11 OVERVIEW OF RESULTS AND DISCUSSION**

An extensive study of practical implementations for EGR and VGT control strategies based on feedback from a UEGO sensor has been performed. Direct control of the exhaust oxygen content was researched as a simple method of using the information made available by the sensor. Compared to independent control, coordinated EGR and VGT control improves the response of the system to disturbances in exhaust oxygen concentration caused by changes in fuelling. However, it was ultimately found that feedback control alone was insufficient for good control system tracking performance.

The model-based feedforward scheme subsequently proposed and implemented in simulation improves significantly the control system tracking performance by compensating in advance for the fuelling instigated disturbances. The new control scheme is a relatively simple extension to the common proportional plus integral feedback compensation scheme developed previously, although the use of a dynamic model may present implementation problems for the fixed-point 16-bit arithmetic processors typical of mass-produced automotive control units. This particular point is becoming less valid as new, more powerful floating point DSP-based automotive control units become widely available, however it must be remembered that the EGR VGT algorithm will be just one of many control features executed by the processor

From the point of view of calibration, a target EGR rate can be obtained for given fuel quantity by setting the exhaust oxygen level, this relationship is more readily comprehensible than the use of airflow and boost pressure setpoints to fix the charge composition. The natural tendency for EGR rate to reduce as fuelling increases for a given exhaust oxygen concentration also assists the calibration process. Exhaust oxygen concentration lends itself well to an adaptive control strategy where the combustion conditions could be altered to match driver style, i.e. less EGR when aggressive driven regimes are identified, more EGR when a more passive style is detected.

The feedforward model will reduce the calibration effort in populating the look-up table of feedforward actuator demands. However, model parameters need to be scheduled with operating point as do the gains from the model output to the EGR and VGT open-loop terms.

Exhaust gas oxygen feedback has never been widely implemented in Diesel engines despite the existence of sensors for many years, this may have more to do with the cost/benefit trade-off associated with the use of such sensors, especially when compared to model-based control and/or other sensor combinations.

Relationship between Oxygen Concentration and Air Fuel Ratio

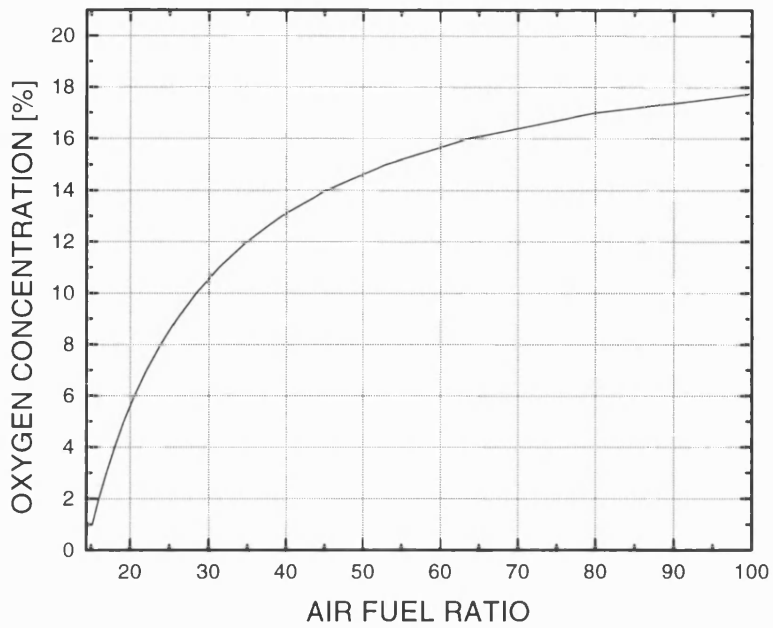


Figure 8.1 Relationship between oxygen concentration and air fuel ratio (no EGR present)



UEGO SENSOR TYPICAL OUTPUT CURVE  
(H/C=1.85 O/C=0)

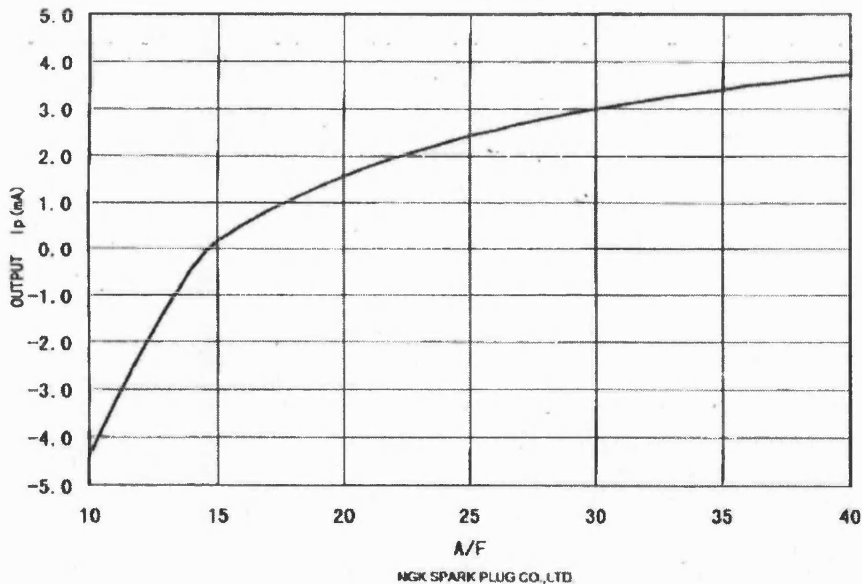
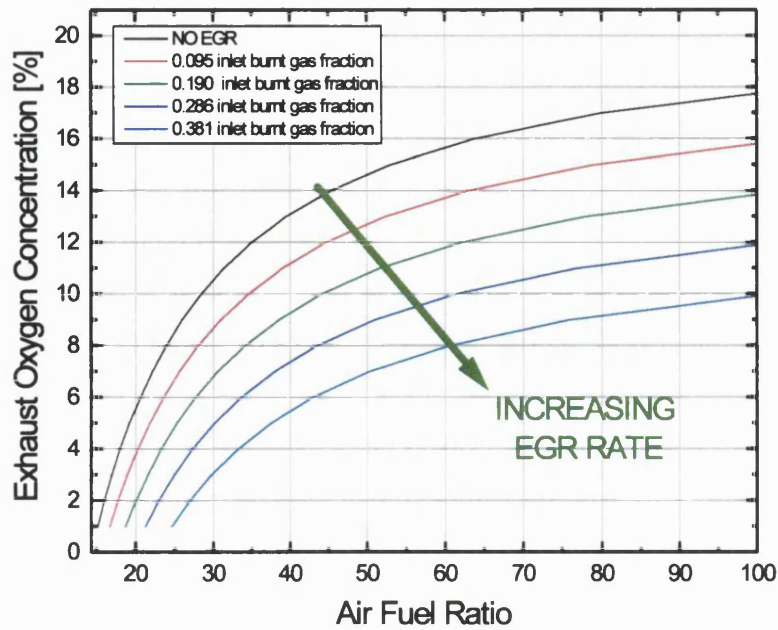
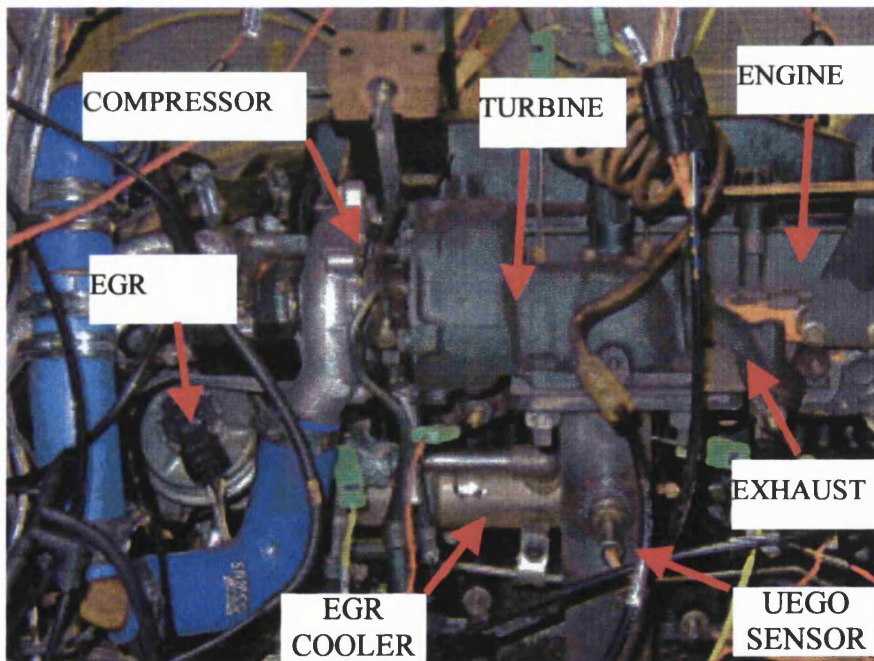


Figure 8.2 UEGO sensor output curve



**Figure 8.3 Relationship between Air Fuel Ratio, Exhaust oxygen Concentration and EGR rate**



**Figure 8.4 Installation details for UEGO sensor (exhaust side on view of engine)**

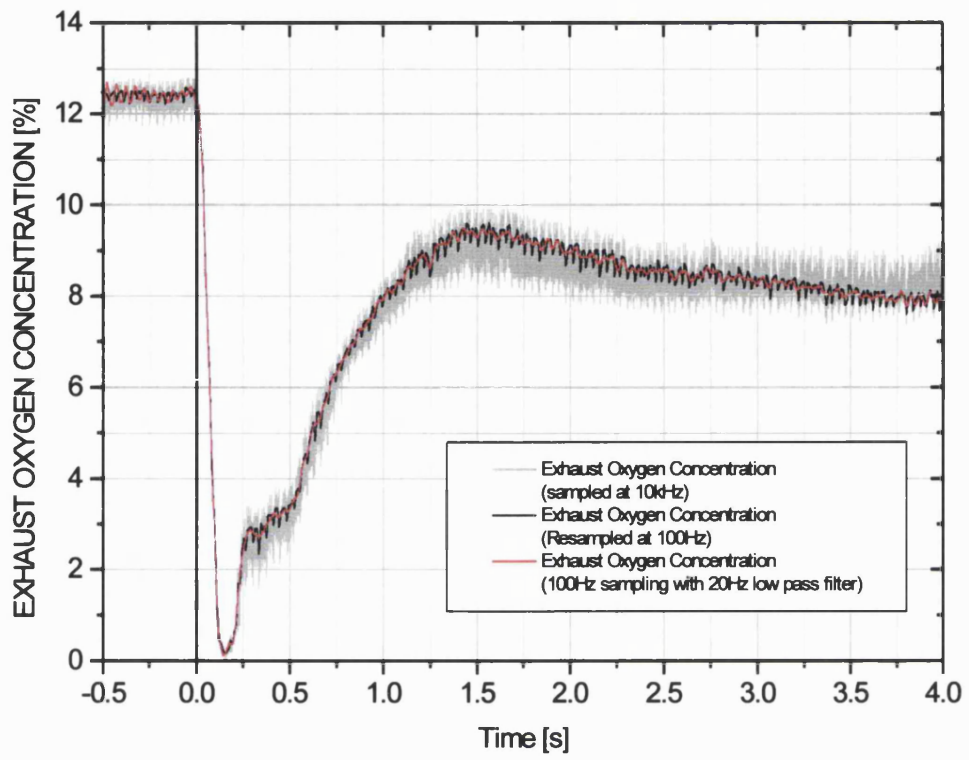


**Figure 8.5 Noise reduction on sensor output**

Tip-in transients at various engine speeds  
Fourier Analysis of UEGO sensor output

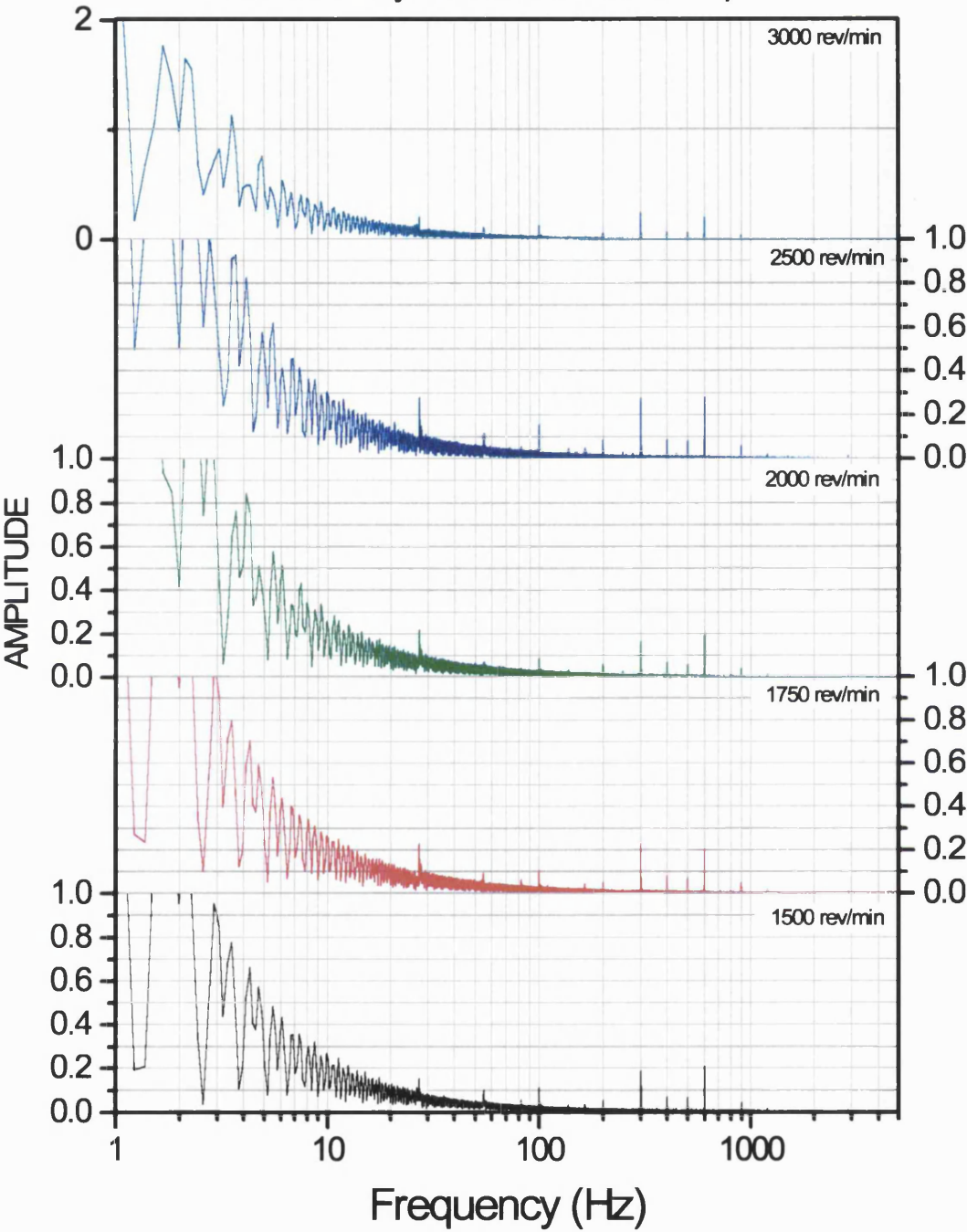


Figure 8.6 Frequency content of UEGO sensor signal for transients at various engine speeds

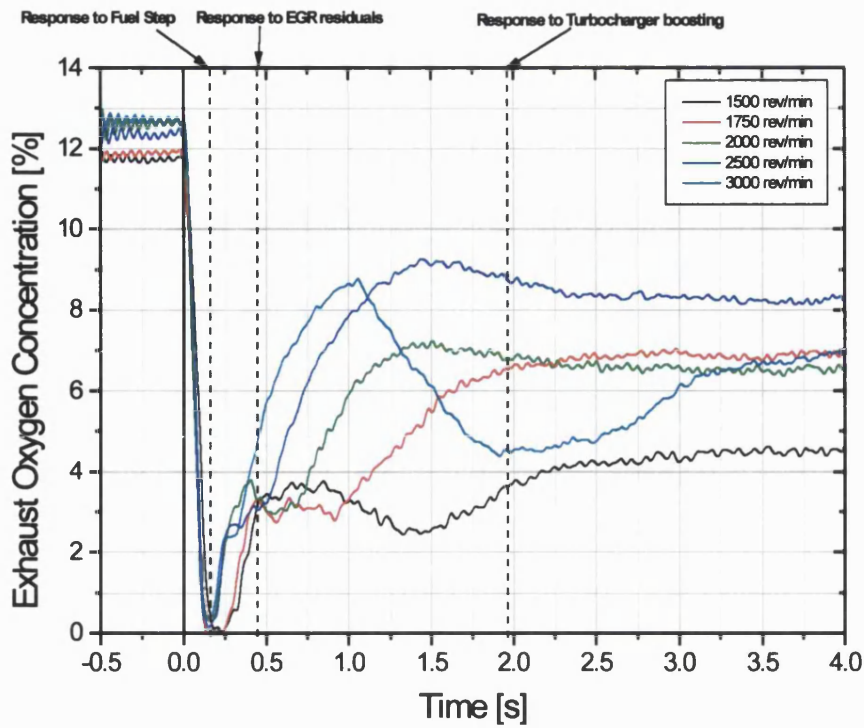


Figure 8.7 Exhaust oxygen Sensor response to a fuel steps at various engine speeds

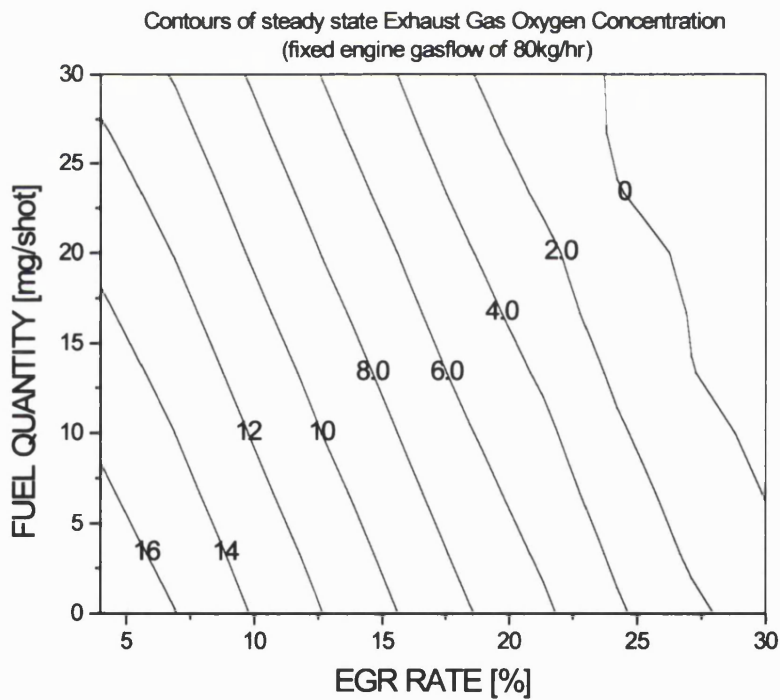


Figure 8.8 Contours of Exhaust Gas oxygen Concentration [%] compared to fuelling and EGR rate for fixed total engine gas flow conditions

1500rpm fuelling step response - P+I Controller UEGO\_1  
 11 jul 2000 Initial testing using UEGO to close the loop on EGR  
 11jul\_002.mat 00071114.dyn

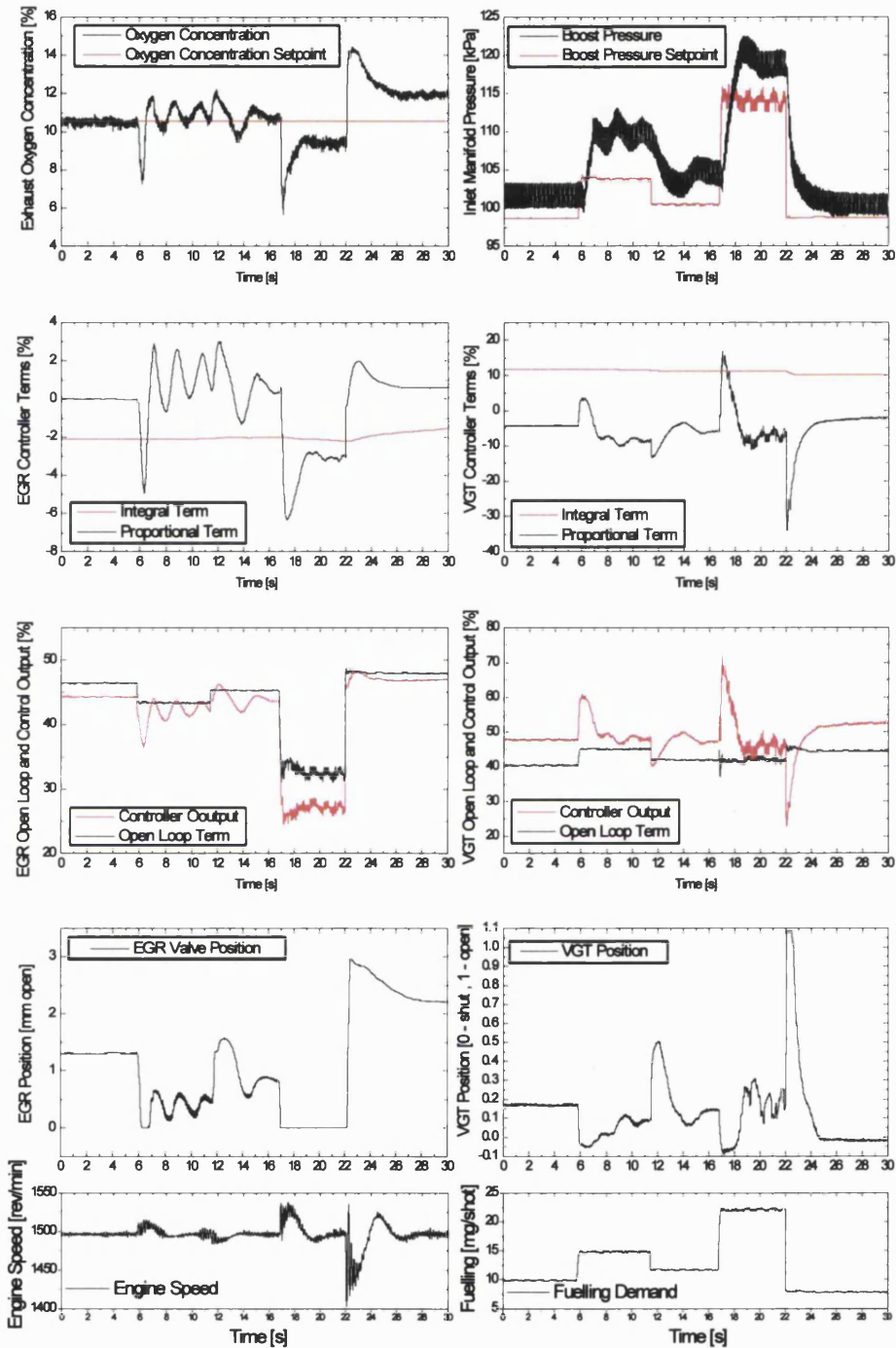


Figure 8.9 Constant speed fuel profile performance for direct replacement of MAF sensor with UEGO sensor



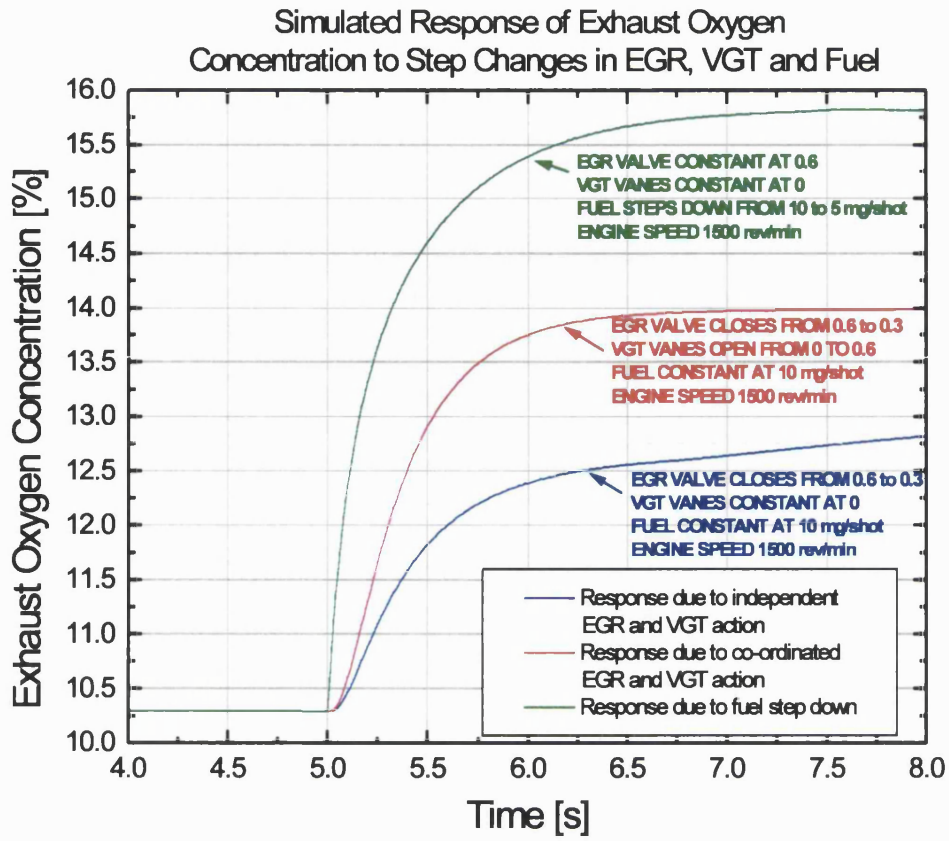


Figure 8.10 Simulated oxygen Concentration response to EGR, VGT and Fuel changes

1500rpm fuelling step response - SISO EGR VGT loops with Fuzzy Error Apportionment  
 50% Fixed Open Loop Term  
 <7jul\_alf004.mat 00072604.dyn>

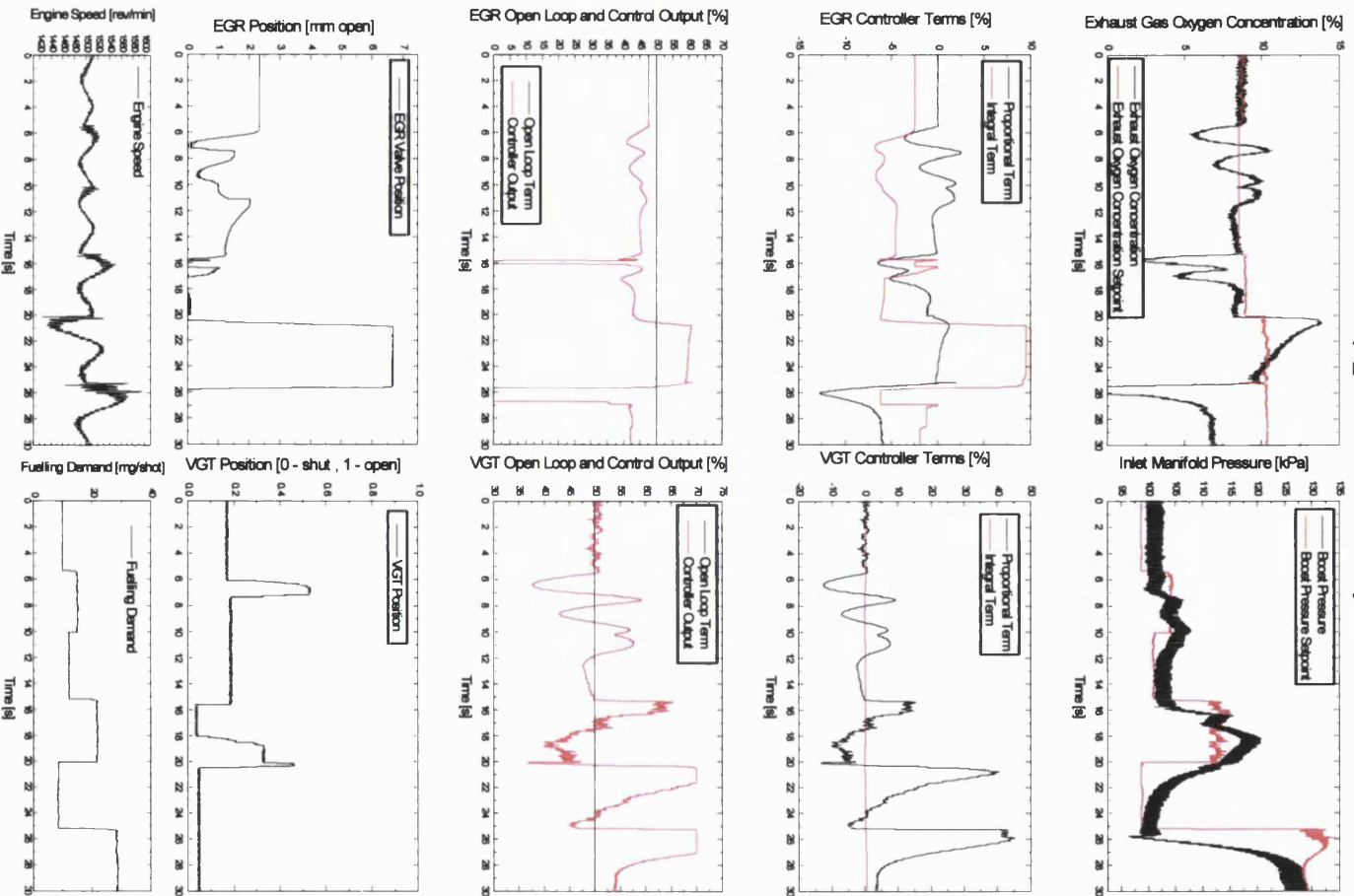
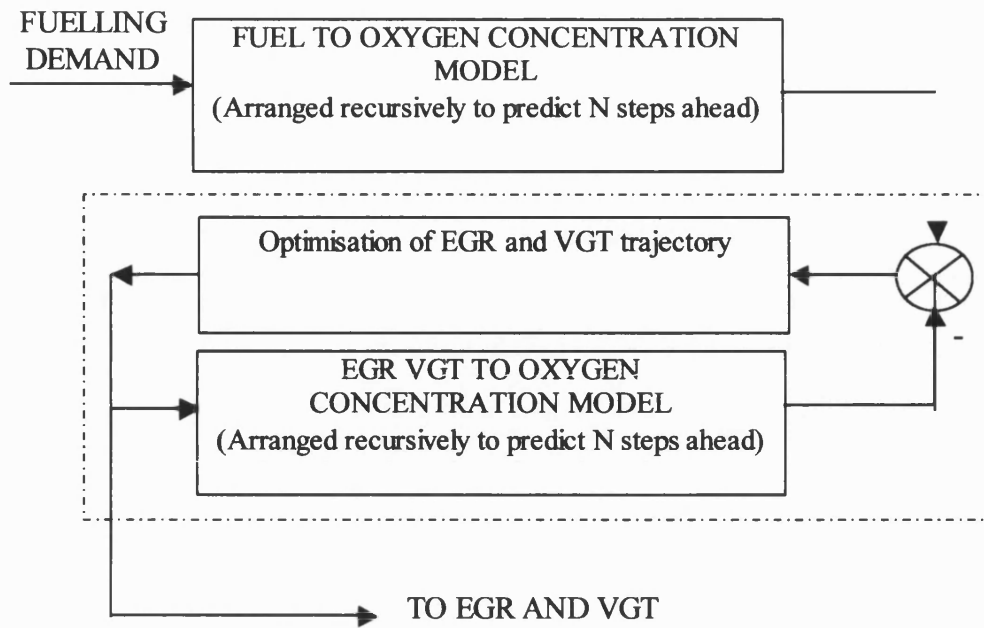
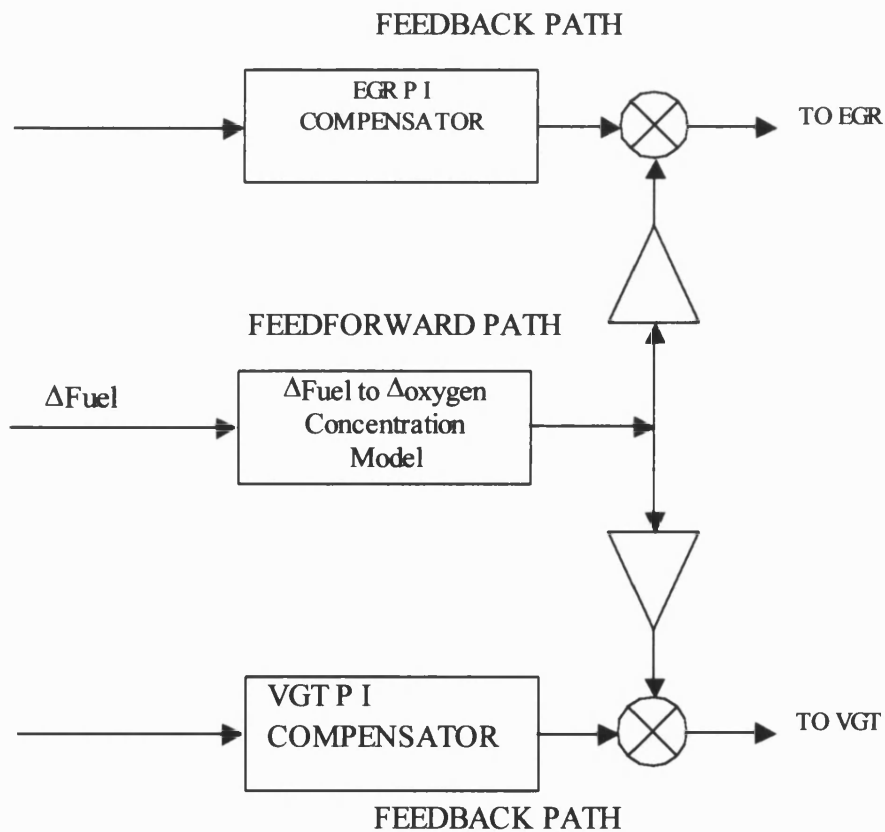


Figure 8.11 Fuelling profile response for coordinated oxygen Concentration Controller



**Figure 8.12 Formulation for a predictive, optimisation-based approach to the Exhaust oxygen Concentration control problem**



**Figure 8.13 Schematic of Feedforward and Feedback control scheme**

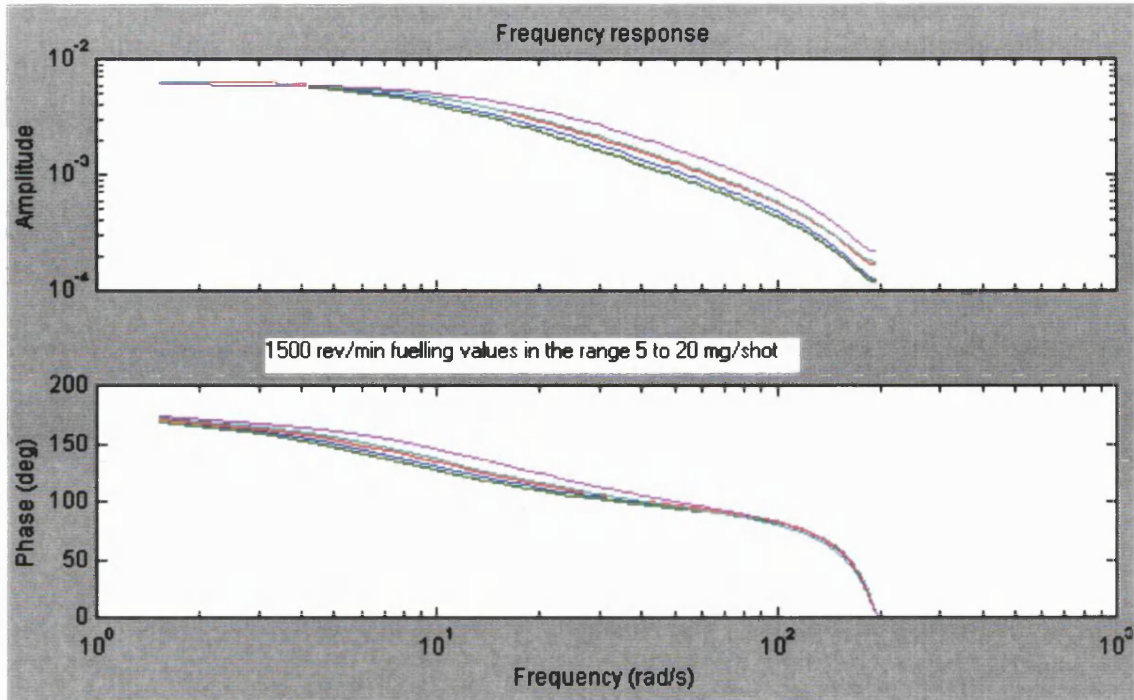


**Figure 8.14** Frequency response for Fuel to oxygen Concentration models at various nominal fuel levels in the range 5-20 mg/shot

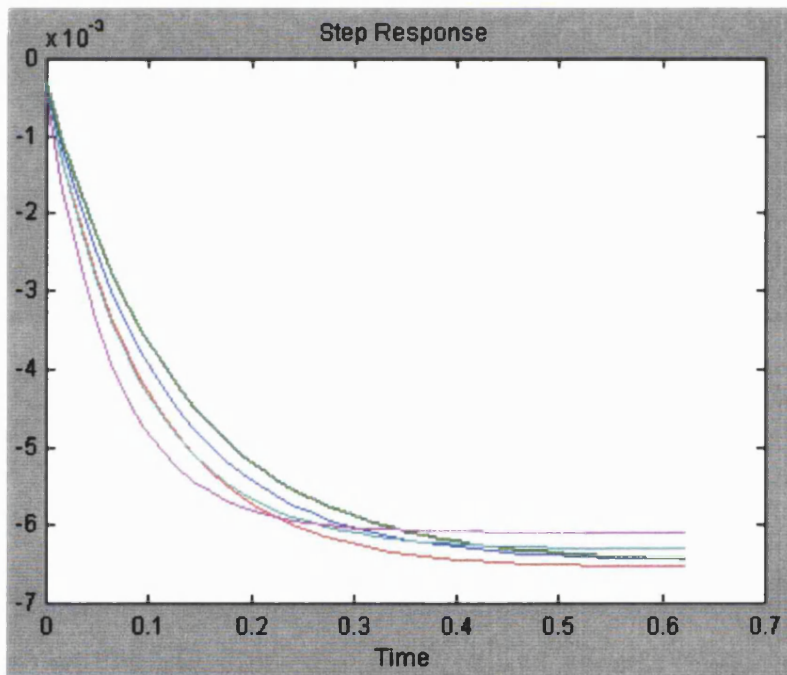


**Figure 8.15** Step responses for Fuel to oxygen Concentration models at various nominal fuel levels in the range 5-20 mg/shot

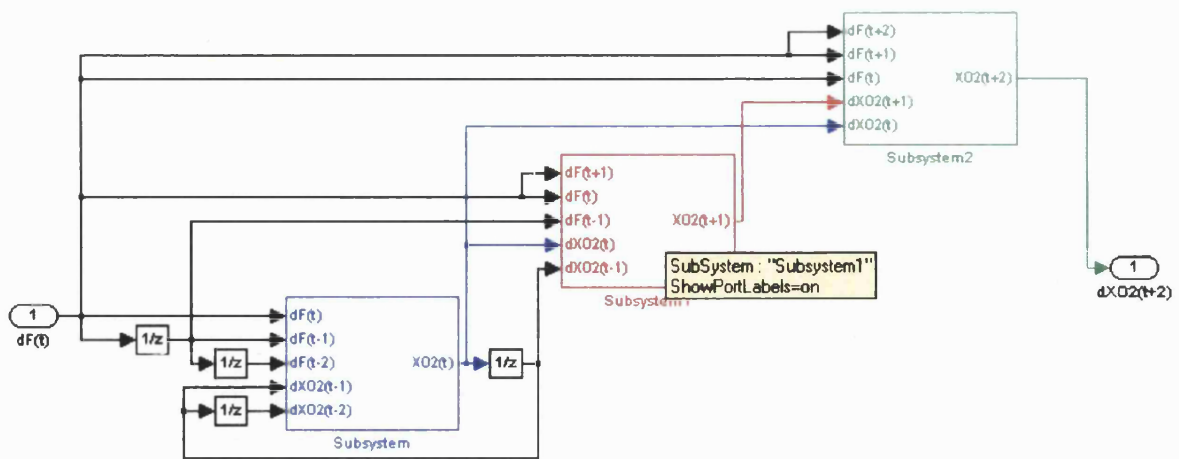


Figure 8.16 Simulink Implementation of oxygen Concentration Disturbance Predictor

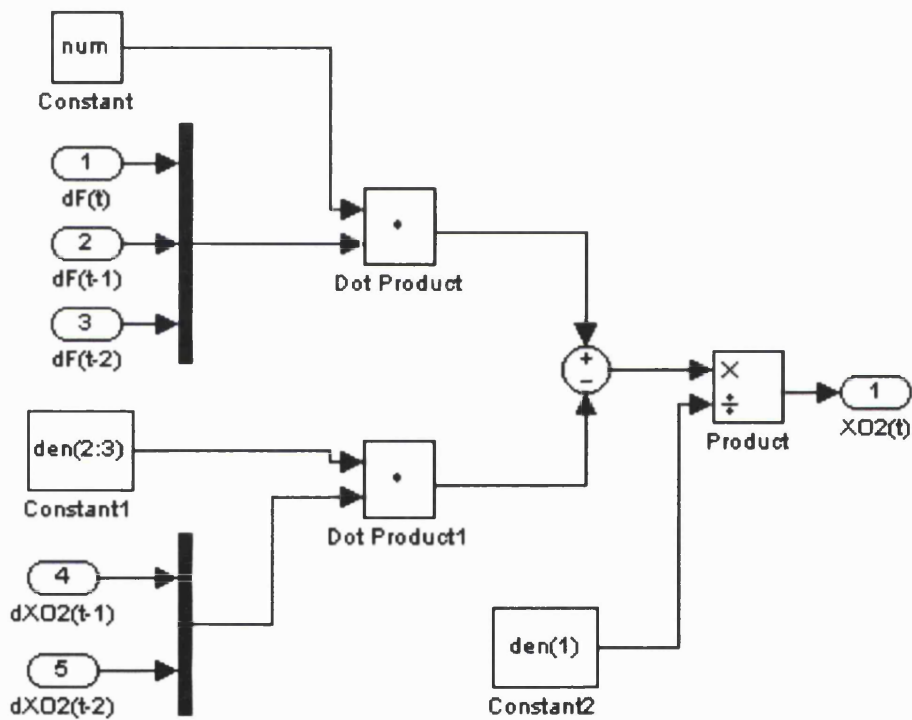


Figure 8.17 Detail of Simulink implementation of recursive algorithm

2 step ahead prediction of rate of change of exhaust oxygen concentration using linearised model of fuel to oxygen concentration compared with the rate of change measured on the non-linear engine model (prediction has been delayed by 2 steps for comparison)

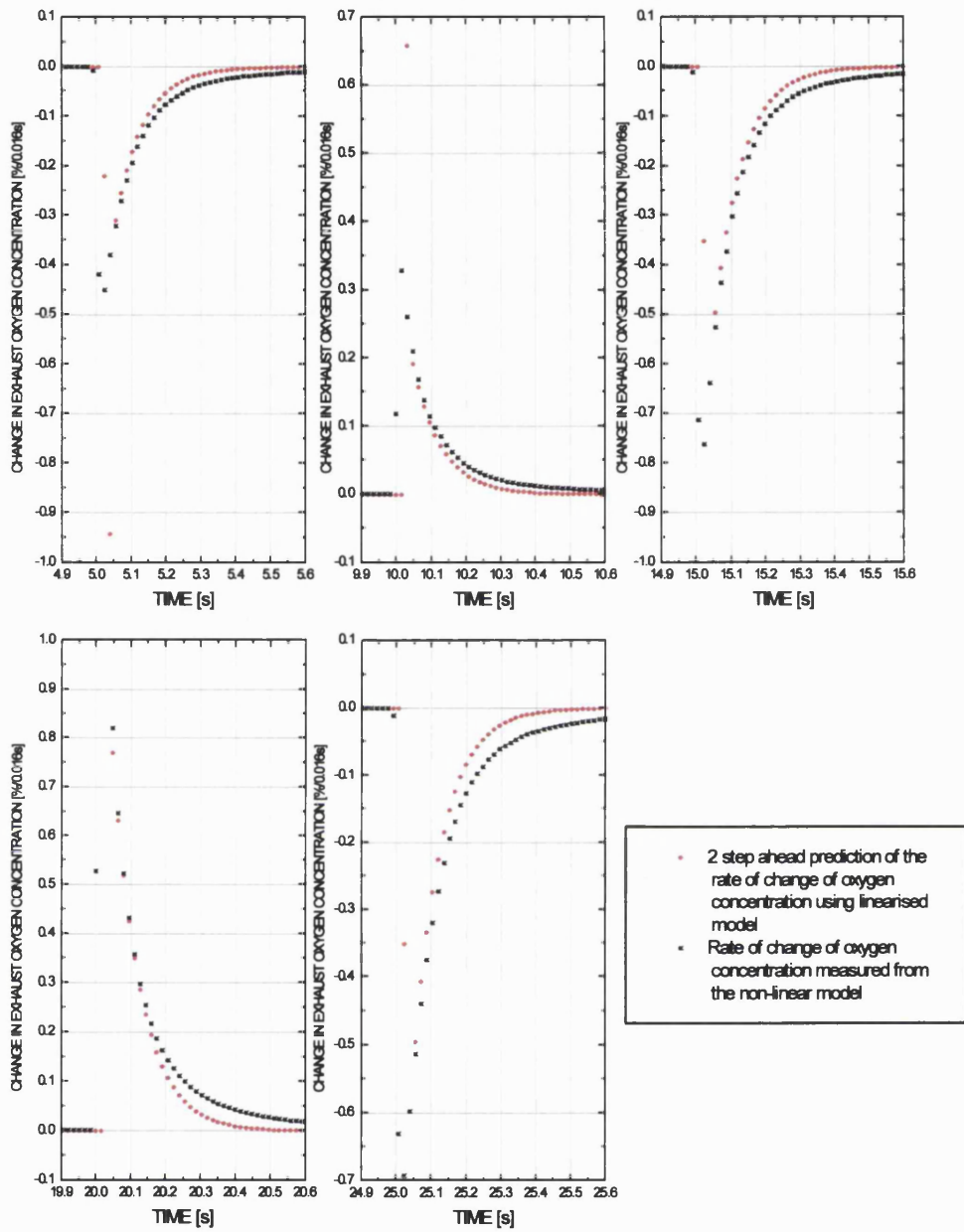
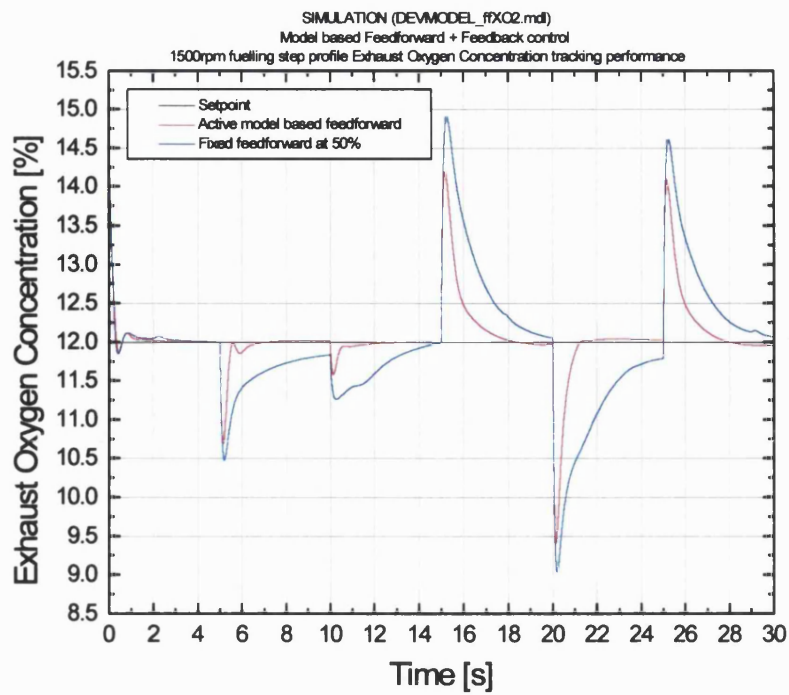
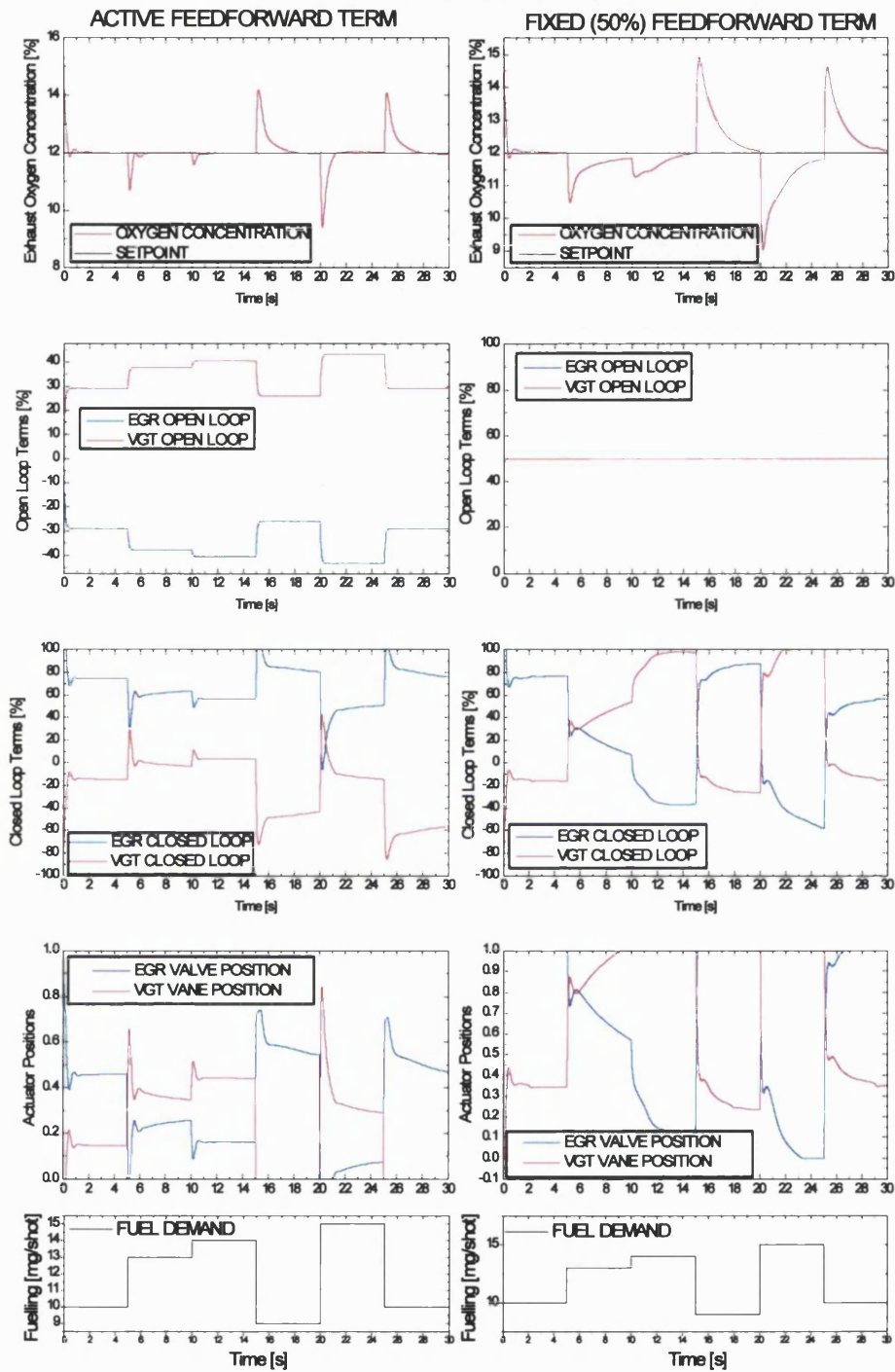


Figure 8.18 Prediction performance of Fuel to oxygen concentration model for various fuel step changes



**Figure 8.19 Comparison of oxygen Concentration tracking over fuel step profile for UEGO feedback control with model-based feedforward against fixed feedforward terms**

SIMULATION (DEVMODEL\_ffXO2.mdl)  
 Model based Feedforward + Feedback control  
 1500rpm fuelling step profile response



**Figure 8.20 Comparison of oxygen Concentration tracking over fuel step profile for UEGO feedback control with model-based feedforward against fixed feedforward terms - Detail**



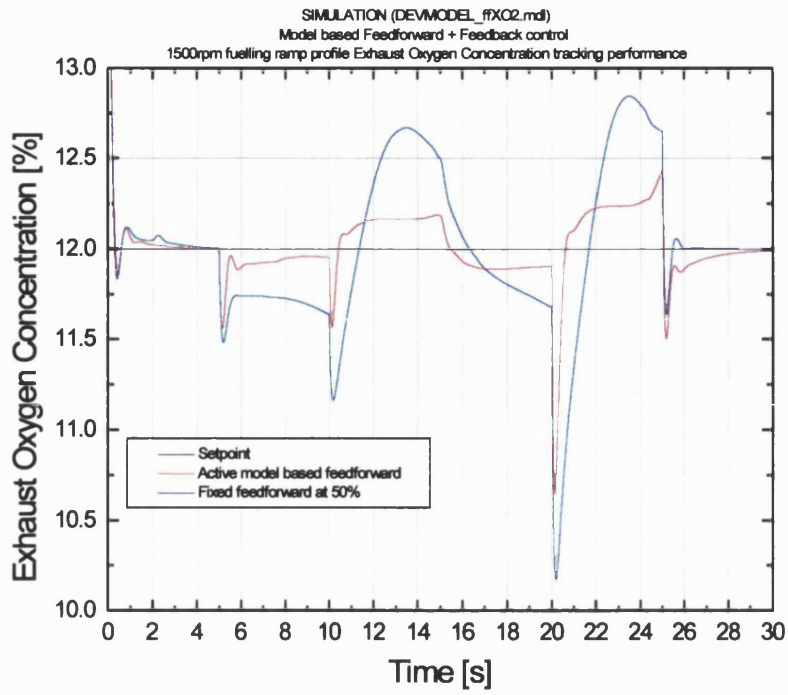


**Figure 8.21 Comparison of oxygen Concentration tracking over fuel ramp profile for UEGO feedback control with model-based feedforward against fixed feedforward terms**

SIMULATION (DEVMODEL\_ffXO2.mdl)  
 Model based Feedforward + Feedback control  
 1500rpm fuelling ramp profile response

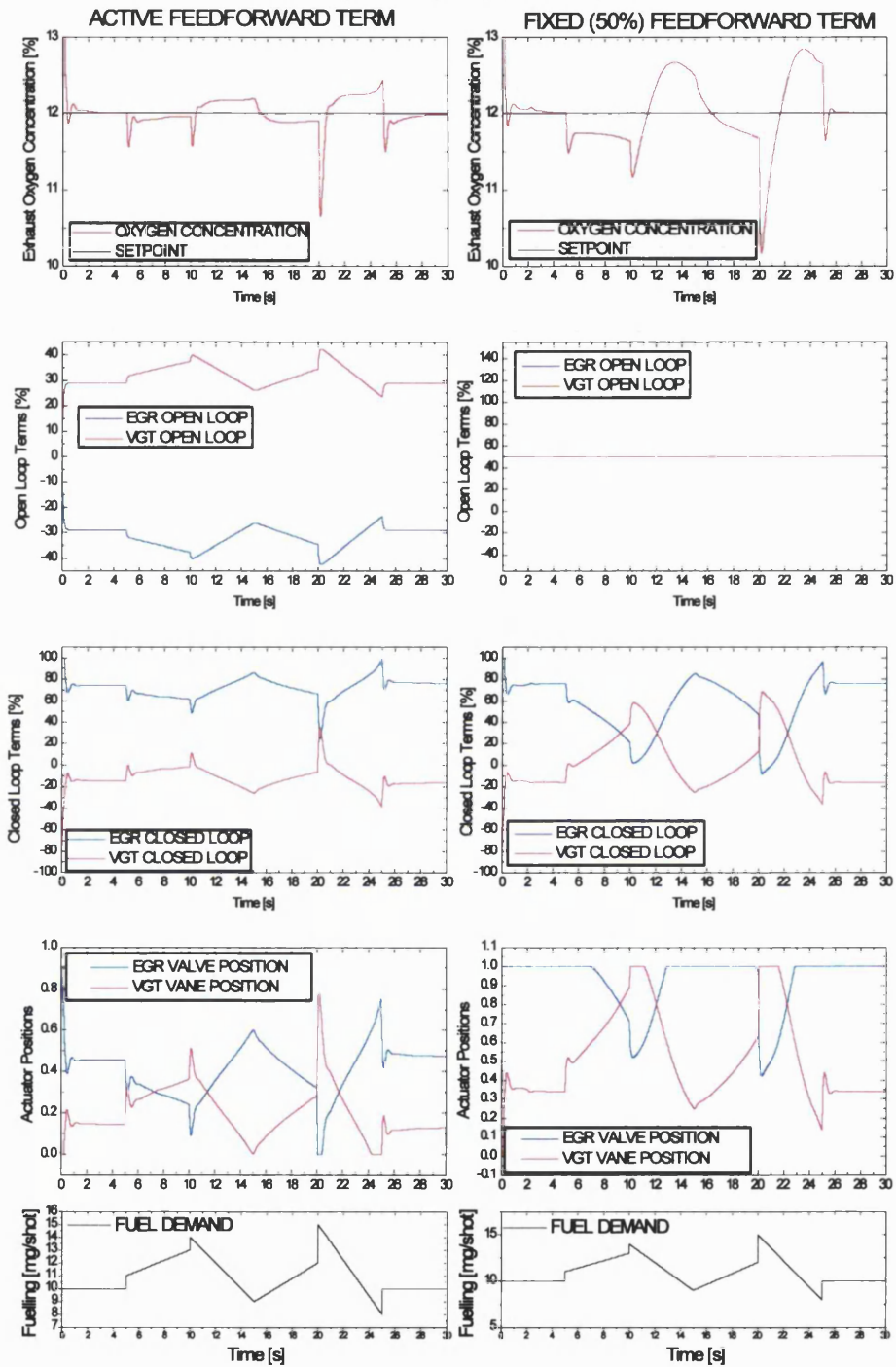


**Figure 8.22 Comparison of oxygen Concentration tracking over fuel ramp profile for UEGO feedback control with model-based feedforward against fixed feedforward terms – Detail**

## Chapter 9 CONTROLLER EVALUATION OVER DRIVE CYCLE

### 9.1 INTRODUCTION

This chapter describes the evaluation of the coordinated controller and the UEGO feedback controllers developed in **chapters 7 and 8** over an emulated European legislative drive cycle, the standard control strategy is used as a baseline against which the relative performances of the new controllers are discussed. The aim is to determine what benefits, if any, the new control schemes offer under the transient conditions of a simulated cycle.

The European legislative cycle is the basis for all emissions and fuel consumption development work in the European market, therefore as a controller evaluation tool it provides a realistic test method for comparing any systems that will alter emissions and fuel consumption. Any benefits or detrimental effects of the new control schemes under evaluation in this section are expected to manifest themselves over the cycle as it covers the operating points around which these systems were designed.

The work is presented as both cumulative (i.e. summed over the section of the cycle in question) and time-based data. The cumulative results provide a single figure for key performance parameters such as NO<sub>x</sub> emissions or Fuel Consumption, facilitating direct comparison between control schemes. Additionally, the emissions legislations specify a cumulative total for each regulated emissions species over the cycle, and now all manufacturers must provide figures for the total fuel consumption over the cycle for their new vehicles, therefore calculating the results in this manner is consistent with current industry practice. However, the cumulative results do not divulge where in the cycle the emissions are being produced, and they do not discriminate between steady state and transient events, therefore the time-based results are necessary.

It is difficult to draw firm conclusion from these tests as repeat testing to give good statistical averaging of the results was not possible. Within the limitations of the test facility and test regime, it is shown that the coordinated controller gives very close performance to the standard control system. The anticipated improvements due to the better EGR dynamics offered by coordination of EGR and VGT systems do not appear to have a great bearing on the cumulative test results, however the choice of target airflow and boost values appears to have a large influence. Although flawed, the UEGO feedback controller demonstrates good NO<sub>x</sub> reduction at the expense of increased smoke production, this is considered to be more a function of the chosen oxygen target rather than the control algorithm itself.

## **9.2 TEST PROCEDURE**

The cycle tests were conducted in two sections, the Extra-Urban section or high-speed section of the ECE15+EUDC legislative cycle first, followed by one of the four repeated Urban sections. This arrangement was adopted to reduce the burden on both the data acquisition system and the test operator when compared with the full 1200 second cycle. Control system data were logged via dSpace at the controller update rate (16 milliseconds or 66.67Hz) whilst general engine signals were acquired through the test facility data acquisition system at 2 Hz over 200 seconds for the ECE15 and over 400 seconds for the EUDC.

The controllers were evaluated with both active and fixed open-loop terms. This is performed as an assessment of how robust the control schemes are to uncertainties in the feedforward path. In real-life the engine system behaviour can change with age and the accuracy of the feedforward look-up tables will generally worsen, controllers that can still function adequately under these circumstances are more robust.

The emulation of the standard controller was performed with the setpoints of the original calibration (referred to as 'as supplied') and the new setpoints designed for the coordinated controllers. The different configurations and the sections of cycle they were tested with are summarised in **Table 9.1**.

## **9.3 STABILITY**

In order to verify stability, the engine was manually driven to the significant operating points in the drive cycle and small fuel step disturbances applied manually to ensure that each controller would settle and not go unstable. The UEGO feedback controller evaluated here was already demonstrated to suffer oscillatory response to step changes in fuelling under certain conditions (**Chapter 8**), however it did not actually go unstable in any of the tests.

No formal stability evaluation was performed for the new control schemes owing to the difficulty involved with analysing the non-linearity posed by the fuzzy logic element in each controller. The new strategies are however very similar to the original strategy which has been carefully calibrated to avoid instability. Taking into account the considerable non-linearities posed by the engine and actuation systems, an analytical stability proof would be very difficult to achieve without simplifications that limit validity, therefore under the circumstances an easier approach would be to test the controllers and identify any stability issues that arise. Given the ease at which controller iterations can be evaluated using the rapid prototyping hardware and software, this is considered a sensible approach.

Test ID	Controller Type	Section of Cycle	Setpoints	Open-loop Term
STD_1	Standard	Urban	New MAF MAP	Active
STD_2	Standard	Extra-urban	New MAF MAP	Active
STD_3	Standard	Urban	New MAF MAP	Fixed @ 50%
STD_4	Standard	Extra-urban	New MAF MAP	Fixed @ 50%
STD_5	Standard	Extra-urban	As supplied	Active
STD_6	Standard	Urban	As supplied	Active
COORD_1	Coordinated	Urban	New MAF MAP	Active
COORD_2	Coordinated	Urban	New MAF MAP	Fixed @ 50%
COORD_3	Coordinated	Extra-urban	New MAF MAP	Fixed @ 50%
COORD_4	Coordinated	Extra-urban	New MAF MAP	Active
UEGO_1	UEGO	Extra-urban	New O <sub>2</sub> MAP	Active
UEGO_2	UEGO	Extra-urban	New O <sub>2</sub> MAP	Fixed @ 50%

**Table 9.1 Summary of drive cycle test program**

## 9.4 LIMITATIONS

The tests were performed on a fully warmed-up engine, however it was later discovered that problems with the control of the engine coolant temperature control caused significant drops in coolant temperature over two of the tests (STD\_4 & UEGO\_2). The results from these two tests have to be excluded from direct comparison as the emissions results are strongly affected by the differing engine temperatures.

The test facility data acquisition was performed at 2Hz as opposed to a faster rate due to the inability of the post-processing system to handle extremely large files generated at higher acquisition rates, this is due to the large number (100+) of channels that are actually recorded. The relatively large sample times make analysing the time-based data difficult as the order of improvements in airflow offered by coordinated control is less than this sample time.

The UEGO feedback controller evaluated in this section is *not* the model-based feedforward controller designed and evaluated in simulation at the end of **Chapter 8**, as this was designed after this test program had been completed. The controller implemented here is described in **Chapter 8** under *section 8.8*, it uses the fuzzy logic-based cross coupling of input errors to achieve coordinated EGR and VGT control action for exhaust oxygen tracking.

The UEGO controller was evaluated over the EUDC section only, this was because the gearbox on the test rig failed before the Urban section of the cycle could be performed for this controller. This also served as a convenient end to the testing program as no replacement gearbox was available.

## 9.5 Cumulative Results

Cumulative results over each section of the cycle were calculated for NO<sub>x</sub>, smoke and fuel consumption. In the absence of any measurement capability for particulate matter, the integrated smoke opacity was used as a measure of particulate emissions. Work performed by Fosberry and Gee [94] correlates smoke opacity to filter smoke, and the well-known study by Grieves and Wang [95] correlates filter smoke and hydrocarbons with particulate matter. Drawing from these two studies it is possible to justify the use of smoke opacity to create a quantitative representation of particulate emissions for use solely as a comparative measurement. Details of the emissions calculations can be found in **Appendix E**.

### 9.5.1 URBAN SECTION OF CYCLE

TEST	STD_1	STD_3	STD_6	COORD_1	COORD_2
Open-Loop Term	Active	50%	active	active	50%
SETPOINTS	new MAF MAP	new MAF MAP	Standard MAF MAP	new MAF MAP	new MAF MAP
NO <sub>x</sub> [g/km]	0.473	0.363	0.269	0.288	0.399
SMOKE [km <sup>-1</sup> ]	0.006	0.005	0.006	0.006	0.007
FUEL [g/km]	75.9	68.1	70.2	74.0	71.9
DISTANCE [km]	0.989	0.985	0.987	0.989	0.987
FUEL [l/100km]	9.039	8.110	8.359	8.807	8.558
T <sub>smoke&gt;10%opacity</sub> [s]	1	1	0	2.5	1

**Table 9.2 Summary of controller performance over Urban section of drive cycle**

**Table 9.2** summarises the results over the Urban section of the cycle, the data shown in red represent the worst results for each of the categories, and those in green the best. These results are also given as trade-off plots for NO<sub>x</sub> vs. Smoke (**Figure 9.1**) and NO<sub>x</sub> vs. Fuel Consumption (**Figure 9.2**).

#### 9.5.1.1 STANDARD CONTROLLER

The standard controller was tested under three different conditions, the first using 'as supplied' setpoints and active open-loop (STD\_6). This gives the best overall performance on the Urban section of the cycle in terms of NO<sub>x</sub>, Smoke and Fuel Consumption (**Figure 9.1** and **Figure 9.2**), this is not surprising considering this is the best optimised and most developed of all the controller / setpoint configurations tested here. This controller was also tested with the custom setpoints designed for the coordinated controller, these cycles were performed with and without assistance from the open-loop control term (STD\_1 and STD\_3 respectively). On the NO<sub>x</sub> / Smoke trade-off (**Figure 9.1**) the new setpoints cause the controller to tend towards high NO<sub>x</sub> and low Smoke, the highest NO<sub>x</sub> level of the Urban section tests was achieved with active open-loop and the new setpoints.

Examining the EGR versus VGT position scatter plot in **Figure 9.3** it can be seen that with active open-loop (STD\_1), the controller tends to use low EGR and VGT openings, this results in low EGR rates and high NO<sub>x</sub>. Without open-loop assistance (STD\_3) the controller maintains wider VGT and EGR settings allowing more EGR flow and hence reducing NO<sub>x</sub>.

From the point of view of Fuel Consumption (**Figure 9.2**), the small EGR and VGT openings for the STD\_1 test cause high pumping losses and as a consequence, the highest fuel consumption of the test. For the case of STD\_3, the low backpressures resulting from the higher EGR and VGT settings give rise to the lowest fuel consumption of all the Urban tests.

#### 9.5.1.2 COORDINATED CONTROLLER

The coordinated controller with a fixed open-loop term (COORD\_2) has the worst emissions performance over the Urban scenario, suffering the highest smoke levels and second highest NO<sub>x</sub>. The lack of open-loop assistance to the controller affects the attainable EGR and VGT positions, this can be seen in **Figure 9.4**. In this plot of VGT vane position versus EGR valve position the fixed open-loop test results are scattered more over the upper region of the graph meaning that open VGT vane settings were used more, this results in lower EGR rates as the driving pressure differential will be low and hence the NO<sub>x</sub> high.

The high smoke is a transient phenomena as usually increased NO<sub>x</sub> is countered by reduced Smoke (particulates) due to the trade-off. The lack of open-loop assistance in closing the EGR valve in response to certain tip-in transients will result in low transient air fuel ratios and as a consequence, transient smoke. This is reflected by the values for time spent above 10% smoke opacity shown in **Table 9.2**. This measurement has been included to indicate the levels of visible smoke produced by each controller. A value of 10% opacity corresponds approximately to the lower limit for visible smoke. It should be noted that because the sample interval was relatively large (0.5s) the resolution of this calculation is low and hence the resultant times are likely to be greater than they were in reality.

The coordinated controller with fixed open-loop term (COORD\_2) does achieve better fuel consumption than with active open-loop (COORD\_1) as demonstrated in **Figure 9.2**, this is again due to the open VGT vane positions and resultant low backpressure which reduces engine pumping work. The higher fuel consumption of the active open-loop controller can be traced back to the lower vane positions being used, as seen by the large concentration of points near the origin of **Figure 9.4**. These combinations of settings do drive higher EGR rates and as a consequence the NO<sub>x</sub> emissions are significantly lower for the active open-loop controller. Smoke has also reduced (**Figure 9.1**) as a result of the improved command over the EGR valve.

Figure 9.5 illustrates to what extent coordinated action was actually used over this section of the cycle, the non-zero values on the z-axis correspond to coordinated action to either increase or decrease compressor mass airflow. The boundaries of coordinated operation are clear.

Examining Figure 9.6 it can be seen that standard controller (blue points) has a marginally larger scatter of tracking error than the coordinated controller (red points) when using the custom setpoints. The RMS values for tracking error are given on the plot and confirm the slight advantage that the coordinated controller has.

## 9.5.2 EXTRA-URBAN SECTION OF THE CYCLE

TEST	STD_2	STD_4	STD_5	COORD_4	COORD_3	UEGO_1	UEGO_2
Open-Loop Term	active	50%	active	active	50%	active	50%
SETPOINTS	new MAF MAP	<i>new MAF MAP</i>	standard MAF MAP	new MAF MAP	new MAF MAP	new O <sub>2</sub> MAP	<i>new O<sub>2</sub> MAP</i>
NO <sub>x</sub> [g/km]	0.390	<i>0.842</i>	0.267	0.251	0.262	0.209	0.215
SMOKE [km <sup>-1</sup> ]	0.005	<i>0.004</i>	0.005	0.005	0.005	0.006	<i>0.007</i>
FUEL [g/km]	45.0	<i>45.3</i>	45.4	45.0	45.0	45.1	<i>46.6</i>
DISTANCE [km]	6.918	<i>6.934</i>	6.920	6.923	6.920	6.923	<i>6.918</i>
FUEL [l/100km]	5.354	<i>5.395</i>	5.405	5.351	5.347	5.366	<i>5.545</i>
T <sub>smoke&gt;10%opacity</sub> [s]	8	<i>1</i>	15.5	12.5	9.5	17	<i>23.5</i>

**Table 9.3 Summary of controller performance over Extra-Urban section of cycle**

Table 9.3 summarises the emissions and fuel consumption results for the controllers over the Extra-Urban section of the legislative cycle. The data shown in red represent the worst results for each of the categories, and those in green the best. The results for fuel consumption are all coloured green save for the UEGO\_2 test as the values are considered too similar for their to be any distinction between them when taking into account measurement error. The two columns where the figures are given in *italics* represent the two tests where engine coolant temperature control failed, this is illustrated by the time-based engine coolant temperature data given in Figure 9.7. Although they cannot be included in the comparison these two tests are plotted in the trade-off graphs (Figure 9.8 and Figure 9.9) and are consistent with the effects that such a temperature change would have on NO<sub>x</sub>, smoke and fuel consumption.

Examining Figure 9.8, the NO<sub>x</sub> / Smoke trade-off is more apparent than it was in the Urban section results, the grey line represents an approximation to the trade-off line and it can be seen how the different controller / setpoint configurations fit this curve well.

### 9.5.2.1 STANDARD CONTROLLER

Over the Extra-Urban section the standard controller ‘as supplied’ does not give the best overall performance, in both the NO<sub>x</sub> / Smoke trade-off (Figure 9.8) and the NO<sub>x</sub> / Fuel



Consumption trade-off (**Figure 9.9**), the coordinated controller (with and without active open-loop term) marginally outperforms the standard controller.

The new setpoints applied to the standard controller (STD\_2) shift the NO<sub>x</sub> / Smoke trade-off towards the increased NO<sub>x</sub> side of the plot, the difference in operating characteristics can be deduced from **Figure 9.10** which plots EGR position against VGT position. The custom setpoints maintain wider VGT openings, thus reducing the EGR driving pressure difference compared to the 'as supplied' setpoints (STD\_5), therefore less EGR flows and NO<sub>x</sub> is higher while smoke decreases. The lower pressure difference also results in less pumping work and lower fuel consumption as seen in **Figure 9.9**.

#### 9.5.2.2 COORDINATED CONTROLLER

The coordinated controller appears to perform better than the standard control over this section of the cycle, however the results are very close and repeat testing would have to be carried out in order to draw any firm conclusions on this. The wider VGT openings denoted in the scatter plot in **Figure 9.10** corroborate the fuel consumption improvements. The tabulated values of time spent over 10% smoke opacity fall in the middle of the range of results and are generally better than the standard controller in 'as-supplied' guise.

The NO<sub>x</sub> / Smoke trade-offs for the coordinated controller with custom setpoints (COORD\_3 & COORD\_4) compared with the standard controller with setpoints 'as-supplied' (STD\_5) are very close, the active and fixed open-loop Extra-Urban tests for the coordinated controller also show minimal variation suggesting good controller robustness. Outside of the low speed and low load operating region, the coordinated controller should behave in the same manner as the standard controller. The Extra-Urban section of the cycle concentrates on engine operating points outside of this region as can be seen in **Figure 9.11**, explaining the similarity in results with the standard controller. The operating envelope for co-ordination is bounded by 2000 rev/min and 20 mg/shot; there is scope for widening the coordinated operating envelope by tuning the fuzzy logic Membership Functions. The 2000 rev/min boundary is quite conservative and increasing this to 2500 rev/min would enable coordinated action over a much greater proportion of the Extra-Urban cycle, potentially bringing performance improvements.

Examining **Figure 9.12** it can be seen that standard controller has a larger scatter of tracking error, particularly in excessive boost and airflow region corresponding in general to tip-outs (though also includes the case when the system overshoots the target airflow and boost). The RMS error values for tracking error are given on the plot, clearly the cross-coupled controllers have a lower overall error, hence better tracking.

### 9.5.2.3 UEGO FEEDBACK CONTROLLER

Unsurprisingly, the UEGO controller test results give lowest NO<sub>x</sub> emissions and highest smoke due to the excessive EGR rates. The controller uses a low exhaust oxygen content target, generally lower across the cycle than is achieved by the other airflow/boost tracking controllers. This results in high EGR rates and as a consequence high smoke. The O<sub>2</sub> setpoints were perhaps too low and higher mapped values would certainly improve the smoke emissions results. The trade-off between smoke and NO<sub>x</sub> is very easy to deal with through the use of this one parameter. Interestingly the UEGO\_1 test result for time spent over 10% smoke opacity is not a great deal longer than the 'as-supplied' standard controller, the higher cumulative smoke result is thus due more to steady state than transient smoke. Examination of **Figure 9.10** shows that wide open EGR settings and lower VGT combinations are used to drive the high EGR rates.

## 9.6 Time-Resolved Data

### 9.6.1 Urban Section of Cycle

**Figure 9.13** indicates where in the Urban section of the cycle coordinated action was employed during the COORD\_1 test. The upper plot is engine speed, the mid plot is fuelling and the lower plot is the amount of airflow error being fed to the VGT control loop, representing the level of coordinated EGR and VGT action to track airflow. Co-ordination is evident through most of the cycle, and a clear correspondence with transient events (pullaway, gearshift, tip-in, tip-out) can be seen. The co-ordination is inactive at engine speeds above 2000 rev/min and for large fuelling peaks. The drive cycle controller can be quite 'heavy-footed', displaying large peaks in fuelling demand during transient events. These peaks deactivate the coordinated control as they exceed the fuelling range where coordinated action is applicable; this reduces the effectiveness of the coordinated control under these circumstances and explains why coordinated action is not used in the first pullaway, for example.

In **Figure 9.14** the airflow tracking for the coordinated controller is shown, the three detail windows show the EGR and VGT actuator behaviour over three different sections of the cycle where coordination is active (indicated by the blue line on the main plot). The co-ordination is exhibited as symmetrical movements of the actuators, either the EGR opening as the VGT closes (to increase airflow) or vice-versa.

Comparing the airflow tracking plots for the coordinated and standard controllers (**Figure 9.15**), the biggest difference appears to be in the activity of the VGT as illustrated in the detail windows. The standard controller is more busy than it is using the standard setpoints, the

VGT behaviour is often oscillatory, this is likely to be due to the boost pressure measurement which carries a lot of noise, more significantly so at low boost pressures. The VGT loop proportional gain is relatively high in this controller (using the standard ECU gains ‘as-supplied’) therefore the P term can carry the noise through to the actuators. This is usually not a problem when the setpoints and open-loop terms are chosen to keep the VGT closed but in this case the new setpoints results in poor VGT performance. The coordinated controller VGT action is much more stable by comparison.

**Figure 9.16** describes the airflow tracking and actuator behaviour for the coordinated controller with fixed 50% open-loop term, the lack of open-loop assistance has greatly reduced the amount of movement from the EGR and VGT actuators, however, airflow tracking does not appear to have been degraded as a result.

An emissions comparison between the coordinated and standard controllers is plotted in **Figure 9.17**. The upper plot shows NO<sub>x</sub> emissions, the coordinated controller appears to be achieving lower NO<sub>x</sub> over most of the cycle. The level of CO<sub>2</sub> in the inlet manifold (4<sup>th</sup> plot) represents the level of recirculated gases, it can be seen that the EGR levels are in general higher for the coordinated controller. The setpoints are the same for both controllers, but the difficulty the standard controller has with stable VGT control may account for its lower EGR rates. The smoke trace indicates that the coordinated controller is generally performing better, with a reduction in the number of smoke spikes even though higher EGR rates are present.

### 9.6.2 Extra Urban Section of Cycle

**Figure 9.18** illustrates where in the EUDC section of the cycle the coordinated controller is active. It can be seen that over this section of the cycle there is very little coordinated action, much of it being in response to the transient fuelling events associated with pullaway and the first three gear changes. Once the engine speed exceeds 2000 rev/min, the coordinated action is reduced to zero, becoming active again in response to the tip-out at 100 seconds where engine speed falls below 2000 rev/min, and the subsequent tip-in at 172 seconds. The gearchange from fourth to fifth does not exploit coordinated action as the engine speed remains outside the coordinated operating bound.

The airflow tracking for the coordinated controller over the Extra-Urban section is illustrated in **Figure 9.19** with detail plots of EGR and VGT movements at points where co-ordination is active. Coordinated EGR-VGT movement can be seen in all three detail plots, though it is very difficult to determine the effect on airflow tracking from analysing the airflow response, partly because any improvements in airflow will be on a time scale less than the 0.5 seconds sample interval. Comparing the coordinated airflow tracking to the standard controller (see

**Figure 9.20)** the immediate observation is that the EGR and VGT actuators are less busy under coordinated control, as seen with the Urban cycle tests.

**Figure 9.21** describes the airflow tracking for the case of the coordinated controller with fixed 50% open-loop term. The instances where coordinated action is used are the same as for the case with fully active open-loop term, however examining the EGR VGT actuator behaviour illustrates how much it influences the actuator movements and contradicts the observations made about robustness from the cumulative results. The levels of movement (both coordinated and independent) are lower, this is due to the controller gains being low resulting in limited closed-loop response.

A comparison between the emissions characteristics of the coordinated controller and the standard strategy is given in **Figure 9.22**. The coordinated controller achieves lower  $\text{NO}_x$  for most of the cycle, however much of this reduction is due to better steady state EGR levels during the critical sections. The plot of inlet  $\text{CO}_2$  confirms this, from 275 seconds onwards the EGR level is clearly higher for the coordinated controller. The engine operating points for this section of the cycle are outside the envelope for coordinated control therefore the two controllers should behave identically, tracking the same setpoints. However, the '*disable EGR on overboost*' feature of the standard control strategy was activated, this resulted in closing the EGR valve over this section leading to higher airflow and boost. This particular feature is included to address the potential for the EGR valve to open during a large tip-in transient, should the boost pressure overshoot the airflow would do so as well, and the EGR control loop would open the valve to reduce the airflow. At high loads this is clearly undesirable therefore the protection mechanism is used.

The smoke plot indicates that the coordinated controller produces lower smoke peaks but this should be considered in the context of where the coordinated action is being used. The large peak at 40 seconds into the test is reduced, this can be attributed to coordinated action as the event corresponds to an instance of co-ordination (see **Figure 9.18**). However other reductions in peak smoke occur when the coordinated control is inactive, and are due to lower EGR levels and variability in pedal behaviour between tests. The quantity of smaller smoke spikes has increased, particularly over the final phase of the cycle (250 - 400 seconds), this is due to the higher EGR levels experienced with the coordinated controller in this region. The oxygen concentration trace in **Figure 9.22** reinforces these observations, with slightly lower levels for most of the operating region, and significantly lower values for the last section of the cycle.

In **Figure 9.23** the effect of the fixed open-loop term on emissions can be seen. Most significantly, the reduced actuator authority has led to increased smoke, due to the limited response of the EGR and VGT systems.

The UEGO feedback controller tracking performance is shown in **Figure 9.24**, the use of co-ordination between EGR and VGT actuators to achieve the target oxygen concentrations can be seen, as can the wide open EGR in combination with low VGT settings used to drive such high EGR flows. The tracking error is poor over the steady state regions of the cycle, the integral gains are too low for this controller hence poor steady state error. Higher integral gain on the VGT circuit will help alleviate the saturation of the EGR valve, as in many of the steady state cases, the EGR valve opens to reduce the oxygen content, however the VGT does not close down far enough to sufficiently increase the EGR flow, therefore the EGR valve continues to open.

The emissions results for the UEGO controller are plotted in **Figure 9.25** against the results of the standard controller for comparison. The lower exhaust oxygen concentrations obtained with this controller can be seen in the third frame of the figure, the corresponding high EGR rates are shown by the inlet CO<sub>2</sub> trace below. The result on NO<sub>x</sub> is a substantial reduction, though it is interesting to note that in the steady state region between 50 and 100 seconds, although the increase in EGR rate is large, the resultant NO<sub>x</sub> reduction is relatively small. A higher recirculation rate means that less gas is actually flowing out of the exhaust (tailpipe) of the engine, therefore, a reduced *concentration* of NO<sub>x</sub> in a reduced flow of gas leads to a greater overall reduction in emissions. In this particular region the increase in steady state smoke that accompanies the reduced NO<sub>x</sub> can be seen on the opacity plot.

The high levels of EGR mean greater residual levels in the inlet manifold, this will increase the instances of transient smoke as the residuals will take longer to reduce and so are more likely to cause unfavourable air fuel ratios during transients. This is evident from the smoke peaks at all the transient events, and the number of instances where the oxygen concentration approaches zero.

## **9.7 SUMMARY OF RESULTS & DISCUSSION**

A drive cycle evaluation of the tracking control performance and emissions behaviour of a selection of the control strategies developed in this project has been performed. The new controller designs have been compared against the standard control strategy. It is difficult to draw firm conclusions from the results due to the lack of repeat testing.

Both of the new control strategies demonstrated in this study are generic to Diesel engines equipped with VGT and EGR systems, a configuration which is practically standard for current passenger vehicle engines.

Over the urban section of the cycle, the standard controller appears to perform better than the coordinated strategy, although optimisation of the coordinated controller setpoints and gains may improve its performance. The Extra-Urban testing shows the coordinated control to be slightly better, though the results are close enough to be considered the same due to experimental scatter, this is more likely considering the extent to which co-ordinated action is used in this section.

It is encouraging that using a co-ordinated controller and roughly chosen setpoints does not significantly deteriorate the engine emissions and fuel economy. Disappointingly, the improvements in transient EGR behaviour shown by the constant speed testing used to develop the controller are not reflected in the drive cycle emissions performance. However, it must be noted that the drive cycle conditions are very specific and it would be fair to say are seldom reflected in real-life driving conditions. The transient conditions where co-ordinated action would actually be of use are not that common in the legislative cycle.

It appears that the choice of setpoints has a stronger influence on the drive cycle cumulative performance than the control scheme used to move between these targets. Additionally, changing the setpoints used by the standard control scheme degrades its stability by having the VGT active over a region of the operating map where it has a strong influence on EGR flow.

The lack of scatter between the cumulative emissions results for the coordinated controller with active and fixed open-loop controller terms suggests good robustness. However, the time-resolved data indicates that the closeness of these results is an averaged effect and the actual tracking performances of the two cases are quite different. This highlights the need to examine the time-based results of drive cycle tests as opposed to relying uniquely on the cumulative results.

It is interesting to note that **Van Nieuwstadt et al [36]** displayed similarly inconclusive results for the drive cycle evaluation of their coordinated control strategies, this substantiates the suggestion that the legislative cycle cannot be used to illustrate the benefits of coordinated control.

The UEGO feedback controller achieves strong NO<sub>x</sub> reductions through the highest EGR rates of all the controllers, however the smoke and fuel consumption figures suffer as a result. The UEGO controller was not shown to give completely satisfactory performance over the constant speed fuelling profiles used in its development, however when tested over a drive

cycle the results are still in the region of those for the other controllers. Higher oxygen concentration targets may well improve the system performance by bringing smoke production down to levels comparable with the other controllers.

Were it possible to test this controller with the feedforward compensation scheme developed in **Chapter 8** and more carefully chosen setpoints, it is probable that this system would show at the very least equivalent behaviour to the well optimised standard controller. If so, the UEGO feedback approach offers a substantially reduced calibration effort. This is because the relationship between exhaust oxygen, fuel level and EGR rate is known, allowing an EGR rate to be specified without having to perform time consuming engine mapping exercises in order to determine the boost pressure and mass airflow levels required to achieve the same level of EGR.

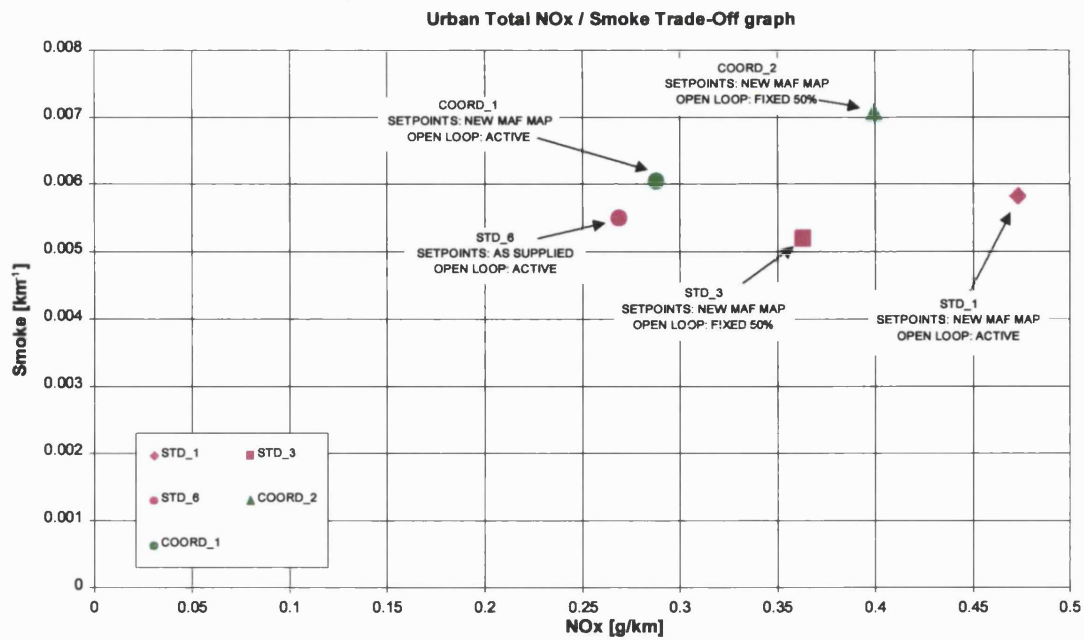


**Figure 9.1 NO<sub>x</sub> / Smoke trade-off over Urban (first 200 seconds) section of drive cycle**

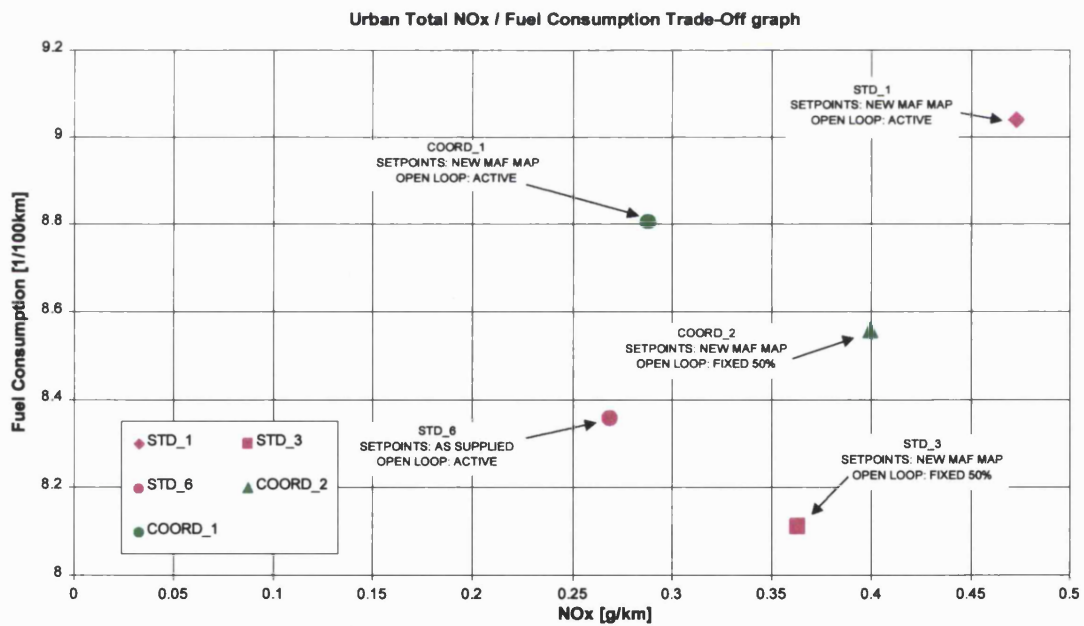


**Figure 9.2 Fuel Consumption / NO<sub>x</sub> trade-off over Urban section of cycle**



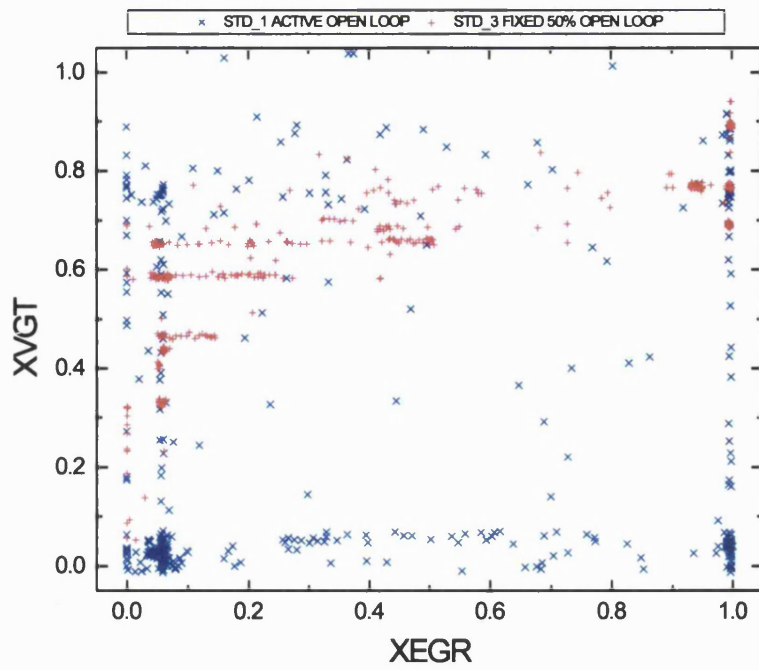


**Figure 9.3 EGR and VGT positions over Urban section of cycle for standard controller with new setpoints**

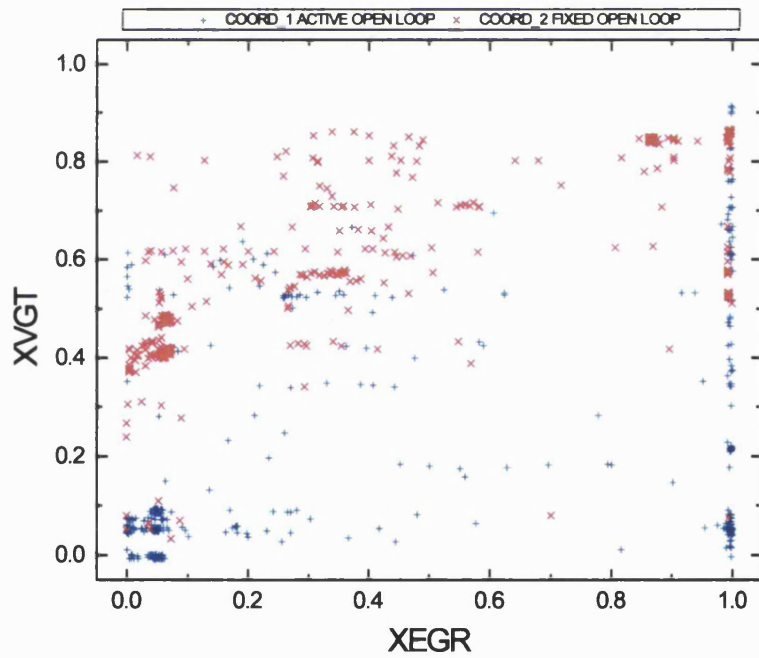


**Figure 9.4 EGR and VGT positions over Urban section of cycle for coordinated controller with new setpoints**

Areas of engine operating map over ECE15 section of drive cycle for which coordinated control is active

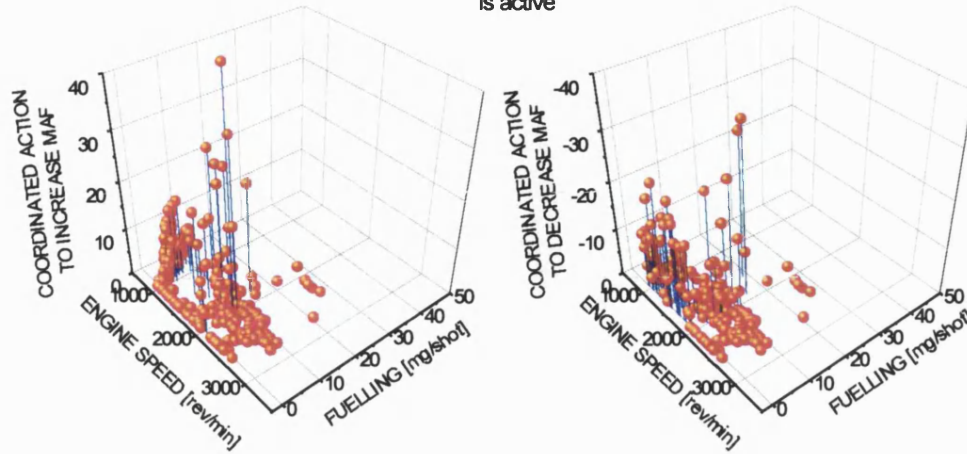


Figure 9.5 Operating envelope for coordinated controller over Urban section of cycle

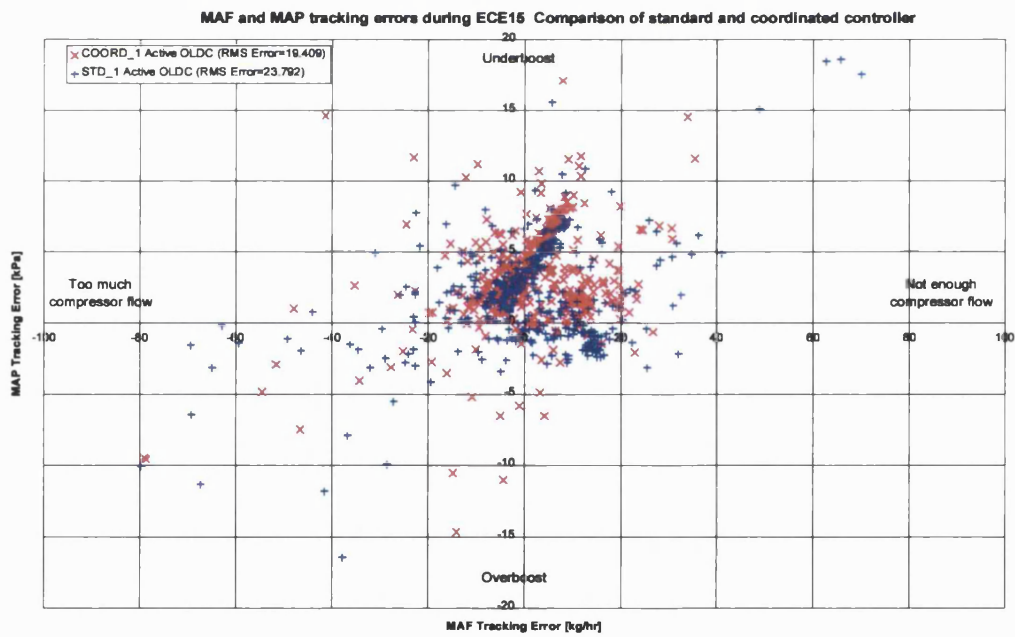


Figure 9.6 Airflow vs boost tracking error comparison for standard and coordinated controllers over Urban section of cycle

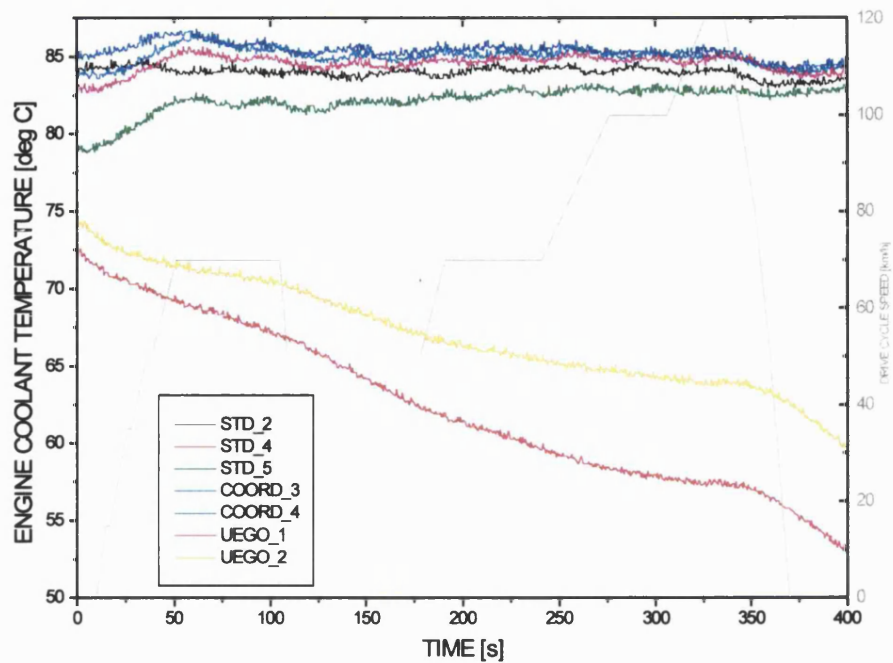


Figure 9.7 Engine coolant temperature over Extra-Urban section of cycle, illustrating the 2 instances where coolant temperature dropped during the test

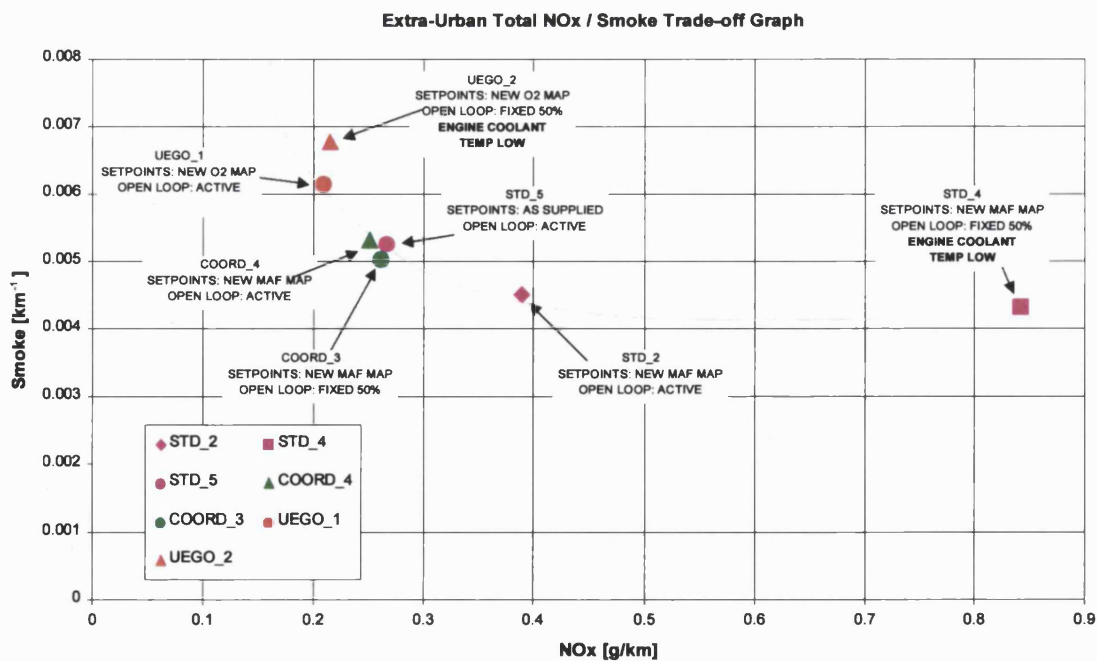
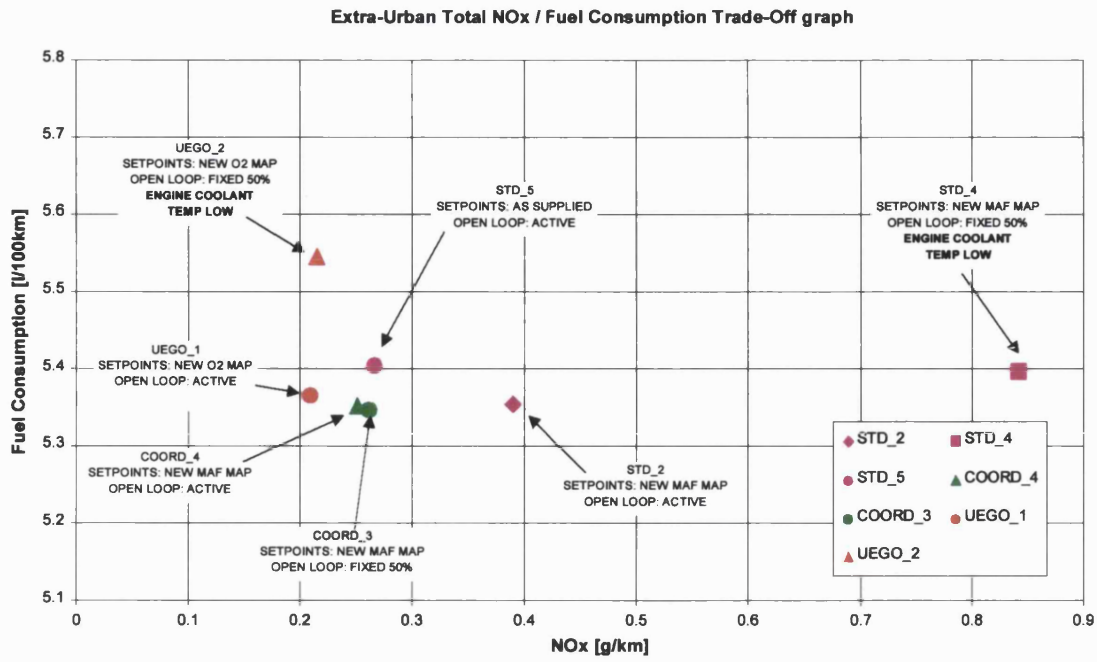
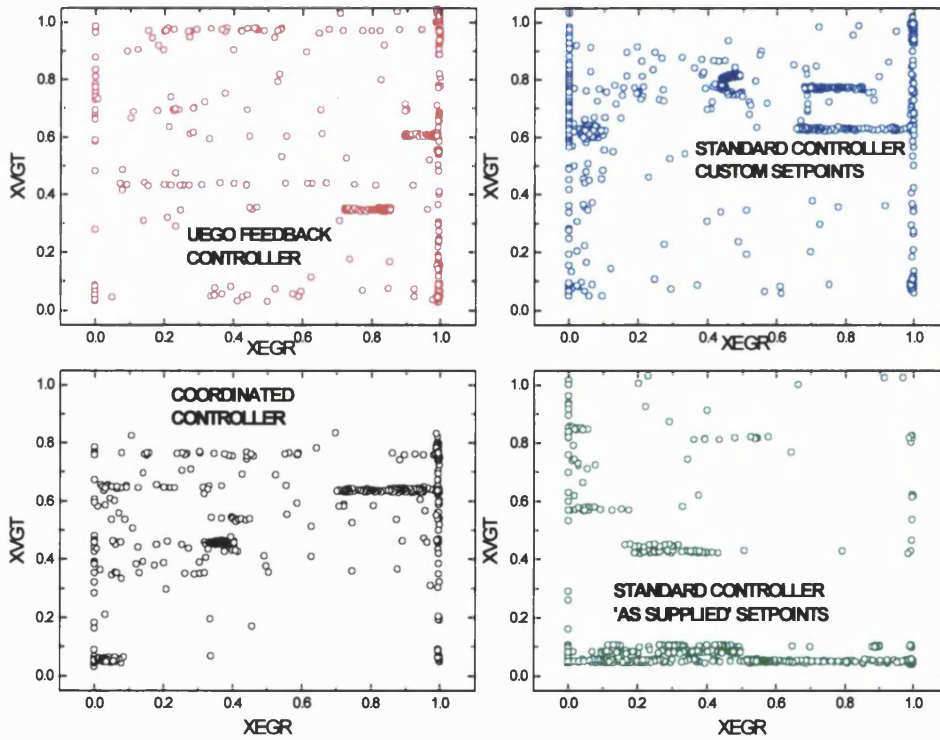


Figure 9.8 NO<sub>x</sub> / Smoke trade-off over EUDC section of drive cycle



**Figure 9.9 NO<sub>x</sub> / Fuel Consumption trade-off over EUDC section of cycle**



**Figure 9.10 EGR and VGT positions over Extra-Urban section for the different controllers**

Areas of engine operating map over EUDC section of drive cycle for which coordinated control is active

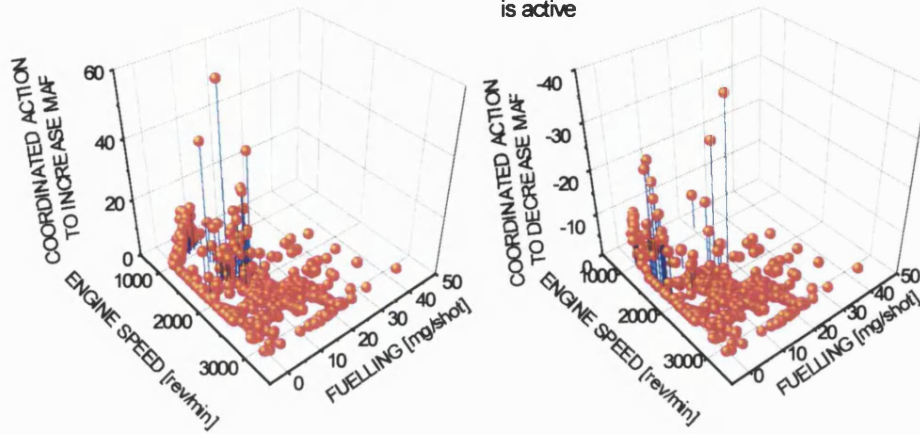


Figure 9.11 Use of coordinated action for coordinated controller over Extra-Urban section of cycle

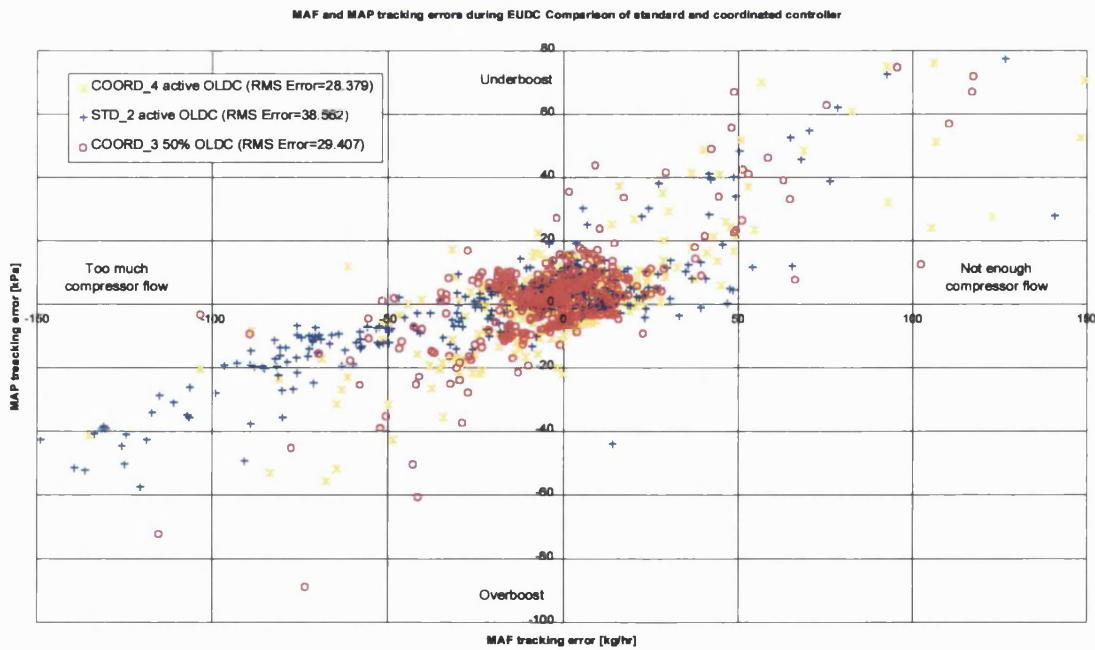


Figure 9.12 Airflow vs. boost tracking error comparison for standard and coordinated controller over EUDC section of cycle

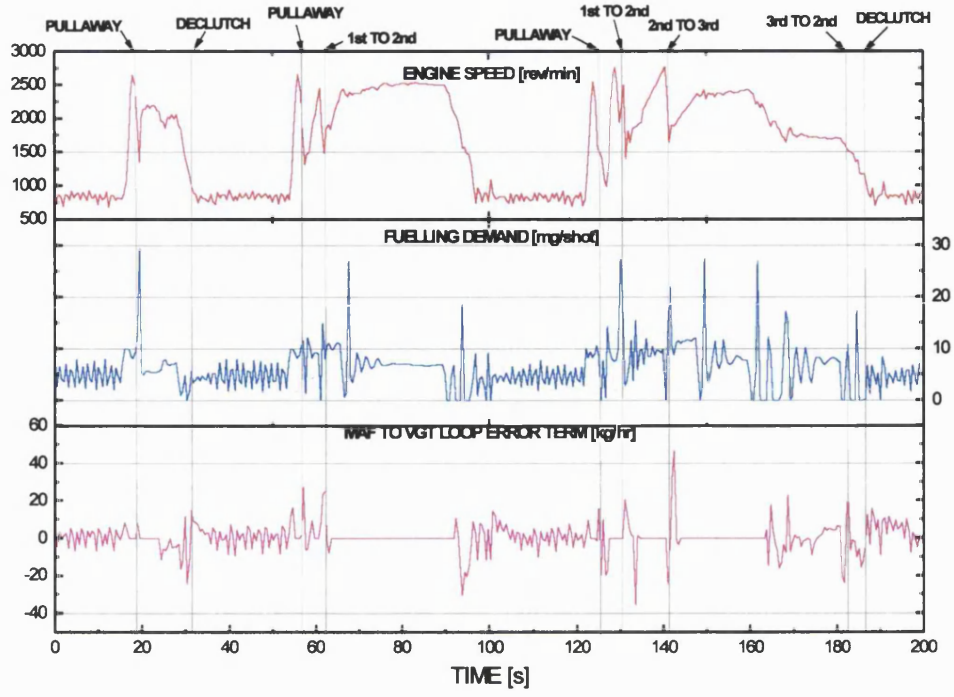


Figure 9.13 Transient events and coordinated action over Urban section of cycle

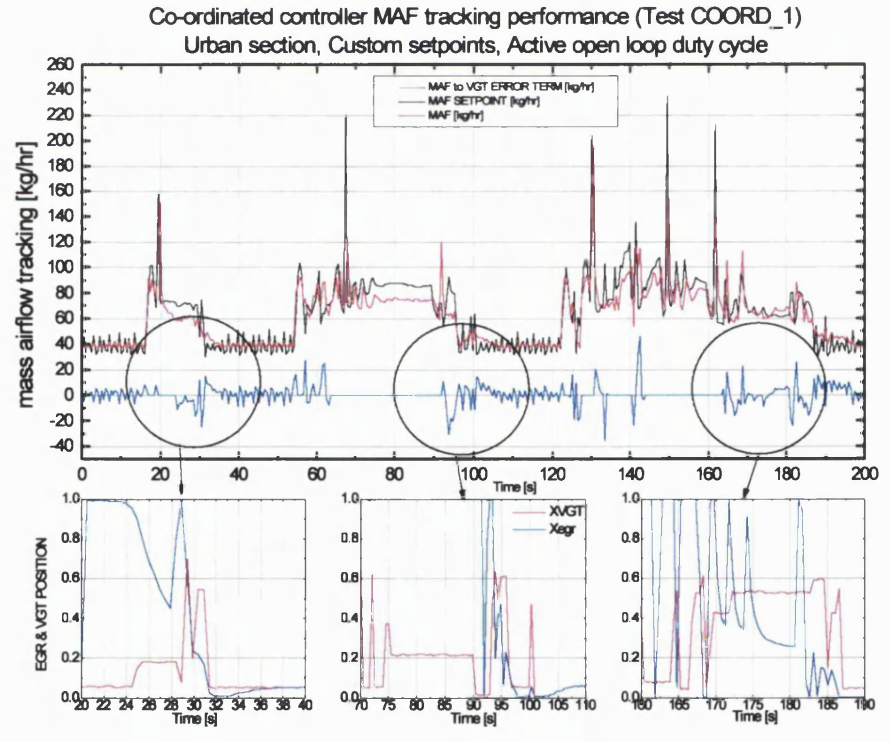
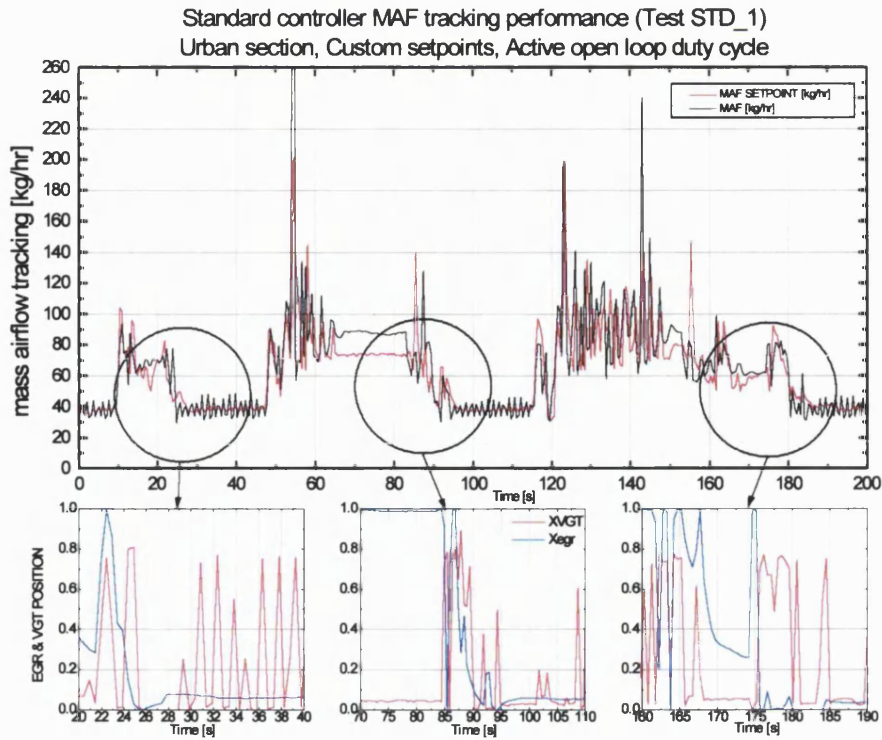
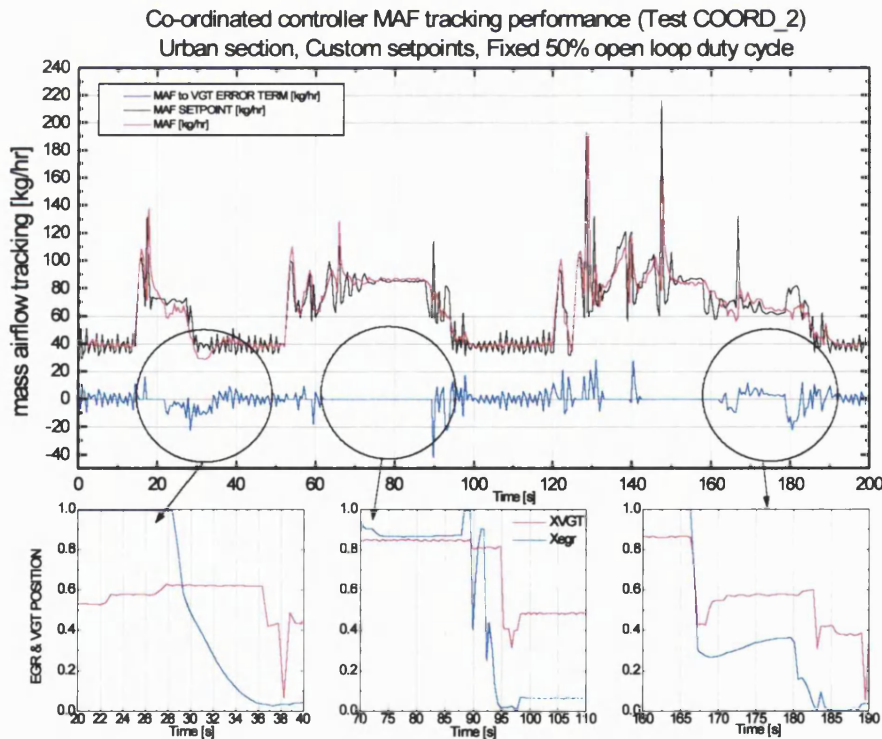


Figure 9.14 Airflow tracking and EGR VGT position detail for coordinated controller over Urban section of cycle



**Figure 9.15** Airflow tracking and EGR VGT position detail for standard controller over Urban section of cycle



**Figure 9.16** Airflow tracking and EGR VGT position detail for coordinated controller with fixed 50% open-loop term over Urban section of cycle

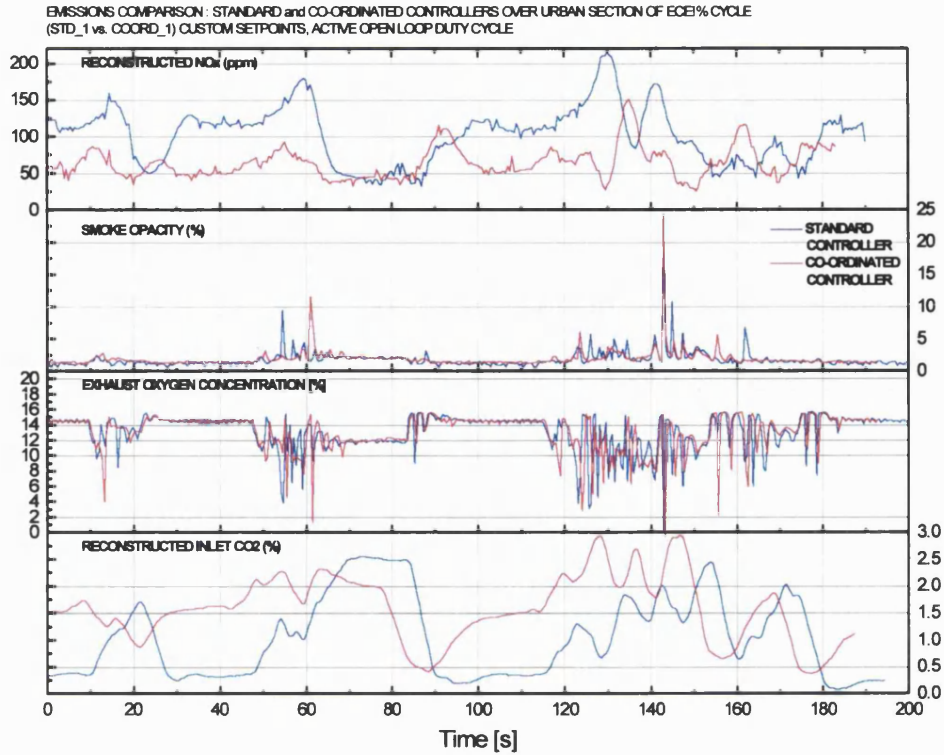


Figure 9.17 Emissions comparison of standard and coordinated controllers over Urban section of cycle

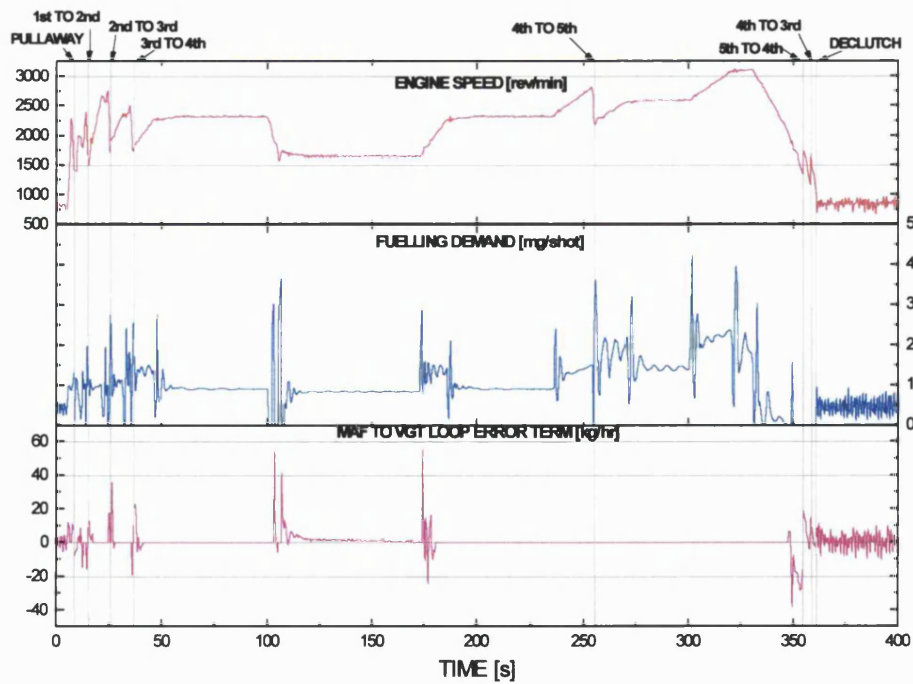
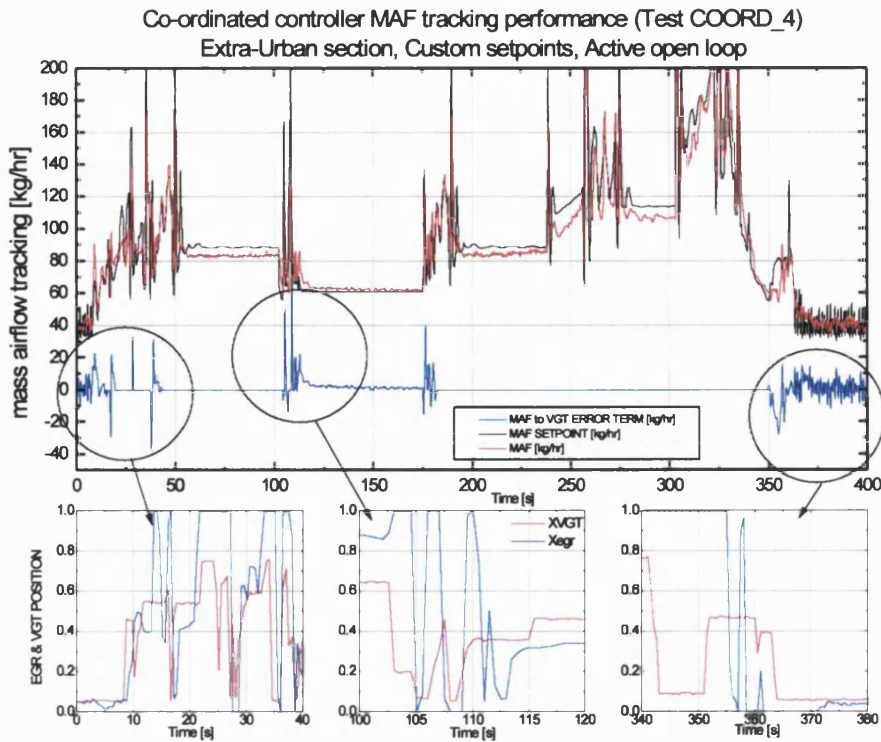
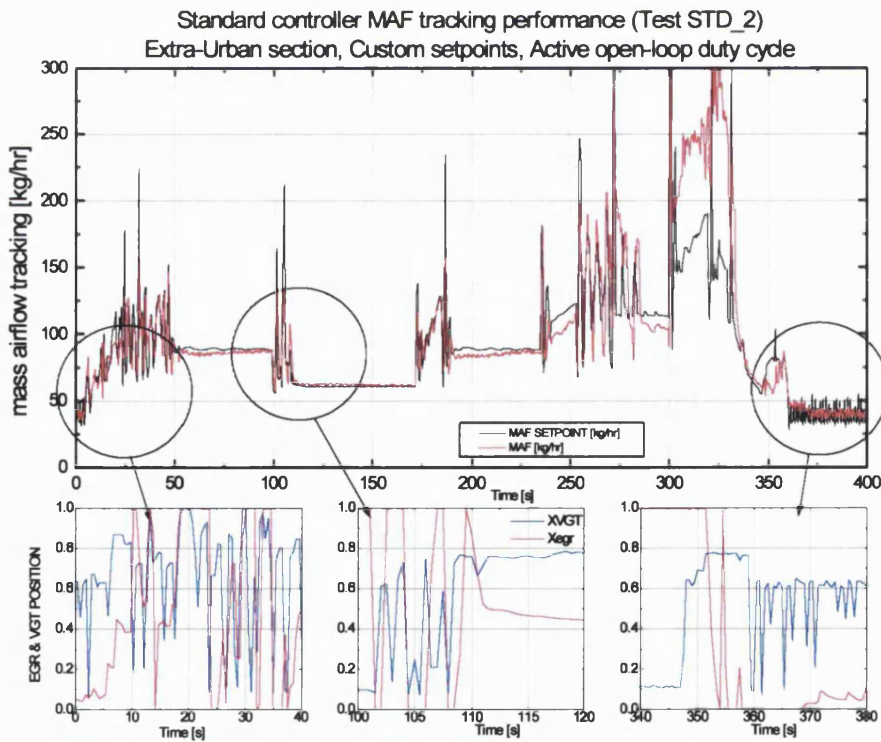


Figure 9.18 Transient events and coordinated action over Extra-Urban section of cycle





**Figure 9.19** Airflow tracking and EGR VGT position detail for coordinated controller over Extra-Urban section of cycle



**Figure 9.20** Airflow tracking and EGR VGT position detail for standard controller over Extra-Urban section of cycle

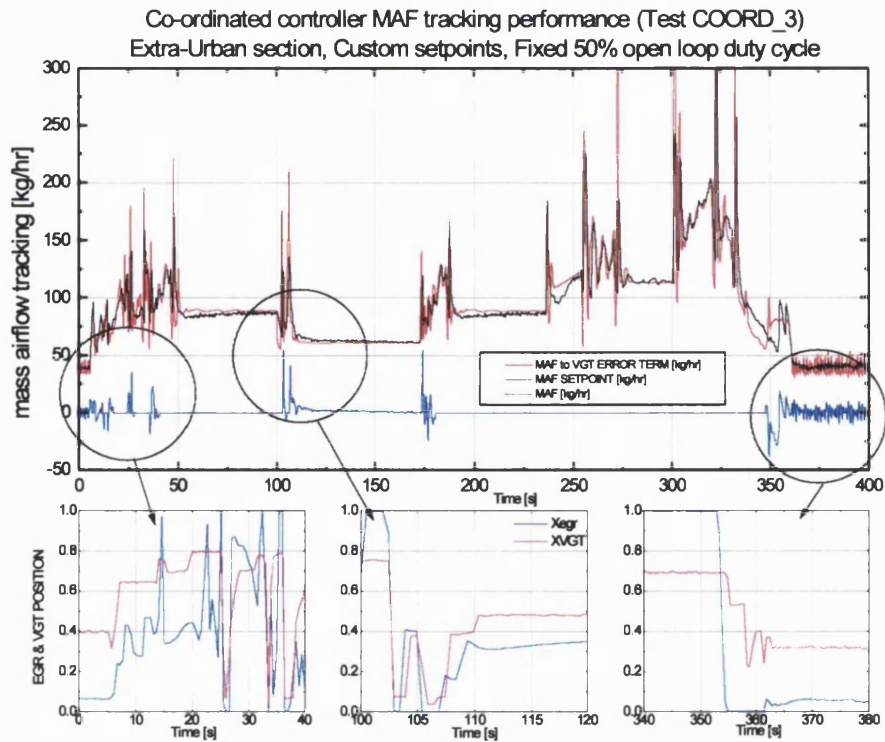


Figure 9.21 Airflow tracking and EGR VGT position detail for coordinated controller with fixed 50% open-loop term over Extra-Urban section of cycle

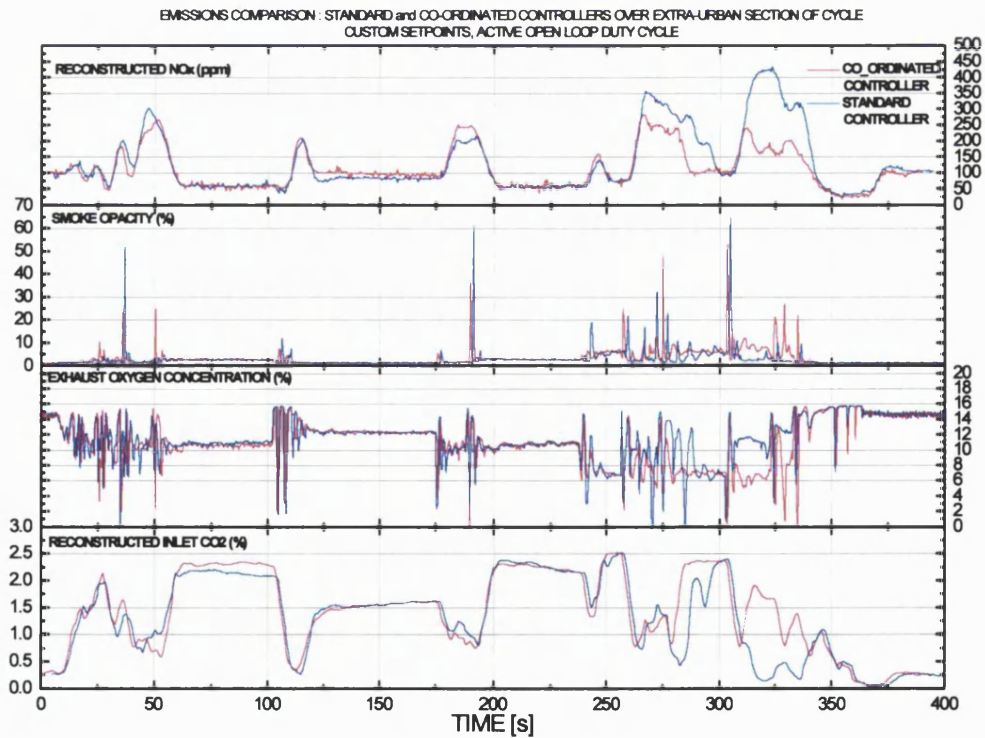
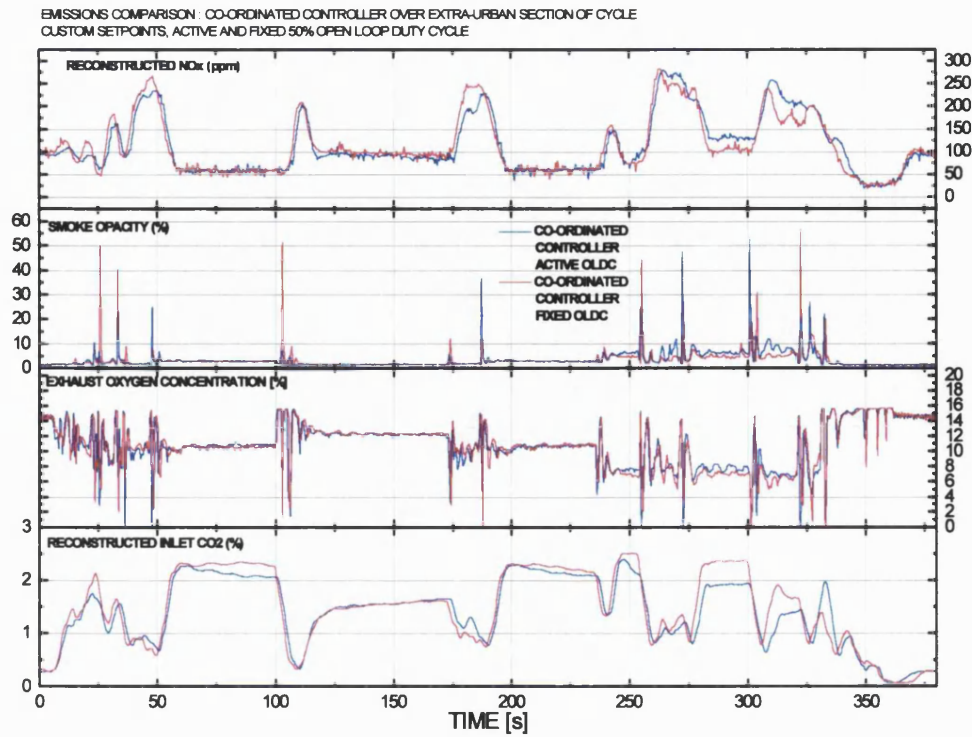
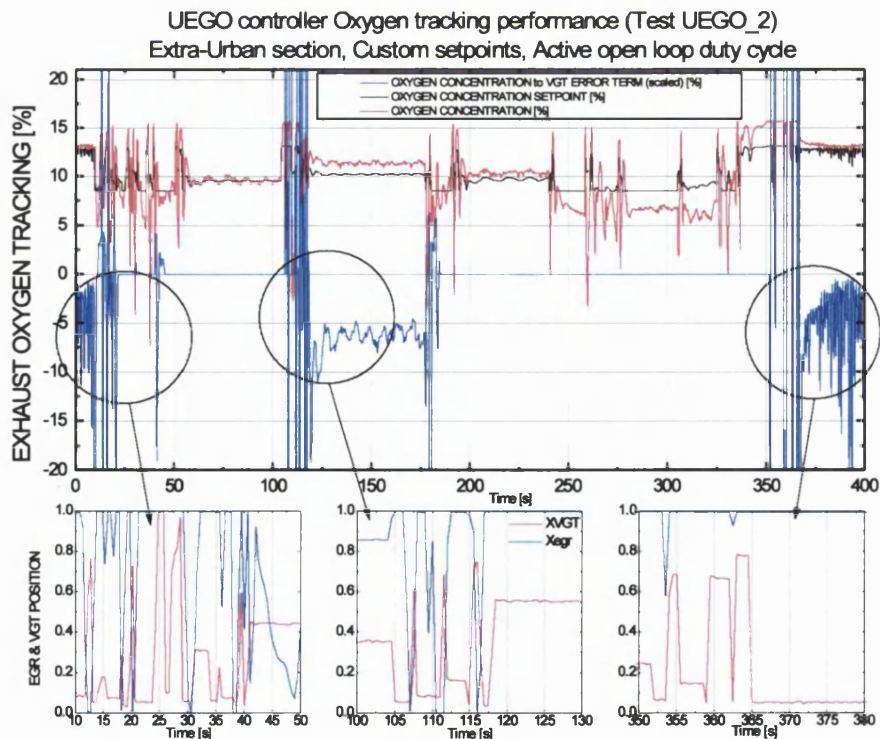


Figure 9.22 Emissions comparison of standard and coordinated controllers over Extra-Urban section of cycle



**Figure 9.23 Emissions comparison of coordinated controller with fixed and active open-loop term over Extra-Urban section of cycle**



**Figure 9.24 Exhaust oxygen tracking and EGR VGT position detail for UEGO controller over Extra-Urban section of cycle**

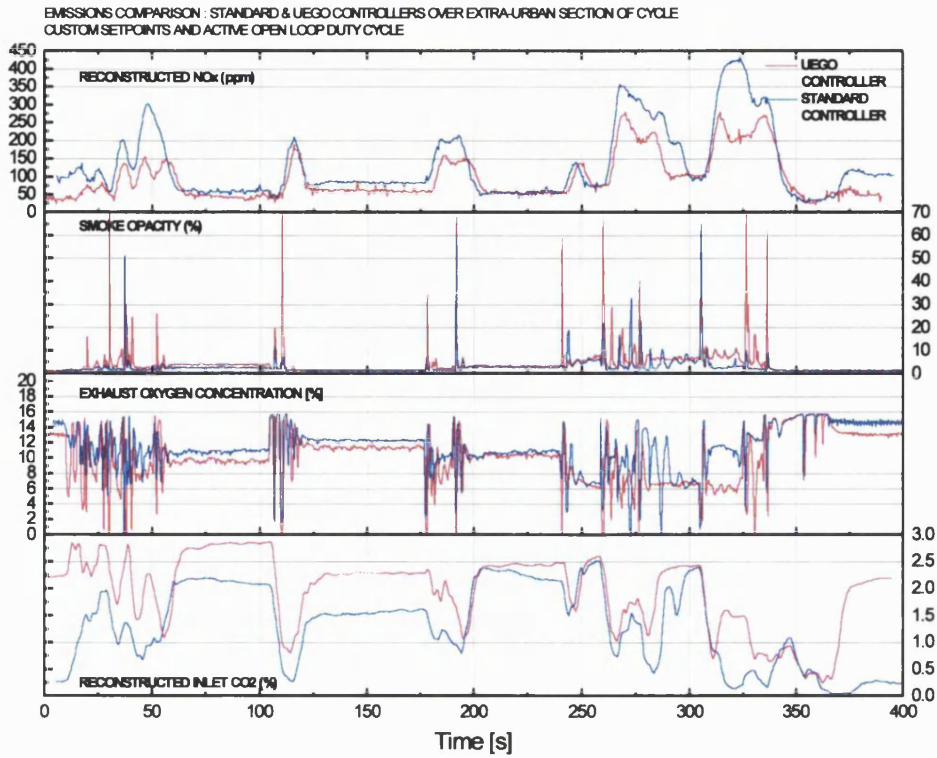


**Figure 9.25 Emissions comparison of UEGO controller over Extra-Urban section of cycle**

## **Chapter 10 CONCLUSIONS & FURTHER WORK**

### **10.1 CONCLUSIONS**

An extensive study of the performance and control of a High Speed Direct Injection Diesel Engine has been performed. Through experimental characterisation and analysis of contemporary research programs, several development areas were identified and investigated using simulation and experimental based techniques.

The VGT actuation mechanism and boost pressure-based feedback control scheme currently used on the engine conspire to create dynamic behaviour problems in response to certain tip-in transient manoeuvres. It is also demonstrated that independent control of EGR and VGT systems serves to reduce the attainable transient airflow response. Additionally, the use of steady state airflow and boost pressure schedules to characterise the combustion conditions is less accurate compared to a physical feedback parameter of the actual conditions such as an oxygen concentration measurement.

A control scheme has been designed to address issues in the engine transient performance under large tip-in conditions. The exhaust pressure feedback-based system demonstrates large improvements over conventional VGT control systems through better management of the exhaust manifold pressure, thus reducing pumping work and fuel consumption, improving transient torque delivery and reducing transient emissions. In this particular study the control scheme improves the behaviour of vacuum actuated swivelling VGT mechanisms which have their own unique behavioural quirks, however the technique is generic and offers better control for VGT systems by reducing the time delays between actuation and feedback.

Controllers that exploit the cross-coupled nature of the EGR and VGT systems have been synthesised and shown to improve the response of transient airflow under certain engine operating regimes. Fuzzy logic is demonstrated as a practical means of achieving the selective co-ordination of the systems without need for overly complicated model-based control schemes. Again, the technique developed here is generic and can be applied to any engine equipped with VGT and external EGR.

An alternative control method for EGR rate control using exhaust gas Oxygen feedback with a UEGO sensor has also been investigated and shown to offer potential for good EGR control. In order to reject the high frequency disturbances caused by the fuel injection, a feedforward model-based strategy is required; a simple implementation of such a scheme has been demonstrated in simulation.

Legislative drive cycle testing has been used to evaluate the performance of the coordinated airflow controller and UEGO feedback controller compared to various configurations of the standard control system. It was difficult to draw firm conclusions as to whether or not the coordinated control gave better drive cycle performance due to the similarity of the test results to those of the standard controller and the lack of repeat testing. It is concluded that the legislative cycle is unlikely to highlight differences in the control algorithms used here, but will reflect more the choice of setpoints used by the controllers.

This study has made extensive use of simulation and rapid-prototyping techniques. The accurate simulation of a complex non-linear system such as the turbocharged Diesel engine is a difficult task, but given the flaws in the simulation method the resulting model has proved itself to be very useful in control design and evaluation. Sub-models have also been developed during the course of this work that increase the functionality of the basic model and better represent the engine transient behaviour.

The rapid-prototyping hardware and software has enabled control schemes to be implemented, evaluated and iterated within extremely short timescales, to the extent that controller development could take place largely on the test bed rather than in simulation. This single factor has allowed the development to be carried out in a very practical manner, working within similar constraints to production engine control systems.

Considerable effort has been made in developing a method of extracting useful signals from the existing engine management system for use in the custom strategies running externally. The resultant method can be used with any engine management system that operates the CAN Calibration Protocol providing some basic information about the control strategy is available, and offers a cost effective solution to the problem of bypassing certain aspects of an existing control strategy.

Additionally, a custom driver emulation system has been developed in the course of this project that permits arbitrary driving cycles to be performed automatically on the test bed engine, including clutch and gearchange operations. This has allowed the evaluation of systems using the legislative cycles as mentioned previously, and creates a highly flexible test facility.

The new control schemes developed in this work improve control performance with a very efficient computational implementation, and the benefits of the PID feedback compensation scheme are retained. This provides a very practical solution for the mass-production automobile market to the otherwise complex transient optimisation problem.

## **10.2 FURTHER WORK**

The greatest limitation to this work has been the short period available for evaluating the new control schemes on the test rig. Repeated drive cycle testing to average the cumulative performance would be beneficial from statistical point of view. Additionally, the development of custom drive cycles would allow a better evaluation of the new strategies, such as including large tip-in transients as experienced when overtaking for example.

The setpoints used for the coordinated controllers were not optimal but merely chosen to demonstrate the controller, given that the resultant performance was very close to the original strategy, a more thorough calibration exercise is likely to improve performance. An on-line optimisation technique was used on the engine model as an initial setpoint generation method, however, discrepancies between simulation and the real engine prevented these from being successfully employed on the test bed. With the rapid prototyping hardware it is possible to apply this same optimisation technique direct to the engine, allowing substantial reductions in strategy calibration requirements.

The successful control schemes developed here are essentially simple extensions to the existing 'standard' strategy and are modular in nature. It would be possible to combine these new schemes into one global strategy that offered improved performance over a wide range of engine conditions, as opposed to the individual treatment given here. A further study of which sensor and control combinations are most effective would be a useful continuation of this work, for example, using exhaust pressure and UEGO feedback, or inlet and exhaust manifold pressure for a global strategy.

## REFERENCES

---

- 1 "Transient Modelling of a DI TCi Diesel Engine", Brace, C., University of Bath, PhD Thesis 1996
- 2 "The Dynamic Behaviour of a High Speed Direct Injection Diesel Engine", Wijetunge, R., Brace, C., Hawley, J., Vaughan, N., Horrocks, R., Bird, G., University of Bath, Ford Motor Company, SAE990829
- 3 "Internal Combustion Engine Fundamentals", Heywood, J., p.491-566 Chapter 10 Combustion in Compression Ignition Engines, 1988 McGraw-Hill Book Co, ISBN 0-07-100499-8
- 4 "European Emission Standards to the Year 2000", Dunne, J, Greening, P, Department of Transport, UK, IMechE conference proceedings "Worldwide Engine Emissions Sandards and How to Meet them", 25-26 May 1993
- 5 Course Notes, 14<sup>th</sup> Annual Short Course on Diesel Particulates and NO<sub>x</sub> Emissions, 30<sup>th</sup> March-3<sup>rd</sup> April 1998, University of Leeds
- 6 "Review of Literature on the Possible Carcinogenicity of Automotive Emissions: Final Report", Grasso, P, Mann, A., Irvine, D., The Robens Institute, University of Surrey UK, British Airways Health Services, UK, October 1998
- 7 "Introduction to Internal Combustion Engines: Second Edition" Stone, R., p.93, Chapter 3, 1992 The Macmillan Press Ltd., ISBN 0-333-55084-6
- 8 "Internal Combustion Engine Fundamentals", Heywood, J., p.620-626 Chapter 11 Pollutant Formation and Control, 1988 McGraw-Hill Book Co, ISBN 0-07-100499-8
- 9 "A Study of Unburnt Hydrocarbon Emission in Small DI Diesel Engines", Tsurushima, T., Zhang, L., Ishii, Y., ISUZU Advanced Engineering Centre, SAE Paper 1999-01-0512
- 10 "Multicomponent Absorption on Diesel Particulate Matter", Johnson, J., Kittelson, D., Proceedings of the 4<sup>th</sup> International Aerosol Conference, 29<sup>th</sup> August – 2<sup>nd</sup> September 1994, Los Angeles USA
- 11 "Internal Combustion Engine Fundamentals", Heywood, J., p.642-646 Chapter 11 Pollutant Formation and Control, 1988 McGraw-Hill Book Co, ISBN 0-07-100499-8
- 12 "NO<sub>x</sub> Control Using EGR", Ladommatos N, Brunel University
- 13 "The effects of carbon dioxide EGR on Diesel engine emissions", Ladommatos N, Abdelhalim S, Zhao H, Brunel University, Proceedings of the IMechE C517/028/96
- 14 "The effects on Diesel Combustion and Emissions of Reducing Inlet Charge Mass Due to Thermal Throttling with hot EGR", Ladommatos N, Abdelhalim S, Zhao H, Hu Z, Brunel University, SAE980185
- 15 "The influence of CO<sub>2</sub>(carbon dioxide) and H<sub>2</sub>O(water) in EGR on particulate NO<sub>x</sub> emissions", Ladommatos N, Zhao H, Abdelhalim S, Hu Z, Brunel University, UnICEG Minutes -Appendix 96/3/1/, 9th Jan, 1997. UMIST
- 16 "The Effect of Exhaust Gas Recirculation on Soot Formation in a High-Speed Direct Injection Diesel Engine", Ladommatos N, Balian R, Horrocks R, Cooper L, University of Brunel, Ford Motor Co., SAE960841
- 17 "Introduction to Internal Combustion Engines: Second Edition" Stone, R., p.338, Chapter 9, 1992 The Macmillan Press Ltd., ISBN 0-333-55084-6
- 18 "Variable Geometry Turbocharging for Lower Emissions and Improved Torque Characteristics", Hawley, J., Wallace, F., Pease, A., Cox, A., Horrocks, R., Bird, G., University of Bath, Ford Motor Company, IMechE Journal of Automobile Engineering, 1998
- 19 "Optimisation of Heavy Duty Diesel Engine Transient Emissions by Advanced Control of A Variable Geometry Turbocharger", Pilley A, Noble A, Beaumont A, Needham J, Porter B, Ricardo Consulting Engineers Ltd., SAE890395
- 20 "Turbocharging the Ford 2.5l HSDI Diesel engine", Bostock P, Cooper L, Ford Motor Company



- 
- 21** "Simulation of a variable geometry turbocharged Diesel engine for control algorithm development", Truscott A, Porter B, Ricardo Consulting Engineers Ltd., Proceedings of the IMechE C524/127/97
- 22** "A study of an EGR Control System for Diesel Based on an Intake/Exhaust System model", Itoyama H, Uchida M, Miwa H, Nissan Motor Co. Ltd., SAE970621
- 23** "EGR Feedback control on a Turbocharged DI Diesel Engine", Amstutz A, Del Re L, Federal Institute of Technology, Zurich CH, IMechE publication C448/010/92
- 24** "Parameter Scheduling Controller for Exhaust Gas Recirculation (EGR) System", Olbrot A, Berri M, Asik J, Wayne State University and The Ford Motor Company, SAE970620
- 25** "The Design and Implementation of an Integrated Variable Geometry Turbocharger Control Strategy for a Passenger Car Diesel Application", Walker D, 1998 MSc Thesis, Department of Aeronautical & Automotive Engineering and Transport Studies, Loughborough University
- 26** "Modelling and Identification of a Current to Vacuum Transducer and VNT actuator", Moraal P, Kolmanovsky I, Van Nieuwstadt M, Proceedings of the IEEE / ASME International Conference on Advanced Intelligent Mechatronics, September 19-23 Atlanta USA, p.257-262
- 27** "Transient Investigation of Two Variable Geometry Turbochargers for Passenger Vehicle Diesel Engines", Brace C, Wijetunge R, Hawley J, Vaughan N, Wallace F, Horrocks R, Bird G, University of Bath, Ford Motor Co UK, SAE 991241
- 28** "Using and electronically controlled VGT to improve engine transient performance", Jain D, Schwitzer Inc.
- 29** "Optimisation of the transient performance of a turbocharged Diesel engine using turbocharging and fuel injection controls", Arcoumanis C, Chan S, Bazari Z, Imperial College of Science Technology and Medicine UK, Lloyds Register, IMechE
- 30** "Optimisation of a Heavy-Duty Diesel Engine Transient Emissions by Advanced Control of a Variable Geometry Turbocharger", Pilley A, Noble A, Beaumont A, Needham J, Porter B, Ricardo Consulting Engineers Ltd, SAE890395
- 31** "Model Based Development of Engine Control Algorithms", Dekker H, Sturm W, TNO Road-Vehicles Research Institute NL, IMechE Publication C499/021/96
- 32** "DI Diesel Engine with Variable Geometry Turbocharger (VGT): A Model Based Boost Pressure Control Strategy", Buratti, R., Carlo, A., Lanfranco, E., Pisoni, A., Meccanica 32, 1997.
- 33** "Nonlinear Control of Turbocharged Diesel Engines -An Integrated Powertrain Control Perspective", Fredriksson J, 1999 Licentiate of Engineering Thesis, Department of Signals and Systems, Chalmers University of Technology, Sweden
- 34** "Issues in Modelling and Control of Intake Flow In Variable Geometry Turbocharged Engines", Kolmanovsky I, Moraal P, Van Nieuwstadt M, Stefanopoulou A, The Ford Motor Company, IFIP 1997
- 35** "A Comparison of SISO and MIMO designs for EGR-VGT control of a High Speed Diesel Engine", Van Nieuwstadt M, Moraal P, Kolmanovsky I, Stefanopoulou A, The Ford Motor Company, IFAC workshop on Advances in Automotive Control, Ohio, February 1998
- 36** "Coordinated EGR-VGT Control for Diesel Engines: an Experimental Comparison", Van Nieuwstadt M, Kolmanovsky I, Moraal P, The Ford Motor Company, SAE000266
- 37** "EGR VGT Control Schemes: Experimental Comparison for a High Speed Diesel Engine", Van Nieuwstadt M, Kolmanovsky I, Moraal P, Stefanopoulou A, Jankovic M, IEEE Control Systems Magazine June 2000 p.64-79
- 38** "Constructive Lyapunov control design for turbocharged Diesel engines", Jankovic M, Kolmanovsky I, IEEE Transactions on control system technology Vol 8 Issue 2 March 2000 p.288-299
- 39** "Robust Control of Diesel Internal Combustion Engines", Moynihan E, PhD Thesis, Cambridge University 1998

- 
- 40** "Control Technology for Future Low Emissions Diesel Passenger Cars", Porter B, Ross-Martin T, Truscott A, Ricardo Consulting Engineers Ltd., IMechE Publication C517/035/96 1996
- 41** "Reduction of steady-state NO<sub>x</sub> levels from an automotive Diesel engine using optimised VGT/EGR schedules", Hawley J, Wallace F, Cox A., Horrocks R, Bird G, University of Bath UK, Ford Motor Co. UK, SAE990835
- 42** "Turbocharger and EGR Control in an Automotive DI Diesel Engine", Capobianco M, Gambarotta A, University of Genoa Italy, Proceedings of the 3<sup>rd</sup> International Conference on Internal Combustion Engines: Experiments and Modeling 17<sup>th</sup>-20<sup>th</sup> September 1997 Capri – Naples, Italy
- 43** "Experimental Characterisation of Turbocharging and EGR systems in an Automotive Diesel Engine", Capobianco M, Gambarotta A, Zamboni G, University of Genoa, Italy, IMechE publication C517/027/96
- 44** "Sliding Mode : Control Engineering in Practice", Young K, Özgüner Ü, p.150-162 Proceedings of the American Control Conference, San Diego 1999
- 45** "Variable Structure Systems with Sliding Modes", Utkin V, p212-222 IEEE Transactions of Automatic Control, Vol ac-22, no.2, April 1977
- 46** "Sliding Mode Control of Automotive Engines", Moskwa J, p687-693 Transactions of the ASME, Journal of Dynamic Systems, Measurement and Control, December 1993, Vol. 115
- 47** "Nonlinear Diesel Engine Control and Cylinder Pressure Observation", Kao M, Moskwa J, Powertrain Control Research Laboratory, University of Wisconsin-Madison, p183-192 Transactions of the ASME, Journal of Dynamic Systems, Measurements and Control, June 1995 Vol. 117
- 48** "Nonlinear Algorithms for Simultaneous Speed Tracking and Air-fuel Ratio Control in an Automobile Engine", Pfeiffer J, Hedrick J, University of California, Berkely USA, SAE990547
- 49** "Secondary O<sub>2</sub> Feedback Using Prediction and Identification Type Sliding Mode Control", Yasui Y, Akazaki S, Ueno M, Iwaki Y, Honda R&D CO. Ltd., SAE 000936
- 50** "Variable Structure Control Method for Fuel-Injected Systems", Cho D, Oh H, Princeton University, Princeton USA, p.475-481 Transactions of the ASME Journal of Dynamic Systems, Measurement and Control, September 1993, Vol. 115
- 51** "Gain Bounds in the Minimal Controller Synthesis Algorithm", Stoten D, Sebusang S, University of Bristol, 1998 Proceedings of the ImechE Vol 212 Part 1 p.345-360
- 52** "Evaluation of Turbocharger Power Assist System Using Optimal Control Techniques", Kolmanovsky I, Stefanopoulou A, Ford Motor Company USA, University of California, Santa Barbara, SAE 200519
- 53** "Optimal Control of an Automotive Powertrain System during Rapid Load Transients", Karrison J, Jacobson B, Chalmers University of Technology Sweden, IMechE Symposium on Integrated Powertrains and their Control, University of Bath 19 September 2000
- 54** "Intelligent Control Systems: Are they for Real?", Shoureshi R, Purdue University, West Lafayette, IN 47907-1288, Transactions of the ASME, Journal of Dynamic Systems, Measurement, and Control, June 1993, Vol. 115, p392-401
- 55** "Virtual Sensing: A neural Network-based Intelligent Performance and Emissions Prediction System for On-Board Diagnostics and Engine Control", Atkinson C, Long T, Hanzevack E, West Virginia University USA, Neurodyne Inc. SAE 980516
- 56** "Engine Knock Estimation using Neural Networks based on a real world database", Ortmann S, Rychetsky M, Glesner M, Groppo R, Tubetti P, Morra G, Darmstadt University of Technology, FIAT research centre, SAE 980513
- 57** "Transient A/F Estimation and Control Using a Neural Network", Asik J, Peters J, Meyer G, Tang D, Ford Motor Co.USA, SAE 970619
- 58** "Transient Air-Fuel Ratio Control Using Artificial Intelligence", Lenz U, Schroeder D, Technical University of Munich, SAE 970618

- 
- 59** "Transient Exhaust Gas Improvement by Adaptive Neural Network", Takagi S, Takeshi S, Morita S, Takiyama T, Takigawa M, Osaka City University, Japan, Matsushita Electric Industrial Co., Japan, 1997 JSAE Review (1998) 19, p.15-19
- 60** "Turbocharger Modelling for Automotive Control Applications", Moraal P, Kolmanovsky I, Ford Motor Company, SAE 990908
- 61** "Fuzzy Logic Toolbox for use with Matlab", 1998, The MathWorks, Inc., Natick MA, USA.
- 62** "Digital Control Systems", Paraskevopoulos P, 1996, Prentice Hall, p.330-358
- 63** "Fuzzy Control and Fuzzy Systems", Pedrycz, W, 1989, Research Studies Press Ltd.
- 64** "Fuzzy Thinking", Kosko B, 1994 Flamingo
- 65** Bolander, W., "Powertrain Applications of Fuzzy Logic", SAE TOPTEC Electronic Engine Controls, 7-9 September 1998, Turin, Italy.
- 66** "A Fuzzy Decision-Making System for Automotive Applications", Soliman A, Kim Y, Rizzoni G, Candau J, The Ohio State University, USA, University of Valladolid, Spain, SAE 980519
- 67** "Use of Fuzzy Logic for Engine Idle Speed Control", Abate M, Dosio N, FIAT Research Centre, Italy, SAE 900594
- 68** "Impact of Alternative Controller Strategies on Exhaust Emissions from an Integrated Diesel / CVT powertrain" Deacon M, Brace C, Vaughan N, Burrows C, Horrocks R, University of Bath UK, Ford Motor Company UK, 1999 Proceeding of the ImechE vol 213 Part D p.95-107
- 69** "Vehicle Driveability – The Development of an Objective Methodology", Dorey, R., Martin, E., Ricardo Consulting Engineers, SAE201326
- 70** "The Potential for Simulation of Driveability of CVT vehicles", Wicke, V., Brace, C., Vaughan, N., University of Bath, SAE 00PC218
- 71** "Performance Feel QFD – Generic Test Specification No.101-03" Internal Document, Ford Motor Company, Diesel Engineering, Dunton UK
- 72** "Real Time Powertrain Simulation for Dynamic Engine Testing Using a Hydrostatic Dynamometer", Dorey, R.E., Guebeli, M., IEE Colloquium on Powertrain Control, 16 May 1990
- 73** "Model 107 Opacimeter: Users Manual", Celesco (Telonic Berkely), 1992
- 74** "HFR200 High Frequency FID: User Manual & Specification", Cambustion, 1998
- 75** "Ford Puma CP4 Turbocharger Comparison Steady State And Dynamic Testing", Cooper, A., Wijetunge, R., 14 April 1999, Vol 1 Issue 2, University of Bath Internal Document
- 76** "Comparison of Variable Geometry Turbocharging (VGT) over Conventional Wastegated Machines to achieve Lower Emissions", Pease, A., Hawley, G., Wallace, F., Cox, A., Horrocks, R., Bird, G., University of Bath, Ford Motor Co., Autotech 98 conference paper ref L07/C524-70
- 77** "Real-Life Vehicle Exhaust Emissions Performance Compared with Legislative Cycles", Farnlund, J., Bale, C., Rototest AB, Sweden, Knibb Gormezano & Partners, Harrogate, UK, IMechE publication C575/030/99
- 78** "Signal Reconstruction Techniques for Improved Measurement of Transient Emissions", Beaumont, A., Noble, A., Pillely, A., Ricardo Consulting Engineers Ltd, SAE900233
- 79** "Some Experiences of the Measurement of Regulated Pollutants on Transient Conditions", De Petris, C., Diana, S., Giglio, V., Police, G., Instituto Motori, CNR, Naples, Italy
- 80** "Dynamic Engine Modelling for Improved Control", Pillely, A., Noble, A., de Boer, C., Beaumont, A., Ricardo Consulting Engineers Ltd
- 81** "The Analysis of Mean Value Engine Models", Hendricks, E., The Technical University of Denmark, SAE 890563

- 
- 82** "Modelling and Validation of Automotive Engines for Control Algorithm Development", Moskwa, J., Hedrick, J., University of Wisconsin-Madison, University of California-Berkeley, Transactions of the ASME, Journal of Dynamic Systems, Measurement and Control, June 1992, Vol 114
- 83** "Automotive Engine Modelling for Real-Time Control Using MATLAB/SIMULINK", Weeks, R., Moskwa, J., Modular Systems, University of Wisconsin-Madison, SAE 950417
- 84** "Modelling and Real-Time Simulation of Diesel Engines for Control Design", Isermann, R., Sinsel, S., Schaffnit, J., Darmstadt University of Technology, SAE 980796
- 85** "Dynamic Turbocharged Diesel Engine Simulator for Electronic Control System Development", Watson, N., Imperial College London, UK, Transactions of the ASME, Journal of Dynamic Systems, Measurement and Control, March 1984, Vol 106
- 86** "Mean Value Modelling of a Small Turbocharged Diesel Engine", Jensen, J., Kristensen, S., Sorensen, S., Houbak, N., Technical University of Denmark, SAE 910070
- 87** "On the validity of Mean Value Engine Models during Transient Operation", Chevalier, A., Müller, M., Hendricks, E., Ford Motor Company, Delphi Automotive Systems, Technical University of Denmark, SAE 201261
- 88** "A Model for Load Transients of Turbocharged Diesel Engines", Payri, F., Reyes, E., Serrano, J., Universidad Politécnica de Valencia, SAE 990225
- 89** "Turbocharging the internal combustion engine", Watson, N., Janota, M. , 1982 Macmillan, p.158 "The radial flow turbine"
- 90** "Fuzzy Control and Fuzzy Systems", Pedrycz, W., Research Studies Press Ltd. 1989, ISBN 0863800815, chapter 4, p.111 "Design Aspects of the Fuzzy Controller"
- 91** "Digital Control Systems", Paraskevopoulos, P., 1996 Prentice Hall Europe, ISBN 0099989796, ch.11 "An intelligent approach to control: Fuzzy Controllers"
- 92** Stone, R., 'Introduction to Internal Combustion Engines', 1992, The Macmillan Press Ltd, p.173-175
- 93** Ljung, L., "System Identification Toolbox for Use With Matlab", 1997 The Mathworks inc.
- 94** "Some Experiments on the Measurement of Exhaust Smoke Emissions from Diesel Engines", Fosberry, R., Gee, D., MIRA Report 1961/5
- 95** "Origins of Diesel Particulate Mass Emissions", Greeves, G., Wang, C., SAE810260

# Appendix A- RAPID PROTOTYPING OF CONTROL STRATEGIES ON THE TEST BED ENGINE

## A.1 INTRODUCTION

This appendix describes the end result of extensive research into the best method of applying custom control strategies onto the test bed engine within the limitations of hardware and cost imposed by the project. A full description of this research, including the background information on CAN (Control Area Network) and its calibration protocol are given in <sup>1</sup>.

## A.2 OVERVIEW

In order to evaluate new engine control strategies a method of applying controller code in real time to the engine hardware is necessary. The real-time hardware used for running the custom control strategies is made by dSpace GmbH (see <http://www.dSpace.de>) and is practically an industry standard. It consists of a Digital Signal Processor (DSP, as the equipment shall henceforth be referred to as) and various I/O cards. The system is directly compatible with the Matlab / Simulink simulation and analysis environment, providing a convenient and powerful method of generating models and then executing them in real time. Controllers can be developed using, for example, an engine simulation or any of the control design tools provided by the Matlab environment, downloaded as compiled C code onto the dSpace processor and run in real time using real world inputs and outputs. The generation of C code is taken care of by software known as the Real Time Workshop, the process is referred to as Rapid Prototyping as it enables new designs to be developed and evaluated over very short timescales.

Existing solutions to the problem of efficiently implementing custom control code on an engine are not possible in this case due to cost and flexibility requirements, therefore a new method was sought.

Although a completely non-intrusive system making use of the CAN bus was desired, initial investigations found this to be infeasible therefore a hybrid method was proposed (see **Figure A.1**). It was decided to 'hard wire' the control outputs from the DSP to the vacuum drivers that control the EGR and VGT actuators; this required the construction of a current amplifier in order to provide a suitable output from the DSP to drive the Electronic Vacuum Regulators (EVR).

---

<sup>1</sup> "Investigation of a CAN-based Rapid Prototyping Method for Engine Control Strategies", Wijetunge, R., University of Bath, Internal Report

The variables used in the custom strategy are still acquired from the existing Engine Control Unit (henceforth referred to as the ECU) via the CAN bus, but instead of requesting each variable individually they are streamed continuously from the ECU to the DSP. This is made possible by the data acquisition feature of the CAN Calibration Protocol, a list of variables that the user wishes to acquire can be defined within the ECU and then the acquisition started; once this is done, the ECU will stream the variables continuously to the calibration tool via the CAN bus.

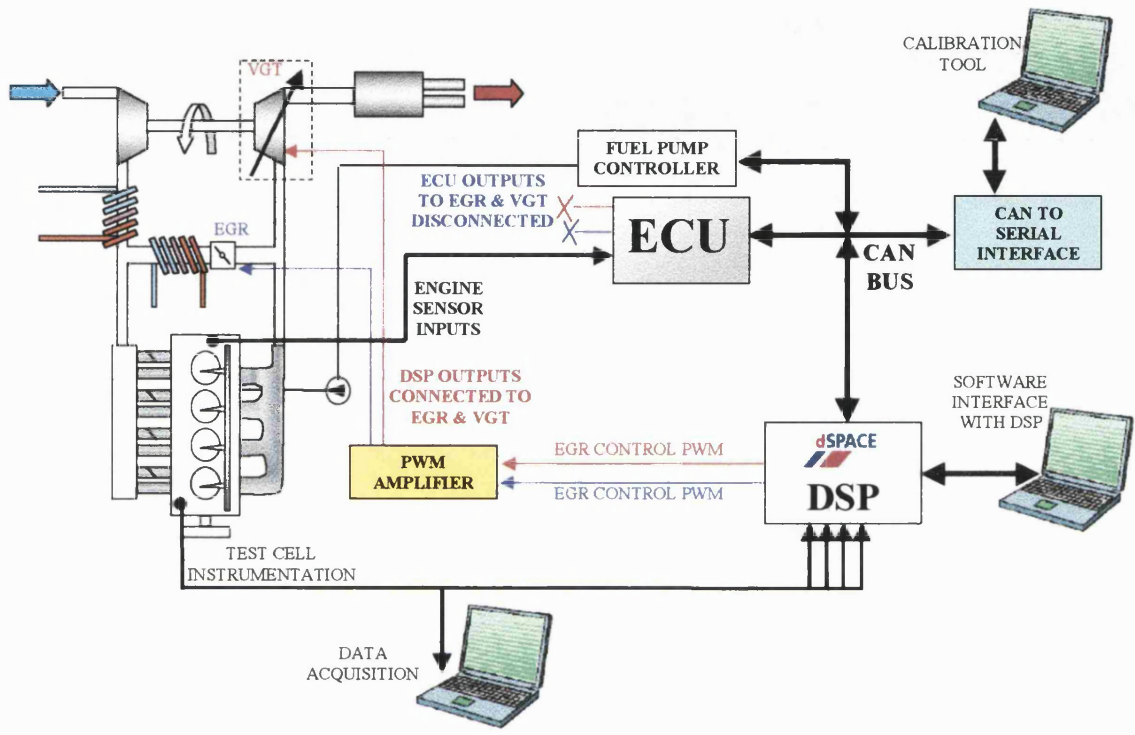


Figure A.1 Schematic of implementation

### A.3 IMPLEMENTATION DETAILS

#### A.3.1 DEFINING THE ACQUISITION LIST

The calibration tool (in this case the **Kleinknecht Gredi MCS 3.0** system) is used to define the list of variables to be transferred, reducing the implementation effort on the DSP. The variables required in the custom strategy are selected for display from the variables list window in the calibration tool. The variables that appear on screen are the variables that will be sent over the bus, the order in which they are sent being same as the order in which they appear on screen.

### A.3.2 DECODING THE CAN MESSAGES

The Simulink model for CAN message handling performs three tasks: it intercepts the messages, buffers them and finally decodes them into engineering units. The dSpace system does not provide hardware buffers for the CAN messages, therefore incoming frames must be dealt with as soon as they arrive, if not they will be overwritten by the preceding message.

As only three variables in the 16-bit signed integer form can be transferred by any one CAN frame, the messages arrive in batches corresponding to the total number of variables being transferred divided by three. The time between successive frames in a batch is approximately 250  $\mu$ s, the time between batches matches the ECU refresh rate of 16 ms. It would be extremely wasteful of DSP resources to run the system at an execution rate that could continuously resolve the smallest interval (e.g. 200  $\mu$ s timestep) therefore an interrupt driven system with software buffering was developed.

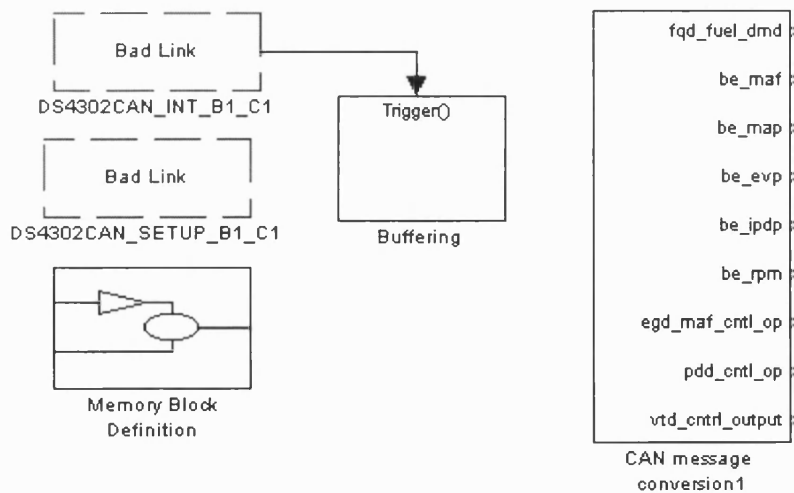


Figure 2 Top level of the Simulink CAN message handling model

The top level of the model is shown in **Figure 2**, the elements shown are:

- 1) The CAN message interrupt generator (labelled DS4302CAN\_INT\_B1\_C1)  
This will generate an interrupt flag every time a particular can message arrives in the CAN mailbox; it is a standard component in the dSpace ds4302 CAN blockset for Simulink.

- 2) The software buffer (labelled 'Buffering'). This is a system that only executes when the interrupt from the CAN message receive interrupt block is flagged, it then stores the values in the CAN frame that has just arrived into a predefined location in memory.
- 3) Memory description (labelled Memory Definition Block). This block defines the memory locations that act as buffers for the incoming messages.
- 4) Message conversion (labelled CAN Message Conversion 1). This block reads the batches of values from the buffer area and converts them into the engineering unit values for use in the strategy.

Each of the last three sections are now described in detail.

### **A.3.3 SOFTWARE BUFFER (2)**

The block components are shown in **Figure A.3**. The DS4302CAN\_RX\_B1\_C1 block is the standard message receiver block from the Simulink DS4302 blockset. It return the values of the variables in the CAN frame. The received message is a data acquisition object, its composition is shown in **Figure A.4**. The PID (Packet IDentification) byte is used to identify the batch of variables that are contained in the message. For example, if nine variables have been selected for transmission using the calibration tool, these variables will be sent in a batch of  $9/3=3$  separate CAN frames. Variables 1 to 3 arrive in frame 1, this will have the PID of 0, variables 4 to 6 arrive in the next frame with a packet ID of 1 and finally variables 7 to 9 arrive in the final frame with a packet ID of 2.

In the Simulink model, the PID and the six data bytes are transferred from the CAN receive block to the buffer block every time the CAN interrupt occurs; this is achieved by putting the enable trigger in the Simulink subsystem.

The buffer sub-block is shown in **Figure A.5**. This block has the function of allocating the six variables from the data section of the CAN frame to a particular buffer area depending on the PID. If the packet ID is 0 then the variables are channelled into the PID=0 buffer area and so on.

The actual buffer block is detailed in **Figure A.6**, it simply transfers the variables to the predefined memory locations.

No further processing (e.g. reconstructing the original 16-bit variables from the 2 byte format) is performed in this subsystem in order to minimise the computational load of this part of the model. This is because the interrupt driven system has priority over all other tasks and therefore should be as unobtrusive as possible.



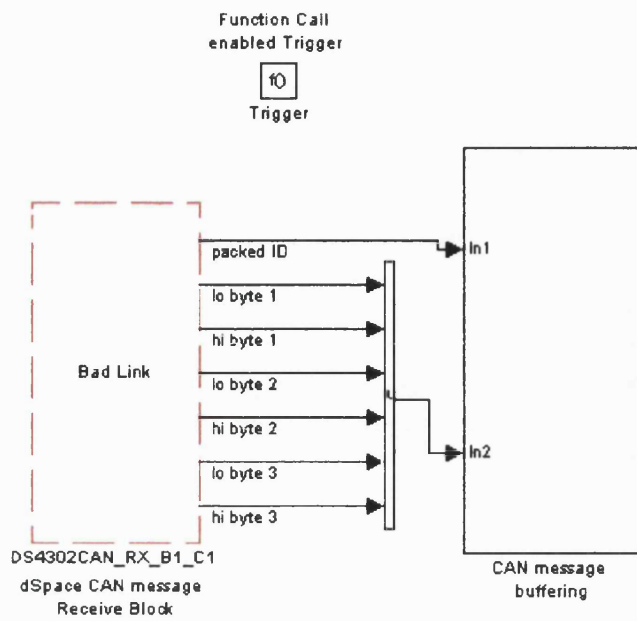


Figure A.3 Detail of software buffer

IDENTIFIER	PID	BYTE 1	BYTE 2	BYTE 3	BYTE 4	BYTE 5	BYTE 6	BYTE 7
------------	-----	--------	--------	--------	--------	--------	--------	--------

Figure A.4 Data acquisition CAN frame composition

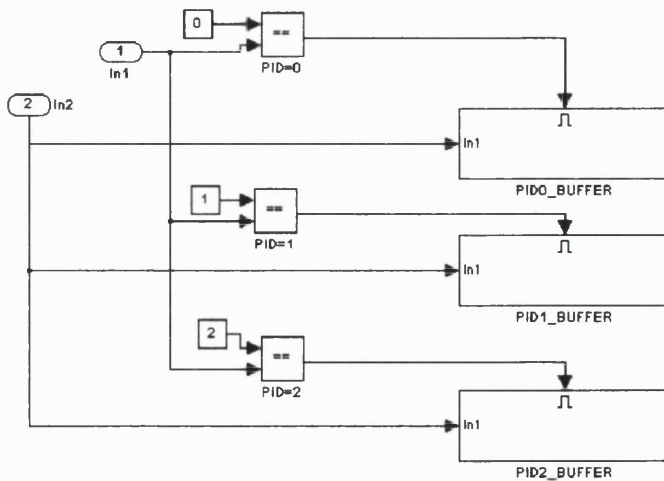


Figure A.5 Buffer allocation detail

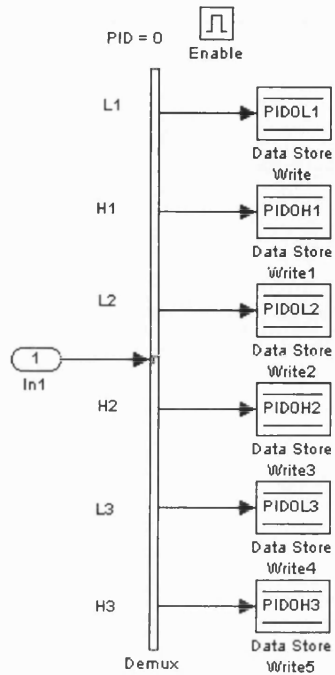


Figure A.6 Buffer detail

### A.3.4 Memory Definition (3)

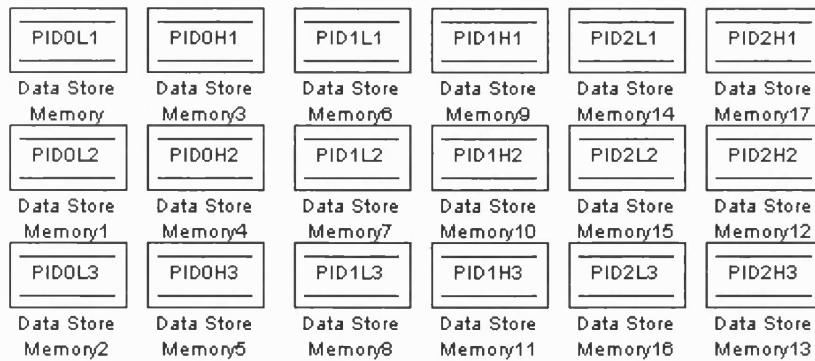


Figure A.7 Memory allocation blocks

The memory definition block consists of (2\*number of variables transmitted) Simulink Data Store Memory definition blocks, see **Figure A.7**.

### A.3.5 MESSAGE CONVERSION (3)

The message conversion block reconstructs the variables from the separate bytes transmitted in the CAN frame; this is performed at the update rate of the custom control strategy. **Figure A.8** shows the first level down of the Simulink implementation, each group of variables in the batch is dealt with by individual blocks.

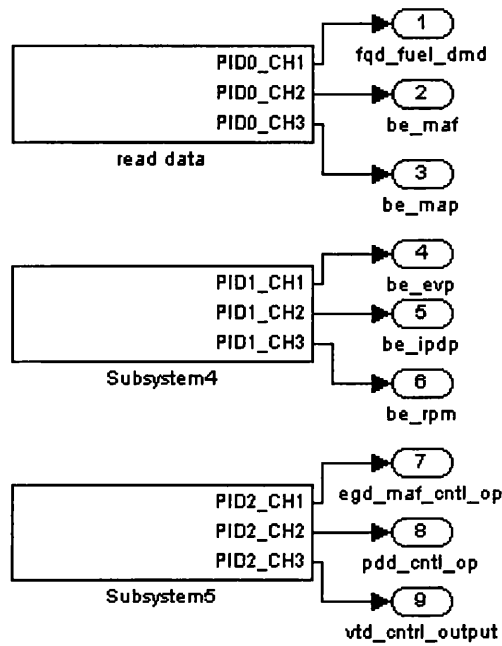


Figure A.8 First level of the decoding model

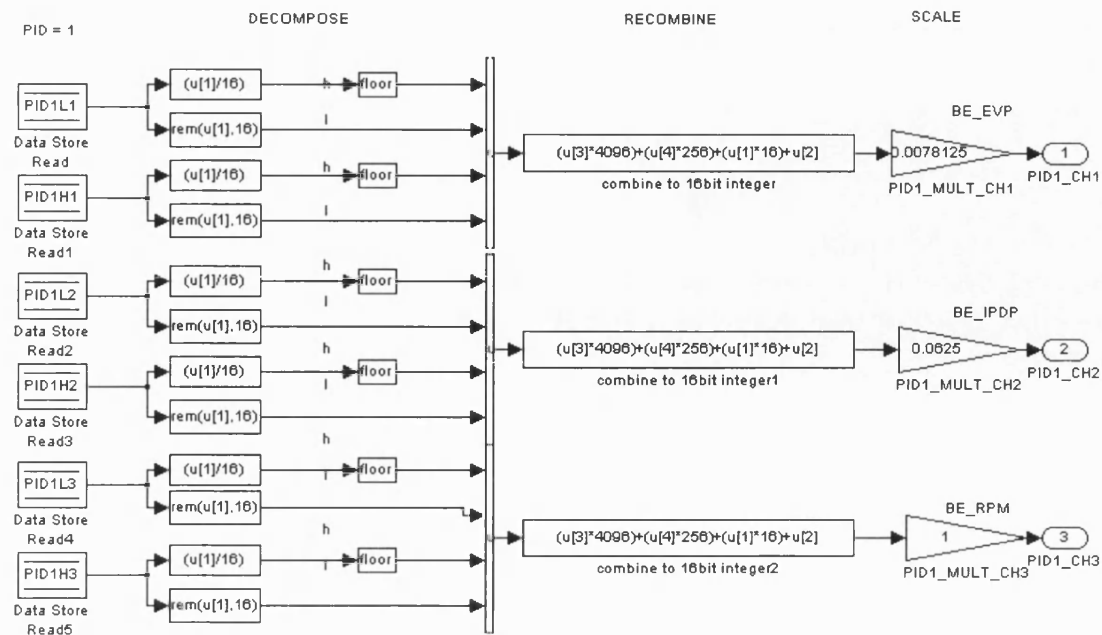


Figure A.9 The actual message conversion from lo / hi byte format to engineering units

The composition of one of these individual conversion blocks is shown in **Figure A.9**, the conversion process flows from left to right in the diagram. The bytes of data from the CAN frame are read from the memory locations every 16 ms, they are then combined into 16-bit values and converted to engineering units by the process shown in the figure to create the original values used in the ECU. Lastly, these values are scaled to real engineering units, the scale factors can be found in the \*.ROB file used by the calibration tool as shown in **Figure A.10**.

```

<from PUPE1RSW.ROB>
.....
3,$0,0p,250p,$3450,1,,vtc_os_cal,,x/16,0

PROVARI2
0
$0000
3,$0,0p,10p,$078e,1,,be_evp,mm_opened,x/128,2
3,$0,0p,255p,$0bcc,1,,fqd_fuel_dmd,mg/stroke,x/64,3
3,$0,0p,1000p,$0790,1,,be_maf,kg/hr,x/8,1
3,$0,0p,250p,$0796,1,,be_map,kPa,x/16,2
                                |
                                scale factor to convert be_map
                                to engineering units

```

**Figure A.10 Scale factors for variables given in \*.ROB file**

## **A.4 EGR FAULT HANDLING**

Care must be exercised when implementing this scheme, as the ECU has an error handling strategy for the EGR valve. This must first be disabled otherwise it will register a fault and alter the ECU calibration to a fault handling mode, this will result in erroneous values of EGR valve position being registered. Only the EGR valve has such a feature; it uses the position feedback from the valve to test that when the ECU demands a certain control level, the resulting EGR valve position falls within acceptable bounds. Also, upon cranking of the engine, the ECU requests zero EGR valve position, and recalibrates the position feedback to cater for any offset that may have occurred in the system. It is more straightforward to ensure that when starting the engine the custom strategy outputs zero demand than it is to override the ECU offset routine, as well as the fact that to achieve a good start it is better to crank the engine without EGR.

The range checking function can be overridden by using the calibration tool to set the following parameters to high values (e.g.16000): **aic\_evp\_slw\_bkt\_lek** and **aid\_evp\_mg\_bkt\_lek** , this has

the effective of preventing the fault counter from ever reaching the threshold that causes a fault to be flagged.

## **A.5 PROCEDURE**

The procedure to be followed for using this rapid prototyping method can be summarised as follows:

- 1) Select the variables required for the custom strategy using the calibration tool, the ECU must be 'alive' when doing this. (This step need not be repeated providing the same variables are to be used each time)
- 2) Switch off the ECU
- 3) Download the custom strategy onto dSpace
- 4) Ensure that the custom strategy output to the EGR valve is 0
- 5) Switch on power to the ECU, let the calibration tool perform its download
- 6) Start the engine
- 7) Enable the EGR valve output of the custom strategy

## Appendix B - DERIVATION OF TURBINE MASS FLOW

The turbocharger turbine mass flow is a useful variable for the evaluation of turbine performance, however it is neither straightforward nor convenient to measure. In order to produce plots of turbine mass flow vs. pressure ratio for the transient tests a method of deriving the turbine flow from other measurements is required.

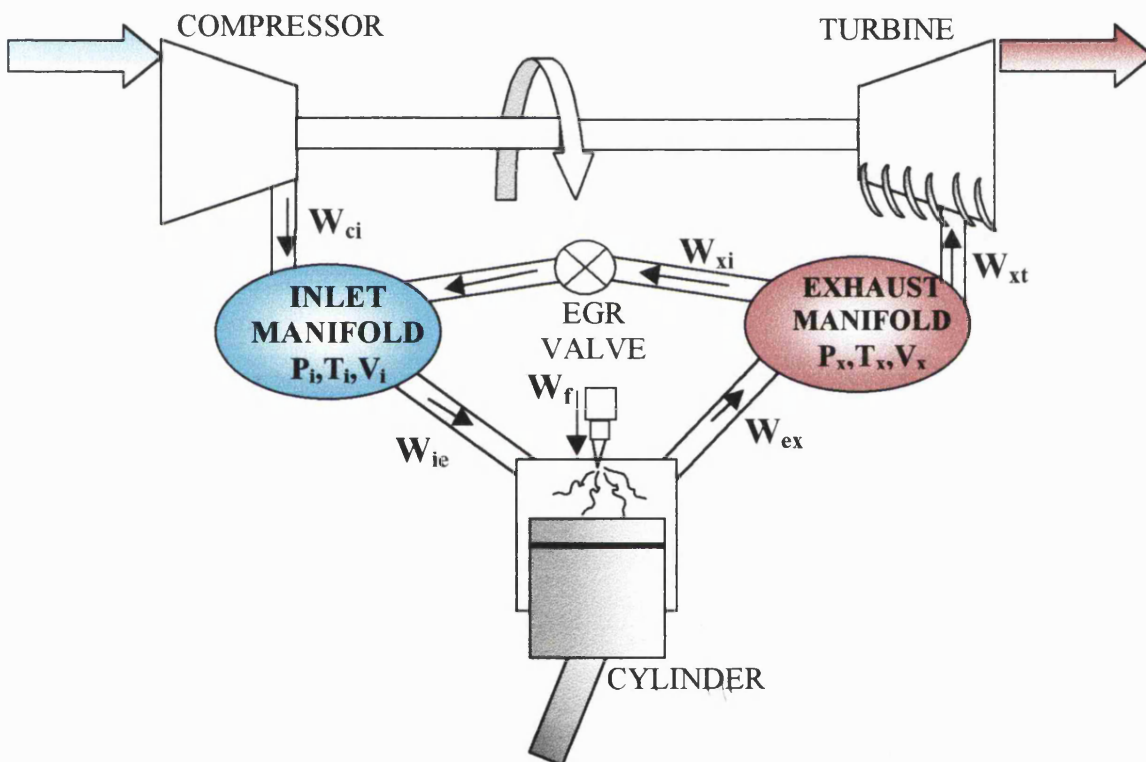


Figure B.1 Gas dynamics schematic of EGR VGT plant

Figure B.1 describes the EGR VGT plant in terms of its gas dynamics, where  $W$  refers to mass flow rates,  $p$  to pressures,  $T$  to temperatures and  $V$  to volumes. The subscripts refer to the compressor ( $c$ ), inlet manifold ( $i$ ), cylinder ( $e$ ), exhaust manifold ( $x$ ), turbine ( $t$ ) and fuel ( $f$ ). Where multiple subscripts are used this defines conditions from the 1<sup>st</sup> subscript to the 2<sup>nd</sup>, e.g.  $W_{ci}$  is the flow from compressor to inlet manifold,  $W_{xi}$  is the EGR flow etc.

The pressure in the manifolds is related to mass, volume and temperature by the perfect gas law (B.1):

$$pV = mRT \quad (\text{B.1})$$

where  $R$  is the universal gas constant.

The rate of change in manifold pressure is therefore related to rate of change of manifold mass content by equation (B.2):

$$\frac{dp}{dt}V = \frac{dm}{dt}RT \quad (\text{B.2})$$

The rate of change of manifold mass will be the sum of the flows entering and leaving the manifold. For the inlet this is given by equation (B.3):

$$\frac{dp_i}{dt} \frac{V_i}{RT_i} = W_{ie} - W_{ci} - W_{xi} \quad (\text{B.3})$$

For the exhaust manifold this is described by equation (B.4):

$$\frac{dp_x}{dt} \frac{V_x}{RT_x} = W_{ex} - W_{xt} - W_{xi} \quad (\text{B.4})$$

The mass flow through the cylinders is defined by equation (B.5):

$$W_{ex} = W_{ie} + W_f \quad (\text{B.5})$$

By rearranging equations (B.3) and (B.4) and substituting them into equation (B.5), the expression given by equation (B.6) is derived.

$$\frac{dp_x}{dt} \frac{V_x}{RT_x} + W_{xt} + W_{xi} = W_f + W_{ci} + W_{xi} + \frac{dp_i}{dt} \frac{V_i}{RT_i} \quad (\text{B.6})$$

Equation (B.6) can then be rearranged to give an expression for mass flow through the turbine as a function of measured variables (B.7):

$$W_{xt} = W_f + W_{ci} + \frac{dp_i}{dt} \frac{V_i}{RT_i} - \frac{dp_x}{dt} \frac{V_x}{RT_x} \quad (\text{B.7})$$

Due to the noise amplifying properties of the differential operation, the pressure signals need to be filtered for best results. This equation can also be used online providing suitable measurements or estimates are available to the control strategy.



## Appendix C - AN OVERVIEW OF FUZZY LOGIC

The basis of fuzzy logic is the degree to which an input to a system belongs a particular set, once this is established logical rules can be applied to the sets in order to map the inputs to the outputs.

The main elements of the fuzzy system are:

- 1) Fuzzification interface
- 2) Rule Base
- 3) Inference Engine
- 4) Defuzzification interface

These are illustrated in the context of a feedback control system in **Figure C.1**.

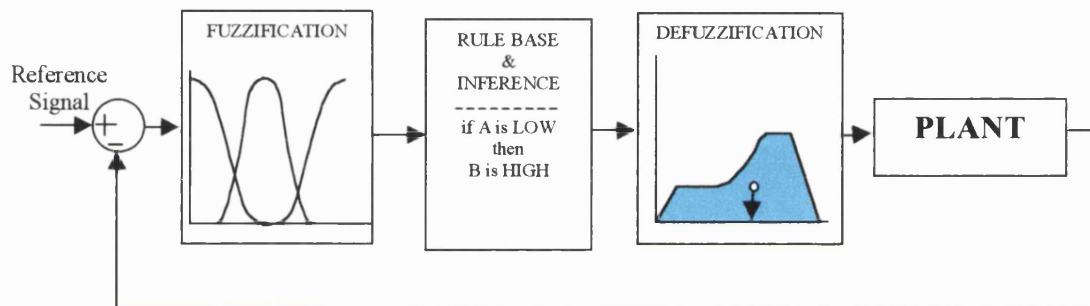


**Figure C.1 Elements of a fuzzy controller**

To illustrate the working of fuzzy logic more clearly, a simple room temperature control example is proposed;

Room temperature is measured and fed into a fuzzy system, the fuzzification of the input is illustrated in **Figure C.2**. The fuzzy system must decide what to do with the room heater (its control output) for any given input. A graphical representation of a fuzzy system to achieve this is given in **Figure C.3**.

### **C.1 FUZZIFICATION**

This is the process that takes physical inputs and produces fuzzy representations of these inputs. The whole concept of fuzzy logic revolves around the extent to which a value belongs to particular sets. The Membership Function is a shape function that represents a set of values. This is illustrated in the example input fuzzification of room temperature (**Figure C.2**), there are three input membership functions, COLD, WARM and HOT. The measured temperature intersects two

of these Membership Functions, COLD and WARM, therefore it can be said to belong to both the cold and warm sets. If a line is drawn from the point of intersection with the Membership Function to the y-axis, this describes to what extent the input value is a member of each set. It can be seen that the measured temperature is more a member of the WARM set than the COLD set. Membership values range from 0 for definitely not a member to 1 for definitely a member. The intermediate values describe the imprecision involved in classifying the value into a set, for instance 0.7 COLD and 0.3 WARM can be interpreted as 70% sure it is COLD and 30% sure it is warm.

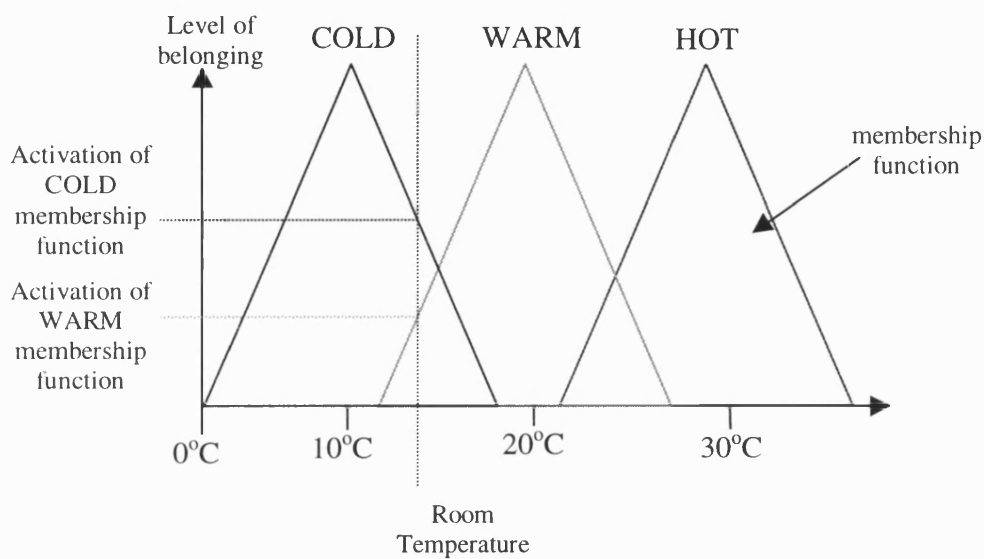


Figure C.2 Fuzzification example

## C.2 RULE BASE

The rule base is the linguistic description of the relationship between input and output.

The desired control action can be encapsulated in 3 logical rules

- 1) *If ROOM TEMPERATURE is COLD then INCREASE HEATER DEMAND*
- 2) *If ROOM TEMPERATURE is WARM then NO CHANGE TO HEATER DEMAND*
- 3) *If ROOM TEMPERATURE is HOT then REDUCE HEATER DEMAND*

Where *INCREASE HEATER DEMAND*, *NO CHANGE TO HEATER DEMAND* and *REDUCE HEATER DEMAND* represent the output Membership Functions.

### **C.3 INFERENCE ENGINE**

The inference engine 'blends' the rules to create an aggregate output. In the example (see **Figure C.3**), two rules are activated, rules 1 and 2, this is because the input temperature activates both COLD and WARM Membership Functions. As is illustrated in the diagram, the inference blends the outputs of each rule by summing them to create a composite shape. In the inference, the logical operators in the rule base are applied using equivalent geometric operations. For example if two inputs are being used and a rule such as "if INPUT1 is A AND INPUT2 is B", the *AND* operation between the two input Membership Functions will be performed by a *MIN* operation on the shapes to produce a composite shape.

### **C.4 DEFFUZIFICATION**

This is the output stage of the fuzzy logic system, the aggregate output of all the rules is converted into a single value by applying a geometric function to the composite output shape, in this example a centre of mass calculation is used to generate the control output.

This simple example illustrates how Fuzzy Logic offers an intuitive approach to control, allowing complex control laws to be built up from simple linguistic rules, these rules can embody operator knowledge and system behaviour.

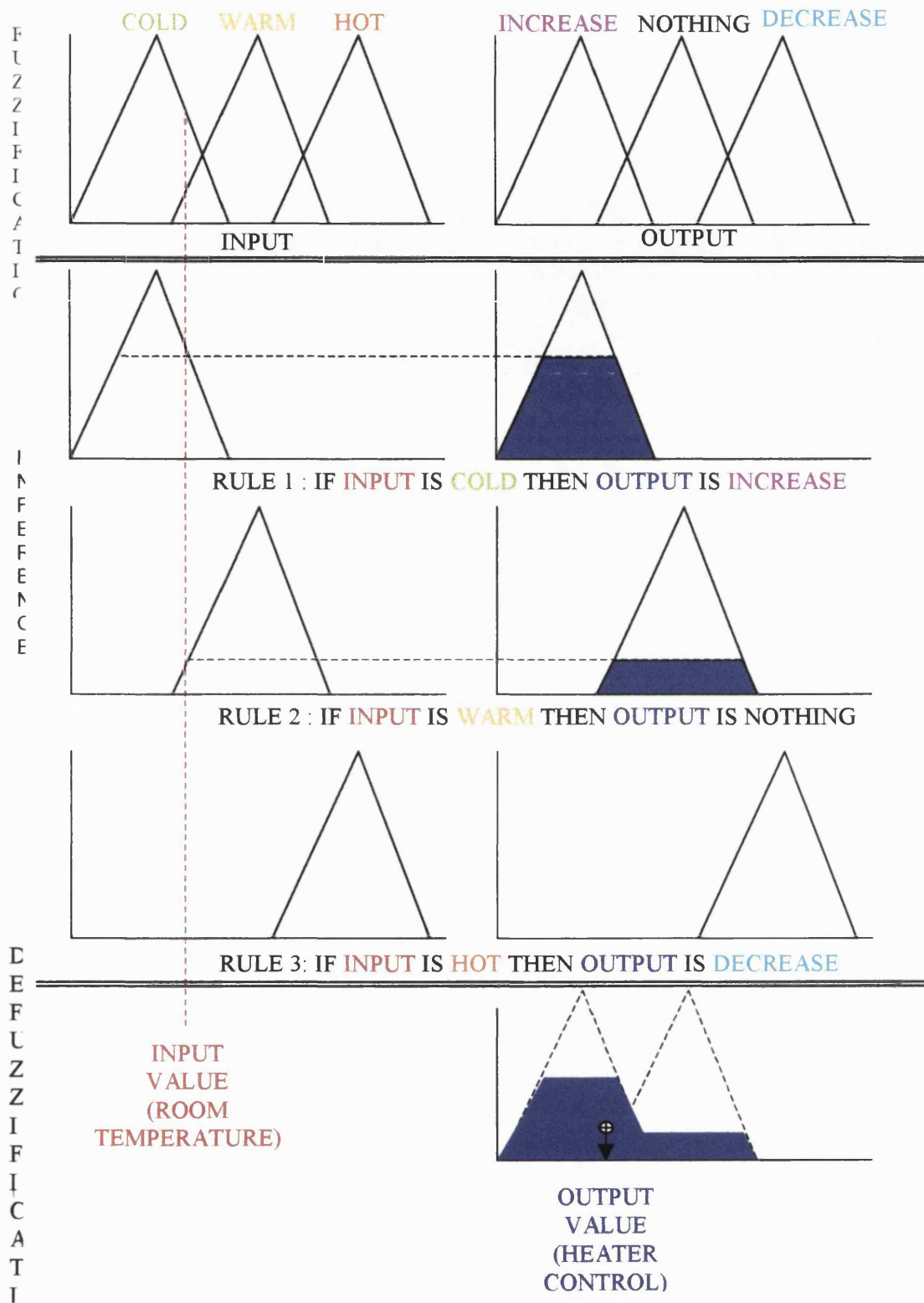


Figure C.3 Fuzzy temperature control example

## Appendix D – DERIVATION OF PREDICTOR ALGORITHM FROM PLANT MODEL

This appendix explains the derivation of a two step ahead prediction model from a linear 2<sup>nd</sup> order system.

The general linear discrete-time system model is given by **Equation D.1**

$$\frac{y(t)}{u(t)} = \frac{d_1 z^2 + d_2 z + d_3}{n_1 z^2 + n_2 z + n_3} \quad (\text{D.1})$$

This expression can be re-arranged to the form:

$$y(t)(n_1 z^2 + n_2 z + n_3) = u(t)(d_1 z^2 + d_2 z + d_3) \quad (\text{D.2})$$

Dividing through by the highest power of z leads to the same expression in terms of powers of the delay operator,  $z^{-1}$ :

$$y(t)(n_1 + n_2 z^{-1} + n_3 z^{-2}) = u(t)(d_1 + d_2 z^{-1} + d_3 z^{-2}) \quad (\text{D.3})$$

The  $z^{-1}$  operator represents a delay of one sample, therefore the above expression can be written as:

$$n_1 y(t) + n_2 y(t-1) + n_3 y(t-2) = d_1 u(t) + d_2 u(t-1) + d_3 u(t-2) \quad (\text{D.4})$$

Where the subscripts (t-1), (t-2) etc.. represent the previous sample values.

Rearranging **Equation D.4** gives an expression for the current output,  $y(t)$ , as a function of previous inputs and outputs:

$$y(t) = \frac{1}{n_1} (-n_2 y(t-1) - n_3 y(t-2) + d_1 u(t) + d_2 u(t-1) + d_3 u(t-2)) \quad (\text{D.5})$$

To predict one step ahead, the samples used in the equation are simply shifted forward in time:

$$y(t+1) = \frac{1}{n_1} (-n_2 y(t) - n_3 y(t-1) + d_1 u(t+1) + d_2 u(t) + d_3 u(t-1)) \quad (\text{D.6})$$

To predict 2 steps ahead, the samples used in **Equation (D.5)** are shifted forward in time again, and **Equation (D.6)** backsubstituted to produce the recursive formula given by **Equation (D.7)**:

$$y(t+2) = \frac{1}{n_1} (-n_2 y(t+1) - n_3 y(t) + d_1 u(t+2) + d_2 u(t+1) + d_3 u(t))$$

$$y(t+2) = \left( \frac{n_2^2}{n_1^2} - \frac{n_3}{n_1} \right) y(t) + \left( \frac{n_2 n_3}{n_1^2} \right) y(t-1) + \frac{d_1}{n_1} u(t+2) + \left( \frac{d_2}{n_1} - \frac{n_2 d_1}{n_1^2} \right) u(t+1) + \left( \frac{d_3}{n_1} - \frac{n_2 d_2}{n_1^2} \right) u(t) - \frac{n_2 d_3}{n_1^2} u(t-1) \quad (\text{D.7})$$

## Appendix E - CUMULATIVE EMISSIONS CALCULATIONS

For the purposes of comparing controllers over the legislative drive cycle, it is convenient to generate cumulative values for the important exhaust emissions and fuel consumption. In this study the measurements of smoke, Oxides of Nitrogen and fuel consumption have been used to characterise the performance of the particular strategy under test.

In the absence of particulate matter measurement, the smoke measurement has been used to give an indication of the level of particulates in the exhaust; this is a well-established approximation. There are two smoke measurement devices; the first is an opacimeter which works by shining a beam of light through the exhaust plume and measuring the amount that falls on a detector, the result being a percentage opacity. The second system draws the sample gas through a filter paper, the smoke deposits on the paper and the reflectivity of the deposit is measured as a filter smoke number (FSN). The opacimeter is the only device of the two capable of continuous measurement, hence was used for this study. The results from this measurement are less accurate, especially at low levels, but the benefits are that the system can track the rapid smoke peaks associated with tip-in transients.

The NO<sub>x</sub> measurement uses a chemi-luminescence detector, the result is given as a concentration of NO<sub>x</sub> in the exhaust gas in parts per million (ppm). The analyser output is heavily damped and delayed, therefore the result is treated with the signal reconstruction technique that fits the system step response to a 1<sup>st</sup> order lag and a transport delay.

Fuel consumption was initially measured using the gravimetric fuel flow meter; this device fills a beaker with fuel, the engine is supplied from this beaker, periodic measurement of the weight of the beaker gives the fuel mass flow rate. Unfortunately, the system was not properly initialised (i.e. the beaker was not sufficiently filled) before several of the tests, leading to spurious fuel consumption results as the beaker filled during the cycle. The demanded fuelling signal from the ECU had to be used instead, although this will be slightly inaccurate in absolute terms as it is the demand, not the actual amount delivered by the injectors; the inaccuracy will be consistent across all tests allowing fair comparison.

The following equations describe the derivation of cumulative drive cycle results from the quantities described above:

### SMOKE

$$M_{smoke} = \frac{1}{D_{cycle}} \int_{t=0}^{t=T} \left( \frac{X_{smoke}(t) \dot{m}_{ex}(t)}{3600} * 0.1 \right) dt \quad (E.1)$$

where  $M_{smoke}$  is the total smoke emissions [1/km]

$D_{cycle}$  is the total distance travelled during cycle (from time  $t=0$  to time  $t=T$ ) [km]

$X_{smoke}(t)$  is the smoke opacity at time  $t$  [%]

$\dot{m}_{ex}(t)$  is the exhaust mass flow at time  $t$  [kg/hr]

The 0.1 multiplier represents an arbitrary function to convert the smoke opacity to a representative mass.

### NOx

$$M_{NOx} = \frac{1}{D_{cycle}} \int_{t=0}^{t=T} \left( \frac{X_{NOx}(t) \dot{m}_{ex}(t)}{3600 * 1000} * 1.587 \right) dt \quad (\text{E.2})$$

where  $M_{NOx}$  is the total NOx emissions [g/km]

$X_{NOx}(t)$  is the reconstructed exhaust NOx concentration at time  $t$  [ppm]

The 1.587 multiplier is the relative density of NOx, converting the volume flow to mass flow

### FUEL CONSUMPTION

$$M_{fuel} = \frac{1}{D_{cycle}} \int_{t=0}^{t=T} \left( \frac{X_{fuel}(t) N_{eng}(t)}{2 * 60 * 1000} \right) dt \quad (\text{E.3})$$

where  $X_{fuel}(t)$  is the fuelling demand at time  $t$  [mg/shot]

$N_{eng}(t)$  is the engine speed at time  $t$  [rev/min]

MICROCAL ORIGIN 5.0 SCRIPT TO IMPLEMENT ABOVE CALCULATIONS

The following script was used to implement the calculations in the data analysis package Mircocal Origin (<http://www.microcal.com>)

<dc\_opj\_macro.txt>

```
%Z=%H
emissions!wks.addcol(MdotEx)
doc -uw
emissions_MdotEx=(%Z_MAFfox+%Z_Mdotfuel)

%Z!wks.addcol(speed)
doc -uw
%Z_speed=(%Z_aa45)/3600
integrate(%Z_speed)
dist=integ.area

emissions!wks.addcol(MassNOx)
doc -uw
emissions_MassNOx=(emissions_MdotEx)*(emissions_rconNOxwet)*1.587/(3600*1000)

integrate(emissions_MassNOx)
NOx=integ.area

TOTNOx=NOx/dist

TOTNOx=
emissions!wks.addcol(MassSmoke)
doc -uw
emissions_MassSmoke=(emissions_MdotEx)*(emissions_smoke)*0.1/3600

integrate(emissions_MassSmoke)
Smoke=integ.area

TOTSmoke=Smoke/dist

TOTSmoke
```